Profiling for Natural Products with $GABA_A$ Receptor Modulatory and Immunosuppressant Activities

Inauguraldissertation

zur
Erlangung der Würde eines Doktors der Philosophie

vorgelegt der

Philosophisch-Naturwissenschaftlichen Fakultät

der Universität Basel

von

Nova Syafni

2021

Genehmigt von der Philosophisch-Naturwissenschaftlichen Fakultät
auf Antrag von

Prof. Dr. Matthias Hamburger

PD Dr. Martin Smiesko

Dr. Emerson F. Queiroz

Basel, den 15.12.2020

Prof. Dr. Martin Spiess

Dekan

TABLE OF CONTENTS

LIST OF ABBREVIATIONS **5**
SUMMARY **6**
ZUSAMMENFASSUNG **9**
1. AIM OF THE WORK **12**
2. INTRODUCTION **15**
2.1. Natural Products in Drug Discovery **16**
2.1.1. Drug-like compounds from nature **16**
- Natural products as sources of drugs 16
- Challenges of natural product-based drug discovery 17
- Tracking bioactive natural products 19
2.1.2. GABAergic natural products **23**
- Traditional medicine as a source of information for CNS drug discovery 23
- GABAergic drugs 24
2.1.3. Natural products with immunosuppressant properties **25**
- Traditional medicine as a source of information for immune suppression 25
- Currently available immunosuppressant agents 25
2.2. The $GABA_A$ Receptor **29**
- The function of $GABA_A$ receptors 30
- $GABA_A$ receptors as targeted assays 32
2.3. HPLC-Based Activity Profiling with $GABA_A$ Receptor Assays **36**
2.3.1. *Xenopus* oocyte assay **36**
- Principle 37
- Advantages and challenges 38
2.3.2. Zebrafish larvae locomotor-activity model **39**
- Principle 39
- Advantages and challenges 40
2.3.3. Fluorometric Imaging Plate Reader (FLIPR) assay **41**
- Principle 42
- Advantages and challenges 44
- Chinese Hamster Ovary (CHO) cells in expressing $GABA_A$ receptors 44

2.4. HPLC-Based Activity Profiling for Immunosuppressant Activity 47

- Role of T cells in the immune system..... 47

- T lymphocyte proliferation assay..... 49

3. RESULT AND DISCUSSION.....54

3.1. HPLC-Based activity profiling for $GABA_A$ receptor modulators in *Murraya exotica* **.** 55

3.2. Clerodane diterpenes from *Casearia corymbosa* as allosteric modulators at the neurosteroid binding site of $GABA_A$ receptors**.....** 72

3.2. Immunosuppressant flavonoids from *Scutellaria baicalensis* 1399

4. CONCLUSION AND OUTLOOK.....164

ACKNOWLEDGEMENTS.....169

LIST OF ABBREVIATIONS

APCI	atmospheric pressure chemical ionization
BBB	blood-brain barrier
CFSE	carboxyfluorescein diacetate succinimidyl ester
CHO cells	Chinese hamster ovary cells
CNS	central nervous system
COSY	correlated spectroscopy
DAD	diode array detector
DCM	dichloromethane
DMSO	dimethyl sulfoxide
DNP	dictionary of natural products
ECD	electronical circular dichroism
EC_{50}	half maximal effective concentration
ELSD	evaporative light scattering detector
ESI	electron spray ionization
EtOAc	ethyl acetate
FACS	fluorescence-activated cell sorting
FBS	fetal bovine serum
FDA	food and drug administration
FLIPR	fluorescence imaging plate reader
$GABA_A$ receptor	γ—aminobutyric acid type A receptor
HMBC	heteronuclear multiple bond correlation
HPLC	high performance liquid chromatography
HSQC	heteronuclear single quantum coherence/correlation
HTS	high-throughput screening
IC_{50}	half maximal inhibitory concentration
MS	mass spectroscopy
NOESY	nuclear Overhauser effect spectroscopy
NMR	nuclear magnetic resonance
MTC	maximal tolerated concentration
NP/NPs	natural products
PAM	positive allosteric modulator
PDA	photodiode array
PREGS	pregnenolone sulfate
PTZ	pentylenetetrazol
ROESY	rotating frame nuclear Overhauser effect spectroscopy
TEVC	two-microelectrode voltage clamp
UV-Vis	ultraviolet-visible

SUMMARY

HPLC-based activity profiling is an effective approach for tracking active compounds in an extract. In this doctoral thesis, this approach was applied to discover new scaffolds for Gamma-aminobutyric acid type A ($GABA_A$) receptor modulators and immunosuppressant agents from natural origin.

$GABA_A$ receptors are the major inhibitory neurotransmitter in the human brain. They are also a therapeutic target in drug discovery. Lack of subtype-selectivity of GABAergic drugs correlates with undesireable side-effects. Benzodiazepines, barbiturates, neurosteroids, anesthetics, and alcohol are well-known modulators of $GABA_A$ that bind to its receptor. Some methodological approaches have been developed for investigating $GABA_A$ receptor modulator pharmacology and functional response. The gold standard for the functional assay of GABA is *in vitro Xenopus* oocyte assay, which is expressing the $\alpha_1\beta_2\gamma_{2s}$ subunit compositions. This method was applied as primary screening for the *in vivo* in house assay utilizing zebrafish larvae in this research.

The HPLC-based activity profiling and screening using zebrafish larvae locomotor assay allowed us to identify active compounds in dichloromethane (DCM) extract of twigs and leaves of *Murraya exotica* L. Ten compounds were isolated from DCM extract consisting of six coumarins and four polymethoxyflavones. The active compound was identified as osthol (**9**). It potentiated $GABA_A$-induced chloride currents by 487 ± 42%, with an EC_{50} of 46 ± 10 μM in *Xenopus* oocyte assay. The adjacent compound in the activity profiling showed a related structure (coumurrayin (**10**)) with an additional methoxy group, but it showed a neglectable effect. Furthermore, the physicochemical properties of these two compounds were calculated *in silico*. The result shows that both compounds are favourable for oral bioavailability and blood-brain barrier (BBB) permeability.

A library of 798 ethyl acetate (EtOAc) extracts was screened in fluorometric imaging plate reader (FLIPR) assay. This functional assay utilized Chinese hamster ovary (CHO) cells stably transfected with $GABA_A$ receptors of $\alpha_1\beta_2\gamma_2$ subunit composition. The active extracts were further checked for concentration-dependent effects. Afterwards, the active extracts were submitted to HPLC-based activity profiling to localize the active compounds in the extracts. This screening resulted in two active extracts, which one of them was an EtOAc extract from

Casearia corymbosa Kunth leaves. Eight compounds were isolated from active time windows, and one compound was obtained from an adjacent fraction. All of the compounds were clerodane-type diterpenoids, of which five were new. All compounds were screened in FLIPR assay. Five compounds (**1**, **3**, **5**, **7**, **8**) exhibited activation for allosteric $GABA_A$ receptor modulators and were further assessed for concentration-response and determination of EC_{50} values. Compounds **3**, **7**, and **8** displayed significantly enhanced potentiation of GABA with EC_{50}'s of 0.51, 4.57, and 1.36 μM, respectively. In contrast, compounds **1** and **5** did not show concentration-dependent effect.

Compound **8** was further evaluated to identify allosteric $GABA_A$ receptor modulatory binding sites in FLIPR assay. In order to evaluate the affinity to the benzodiazepines binding site, compound **8** (5 μM) combined with increasing concentrations of flumazenil and increasing concentrations of compound **8** combined with diazepam (2 μM) were tested. For the barbiturates binding site, increasing concentrations of compound **8,** combined with etazolate (0.78 μM) were assessed. For the neurosteroids binding site, the same treatments as for benzodiazepine binding site assessments were used consisting of compound **8** with increasing concentrations of pregnenolone sulfate (PREGS) and increasing concentrations of **8** with a fixed concentration of allopregnanolone at 0.25 μM. The results showed that additive potentiation could be observed in the addition of diazepam, etazolate, and allopregnanolone. However, decreasing activation was observed with the addition of compound **8** at the highest concentration of PREGS. This suggests that compound **8** and PREGS bind at the same sites on the neurosteroid $GABA_A$ receptors with compound **8** being the first reported non-steroidal compound interacting at the neurosteroid binding site.

Toxicity and side effect issues in immunosuppressant drugs were the driving force in searching for a natural product as a source of immunosuppressive agents. A library of 435 extracts from traditional Chinese herbal medicines was screened for inhibition of human T lymphocyte proliferation. One of the active extracts without concomitant toxicity, a DCM extract from the roots of *Scutellaria baicalensis*, was submitted to HPLC-based activity profiling for tracking the active compounds. Seventeen flavonoids were isolated in the time active windows and its adjacent fractions. The isolated flavonoids possessed unusual substitution patterns in B-ring, with preferred substitutions at C-1' and C-6' and lack of substitutions at C-3' and C-4'. All active compounds showed cytotoxicity at a concentration of

100 µg/mL. Compounds **2**, **4**, **8**, and **12** displayed moderate activity with EC_{50} values of 55.9, 45.9, 61.6, and 50.2 µM, respectively. High immunosuppressant activity was exhibited by compounds wogonin (**11**), chrysin (**13**), skullcapflavone (**14**), and oroxylin A (**16**) with EC_{50} values of 20.2, 22.2, 12.2, and 39.0 µM, respectively.

All structures of the isolated compounds were determined by off-line 1D and 2D NMR (COSY, HSQC, HMBC) and HPLC-ESI-MS. High-resolution MS was also applied for some isolated compounds. Absolute configurations were determined by ECD and NOESY. Optical rotation was recorded for chiral compounds.

ZUSAMMENFASSUNG

HPLC-basiertes Aktivitäts-Profiling ist ein effektiver Ansatz, um aktive Verbindungen in einem Extrakt zu lokalisieren. In dieser Dissertation wurde dieses Verfahren zur Entdeckung neuer Strukturen für γ- Aminobuttersäure A ($GABA_A$) – Rezeptor-Modulatoren und immunosupressiven Substanzen natürlichen Ursprungs angewendet.

$GABA_A$-Rezeptoren sind die Hauptgruppe inhibierender Neurotransmitter im menschlichen Gehirn. Sie sind daher ein therapeutisches target in der Wirkstoffforschung. Mangel an Subtyp-Selektivität von GABAergen Arzneimitteln korreliert mit unerwünschten Nebenwirkungen. Benzodiazepine, Barbiturate, Neurostereoide, Anästhetika und Alkohol wirken bekannterweise modulierend an $GABA_A$-Rezeptoren. Es wurden bereits verschiedene methodische Ansätze entwickelt zur Untersuchung der Pharmakologie und funktionellen Wirkung von $GABA_A$-Rezeptor-Modulatoren. Der sogenannte Goldstandard für funktionelle Assays von GABA *in vitro* ist der *Xenopus* Oozyten Assay, welches die Untereinheiten $\alpha_1\beta_2\gamma_{2s}$ exprimiert. Diese Methode wurde als primäres *in vivo* Screening für die in dieser Arbeit verwendete in-house Zebrafischlarven Assay angewendet.

Das HPLC-basierte Aktivitäts-Profiling und Screening (Zebrafischlarven-Locomotor-Assay) ermöglichte die Identifizierung aktiver Verbindungen im Dichlormethan (DCM)-Extrakt der Zweige und Blätter von *Murraya exotica* L. Zehn Verbindungen konnten aus dem DCM-Extrakt isoliert werden. Dabei handeltes es sich um sechs Cumarine und vier Polymethoxyflavone. Die aktive Verbindung wurde als Osthol (**9**) identifiziert. Osthol erhöhte die $GABA_A$-induzierten Chloridströme um 487 ± 42%, bei einem EC_{50} von 46 ± 10 μM im *Xenopus* Oozyten Assay. Eine benachbarte Verbindung im Aktivitäts-Profiling, Coumurrayin (**10**), besass eine verwandte Struktur mit einer zusätzlichen Methoxygruppe, ihre Aktivität war jedoch vernachlässigbar. Darüber hinaus wurden die physikochemischen Eigenschaften der zwei Verbindungen *in silico* berechnet. Das Resultat zeigte, dass beide Verbindungen günstige orale Verfügbarkeit sowie Permeabilität zur Blut-Hirn-Schranke aufweisen.

Eine Bibliothek von 798 Ethylacetat- (EtOAc) Extrakten wurde mittels FLIPR (fluorometric imaging plate reader) Assay gescreent. In diesem funktionellen Assay wurden chinesische Hamsterovarien- (CHO) mit $GABA_A$-Rezeptoren mit den Untereinheiten $\alpha_1\beta_2\gamma$ transfiziert. Die Extrakte, welche eine Aktivität aufwiesen, wurden weiter auf

konzentrationsabhängige Effekte untersucht. Anschliessend wurden diese Extrakte mittels HPLC-basiertem Profiling auf ihre für die Aktivität verantwortlichen Verbindungen untersucht. Der EtOAc-Extrakt von den Blättern von *Casearia corymbose* Kunth. zeigte beim Screening eine starke Aktivität. Insgesamt acht Verbindungen wurden aus dem entsprechenden Zeitfenster isoliert sowie eine Verbindung aus einer nächsten Fraktion. Bei allen Strukturen handelte es sich um Diterpenoide vom Clerodan-Typ, von denen fünf neu waren. Alle Verbindungen wurden folglich mit dem FLIPR-Assay gescreent. Fünf Verbindungen (**1**, **3**, **5**, **7**, **8**) zeigten eine Aktivierung als allosterische $GABA_A$-Rezeptor-Modulatoren und wurden weiter auf konzentrationsabhängige Effekte und EC_{50}-Werte untersucht. Die Verbindungen **3, 7** und **8** zeigten signifikante Potenzierung von GABA mit EC_{50}-Werten von 0.51, 4.57 und 1.36 µM. Im Gegensatz zeigten die Verbindungen **1** und **5** keinen konzentrationsabhängigen Effekt.

Verbindung **8** wurde weiter mittels FLIPR-Assay untersucht, um mögliche allosterische modulierende $GABA_A$-Rezeptor Bindungsstellen zu identifizieren. Um die Affinität zur Bindungsstelle für Benzodiazepine zu evaluieren, wurden Verbindung **8** (5 µM) in Kombination mit steigenden Konzentrationen von Flumazenil, sowie steigende Konzentrationen von **8** in Kombination mit Diazepam (2 µM) getestet. Für die Bindungsstelle der Barbiturate wurden steigende Konzentrationen der Verbindung **8** kombiniert mit Etazolat (0.78 µM) untersucht. Für die Neurosteroid-Bindungstelle wurden, ähnlich wie für die Benzodiazepin-Bindungstelle, Verbindung **8** und steigende Konzentrationen von pregnenolone sulfate (PREGS), sowie steigende Konzentrationen von **8** in Kombination mit einer konstanten Konzentration von 0.25 µM Allopregnanolon getestet. Die Ergebnisse zeigten eine additive Potenzierung bei Zugabe von Diazepam, Etazolat und Allopregnanolon. Jedoch wurde eine Abnahme der Aktivierung beobachtet bei Zugabe von Verbindung **8** mit der höchsten Konzentration an PEGS. Diese Beobachtung legt nahe, dass Verbindung **8** und PEGS eine Affinität zur gleichen Bindungsstelle am neurosteroidalen $GABA_A$-Rezeptor haben und somit Verbindung **8** die erste beschriebene nicht-steroidale Substanz mit Affinität zur neurosteroidalen Bindungsstelle darstellt.

Die Toxizität und unerwünschten Nebenwirkungen von immunosupressiven Medikamenten war die zugrunde liegende Motivation neue immunosupressive Substanzen bei Naturstoffen zu suchen. Eine Bibliothek mit Extrakten aus 435 traditionellen chinesichen Arzneipflanzen wurde auf Inhibition der menschlichen T Lymphozyten Proliferation gescreent. Einer der aktiven Extrakte ohne begleitende Toxizität war ein Extrakt aus den Wurzeln von

Scutellaria baicalensis. Der Extrakt wurde dem HPLC-basierten Aktivitäts-Profiling unterzogen. Siebzehn Flavonoide wurden aus dem aktiven Zeitfenster und den angrenzenden Fraktionen isoliert. Die isolierten Flavonoide wiesen ein ungewöhnliches Substitutionsmuster im B-Ring auf, mit einer bevorzugten Substitution in C-1' und C-6' und gleichzeitig keine Substitution in C-3' und C-4'. Alle aktiven Verbindungen waren zytotoxisch bei einer Konzentration von 100 µg/mL. Die Verbindungen **2, 4, 8,** und **12** hatten eine moderate Aktivität mit EC_{50}-Werten von 55.9, 45.9, 61.6 und 50.2 µM. Wogonin (**11**), Chrysin (**13**), Skullcapflavon (**14**) und Oroxolyn A (**16**) zeigten eine hohe immunosupressive Aktivität mit EC_{50}-Werten von 20.2, 22.2, 12.2 und 39.0 µM.

Alle Strukturen der isolierten Verbindungen wurden durch off-line 1D, 2D NMR (COSY, HSQC, HMBC) und HPLC-ESI-MS aufgeklärt. Hochauflösende MS wurde bei einigen isolierten Verbindungen auch angewendet. Die absolute Konfiguration wurde durch ECD und NOESY Experimente bestimmt. Zusätzlich wurde die optische Drehung bei chiralen Verbindungen gemessen.

1. AIM OF THE WORK

Natural products play a vital role as a source of new scaffolds in drug discovery and development. In our group, we have established a technology platform for library-based lead discovery [1,2]. The core features in this platform are an extract library in 96-well format, a customized database for sample management, automated liquid handling, HPLC-based tracking of bioactivity *via* microfractionation for off-line bioassay, and on-line (DAD, ESI- and APCI-MS) and off-line (microprobe NMR) spectroscopy for structure elucidation. This platform was used to guide the research on HPLC-based activity profiling of $GABA_A$ receptor modulatory and immunosuppressant activities from plant origin.

The first topic of the thesis was aimed at the application of three different validated bioassays for the discovery of new scaffolds targeting the $GABA_A$ receptor modulators. The samples were selected based on the activity of the extract in a functional two-microelectrode voltage clamp assay with *Xenopus* oocyte and zebrafish larvae locomotor-activity assay [3,4]. The *Xenopus* oocyte format is the gold standard for investigating GABA-chloride ion channels, and zebrafish larvae is used to observe the seizure-like behaviour triggered by the $GABA_A$ receptor antagonist pentylenetetrazol (PTZ). In the zebrafish assay, if the extract significantly decreased larval locomotion provoked by the $GABA_A$ receptor antagonist, then it was submitted to HPLC-based activity profiling for localization and characterization of targeted compounds.

The next methodological approach for the discovery of GABA active compounds was FLIPR format (Fluorescence Imaging Plate Reader) [5,6]. This method can screen samples on a semi-high throughput scale compared to previous assays. The assay was developed using the active-plants extracts in *Xenopus laevis* oocytes transiently expressing $GABA_A$ receptors of $\alpha_1\beta_2\gamma_{2s}$ subunit composition. FLIPR assay employs fluorescence-based dyes for observation of real-time membrane potential changes associated with ion channel activation [6,7,8]. A membrane potential-sensitive dye detects changes in voltage across the cell membrane. Binding to the receptor leads to hyperpolarization and an increase in fluorescence readout. The validated FLIPR assay for $GABA_A$ receptor modulators was applied to screen the EtOAc extract library of our group. Extracts with the threshold of more than 35% activation were further tested for their concentration response. The concentration-response curve will inform the potential of extract in concentration dependent-manner. The hit extracts were submitted to HPLC-based activity profiling and chosen to be the priority for further investigation to identify the active

compounds. The most active compounds will be assessed for the identification of allosteric binding sites.

The last project was the application of T lymphocyte proliferation assay in the investigation of immunosuppressive drugs from natural products [9,10]. The screening samples were from traditional Chinese medicinal plants available in our extract library. The bioassay was carried out by inhibiting human T lymphocyte proliferation. Then, immunosuppressive activity and toxicity of extracts were assessed by FACS Calibur analysis. The extracts which displayed immunosuppressive activity without concomitant toxicity were applied to HPLC-based activity profiling to localize the compounds responsible for the activity of the extract.

References

[1] Potterat, O., and Hamburger, M. Concept and technologies for tracking bioactive compounds in natural product extract: generation of libraries, and hyphenation of analytical processes with bioassays. *Nat. Prod. Rep*. 2013. 30, 546-564.

[2] Potterat, O., and Hamburger, Combined use of extract libraries and HPLC-based activity profiling for lead discovery: potential, challenges, and practical considerations. *Planta Med*. 2014. 80, 1171-1181.

[3] Zaugg, J., Baburin, I., Strommer, B., Kim, H-J., Hering, S., and Hamburger, M. HPLC-based activity profiling: discovery of piperine as a positive $GABA_A$ receptor modulator targeting a benzodiazepine-independent binding site. *J. Nat. Prod*. 2010. 73, 185-191.

[4] Moradi-Afrapoli, F., Ebrahimi, S., N., Smiesko, M., and Hamburger, M. HPLC-based activity profiling for $GABA_A$ receptor modulators in extracts: validation of an approach utilizing a larval zebrafish locomotor assay. *J. Nat. Prod*. 2017. 80, 1548-1557.

[5] Faleschini, M. T., Maier, A., Fankhauser, S., Thasis, K., Hebeisen, S., Hamburger, M., and Butterweck, V. A FLIPR assay for discovery of $GABA_A$ receptor modulators of natural origin. *Planta Med*. 2019. 85; 925-933.

[6] Joesch, C., Guevarra, E., Parel. S. P. Bergner, A., Zbinden, P., Konrad, D., and Albercht, H. Use of FLIPR membrane potential dyes for validation of high-throughput screening with FLIPR and μARCS technologies: identification of ion channel modulators acting on the $GABA_A$ receptor. *J. Biomol Screen*. 2008. 13, 218-228.

[7] Baxter, D. F., Kirk, M., Garcia, A. F., Raimondi, A., Holmqvist, M. H., Flint, K. K., Bojavic, D., Distefano, P. S., Curtis, R., and Xie, Y. A novel membrane potential-sensitive fluorescent dye improves cell-based assay for ion channels. *J. Biomol. Screen*. 2002. 7, 79-85.

[8] Arkarin, M. R., Connor, P. R., Emkey, R., Garbison, K. E., Heinz, B. A., Wiernicki, T. R., Johnston, P. A., Kandasamy, R. A., Rankl, N. B., and Sittampalam, S. FLIPR™ assay for PCR and ion channel targets. Assay Guidance Manual. 2012. 1-33.

[9] Reinhardt, J., K., Klemd, A., M., Danton, O., Mieri, M., D., Smiesko, M., Huber, R., Burgi, T., Grundemann, C., and Hamburger, M. Sesquiterpene lactones from *Artemisia argyi*: absolute configuration and immunosuppressant activity. *J. Nat. Prod*. 2019. 82, 1424-1433.

[10] Zimmermann-Klemd, A. M., Reinhardt, J. K., Morath, A., Schamel, W. W., Steinberger, P., Leitner, J., Huber, R., Hamburger, M., and Gründemann, C. Immunosuppressive activity of *Artemisia argyi* extract and isolated compounds. *Front. Pharmacol*. 2020. 11; 1-13.

2. INTRODUCTION

2.1. Natural Products in Drug Discovery

In ancient times humans learned from nature how to survive. Nature remained as an only source for providing all human needs ranging from foods, cosmetics to medicines. Plants, in particular, have formed the basis of sophisticated traditional medicine [1]. Written documentation of approximately 1000 plant-derived substances used in Mesopotamia and 700 drugs were documented in the Ebers Papyrus dating from 1500 BC in Egypt. Ancient cultures such as Egyptian, Chinese, and Indian are well known for using medicinal plants in the time before Christ. After that, the Greeks and the Romans contributed substantially to the rational development of herbal medicine in the western world, such as Dioscorides (AD 100), Galen (AD 130-200) [1]. Over the centuries, many scholars had added considerable knowledge about medicinal plants, as like Paracelsus (1493-1541), who had influential contributions in medical and pharmaceutical intervention and concepts at the time. In 1804, Friedrich Serturner reported the first isolation of morphine from opium (*Papaver somniferum*). Up to date, many approaches have been taken by many scientists to find compounds that can be used as medicine [2,3].

2.1.1. Drug-like compounds from nature

Natural products as sources of drugs

Nature remains a successful source of inspiration for drugs. Approximately, 6% of all plants have been studied for their biological activities and about 15% for their phytochemistry [3]. Medicinal plants in the defined mixture were classified as botanical drugs approved by the FDA for decades [4]. World Health Organization (WHO) estimated that approximately 80% of global people rely on traditional medicines for their primary health care; around 20% population in developed countries use plant products in their health care system [1].

Over the past four decades, the approved drugs (~37%) were derived and inspired by natural products [4]. It has been shown that the majority of the available antibacterial and anticancer drugs in the market are from natural products. Most of the antibacterials have been discovered from natural products obtained from microbial resources [5]. For example, these antibacterials are β-lactam antibiotic, penicillin, from *Penicillium* fungi (1938) and macrolides antibiotic, fidaxomicin, from the fermentation of *Dactylosporangium aurantiacum* subsp. *hamdenensis* (NRRL 18085) (2011) [1,5]. Paclitaxel, as a remarkable antitumor, was reported in 1971 from the bark of *Taxus brevifolia* [6]. It has a unique mechanism of action in promoting

tubulin polymerization and stabilization of microtubules against depolymerization (microtubule assembly) [7]. Marine natural products significantly have contributed to marine drug development. Most of the marine natural products have cytostatic and cytotoxic activity because of their role as a chemical defense. Moreover, Cephalosporin C obtained from *Acremonium chrysogenum* has contributed to a new class of antibiotics from marine natural products [8].

Some common marketed drugs were obtained from plant origin. Cinchona tree was accidentally found to treat fever in 1630. It was used as a standard treatment for malaria for thousands of years. In 1820, quinine was isolated from the bark of the Cinchona tree by Pierre Joseph Pelletier and Joseph Caventou. From Chinese traditional medicine, *Artemisia annua,* artemisinin isolated and approved as an anti-malarial agent in 1971 [1]. Salicin was first isolated from the bark of willow trees by German pharmacist Johan Andreas Buchner in 1828 and known for the treatment of rheumatic diseases [10]. In 1839, salicin was synthesized into salicylic acid as an active drug-form of the drug.

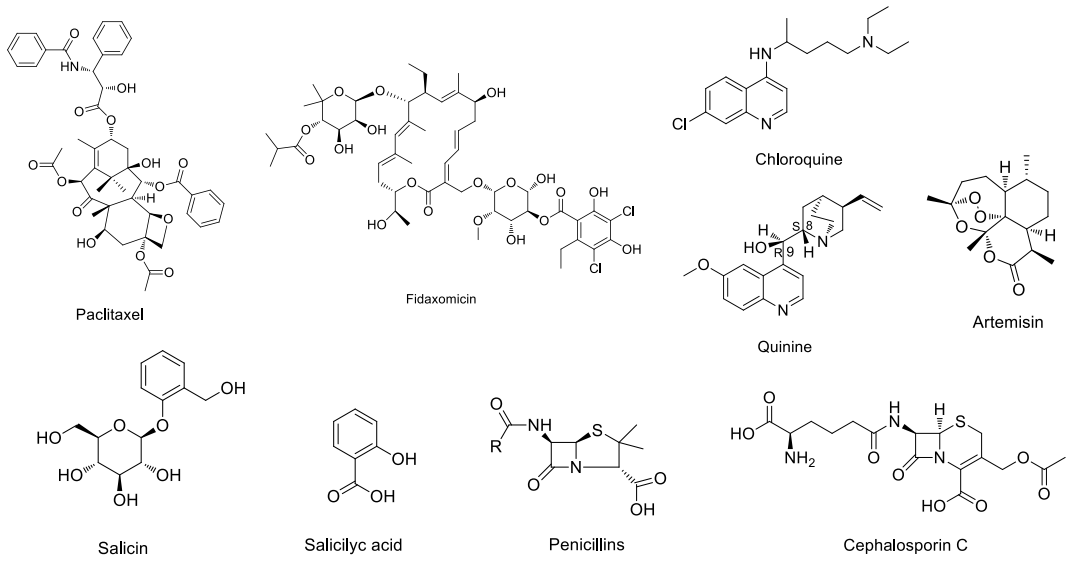

Figure 2.1.1. Structures of representative natural product-derived drugs.

Challenges of natural product-based drug discovery

In the past 30 years, reports on new natural product-derived medicines going into the clinical trial were declined, due to many factors [11]. In the 1980s and 90s, the pharma

companies changed the process of drug discovery to automated assays enabling high throughput screening (HTS) up to millions of vast library of compounds within a few weeks. The compounds library was prepared with combinatorial chemistry, a new synthetic strategy, instead of isolated from nature. The traditional approach of extracts from plants and microorganisms was not an option in HTS because it requires tedious and resource-intensive purification to identify the active compounds from the complex mixture extract, which often yielded only in a tiny amount. The number of reported natural compounds is also considered to be a challenge that added a barrier to the natural product-based drug discovery because the number of newly isolated compounds does not match with the required-amount of compounds for high throughput screening. In some cases, an assay for biological activity using natural product extracts ended up in the identification of known rather than novel compounds and sometimes with the synergistic and simultaneous action of several substances [12]. HTS assays of natural product extracts face many challenges, especially on the convention of biological diversity such as the Rio Convention and the Nagoya Protocol.

Innovative HTS approach with combinatorial chemistry technique has provided only three approved drugs [4]. The first one is an antitumor compound known as sofanib for treating renal cell carcinoma (Nexavar) from Bayer, which the FDA approved in 2005. The second one is ataluren (Translarna), which was approved by the EU in 2014. And the last one is vemurafenib, which received approval from the FDA in 2011. Compared to those amounts of substances used for HTS and NPs, it seems that the quantity cannot guarantee the success rate in drug discovery [13]. Hit rates of HTS are determined by three quality factors, such as chemical diversity, lead-likeness, and biological relevance.

Even though pharmaceutical industries had abandoned natural products, there is an irreplaceable natural hint. NPs are sterically rich and provide a diversity of chemical structures unmatched by any synthetic chemical compounds or combinatorial chemistry approach [13]. NPs are purposefully made through natural selection and can recognize their cognate biologically relevant receptors or targets [11]. Analysis of the Dictionary of Natural Products (DNP) revealed that around 60% of the reported compounds are drug-like NPs, based on Lipinski's rule of five and only about 10% performed two or more violations of them. The ability of NPs to interact with specific proteins for their mechanism of actions inspire drug discovery and development [13].

Tracking bioactive natural products

Current challenges in NPs research led to an innovative and multidisciplinary approach with advanced technologies. With the HTS approach, activity screening needs to have a vast material library. Data library can be generated from diversity in nature or synthesis. To apply all technologies and knowledge with NP research, some steps to trace the active compounds can be used. The general procedure to discover drug-lead from NPs includes; a) extracts screening, b) dereplication of targeted compounds, c) bioassay-guided purification and isolation, d) structure elucidation of targeted compounds [13,14,15]. The following is a brief description of each step:

a) Extracts screening

There are some suitable forms of NP samples for screening: crude extracts, pre-fractionated libraries, semi-purified, pre-fractionated libraries of semi-purified extracts, and pure NPs. Screening the whole extracts and degree of pre-purification extracts lead to some biases of bioassay screenings and the effort to purify targeted substances. Since the most biologically active substances could be major or minor components, pre-fractionated libraries can do profiling of the whole extract into different fractions to avoid the loss of minor components [13,15].

The success of extract screening must be established and validated by the targeted assays. Ideally, an HTS assay should be relatively simple, straightforward, cost-effective, comprises a minimum number of steps, capable of automation, robust, and highly reproducible with a simple readout. The assay should be able to perform in a low volume, thus requiring small amounts of materials and reagents. Importantly, the assay should reflect the biological situation to be assessed [13].

b) Dereplication of targeted compounds

Dereplication can be defined as the identification of known NPs from extracts identified as active in a bioassay through spectral fingerprint data combined with library searching [15]. Dereplication usually requires an analytical step where extracts or fractions are subjected to

chromatographic separation, which can be coupled to multiple detectors such as UV-Vis, mass spectrometry, light scattering, as well as capillary-flow NMR. The analytical data collected can then be used for in-house library matching as well as for comparison to the database of known natural products such as the DNP, AntiBase, or MarinLit. Some ubiquitous interfering compounds can be found during dereplication, such as tannins, fatty acids, saponins, or known compounds that either from the literature or in-house knowledge are known to interact with the target of interest [13]. Dereplication can be used to prioritize the extracts and fractions for chemical isolation based on the identification of multiple extract or fractions that contain the same active component or profile.

c) Bioassay-guided purification and isolation

In the current fast-paced world, the success story of the traditional approach in drug discovery that requires several bioactivity-guided fraction iterative steps seems to be an old-fashioned method [14]. This method needs to be accelerated since it is not compatible with the timelines of modern drug research. With the advanced technology of chromatography and spectroscopy over the last two decades, more efficient alternative approaches have been developed to track bioactivity in complex samples. This approach can obtain reliable data of analysis, purification, and elucidation of the structures of NPs in line with HPLC-based approaches bioactive structural information.

The HPLC-based method here refers to HPLC-based activity profiling [14]. HPLC-based activity profiling has been developed as a highly versatile strategy to accelerate the deconvolution of active extracts. The procedure begins with the fractionation of the bioactive extract by analytical or semipreparative HPLC. Recording UV and MS data are on-line with collecting the fraction into microplates, *via* a T-split of the column effluent. Fractions are dried, re-dissolved in a small amount of a suitable solvent, generally DMSO, and transferred to a bioassay. Bioassay results of each fraction overlay with the on-line UV-Vis chromatogram to match and identify the active peaks (**Figure 2.1.2**). The UV and MS data recorded on-line can be used for early dereplication and estimation of bioactive compounds. The activity profiling of extract and assessment of dereplication can be used for guiding off-line preparative isolation and identification of active peaks.

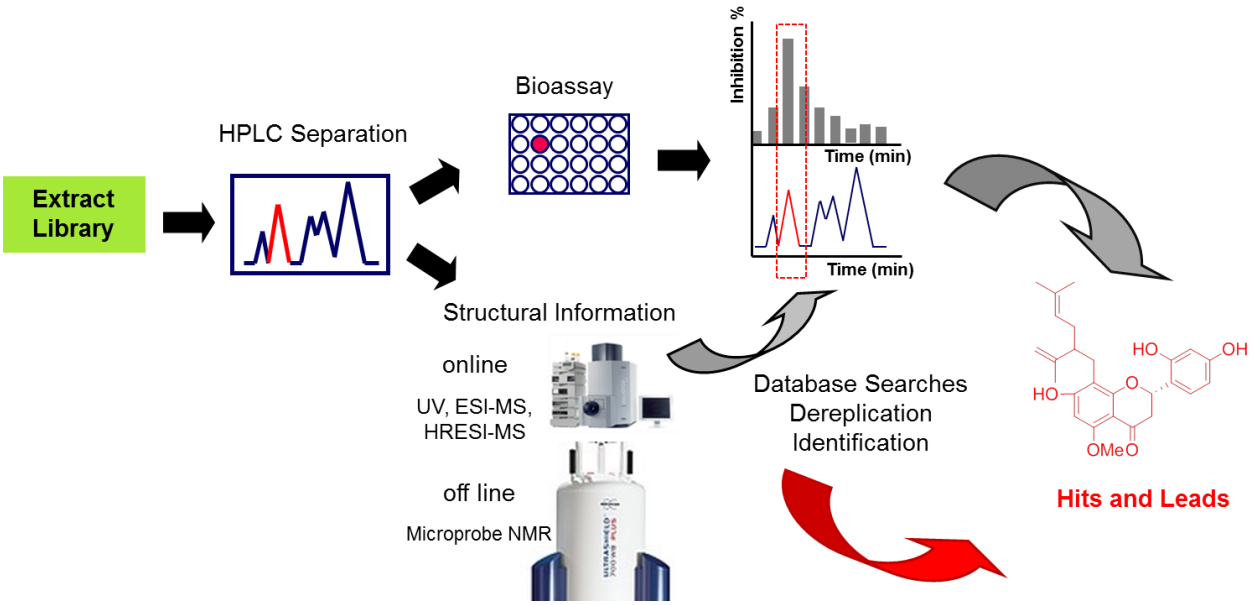

Figure 2.1.2. Experimental platform for HPLC-based activity profiling of bioactive extracts (adopted from Potterat and Hamburger [14])

HPLC-based activity profiling is a powerful strategy to track bioactive substances in complex samples [14]. A miniaturized format assay can run milligram amounts of extracts and microgram amount of pure compounds. This format can be implemented in any laboratory with supporting appropriate HPLC instruments coupled with appropriate detectors (at least UV, MS) and also bioassays. This approach has been successfully applied to localize bioactive substances using different bioassays such as whole-organism assays (tropical parasitic diseases), cell-based antiviral (HIV), and functional assays (e.g., $GABA_A$ receptor modulation, hERG channel inhibition), mechanistic screens (i.e., DYRK1A kinase), and cell-based assay (human T lymphocyte for immunosuppressant) [14,16].

d) Structure elucidation of targeted compounds

The purity of NPs can be characterized by the following criteria [17]:

1. Physical criteria (melting point, boiling point, optical rotation, refractive index)
2. Analytical criteria (elemental composition determined by high-resolution mass spectrometry)
3. Chromatographic criteria (single spot on thin-layer chromatography, single peak on GC, HPLC determined in several systems)

4. Spectroscopic criteria (consistent relative integrals in the ^{1}H NMR spectrum and consistent absorption in the infrared and the UV spectrum).

One of the common issues in NP research is, usually, unknown compounds obtained in a small amount. However, the full characterization of small quantity compounds can be performed by the cutting-edge technology of spectroscopy techniques.

HPLC-based activity profiling provides knowledge about tentative bioactive substances at the early stage of NP research. A variety of HPLC-detectors can detect NPs. Specific patterns of UV absorptions possess characteristics of NP substances, and the absorption occurs in the range of 200 – 550 nm [18]. Among all the HPLC detectors, UV is the most common and widely used, even though it has a particular limitation with compounds that do not possess UV chromophores. However, compounds with a weak chromophore (in the case of most triterpene glycoside) can be detected by UV at short wavelengths (λ_{max} 230 nm). In this case, the UV cut-off of selected solvents should be taken into consideration. Evaporative light scattering detection (ELSD) can be an alternative solution for compounds without or no chromophores. ELSD detector requires the solute components less volatile than the mobile phase. A light beam is directed onto the particles causing scattering of the incident light detected by a photodiode or photomultiplier. ELSD gives a result for equal amounts of the mass present, i.e., a higher peak represents a mass with a higher quantity present.

MS detector in HPLC provides important structural information such as molecular weight, molecular formulas, and diagnostic fragments. This information is crucial for the dereplication and characterization of NPs during the extract screening process [18]. The most common MS-interfaces are electrospray ionization (ESI) and atmospheric pressure chemical ionization (APCI). These ion sources are used for polar, labile, and non-polar, thermally-stable substances, respectively. Some mass spectrometers type can be used, such as single quadrupole (Q), ion trap, time-of-flight (TOF), and triple-quadrupole (QQQ). TOF is the most widely-used mass analyzer for providing information about the accurate mass, the molecular formula, and the very precise ion trace extraction for specific detection.

Sensitivity and the advent of multidimensional NMR spectroscopy have truly revolutionized organic structure determination. With 1D (^{1}H NMR and ^{13}C NMR spectra) and 2D (^{1}H-^{1}H COSY, ^{1}H-^{13}C correlation on HSQC and HMBC), NMR experiments are the routine NMR spectroscopy for small molecules structure elucidation [19]. NOESY and ROESY spectra

can be used to determine relative configurations of small molecules. The assignment of the known compounds can be confirmed through comparing proton spectra with literature NMR data and additional mass analysis. However, unknown compounds require at least full 1D and 2D NMR experiments.

For chiral compounds, some available methods have been used to solve absolute configurations of NPs, such as X-ray crystallography, chemical synthesis, NMR spectroscopy/chiral derivatization, analytical chemistry, and chiroptical approaches. X-ray crystallography is the most robust method in the absolute configuration, but NPs do not always fit with the crystal forms [20]. Electronic circular dichroism (ECD) is one of the powerful chiroptical tools for the absolute configuration assignment of natural products with various chromophores since the 1960s. ECD experiment is a very sensitive and non-destructive technique. Circular dichroism (CD) is the phenomenon of a chiral molecule that absorbs left and right circularly polarized light beams to a different extent. The assignment is based on the closer they match between experimental and calculated ECD spectra.

2.1.2. GABAergic natural products

Traditional medicine as a source of information for CNS drug discovery

Traditional medicines have a success story in CNS drugs. For example, LSD (lysergic acid diethylamide) from ergotamine and psilocin from "magic mushrooms" that is used as a psychedelic drug. Other famous drugs are cannabidiol, a psychoactive drug, from *Cannabis sativa*, cocaine, a CNS stimulant, from *Erythroxylon coca*, and ephedrine, also a CNS stimulant, from herb *Ephedra* [21]. Since 1940 and onward, most NP/NP-inspired drugs are being used as CNS therapeutics, which represent 25% of 1171 approved new molecular entities. Bharate, Mignani, and Vishwakarma pointed out that NPs are specific as CNS active drugs due to their drug-like and lead-like psychochemical properties, blood-brain barrier (BBB) transport, and isoform selectivity. Also, because of their place in the evolutionary scale of things and the prevailing hypothesis on their special role in species-species interaction and mutually assisted survival. In our group, we performed the screening of plant extract library in an *in vitro* functional, automated two-microelectrode voltage clamp assay with *Xenopus laevis* oocytes, which transiently expressed $\alpha_1\beta_2\gamma_{2S}$ $GABA_A$ receptors. The results showed lipophilic extracts

from *Piper nigrum* fruits, *Angelica pubescens* roots, *Acorus calamus* roots, *Biota orientalis* leaves and twigs, *Kadsura longipendunculata* fruits, *Bupleurum chinense* roots, *Pholidota chinensis* stems and roots, *Adenocarpus cincinnatus* roots and tubers, and *Boswellia thurifera* resin possessed positive $GABA_A$ receptor modulating activities [22,23]. From those plants, we isolated responsible active compounds such as piperine (alkaloid) [24], columbianetin acetate, imperatorin, cnidilin, osthol, columbianedin [25], β-asarone, (+)-dioxosarcoguaiacol, (+)-shyobunone, (+)-preisocalamenediol [26], isopimaric acid, sandaracopimiric acid [27], lignan and sesquiterpene compounds [28], aristolactone [29], dihydrostilbenes [30], isoflavone, pterocarpans [31], and dehydroabietic acid (terpenoid) [32], respectively.

GABAergic drugs

GABAergic drugs have been used in clinical practice and approved by many regulatory agencies in the world. Some well-known GABAergic drugs are baclofen, barbiturates, and benzodiazepines. Baclofen is an agonist $GABA_B$ receptor drug used as a muscle relaxant and an antispasmodic agent. Currently, it is studied for the treatment of alcohol dependence and drug addictions [33]. The first barbiturate was synthesized in 1864 by Adolf von Baeyer. Barbiturates were clinically the only drugs for sedatives and hypnotic between the 1920s and the mid-1950s. The dependence and death by overdose of barbiturates made benzodiazepines possible as a psychopharmacological revolution [34]. Chlordiazepoxide (Librium) was the first identified benzodiazepine by Hoffmann-La Roche chemist Leo Sternbach in 1955. Five years later, it was already in the market. Then diazepam (Valium) followed in 1963. The safety concern made benzodiazepine started to be the top prescribed drug in the mid-to-late 1970s [35]. Understanding the mechanism of action of benzodiazepines in the GABA site gives an insight into the additive property and abuse ability of benzodiazepines [36]. After that, multiple other analogues of the benzodiazepine class have been released, such as flurazepam, alprazolam, zolpidem, and lorazepam. The binding site of benzodiazepines is the allosteric modulators of the $GABA_A$ receptor, while the competitive antagonist at the $GABA_A$ receptor is bicuculline. Flumazenil is used clinically to reverse the effects of benzodiazepine agonists [33].

In 2019, a neurosteroid (allopregnanolone) was approved by the FDA as an antidepressant drug as a treatment for women with postpartum depression [37]. Endogenous

steroid, allopregnanolone (brexanolone), is a potent, effective, and broad-spectrum positive allosteric modulator (PAM) of $GABA_A$ receptors. Currently, the $\beta_3(+)/\alpha_1(-)$ intersubunit site is known as a specific allopregnanolone binding site that modulate GABA-allosteric neurosteroid action [38].

2.1.3. Natural products with immunosuppressant properties

Traditional medicine as a source of information for immune suppression

Traditional medicine is a valuable subject to explore different activities through a variety of biological approaches, including immunosuppressant agents. So far, most of the immunosuppressive compounds in nature were reported originally from fungus, bacterium, and marine natural products, while plants are still less reported. Immunosuppressant agents from natural products are like cyclosporine A and rapamycin was obtained from fungus and soil bacterium [39]. The immunosuppressant agents have some issues; one of them is about the difficulties in how to differentiate the activity from associate toxicity of compounds. However, ethnomedical information can lead to valuable drug discovery with a unique mechanism of action and the possibility of low human toxicity. This approach we applied in our group to screen 435 plant extracts from traditional Chinese medicine. The screening assay can differentiate activity on T lymphocyte proliferation and cytotoxicity even at the early stage [16,40]. Some extracts showed immunosuppressive activity such as *Artemisia argyi, Scutellaria baicalensis, and Toddalia asiatica.* From *A. argyi*, sesquiterpene lactones exhibited immunosuppressant activity based on a specific modification of T cell signaling in a non-cytotoxic manner.

Currently available immunosuppressant agents

Small molecules and biologics drugs have been developed and used in clinical practice for immunosuppression. Perry and Neuberger grouped immunosuppressant classes into the following [41]:

1. General immunosuppressants (corticosteroids)
2. Calcineurin inhibitors (cyclosporine and tacrolimus)
3. Anti-metabolites (6-mercaptopurine, mycophenolate mofetil, azathioprine)

4. Inhibitor of TOR (sirolimus and everolimus)
5. Antibodies (OKT3, IL-2R antibodies, Campath 1H)
6. Novel agents (FTY720, leflunomide, FK778, FK779).

Prescribing immunosuppressant agents need to be evaluated and monitored. Effective drug administration is associated with the least toxicity and balanced against the side effect of the drugs. For instance, immunosuppression can increase the risk of sepsis and malignancy, and calcineurin inhibitor has been associated with renal failure or diabetes. All of the side effects of immunosuppressant agents consequently led to supervision and drug monitor for patients taking these drugs [42]. Over the last decade, Remestemcel-l was approved by the FDA as a drug for immunosuppressants [4]. With the cutting-edge of biomedical research, allogeneic stem cell transplantation will be an optional treatment for patients with the side effect of immunosuppression, such as relapsed or high-risk haematological malignancy [43]. Combinatorial drug therapy for immunosuppressant diseases could favour the patients to pan out of the toxicity, side effects, and increase the efficacy of the drug in the future.

References

1. Wermuth, C. G., Aldous, D., Raboisson, P., and Rognan, D. (Editor). The Practice of Medicinal Chemistry, 4th Ed. Newman, D. J., Cragg, G. M., and Kingston, D. G. I. Chapter 5, Natural products as pharmaceuticals and sources for lead structures. Elsevier. 2015. p.121-122. ISBN: 978-0-12-417205-0.
2. Potterat, O., and Hamburger, M. Concept and technologies for tracking bioactive compounds in natural product extract: generation of libraries, and hyphenation of analytical processes with bioassays. *Nat. Prod. Rep*. 2013. 30, 546-564.
3. Verpoorte, R. Pharmacognosy in the New Millennium: Lead finding and Biotechnology. *J. Pharm. Pharmacol*. 2000. 52, 253-262.
4. Newman, D. J., and Cragg, G., M. Natural products as sources of new drugs over the nearly four decades from 01/1981 to 09/2019. *J. Nat. Prod*. 2020. 83, 770-803.
5. O'Connell, K. M. G., Hodgkinson, J. T., Sore, H. F, Welch, M., Salmond, G. P. C., and Spring, D. R. Combating multidrug-resistant bacteria: current strategies for the discovery of novel antibacterials. *Angew. Chem. Int. Ed*. 2013. 52, 10706-10733.
6. Wani, M. C., Taylor, H. L., Wall, M. E., Coggon, P., and McPhail, A. T. Plant antitumor agents. VI. The isolation and structure of taxol, a novel antileukemic and antitumor agent from *Taxus brevifolia*. *J. Am. Chem. Soc*. 1971. 93, 2325-2327.
7. Manfredi, J. J., and Horwitz, S. B. Taxol: An antimitotic agent with a new mechanism of action. *Pharmac. Ther*. 1984. 25, 83-125.
8. Lindequist, U. Marine-derived pharmaceuticals – challenges and opportunities. *Biomol Ther*. 2016. 24, 561-571.
9. Achan, J., Talisuna, A. O., Erhart, A., Yeka, A., Tibenderana, J. K., Baliraine, F.N., Rosenthal P. J., and D'Alessandro, U. Quinine, an old anti-malarial drug in a modern world: role in the treatment of malaria. *Malar. J*. 2011. 10, 1-12.
10. Schrör, K. Acetylsalisilic acid, 2nd Ed. Wiley-VCH. Weinhem, German. 2016. p.5-9.

11. Wright, W. D. Unlocking the potential of natural products in drug discovery. *Microbi Biotechnol*. 2019. 12, 55-57.
12. Thomford, N. E., Senthebane, D. A., Rowe, A., Munro, D., Seele, P., Maroyi, A., and Dzobo, K. Natural products for drug discovery in the 21st century: innovations for novel drug discovery. *Int. J. Mol. Sci*. 2018. 19, 1-29.
13. Avery, V. M., Camp, D., Carroll, A. R., Jenkins, I. D., and Quinn, R. J. 3.07 The Identification of bioactive natural products by high throughput screening (HTS). In: Liu H-W (Ben), Mander L, editors. *Compr. Nat. Prod.* II. Oxford: Elsevier. 2010. p.177-203.
14. Potterat, O., and Hamburger, M. Combined use of extract library and HPLC-based activity profiling for lead discovery: potential, challenge, and practical considerations. *Planta Med*. 2014. 80, 1171-1181.
15. Wilson, B. A. P., Thornburg, C. C., Hendrich, C. J., Grkovic, T., and O'keefe, B. R. Creating and screening natural product libraries. *Nat. Prod. Rep*. 2020. doi: 10.1039/c9np00068b
16. Reinhardt, J. K., Klemd, A. M., Danton, O., Mieri, M. D., Smiesko, M., Huber, R., Bürgi, T., Gründemann, C., and Hamburger, M. Sesquiterpene lactones from *Artemisia argyi:* absolute configuration and immunosuppressant activity. *J. Nat. Prod*. 2019. 82, 1424-1433.
17. Hanson, J. R. Natural products: the secondary metabolites. Royal Society of Chemistry. UK. 2003. p.35-36.
18. Wolfender, J-L. HPLC in natural product analysis: the detection issue. *Planta Med*. 2009. 75, 719-734.
19. Edison, A. S., and Schroeder, F. C. 9.06 NMR-small molecules and analysis of complex mixtures. In: Liu H-W (Ben), Mander L, editors. *Compr. Nat. Prod*. II. Oxford: Elsevier. 2010. p.169-196.
20. Li, X-C., Ferreira, D., and Ding, Y. Determination of absolute configuration of natural products: theoretical calculation of electronic circular dichroism as a tool. *Curr. Org. Chem*. 2010. 14, 1678-1697.
21. Bharate, S. S., Mignani, A., and Vishwakarma, R. A. Why are the majority of active compounds in the CNS domain natural products? A critical analysis. *J. Med. Chem*. 2018. 61, 10345-10374.
22. Zaugg, J. M. Discovery of new scaffolds for $GABA_A$ receptor modulators from natural origin. Universitat Basel, Basel; 2011.
23. Rueda, D. C. Ethnomedicine-based discovery and characterization of plant-derived $GABA_A$ receptor modulators with new scaffolds. Universitat Basel, Basel; 2014.
24. Zaugg, J., Barburin, I., Strommer, B., Kim, H-J., Hering, S., and Hamburger, M. HPLC-based activity profiling: discovery of piperine as a positive $GABA_A$ receptor modulator targeting a benzodiazepine-independent binding site. *J. Nat. Prod*. 2010. 73, 185-191.
25. Zaugg, J., Eickmeier, E., Rueda, D. C., Hering, S., and Hamburger, M. HPLC-based activity profiling of *Angelica pubescens* roots for new positive $GABA_A$ receptor modulators in *Xenopus* oocytes. *Fitoterapia*. 2011. 82, 434-440.
26. Zaugg, J., Eickmeier, E., Ebrahimi, S. N., Baburin, I., Hering, S., and Hamburger, M. Positive $GABA_A$ receptor modulators from *Acorus calamus* by 1D and 2D NMR and molecular modeling. *J. Nat. Prod*. 2011. 74, 1437-1443.
27. Zaugg, J., Khom, S., Eigenmann, D., Baburin, I., Hering, S., and Hamburger, M. Identification and characterization of $GABA_A$ receptor modulatory diterpenes from *Biota orientalis* that decrease locomotor activity in mice. *J. Nat. Prod*. 2011. 74, 1764-1772.
28. Zaugg, J., Ebrahimi, S. N., Smiesko, M., Baburin, I., Hering, S., and Hamburger, M. Identification of $GABA_A$ receptor modulators in *Kadsura longipendunculata* and assignment of absolute configurations by quantum-chemical ECD calculations. *Phytochemistry*. 2011. 72, 2385-2395.
29. Rueda, D. C., Zaugg, J., Quitschau, M., Reich, E., Hering, S., and Hamburger, M. Discovery of $GABA_A$ receptor modulator aristolactone in a commercial sample of the Chinese herbal drug "chaihu" (*Bupleurum chinense* roots) unravels adulteration by nephrotoxic *Aristolochia manshuriensis* roots. *Planta Med*. 2012. 78, 207-210.
30. Rueda, D. C., Schoffmann, A., Mieri, M. D., Raith, M., Jahne, E. A., Hering, S., and Hamburger, M. Identification of dihydrostilbenes in *Pholidota chinensis* as a new scaffold for $GABA_A$ receptor modulators. *Bioorg. Med. Chem*. 2014. 22, 1276-1284.

31. Rueda, D. C., Mieri, M. D., Hering, S., and Hamburger, M. HPLC-based activity profiling for $GABA_A$ receptor modulators in *Adenocarpus cincinnatus*. *J. Nat. Prod*. 2014. 77, 640-649.
32. Rueda, D. C., Raith, M., Mieri, M. D., Schoffmann, A., Hering, S., and Hamburger, M. Identification of dehydroabietic acid from *Boswellia thurifera* resin as a positive $GABA_A$ receptor modulator. *Fitoterapia*. 2014. 99, 28-34.
33. Enna, S. J, and Mohler, H. The GABA Receptors, 3rd Ed. Humana Press. Totowa, New Jersey. 2007. p.9,310.
34. Lopez-Munoz, F., Ucha-Udabe, R., and Alamo, C. The history of barbiturates a century after their clinical introduction. *Neuropsych Dis Treat*. 2005. 1, 329-343.
35. Wick, J. Y. The history of benzodiazepines. *Consult Pharm*. 2013. 28, 538-548.
36. Rudolph, U., and Knoflach, F. Beyond classical benzodiazepines: Novel therapeutic potential of $GABA_A$ receptor subtypes. *Nat. Rev. Drug. Discov*. 2012. 10, 685-697.
37. Zorumski, C. F., Paul, S. M., Covey, D. F., and Mennerick, S. Neurosteroids as novel antidepressants and anxiolytics: GABA-A receptors and beyond. *Neurobiol. Stress*. 2019. 11, 1-10.
38. Sugasawa, Y., Cheng, W. W. L., Bracamontes, J. R., Chen, Z-W., Wang, L., Germann, A. L., Pierce, S. R., Senneff, T. C., Krishnan, K., Reichert, D. E., Covey, D. F., Akk, G., Evers, A. S. Site-specific effects of neurosteroids on GABAA receptor activation and desensitization. *eLife*. 2020. 9, e55331.
39. Mann, J. Natural products as immunosuppressive agents. *Nat. Prod. Rep*. 2001. 18, 417-430.
40. Zimmermann-Klemd, A. M., Reinhardt, J. K., Morath, A., Schamel, W. W., Steinberger, P., Leitner, J., Huber, R., Hamburger, M., and Gründemann, C. Immunosuppressive activity of *Artemisia argyi* extract and isolated compounds. *Front. Pharmacol*. 2020. 11, 1-13.
41. Perry, I., and Neuberger, J. Immunosuppression: towards a logical approach in liver transplantation. *Clin. Exp. Immunol*. 2005. 139, 2-10.
42. Trevillian, P. Immunosuppressants – clinical applications. *Aust Prescr*. 2006. 29, 102-107.
43. Daly, A. Remestemcel-l, the first cellular therapy product for the treatment of graft-versus-host disease. *Drug Today*. 2012. 48, 773-783.

2.2. The $GABA_A$ Receptor

Gamma-aminobutyric acid (GABA), the main inhibitory neurotransmitter of the brain, was identified in 1950 [1]. However, its potency as a central nervous system (CNS) depressant was recognized in the latter years. Glutamate and GABA are major excitatory and inhibitory amino acids neurotransmitters in the CNS [2]. They follow the other slower-acting transmitters, modulators, and ion channels to keep the neuronal balance activity in CNS. GABA receptors have been identified and distinguished pharmacologically and molecularly into $GABA_A$ and $GABA_B$ [3]. $GABA_A$ receptors are pentameric ligand-gated chloride-ion channels, whereas $GABA_B$ receptors are heterodimeric G protein-coupled sites. They exert the effect through increased postsynaptic membrane permeability to modulate chloride ion channels [3,4]. Impairment of GABAergic synaptic transmission associated with psychiatric disorders (schizophrenia, mood disorder, major depression, autism), impaired learning, and sleep abnormalities [5,6].

$GABA_A$ receptors belong to the superfamily of Cys-loop ligand-gated ion channels (LGICs). Its pentameric protein assembled from five protein subunits wall around the central chloride channel, each of them consists of a hydrophilic extracellular N-terminal domain, four transmembrane sequences (TM1-TM4 or M1-M4), and a short extracellular C-terminal domain (**Figure 2.2.1 A**) [7,8]. The hydrophilic extracellular N-terminal domain is in charge of the transmitter and ligand binding and coupling of the binding sites with an ion channel. Extracellular N-terminal is a key for allosteric effects and assembly of various receptor subunits into functional receptors. Four transmembrane regions are responsible binding of hydrophobic ligands, ion selectivity, and channel binding sites. The intracellular loop between transmembrane helices M3 and M4 involves regulatory phosphorylation sites and for anchoring intracellular factors the receptors in appropriate locations (i.e. on the postsynaptic thickening) using interactions with auxiliary and cell structural proteins [2,8]. The cell membrane of pentameric $GABA_A$ receptors consists of two α, two β, and one γ subunit and the interfaces between adjacent subunits are forming ligand-binding sites (**Figure 2.2.1 B, C**) [7,8]. In mammals, $GABA_A$ receptors are assembled by 19 distinct gene subunits (α_1, α_2, α_3, α_4, α_5 α_6, β_1, β_2, β_3, γ_1, γ_2, $\gamma 3$, ε, θ, δ, π, ρ_1, ρ_2, and ρ_3) [3]. Those subunits usually compose GABA isoform with two α subunits, two β subunits, and either one γ subunit or another. The α_1, β_2, and γ_2 are

the major subunit isoforms that are arranged $\gamma_2\beta_2\alpha_1\beta_2\alpha_1$ counterclockwise around the central chloride channel as viewed from the top [8].

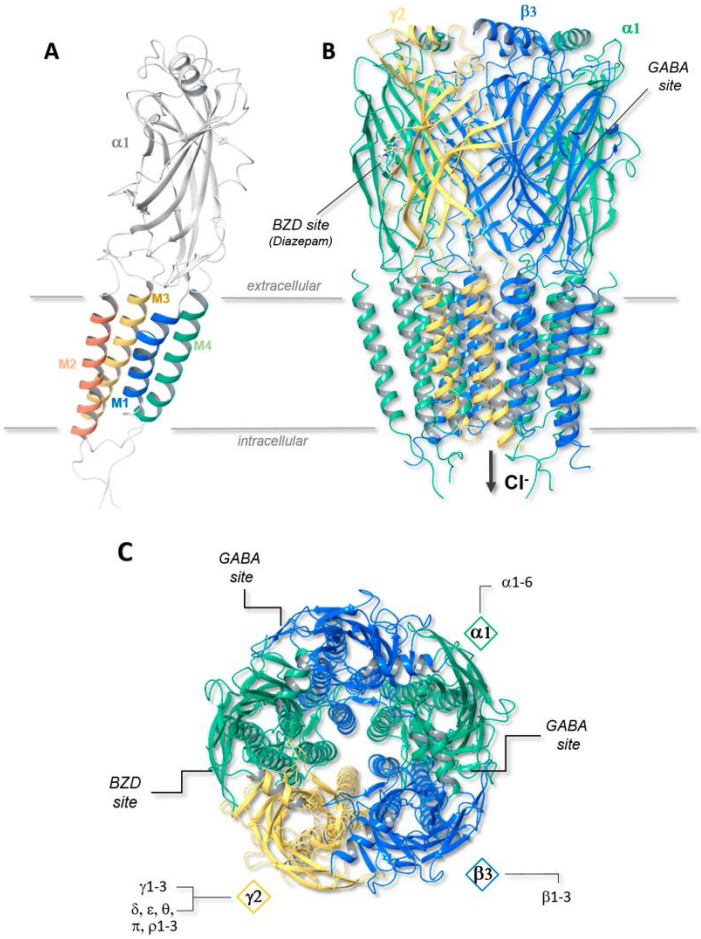

Figure 2.2.1. 3D-reconstruction of $\alpha_1\beta_3\gamma_2$-$GABA_A$ receptors. A, subunit $GABA_A$ receptors contain a long extracellular N-terminus, four transmembrane domains (M1-M4), two short loops that link M1-M2 and M2-M3, a longer intracellular loop between M3 and M4 (modulated by phosphorylation), and a small extracellular C-terminus. B, side view: the heteropentameric $GABA_A$ receptors with α, β, and γ subunits arranged around the central chloride ion channel. C, Top view of $GABA_A$ receptors with GABA binding sites, legends and figures adopted from [9].

The function of $GABA_A$ receptors

The activation of mature $GABA_A$ receptors, under normal conditions, leads to hyperpolarization of cell membrane potential and inhibition of neuronal activity [2]. First, the agonist GABA binds to two binding sites at the α/β subunit interfaces. Then site occupancy leads to change conformational that locks the agonist in the binding pocket. The protein alters conformation and enters one or several closed states. Further conformational changes lead to an opening of the ion pore, which then makes short visits to a ligand-bound closed state [8].

A complex of pentameric protein-structure and ligand-gated ion channels made up $GABA_A$ molecularly distinct subunits [2]. Each of the receptor subunits expresses distinctive

function and distribution in the brain. The majority of $GABA_A$ receptors possess either α_1- or α_2-subunits in combination with a γ_2- and β-subunits [3]. The largest single group of $GABA_A$ receptors appears to be made up of $\alpha_1\gamma_2$- and αβ-subunits. Subunit composition determines the biophysical and pharmacological properties of the site. For instance, α_1- or $\alpha_2\gamma_2\beta$ combination responds to benzodiazepine and non-benzodiazepine anxiolytics and hypnotics. However, lacking γ-subunits in combination with α_4- or α_6 are generally insensitive to the benzodiazepines and related drugs. $GABA_A$ receptors trafficking and localization are regulated in large measure by the subunit composition with, for instance, γ_2 being a key for routing receptors to synapses, while the δ-subunit is typical of $GABA_A$ receptors that gather at extrasynaptic sites.

$GABA_A$ receptors are molecular drug targets containing some binding sites such as benzodiazepines, neurosteroids, barbiturates, intravenous and inhalation anesthetics, and alcohol (**Figure 2.2.2**) [2]. Classical benzodiazepines are clinically used as anticonvulsants, sedatives/hypnotics, anxiolytics, muscle relaxants, and pre-anesthetics. Receptors sensitive to benzodiazepine modulation contain the α_1-, α_2-, α_3-, α_4-, or α_5- subunits in combination with any with the β-subunits and γ_2-subunit [3]. Some selective receptors are well characterized, α_1 subunit associated with sedative-hypnotics, the α_2 and α_3 subunits mediated anxiolytic, and the α_5 subunit associated with cognitive enhancement [8,10]. Other GABA molecular functions are α_3-containing $GABA_A$ receptors that have been characterized as selective agonist agents for psychiatric conditions; these would lack the sedative or extrapyramidal side effects [3,10]. Furthermore, α_5-$GABA_A$ receptors appear to have two allosteric with different affinities. The hypothesis of α_5-$GABA_A$ receptor negative allosteric modulators enhances cognition. Whereas, the α_5-$GABA_A$ receptor positive allosteric modulators may represent a novel approach to the treatment of schizophrenia, which is associate with hippocampal hyperactivity [9]. So far, the benzodiazepines as allosteric modulators of $GABA_A$ receptor function are well characterized than others.

Neurosteroids binding sites have been heavily studied lately. The presence of α subunit is important for neurosteroids potentiation like what Alfarez et al. (2018) has reported a contribution of α1 Gln241 in TM1 as a neurosteroid binding mode [11]. Furthermore, residue of Trp at $TM1_{24}$ position specifically interacts with neurosteroids binding sites, but all 19 genes of $GABA_A$ receptor subunits have a Trp residue. The knock-in/chemogenetic approach observed $GABA_A$ receptors δ-containing subunits in the extrasynaptic are not selective to

neurosteroids [12]. Specific neurosteroids binding sites were lately identified in three sites, e.g. the $\beta_3(+)$-$\alpha_1(-)$ intersubunit, α_1 intrasubunit sites, and β_3 intrasubunit sites [13,14].

In the case of barbiturates and anesthetic, actions via precise $GABA_A$ receptor subtypes are currently still incompletely understood [2,10]. The β subunit in TM2 and TM3 $GABA_A$ receptor regions is an important binding site for barbiturates involving β-subunit methionine 286 and α-subunit methionine 236 pockets [15]. For general anesthetic use (e.g. etomidate and propofol), β_3-containing $GABA_A$ receptors were found mediating through immobilizing action, part of hypnotic action, and respiratory depressant action. In contrast, it was partially deactivated by inhaled anesthetic (enflurane, isoflurane, and halothane) and no hypnotic action of volatile anesthetics [10]. The β_2-containing $GABA_A$ receptors were mediated hypnotic action of etomidate [10]. In a recombinant study, $GABA_A$ receptors contain ε subunit instead of γ_2 subunit would be insensitive to general anesthetics. On the contrary, the biological relevance of this finding need further investigation since ε subunit-containing receptors at low level are indeed sensitive to general anesthetics [3,10].

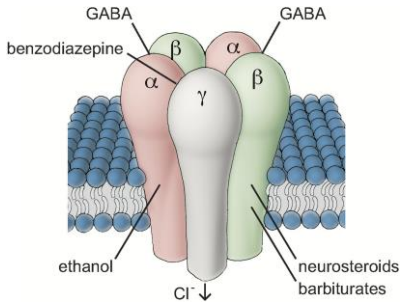

Figure 2.2.2. Schematic representation of a $GABA_A$ receptor illustrating its pentameric structure and the different sites of action for drugs that interact with this site, adopted from [4].

$GABA_A$ receptors as targeted assays

Drug target selection clinically needs to validate the targets. In the case of neurotransmitter receptors, validated targets are molecules related to neurotransmitters mechanism [16]. GABA is the main inhibitor neurotransmitters, with approximately 20% of all neurons in CNS [6]. $GABA_A$ and $GABA_B$ receptors mediate the action of GABA. Between those receptors, $GABA_A$ is a highly validated drug target for the benzodiazepine-type binding sites [16]. Furthermore, a total of 19 genes for $GABA_A$ receptor subunits have been cloned. It

leads the possibility to determine the composition of the site more precisely [2,3]. Molecular characterization of the $GABA_A$ receptor has made possible a more precise definition of the mechanism of action of some drugs and has provided new targets for designing novel therapeutics capable of activating or inhibiting select populations of $GABA_A$ sites [3].

$GABA_A$ receptor assays use cells lines expressing recombinant human $GABA_A$ receptors to evaluate the GABA activities. The assays can be applied in the electrophysiological study, ion flux study, and fluorescence techniques [17,18,19]. Electrophysiological studies can give information about function of $GABA_A$ ion channels, e.g. *Xenopus* oocyte assay, microphysiometry, and ion flux. In *Xenopus* oocyte assay, the enhancement of chloride ion current defined the $GABA_A$ receptors activity that expressed subunit composition of $GABA_A$ receptors [20,21]. At the same time, ion flux as biochemical method, can measure quantitatively $^{36}Cl^-$ radiolabel movement through $GABA_A$ receptors. In case of radio-ligand binding techniques, interaction of radio-labelled ligand to interested receptors were allowed to identify and characterize the ligand-binding site [22]. The binding site altered the affinity of the receptor by competing with that specific ligand, then determined agonist or antagonist activities of tested compounds [23]. For fluorescence techniques, fluorescent-dye is used to measure ion chloride currents or membrane potential of $GABA_A$ receptors. During the assay, $GABA_A$ receptor subunit combination and stoichiometry may effect differently when applied to different cells [20,24].

The α, β, and γ_2 subunit combination are abundant in mammalian brain $GABA_A$ receptors. Alpha (α) and γ subunits at the benzodiazepine site contributed significantly to affinity and efficacy of positive allosteric $GABA_A$ receptor modulators, but not β subunits [17]. Molecular study on $GABA_A$ receptors identified α_1 subunit associate with sedation and target for sedative-hypnotics, agonist selective for α_2 and or α_3 subunit provide anxiolytic without sedation in the preclinical model, α_5 subunit mediate memory enhancement, and the α_3 subunit show possibility for psychiatric disorders, especially for the treatment of deficits in sensorimotor processing [10]. Even though benzodiazepine site is a well-characterized drug target, benzodiazepine as $GABA_A$ receptor drugs can cause sedation, ataxia, cognitive impairment, behavioral tolerance, and potential for abuse [25,26]. However, neurosteroids as endogenous $GABA_A$ receptors are also the targeted assays. Its specific binding sites are detected in transmembrane domain can be a hint for assay development [12,13,14]. The allopregnanolone as positive allosteric modulatory

neurosteroids showed that predominantly bind through $\beta_3(+)/\alpha_1(-)$, while both allopregnanolone and epi-pregnanolone bind to β_3 intrasubunit, promoting receptor desensitization. The α_1 subunit site exhibited various effects in different type of neurosteroids. With the new findings by cryo-EM of $GABA_A$ receptor in lipid bilayer, this will open further functional and structural studies for $GABA_A$ receptor modulation by lipid not only neurosteroids but also receptor target in transmembrane domain [27].

References

1. Brunton, L. L., Lazo, J. S., and Parker, K. L. (Editor). Goodman and Gilman's: The Pharmacological Basis of Therapeutics 11st Ed. Bloom, F. E. Chapter 12, Drugs Acting on the Central Nervous System. McGraw-Hill. USA. 2006. p.330. DOI: 10.1036/0071422803
2. Uusi-Oukari, M., and Korpi, E. R. Regulation of $GABA_A$ receptor subunit expression by pharmacological agents. *Pharmacol. Rev*. 2010. 62, 62-135.
3. Enna, S. J., and Mohler, H. The GABA Receptors, 3rd Ed. Humana Press. Totowa, New Jersey. 2007. p.3-9, 289-300.
4. Olsen, R. W. GABA-benzodiazepine-barbiturate receptor interactions. *J. Neurochem*. 1981. 37, 1-13.
5. Mele, M., Costa, R. O., and Duarte, C. B. Altering in $GABA_A$-receptor trafficking and synaptic dysfunction in brain disorders. *Front. Cell. Neurosci*. 2019. 77, 1-16.
6. Fatemi, S. H., and Folsom, T. D. GABA receptor subunit distribution and FMRP-mGluR5 signaling abnormalities in the cerebellum of subjects with schizophrenia, mood disorders, and autism. *Schizophr. Res.* 2015. 167, 42-56.
7. Goetz, T., Arslan, A., Wisden, W., and Wulff, P. $GABA_A$ receptors: structure and function in the basal ganglia. *Prog. Brain Res*. 2007. 160, 21-41.
8. Sigel, E., and Steinmann, M. E. Structure, function, and modulation of GABA receptors. *J. Biol. Chem*. 2012. 287, 40224-40231.
9. Maramai, S., Benchkroun, M., Ward, S. E., and Atack, J. R. Subtype selective γ-aminobutyric acid type A receptor ($GABA_AR$) modulators acting at the benzodiazepine binding site: an update. *J. Med. Chem*. 2020. 63, 3425-3446.
10. Rudolph, U., and Mohler, H. GABA-based therapeutic approaches: $GABA_A$ receptor subtype functions. *Curr. Opin. Pharmacol*. 2006. 6, 18-23.
11. Alvarez, L. D, and Pecci, A. Structure and dynamics of neurosteroid binding to the the $\alpha_1\beta_2\gamma_2$ $GABA_A$ receptor. *J. Steroid Biochem*. 2018. 182, 72-80.
12. Lu, X., Zorumski, C. F., and Mennerick, S. Lack of neurosteroid selectivity at δ vs. γ2-containing $GABA_A$ receptors in dentate granule neurons. *Front. Mol. Neurosci.* 2020. 13, 1-12.
13. Chen, Z-W., Bracamonte, J. R., Budelier, M. M., Germann, A. L., Shin, D. J., Kathiresan, K., Qian, M-X., Manion, B., Cheng, W. W. L., Reichert, D. E., Akk, G., Covey, D. F, and Evers, A. S. Multiple functional neurosteroid binding sites on GABAA receptors. *Plos Biol.* 2019. 17, 1-27.
14. Sugasawa, Y., Cheng, W. W. L., Bracamontes, J. R., Chen, Z-W., Wang, L., Germann, A. L., Pierce, S. R., Senneff, T. C., Krishnan, K., Reichert, D. E., Covey, D. F., Akk, G., Evers, A. S. Site-specific effects of neurosteroids on $GABA_A$ receptor activation and desensitization. *eLife*. 2020. 9, e55331.
15. Loscher, W., and Rogawski, M. A. How theories evolved concerning the mechanism of action of barbiturates. *Epilepsia*. 2012. 53, 12-25.
16. Hefti, F. F. Drug discovery for nervous system diseases. John Wiley & Sons. Hoboken. New Jersey. 2005. p.43-45.

17. Smith, A. J., and Simpson, P. B. Methodological approaches for the study of $GABA_A$ receptor pharmacology and functional responses. *Anal. Bioanal. Chem*. 2003. 377, 843-851.
18. Smith, A. J., McKernan, R. M., and Atack, J. R. Benzodiazepine modulation of recombinant $\alpha_1\beta_3\gamma_2$ $GABA_A$ receptor function efficacy determination using the cytosensor microphysiometer. *Eur. J. Pharmacol*. 1998. 359, 261-269.
19. Smith, A. J., Alder, L., Silk, J., Adkins, C., Fletcher, A. E., Scales, T., Kerby, J., Marshall, G., Wafford, K. A., McKernan, R. M., and Atack, J. R. Effect of α subunit on allosteric modulation of ion channel function in stably expressed human recombinant γ-aminobutyric acid A receptors determining using ^{36}Cl ion flux. *Mol. Pharmacol.* 2001. 59, 1108-1118.
20. Karim, N., Wellendorph, P., Absalom, N., Johnston, G. A., Hanrahan, J. R., and Chebib, M. Potency of GABA at human recombinant $GABA_A$ receptors expressed in *Xenopus* oocytes: a mini review. *Amino Acids*. 2013. 44, 1139-1149.
21. Zaugg, J., Barburin, I., Strommer, B., Kim, H-J., Hering, S., and Hamburger, M. HPLC-based activity profiling: discovery of piperine as a positive $GABA_A$ receptor modulator targeting a benzodiazepine-independent binding site. *J. Nat. Prod*. 2010. 73, 185-191.
22. Bylund, D. B, and Toews, M. L. Radioligand binding methods: practical guide and tips. *Am. J. Physiol. Lung Cell Mol. Physiol*. 1993. 265, L421-L429.
23. Mohler, H., and Richards, J. G. Agonist and antagonist benzodiazepine receptor interaction in vitro. *Nature*. 1981. 294, 763-765.
24. Mercik, K., Pytel, M., and Mozrzymas, J. W. Recombinant $\alpha_1\beta_2\gamma_2$ $GABA_A$ receptors expressed in HEK293 and in QT6 cells show different kinetics. *Neurosci. Lett*. 2003. 352, 195-198.
25. Olsen, R. W. $GABA_A$ receptor: positive and negative allosteric modulators. *Neuropharmacology*. 2018. 136, 10-22.
26. Nicholson, M. W, Sweeney, A., Pekle, E., Alam, A., Ali, A. B., Duchen, M., and Jovanovic, J. N. Diazepam-induced loss of inhibitory synapses mediated PLCδ/Ca^{2+}/calcineurin signaling downstream of $GABA_A$ receptors. *Mol. Psychiatry*. 2018. 23, 1851-1867.
27. Laverty, D., Desai, R., Uchaski, T. Masiulis, S., Stec, W. J., Malinauskas, T., Zivanov, J., Pardon, E., Steyaert, J., Miller, K. W., and Aricescu, A. R. Cryo-EM structure of the human $\alpha_1\beta_3\gamma_2$ $GABA_A$ receptor in a lipid bilayer. *Nature*. 2019. 565, 516-520.

2.3. HPLC-Based Activity Profiling with $GABA_A$ Receptor Assays

$GABA_A$ receptors are a clinically therapeutic target for drug discovery [1]. Many methodological approaches have contributed to high throughput screening for $GABA_A$ receptor modulation. In this chapter, several assay formats for $GABA_A$ receptor modulation that formed the part of this thesis, namely the *Xenopus* oocyte assay, zebrafish larvae locomotor-activity model, and the FLIPR assay, are discussed in brief. These three assays have been applied to HPLC-based activity profiling [2,3,4,5]. HPLC microfractionation was applied by injecting and separating the extract using linear gradients. The microfractionations were collected every one or three minutes, depends on the assay set up. Microfractionations were tested for $GABA_A$ receptor modulation. The assessment of HPLC microfractionation was able to describe the priority of active fractions in the milligram amount of extracts. The HPLC-UV-MS data of the microfractionations are used for dereplication of substances of extracts or fractions. HPLC profiling and dereplication of the extracts can be a guide to isolate the active compounds at a large scale of plant material.

2.3.1. *Xenopus* oocyte assay

The squid giant axon played a critical role in understanding the changes in membrane potential [6]. The concept of voltage clamp, ion channel, and molecular basis in conductance pathway followed by the ability to record discrete miniature current jumps in excitability inducing material contributed remarkably to develop the patch-clamp technique. On the other side, South African clawed frog, *Xenopus laevis*'s oocytes have been investigated for studying neurotransmitter ion channels [7]. A fully mature oocyte is ideal in size for its microdissection assay and capable to synthesize exogenous protein when it is injected with foreign RNA. The possibility of recording currents of ligand-gated ion channels and the *Xenopus* oocyte's ability to express $GABA_A$ receptor subunits, generated drug-screening format based on an electrophysiological approach, in which this method is called automated fast perfusion of *Xenopus* oocytes. Recording currents of ligand-gated ion channels in the *Xenopus* oocyte expressing $GABA_A$ receptor subunits were generated to an electrophysiology approach for drug screening, which is called automated fast perfusion of *Xenopus* oocytes [7,8].

Principle

Ion channel functional assay is one of the electrophysiological techniques performed by automated two-microelectrode voltage-clamp recording from *Xenopus* oocytes [8,9,10]. The stage V-VI oocyte from *Xenopus laevis* showed a high density of endogenous $Ca2^{+}$-activated Cl^{-} channel. Injection of oocyte with cRNA adequate $GABA_A$ receptors to express $\alpha_1\beta_2\gamma_{2s}$ receptors needs to be done in a healthy defolliculated oocyte (**Figure 2.3.1**) [3,8,11]. After incubation of the oocyte for 24 - 48 hours, it is placed on a cylindrical holding service in the perfusion chamber set up (**Figure 2.3.2**) to increase the stability of oocyte perfusion during the experiment [8,11,12]. The two-electrode voltage clamp (TEVC) can control membrane potential and measure directly ion chloride current changes that occur upon receptor activation. The functional response of drugs potential can be determined by a concentration-effect relationship. Automation, fast, and timed sample application of recording TEVC can improve the reproducible of quantitative data [8,9,11]. The assessment of $GABA_A$ potentiation can be obtained from the enhancement of the chloride current $[(I_{(GABA+Comp)})/(I_{GABA}) - 1]$, which is the comparison between current response in the presence of given compound ($I_{(GABA+Comp)}$) and the control GABA-induced chloride current (I_{GABA}) [3].

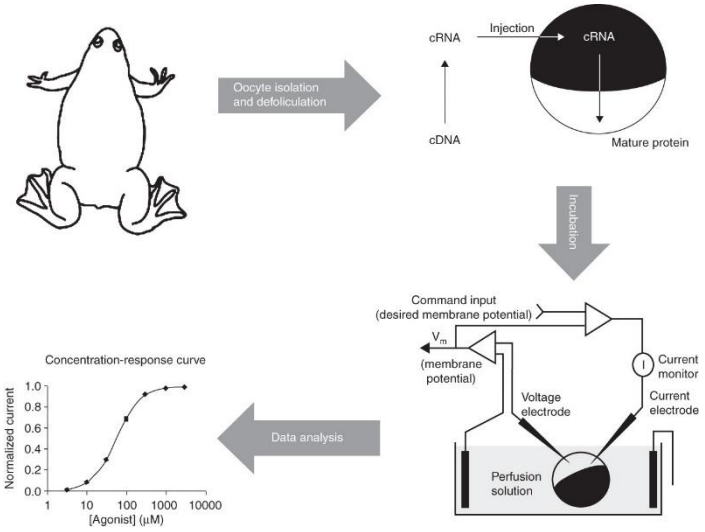

Figure 2.3.1. Schematic workflow of two-microelectrode voltage-clamp experiments using female *Xenopus laevis* for testing $GABA_A$ receptor activity. The oocytes are surgically obtained from the *Xenopus laevis*. The oocytes are then enzymatically defolliculated and injected with cRNA (transcripted from suitable cDNA of $GABA_A$ receptor subunits, $\alpha_1\beta_2\gamma_{2s}$ subtype with ratio 1:1:10). After the incubation, oocytes are ready for TECV measurements (Figures and legends taken from [9].

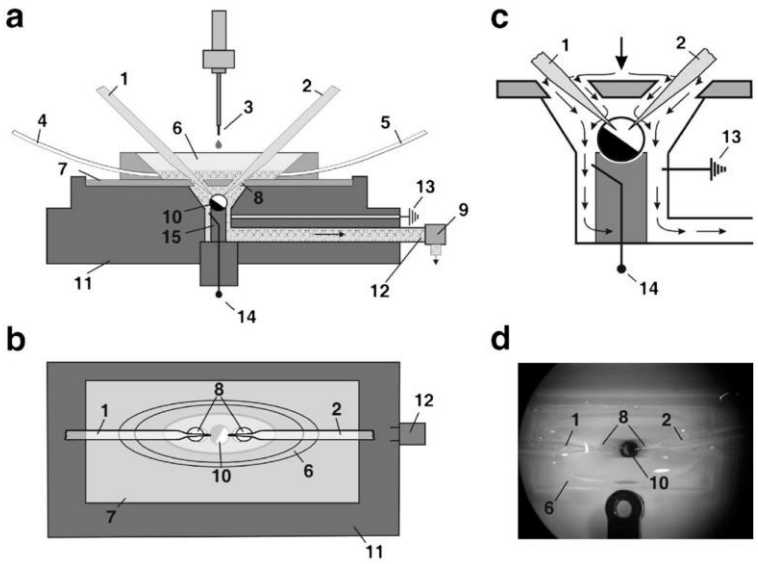

Figure 2.3.2. "Cross-section view (**a**) and top view (**b**) of the oocyte perfusion chamber. Two microelectrodes (1 and 2) are inserted via the sloping access inlet (8) through a glass cover plate (7) into the small (~15 µL) oocyte chamber. The drug is applied by the tip of the liquid handling arm (3) of a TECAN Miniprep 60 to a funnel reservoir made of quartz (6) surrounding the microelectrode access holes. Perfusion of the oocyte (10) that is placed on a cylindrical holding device (15) is enabled employing a syringe pump (9) of the Miniprep 60 connected to the chamber body (11) via the outlet (12). The residual solution is removed from the funnel before drug application via the funnel outlets (4 and 5). In addition to the ground reference electrode (13), the cylindrical holder for the oocyte contains a reference electrode (14) that serves as an extracellular reference for the potential electrode. Salt bridges can be inserted into the side outlet for the ground electrode (13). **c** is a schematic drawing of the solution flow inside the perfusion chamber and in the annular gap around the cylinder with the oocyte. **D** is a photo of the oocyte perfusion chamber. An oocyte (10) is placed on a cylinder and impaled with two microelectrodes (1,2) surrounded by the funnel (6)" (Figures and legends taken from [8].

Advantages and challenges

The ion channel format is a gold standard for studying functional assay [9,11]. The TEVC using *Xenopus* oocyte has some advantages. From the availability of material, the fully mature oocyte up to 10,000 oocytes can be obtained from the same and reused donor frog. Then in living oocyte, the translation of exogenous RNA is occurred with the specificity to express specific subunits of $GABA_A$ receptors into membrane protein and low level of endogenous background channels. The robustness and large size (diameter ~ 1.2-1.3 mm) of the oocyte make them tolerant to repeated impalement of microelectrode and injection pipettes, permitting functional analysis by the number of electrophysiological techniques. The recording results are reproducible and accurate data.

There are several limitations of the *Xenopus* oocyte assay in TEVC [9,11]. First, it requires an animal facility and is labor-intensive, and various factors may affect the quality of the oocytes. Then, the physiological function of oocytes needs optimal temperature at 16-20°C and targeted cRNA/DNA injection. The experiment required a large amount of compound usage because TEVC recordings need a larger volume of the ligand during application. Other disadvantages are a low assay throughput. Post-translational modification of protein might be needed in this assay since proteins interaction and lipid properties in oocyte membranes may express differently in amphibian and mammalian cells.

2.3.2. Zebrafish larvae locomotor-activity model

Zebrafish (*Danio rerio*) is from the family Cyprinidae and a popular freshwater aquarium fish native to South Asia. Zebrafish has been rapidly investigated and published since 1990 [13]. Over the past decade, the zebrafish has been studied for a closer relationship to humans in genetics, morphology, and physiology. These features can facilitate a model disease, drug discovery, target identification, pharmacology, toxicology, and drug development/optimization. Zebrafish have been developed to model human diseases such as cancer, renal disorder, cardiovascular disease, hearing loss, blood disorders, muscular dystrophies, and neurological disease [14,15,16]. Below are brief description of the behavioral model of $GABA_A$ receptor modulators with zebrafish larvae.

Principle

Both larvae and adult zebrafish have responsive behaviors to study. Zebrafish larvae also possess functional livers, kidneys, and blood-brain barriers [16]. However, zebrafish larvae are suitable for behavioral studies since their swimming behavior can evaluate locomotor activity to determine the effect of experimental perturbations. The swimming behavior becomes sustained in larvae once the brain system develops [17,18]. The early stage of zebrafish larval development is investigated for the occurrence of GABA cells [19]. For locomotor activity, 7 days postfertilization (dpf) larvae were used to develop and design the experiments. Larvae at 7 dpf produce reliable active swim time, total distance/travel, and suit for testing the effect of drug treatments on locomotor activity [4,18,20].

A validated assay using zebrafish larvae was established by various parameters in assessing $GABA_A$ receptor modulators [4]. The assay using a pro-convulsant GABA receptor antagonist, pentylenetetrazol (PTZ), which induces seizure-like behavior and increases the locomotor activity of zebrafish larvae [4,21]. It used a single 7-dpf larval in each well of 96-well plate. The larvae were incubated for 3 h with the test samples. The incubation time was assigned before toxicity assessment at four-time points (1.5, 3, 6, and 12 h). Toxicity assessment needs to be done to define the maximal tolerated concentration (MTC). The MTC was set as the highest test concentration in the assay. Concentration PTZ at 10 mM was applied to induce the seizure as it showed a linear concentration-response relationship. The assay was automatically recording the larval motilities over 30 min with an IR-sensitive camera after adding PTZ. $GABA_A$ receptor modulators were determined through a decrease in total movement (distance traveled, mm) and pattern of larval movement during the tracking period (25 min), 5 min after exposure by PTZ does not include in the assessment data. The total movement can be used as a quantitative assessment of the seizure behavior while the pattern of larval movement as average distance traveled over 5 min intervals exhibit different stages of seizure-like behaviors. In the first stage, larvae were observed to increase their swimming activity dramatically, which was followed by a rapid whirlpool-like circling swim behavior, and the last stage is a series of brief clonus-like convulsions leading to a loss of posture (remains immobile for 1-3 s) [21]. The MTC value of test samples can be determined to distinguish less larval motility because of toxicity or the last stage of seizure behavior.

Advantages and challenges

Zebrafish larvae offer some advantages in $GABA_A$ receptor modulators screening [16,21]. First, zebrafish is *in vivo* behavioral animal model which share 70-80% genetic homology similar to human. That fact might increase the translation to *in vivo* mammalian model with less optimization of pharmacological properties. Then, zebrafish larvae expresses blood-brain barrier transporter, which is beneficial in drug discovery of CNS drugs [4,21]. The lack of activity of $GABA_A$ receptor modulators in zebrafish larvae is supported by poor properties of BBB permeability in *in silico* prediction [4].

Zebrafish larvae locomotor assay leaves some hurdles in several aspects [4,21]. In terms of practical work, it has limited assay throughput and labor-intensive. Furthermore, the assay must be performed at certain stages of larvae development that require a fish facility and consecutive arrangements and treatments. Another challenge in the zebrafish assay is the readout selectivity. $GABA_A$ receptor modulators were determined by the movement of the larvae in the validated assay. Therefore, it needs confirmation in cell-based functional assays to identify the binding site of compounds. A drug giving a desired result in the assay might not mean it interacts with the GABA receptor. As the assay use the whole organism with various receptors, the interaction sites between a drug and receptor could not be determined in the assay.

2.3.3. Fluorometric Imaging Plate Reader (FLIPR) assay

Limitation for previous $GABA_A$ receptor modulator assays led to the establishment of high throughput screening by fluorometric imaging plate reader (FLIPR) format [5]. FLIPR is a modern optical screening format that was expanded for quantitative optical screening utilizing cell-based kinetic fluorescence assay [22]. FLIPR was designed by integrating low-level optical detection, precise temperature control, and precise fluid handling at once. The FLIPR assay setup uses a standard 96-well plates that can read each column (8-wells) simultaneously. The assay was developed through validation by using known extracts and drugs for $GABA_A$ receptor modulators activity, diazepam as a positive control. For example, we used active plant extracts that had been reported as allosteric $GABA_A$ receptor modulators in a different assay, e.g., automated two-microelectrode voltage-clamp recording from *Xenopus* oocytes and zebrafish larvae locomotor- activity model [3,4]. The plant extracts and its natural products used for validation of the assay were selected from our extract library: EtOAc extract from barks of *Magnolia officinalis* and magnolol, EtOAc extract from roots of *Valeriana officinalis* and valerinic acid, and EtOAc extract from fruits of *Piper nigrum* and piperine [5]. The FLIPR assay results showed comparable results with previous assay formats.

Principle

FLIPR assays apply fluorescence-based dyes for observation of real-time membrane potential change associated with ion channel activation [23]. The dye is sensitive in membrane potential that detects the change in voltage across the cell membrane [24,25]. When a compound activated chloride ion channels binding to $GABA_A$ receptor binding-sites, it leads to hyperpolarization. At hyperpolarization state, membrane potential-sensitive dye cross from cell surfaces to the inner membrane and remove extracellular fluorescence quenchers. The results are increasing fluorescence readout (**Figure 2.3.3**).

FLIPR assay was validated utilizing Chinese hamster ovary (CHO) cells to express $\alpha_1\beta_2\gamma_2$ $GABA_A$ receptor subunit composition [5]. The procedure of the assay is depicted in **Figure 2.3.4 A**, which shows two different 96-well microtiter formats used in the experiment. The cell plate is a black-walled 96-well plate, while the compound plate is a clear 96-well plate. Both plates are placed in the FlexStation instrument, which contains three drawers, as shown in **Figure 2.3.4 B**. The build-in pipettor takes the pipet tip from the tip rack then it transfers samples in the compound plate to the corresponding well of the cell plate [22,26]. After mixing one row cell plate with a sample from the compound plate, the fluorescence was measured over a duration of 500 seconds automatically for 8 wells simultaneously. The percentage GABA activation was calculated between 270 – 330 s [5].

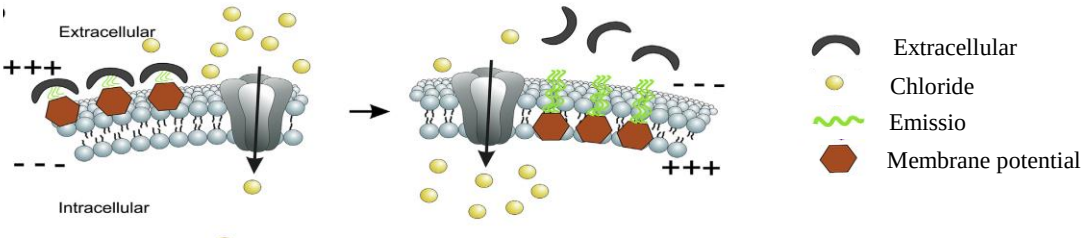

Figure 2.3.3. Membrane potential-sensitive dye assay principle, adopted from [24].

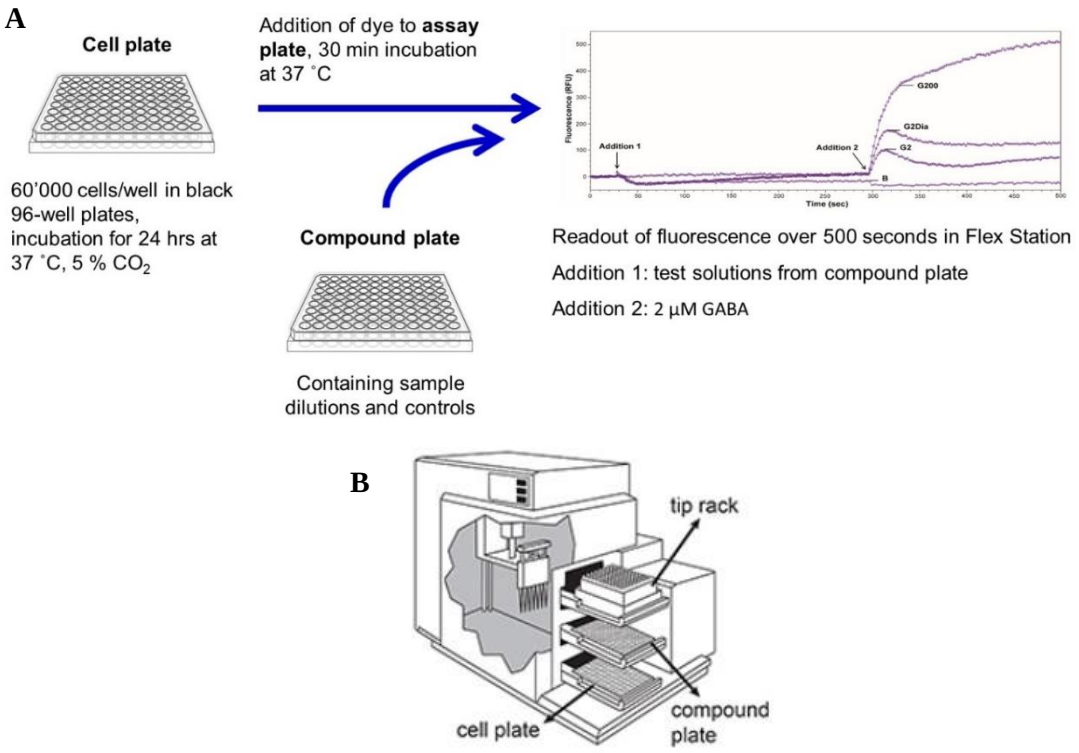

Figure 2.3.4. FLIPR assay procedure (**A**) and FlexStation (**B**), adopted from [26] (Thanks to Faleschini, M. T., for preparing assay procedure figure).

FLIPR assay protocol was developed for HPLC-based activity profiling [5]. It was found the sufficient quantity of plant extracts separation around 0.4 – 1.2 mg. This amount was sensitive to bioassay to localize the active compounds. Since DMSO was used to dissolve samples, DMSO tolerance in the experiment was tested. It concluded that the final DMSO concentration in FLIPR assay without interfering with the assay result was 0.1% for pure testing compound and 0.3% for testing extract. The plant extracts were screened at a single concentration, 20 µg/mL. The extracts showed the percentage of GABA receptors activation of more than 35% was considered hits. Afterward, the activity of the extract was tested in serial dilution, which assessed the properties of extract activity toward concentration response. The extract thus exhibited a great concentration-response curve or activity properties, was then subjected to microfractionation testing. The microfractionation displayed extract activity profiling and localized the active compounds.

Advantages and challenges

FLIPR membrane potential assay overcomes several restrictions for high throughput screening. Even though it is still medium-throughput screening, FLIPR is a robust instrument with high signals as well as easy to use [5,27]. The assay is potentially sensitive, versatile, and amenable to miniaturization and automation. The fluorescence readouts can measure intracellular chloride concentrations. During the measurement, the results can be observed in real-time. In terms of cell-based assays, the FLIPR format possesses some advantages. Since it used $\alpha_1\beta_2\gamma_2$ $GABA_A$ receptor subunit composition, the allosteric modulators can be detected. In this project, allosteric $GABA_A$ receptor modulators were applied for drugs that work as an agonist and antagonist at the benzodiazepine binding sites (diazepam and flumazenil), barbiturate binding sites (etazolate), as well as agonist and antagonist at the neurosteroid binding sites (allopregnanolone and pregnenolone sulfate). In receptor studies, it could be used to distinguish agonist and antagonist in parallel with information of possible binding sites and different functional readouts [28]. The phenotypic readouts are possible if the molecular target is known.

Some limitations of FLIPR assay are included low DMSO tolerance that restricted substances can be applied [5,28]. It also needs to be considered the possibility of fluorescence quenching compounds can interfere especially with extracts. Regarding the price, the dye for the FLIPR assay is also expensive. In terms of cell-based assays, the disadvantages can be found in special engineered cell lines and/or careful selection, cells detached from support. The cell-based assay has a high rate of false positives due to non-specific test compounds on cell function. Regarding cell viability, assay conditions are limited, such as the use of solvent and pH. These disadvantages of cell-based assay can be controlled by special treatment for the cells and assays. Besides, cell-based assays require special infrastructure in the screening laboratory, e.g., cell cultivation facilities, and an automatic system/instrument, to maintain physiological conditions amid the experiment.

Chinese Hamster Ovary (CHO) cells in expressing $GABA_A$ receptors

Chinese hamster ovary (CHO) cells were reported for amplified expression of alpha interferon in 1982 by Kaufman and Sharp [29]. This cell became a model and an important tool

for biomedical research and pharmaceutical products. The cell is able to express a functional recombinant protein, i.e., expressing the $GABA_A$ receptor subunit in FLIPR assay, and easy to cultivates. CHO cells expression system have produced the majority of the recombinant proteins, from 1982-2014 it was reported to reaching up to 35.5% of all recombinant proteins produced worlwide. Comparing to Human Embryonic Kidney (HEK293), CHO cells have a reasonable success rate in whole-cell seal information [24]. To express $\alpha_1\beta_2\gamma_2$ $GABA_A$ receptor subunit composition, CHO cells were maintained in DMEM F-12 nutrient supplemented with 10% FBS, as penicillin/streptomycin (1%), hygromycin B (200 µg/mL), puromycin (5 µg/mL), and zeocin (100 µg/mL) [5]. Cells were incubated in humidified air at 37 °C and 5% CO_2 until 80-90% cell confluency. In this experiment, passage numbers were used from 10 to 30.

References

1. Smith, A. J., and Simpson, P. B. Methodological approaches for the study of $GABA_A$ receptor pharmacology and functional responses. *Anal. Bioanal. Chem*. 2003. 377, 843-851.
2. Potterat, O., and Hamburger, M. Combined use of extract library and HPLC-based activity profiling for lead discovery: potential, challenge, and practical considerations. *Planta Med*. 2014. 80, 1171-1181.
3. Zaugg, J., Barburin, I., Strommer, B., Kim, H-J., Hering, S., and Hamburger, M. HPLC-based activity profiling: discovery of piperine as a positive $GABA_A$ receptor modulator targeting a benzodiazepine-independent binding site. *J. Nat. Prod*. 2010. 73, 185-191.
4. Moradi-Afrapoli, F., Ebrahimi, S. N., Smiesko, M., and Hamburger, M. HPLC-based activity profiling for $GABA_A$ receptor modulators in extracts: validation of an approach utilizing a larval zebrafish locomotor assay. *J. Nat. Prod*. 2017. 80, 1548-1557.
5. Faleschini, M. T., Maier, A., Fankhauser, S., Thasis, K., Hebeisen, S., Hamburger, M., and Butterweck, V. A FLIPR assay for discovery of $GABA_A$ receptor modulators of natural origin. *Planta Med*. 2019. 85, 925-933.
6. Bezanilla, F. Ion channels: from conductance to structure. *Neuron*. 2008. 60, 456-468.
7. Dascal, N. The use of *Xenopus* oocytes for the study of ion channels. *Crit. Rev. in Biochem*. 1987. 22, 317-387.
8. Baburin, I., Beyl, S., and Hering, S. Automated fast perfusion of *Xenopus* oocytes for drug screening. *Pflugers Arch.* 2006. 453, 117-123.
9. Kvist, T., Hansen, K. B., and Br*a*uner-Osborne, H. The use of *Xenopus* oocytes in drug screening. *Expert Opin. Dug Discov*. 2011. 6, 141-153.
10. Papke, R. L., and Smith-Maxwell, C. High-throughput electrophysiology with *Xenopus* oocytes. *Comb. Chem. High Throughput Screen*. 2009. 12, 38-50.
11. Clare, J. J., and Trezise, D. J. Expression and Analysis of Recombinant Ion Channels. In Expression of Ion Channels in *Xenopus* oocytes. Goldin, AL. Wiley-VCH Verlag GmBH&Co. KGaA. Weinheim, Germany. 2006. p.1-21.
12. Khom, S., Baburin, I., Timin, E. N., Hohaus, A., Sieghart, W., and Hering, S. Pharmacological properties of $GABA_A$ receptors containing γ1 subunits. *Mol. Pharmacol*. 2006. 69, 640-649.
13. Meyers, J. R. Zebrafish: development of a vertebrate model organism. *Curr. Protoc. Essent*. 2018. 16, 1-26.
14. Delvecchio, C., Tifenbach, J., and Krause, H. M. The zebrafish: a powerful platform for *in vivo*, HTS drug discovery. *Assay Drug Dev. Techn*. 2011. 9, 354-361.
15. Bowman, T. V., and Zon, L. I. Swimming into the future of drug discovery: *in vivo* chemical screens in zebrafish. *ACS Chem. Biol*. 2010. 5, 159-161.

16. MacRae, C. A., and Peterson, R. T. Zebrafish as tools for drug discovery. *Nat. Rev. Drug Discov*. 2015. 14, 721-731.
17. Drapeau, P., Saint-Amant, L., Buss, R. R., Ching, M., McDearmid, J. R., and Brustein, E. Development of the locomotor network in zebrafish. *Prog. Neurobiol*. 2002. 68, 85-111.
18. Ingebretson, J. J., and Masino, M. A. Quantification of locomotor activity in larval zebrafish: considerations for the design of high-throughput behavioral studies. *Front. Neural Circuits*. 2013. 7, 1-9.
19. Mueller, T., Vernier, P., and Wullimann, M. F. A phylotypic stage in vertebrate brain development: GABA cell patterns in zebrafish compared with mouse. *J. Comp. Neurol*. 2006. 494, 20-634.
20. Colwill, R. M., and Creton, R. Locomotor behaviors in zebrafish (*Danio rerio*) larvae. *Behav. Processes*. 2011. 86, 222-229.
21. Baraban, S. C., Taylor, M. R., Castro, P. A., and Baier, H. Pentylenetetrazole induced changes in zebrafish behavior, neural activity and c-fos expression. *Neuroscience*. 2005. 131, 759-768.
22. Schroeder, K. S., and Neagle, B. D. FLIPR: a new instrument for accurate, high throughput optical screening. *J. Biomol. Screen.* 1996. 1, 75-81.
23. Arkarin, M. R., Connor, P. R., Emkey, R., Garbison, K. E., Heinz, B. A., Wiernicki, T. R., Johnston, P. A., Kandasamy, R. A., Rankl, N. B., and Sittampalam, S. FLIPR^{TM} assay for PCR and ion channel targets. *Assay Guidance Manual*. 2012. 1-33.
24. Prashanth, J. R., Hasaballah, N., and Vetter, I. Pharmacological screening technologies for venom peptide discovery. *Neuropharmacology*. 2017. 127, 4-19.
25. Joesch, C., Guevarra, E., Parel, S. P., Bergner, A., Zbinden, P., Konrad, D., and Albbrecht, H. Use of FLIPR membrane potential dyes for validation of high-throughput screening with the FLIPR and µARCS technologies: identification of ion channel modulators acting on the $GABA_A$ receptor. *J. Biomol. Screen*. 2008. 13, 218-228.
26. Caers, J., Peymen, K., Suetens, N., Temmerman, L., Janssen, T., Schoofs, L., and Beets, I. Characterization of G protein-coupled receptors by fluorescence-based calcium mobilization assay. *J. Vis. Exp.* 2014. 89, 1-10.
27. Baxter, D. F., Kirk, M., Garcia, A. F., Raimondi, A., Holmqvist, M. H., Flint, K. K., Bojanic, D., Distefano, P. S., Curtis, R., and Xie, Y. A novel membrane potential-sensitive fluorescence dye improves cell-based assays for ion channels. *J. Biomol. Screen.* 2002. 7, 79-85.
28. Hill, R. G., Rang, H. P., and Vallance, P. Drug discovery and development. Crock, D. Chapter 8, High-throughput screening. Churchill Livingstone Elsevier. Edinburg, London, New York, Oxford, Philadephia, St Louio Sydney Toronto. 2013. p.101-102.
29. LSF Magazine: Telling the story of Biotechnology. Special issue: Global biotech. 2015. 38-54.

2.4. HPLC-Based Activity Profiling for Immunosuppressant Activity

Epidemiological data showed that the incidence and prevalence of autoimmune diseases increased every year [1,2]. The majority of prescribed immunosuppressive drugs are glucocorticoids, calcineurin inhibitors, antiproliferative/antimetabolic agents, and antibodies [3]. Some of these drugs are also used in autoimmune and immune-mediated diseases [4,5]. Since immunosuppressive agents have serious toxicity issues, it is important to discover immunosuppressive agents from natural products. The discovery was initiated by screening the extract library from known traditional plant medicine, Traditional Chinese Medicine (TCM), which can inhibit T lymphocyte proliferation *in vitro* [6,7]. The promising extracts without concomitant cytotoxicity were subjected to HPLC-based activity profiling [6,7,8]. The milligram amount of extracts were separated by HPLC using an optimized linear gradient and collected every one minute. The results of microfractionation testing and HPLC-UV-MS data of extracts were used to profile the activity of the extracts. It localized the active fraction of the extracts as well as a guidance for isolating the compounds in a large scale.

This chapter briefly reviews T cells' role in immune systems and T cells proliferation assay that were used to isolate immunosuppressive agents in plant extracts.

Role of T cells in the immune system

Pluripotent hematopoietic stem cells residing in bone marrow are central for producing the immune system's cells [9,10]. It provides progenitor cells of lymphoid and myeloid. The lymphoid progenitor contains natural killer (NK) cells such as the T and B lymphocytes, while the myeloid progenitor is composed of the remaining cells such as leukocytes, the erythrocytes, and the megakaryocytes. The immune responses of these immune cells were distinguished into innate and adaptive immune response. Innate immunity reacts immediately to fight against a wide range of pathogens than adaptive immunity [9,11]. Since adaptive immunity takes days to combat potential pathogens, it defeats infection efficiently and generates antibodies against a singular pathogen or its products. Specific response of adaptive immunity is part of lymphocytes' functions. The surface of lymphocytes possesses very specific antigen receptors to recognize and respond to individual antigen. The activated lymphocytes are called effector lymphocytes, while unstimulated lymphocytes are known as naïve lymphocytes. Lymphocytes

have two main types of cells: B lymphocytes (B cells) and T lymphocytes (T cells) [9]. Both cells differentiate in the central lymphoid; B cells are in the bone marrow while T cells are in the thymus. Stimulated B lymphocytes produce antibodies and obtain an identical antigen specificity. These antibodies are known as immunoglobulins (Ig). Its antigen receptors are called membrane immunoglobulin (mIg) or surface immunoglobulin (sIg). However, activated T lymphocytes divide into three general functions: killing (cytotoxic), activation, and regulation [9,10]. In order to reach the final full function of proliferation and differentiation, lymphocytes need co-stimulatory molecules [9,10,12]. Naïve T lymphocytes are helped by co-stimulatory molecules, which are mature dendritic cells expressing cell-surface proteins. The co-stimulatory molecules and together with antigen, activate T lymphocytes. On the other hand, naïve B cells require an activated helper T cell as a second signal. The obvious difference between B cells and T cells is the way their receptors recognize and bind to the antigen. B cells' antigen receptors directly recognize the native antigen that either has been secreted by the pathogen or is expressed on its surface. B cells eventually differentiate into effector plasma cells that secrete antibodies that bind to and neutralize these antigens and pathogens. In contrast, T cell receptors recognize antigens that have been processed, partly degraded, and displayed as peptides bound to proteins on antigen-presenting cells' surface. The main source of the antigens recognized by T cells is cells infected with pathogens, commonly a virus. In this case, the antigen that is recognized by the effector T cells is derived from within the infected cell. Importantly, the T cell receptor will only recognize antigen-derived peptides when these are bound to particular cell-surface glycoproteins (major histocompatibility complex/MHC complex).

T lymphocytes have a specialized defense system that has the ability to recognize peptide fragments of intracellular pathogens or invaders [9,10]. T lymphocytes have two co-receptors for bounding to the correct antigen, CD8 and CD4. CD8 is carried by cytotoxicT cells, and CD8T cells selectively recognize peptides bounding to MHC class I molecules [9,13]. The function of MHC class I molecules is to fight against virus infection by collecting peptides produce in the cytosol and deliver the peptide to the cell surface. The strength of binding between CD8 and MHC class I molecule depends on the glycosylation state of CD8 and the numbers of sialic acid residues in the CD8 carbohydrate structures. Increasing sialic acid residues decrease the strength of the interaction and affect to modulation of antigen recognition. CD4 is carried by helperT cells that are involved in the activation of antigen. CD4T cells

recognize peptides presented by MHC class II molecules. MHC class II molecules can be found on B lymphocytes, dendritic cells, and macrophages. The binding of CD4T cells to MHC class II molecules on B cells stimulates antibody production from B cells. The bounding on macrophages activates these cells to destroy the pathogens in their vehicles.

T lymphocyte proliferation assay

T cells have more complexity to characterize than B cells because T cells contain many different classes with different functions [9]. Cell-surface of lymphocytes express differentially to detect specific antibodies. For instance, T cells contain receptors that can be detected with anti-CD3 antibodies in the human peripheral. Then T-cells split into basis expression of co-receptor proteins which α:β T cells can be distinguished using anti-CD4 antibodies and anti-CD8 antibodies while γ:δ T cells are lack of CD4 and CD8. The expression of the cell-surface protein can be detected with specific antibodies, and it can also be labelled with a fluorescent dye [14,15]. One of the assays that has the ability to measure them is flow cytometry assay [9,16,17]. Flow cytometry has been used for cell investigation, including whole cells, cellular constituents, and T cell functional studies in qualitative and quantitative experiments. Cell proliferation is one of the studies of T cell proliferation. Flow cytometry is equipped with a fluorescence-activated cell sorter (FACS) to analyze separated cells.

Flow cytometer is a technique that essentially applies light scattering and fluorescence measurement for separating and or analyzing cells [16,17]. It is, specifically, used for identifying biological particles. The flow cytometer has a fundamental system such as a fluidic system for transporting cell particles; illumination system for interrogating the particles; an optical and electronics system (detectors) for handling, collecting, and translating the particles; and data storage and computer control system for interpreting, collecting and processing the data.

Cells analyzed with flow cytometry are illuminated in order to emit fluorescence and scattered light. Beforehand, the cell is pre-labelled with an antibody of interest and further conjugated with a fluorescent dye. For example, in experiment setup, carboxyfluorescein succinimidyl ester (CFSE) is used as a robust and long-lived cell dye [18]. It can cross the plasma membrane cell in the diacetylated form of the dye that is carboxyfluorescein diacetate

succinimidyl ester (CFDA, SE). After entering the cell, CFDA enzymatically will transform to fluorescent form (CFSE) by cleavage the acetate from CFDA. Afterwards, the amine-reactive succinimidyl side chain from CFSE reacts quickly with protein in the cell and subsequently label a population of cells up to eight divisions. These process is depicted in **Figure 2.4.1** This dye can be used for both *in vivo* and *in vitro* experiments. Cell labelling also can be done with specific monoclonal antibodies that are already pre-conjugated with fluorescent dye [16].

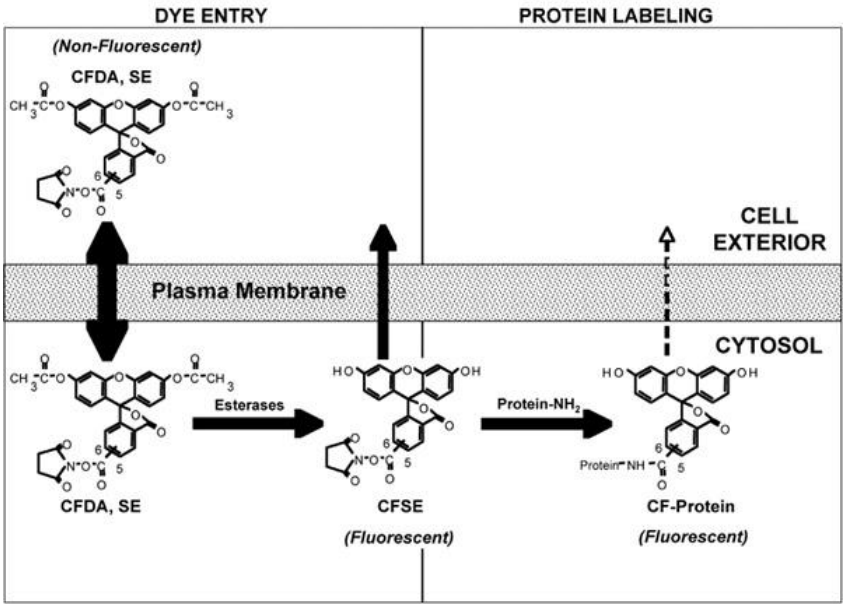

Figure 2.4.1. Illustration of CFSE dye work and label the cell, adopted from [18].

A mixture of labelled cells blend with a volume of saline solution in a flow cytometer; this cell suspension stream is positioned using hydrodynamic focusing with a sheath fluid [16,17]. A single cell passes through sequentially into the laser beam at thousands of cells per second. Then, the fluorophore of labelled-cell get excited and emit fluorescence and or scattered light at particular wavelength then it will be detected by flow cytometer detectors. The light is thus scattered and emitted in all directions (360°), however forward scattered light and the light scattered at 90° are important to generate information of the cell (**Figure 2.4.2 A**). Forward scatter light measures at narrow angles and provides fundamental cell features like the cell dimension, bigger cell will be detected with higher intensity of the forward scatter light. Side scatter light is the result of refracted and reflected light that is scattered at 90° to the incident

beam. Side scatter can identify granularity and membrane topographies of the cell. Forward and side scatter lights correlation can distinguish the cellular debris. Combining these two signals increases dissimilar populations within the same sample-based on size, granularity, and cell surface topography.

Flow cytometry-based experiment has been applied for determining cell apoptosis and necrosis [19]. Since flow cytometry has been established as the fundamental of the apoptotic cell cascade, most apoptosis cases can be distinguished from necrosis by increasing or decreasing forward and side scatter lights from the initial to the final stage of apoptosis. Both apoptosis and necrosis cell-surfaces become exposed to phosphatidylserine. The cell membrane of the initial stage of apoptosis is undamaged compared to the cell membrane of necrosis. In another case, phosphatidylserine has a high affinity to a Ca^{2+}-dependent phospholipid-binding protein, Annexin V [20]. The binding between annexin V and cell surface is indicated as apoptosis that needs a conjugated dye to establish cohesion of the cell membrane. Annexin V binding is labelled with fluorescein isothiocyanate (FITC), which gives green fluorescence signal. Propidium iodide (PI) dye is conjunction with Annexin V can discriminate between intact cells ($FITC^-/PI^-$), apoptotic ($FITC^+/PI^-$), and necrotic cells ($FITC^+/PI^+$). The PI negative ion gives red fluorescence exhibited by Annexin V-$FITC^+/PI^-$ (apoptotic cells) [11,12]. PI is a DNA dye that stains nucleic acid as soon as it passes through cell membrane. Because of the decreasing integrity of membrane cells in the late stage of apoptosis and necrosis, thus PI can easily cross membrane cell. Modification of annexin V and propidium iodide can increase the accuracy of cell death assessment because of the staining of RNA within the cytoplasmic compartment [21].

Analysis data are started by sorting the cell based on user-specification parameters [16,17]. Then the FACS machine determines the cell by an electrical charge. Positively charged cells are collected by a negatively charged plate, and vice versa. The measured data from the flow cytometer is converted into digital data, then interpreted by a computer. Better hardware components, reagents, and software data analysis contribute to the simplification of flow cytometry-analysis [16]. The flow cytometry's data can be represented in histograms (one dimensional/1D) and dot-plots (two-dimensional histogram/2D). A histogram displays a single parameter, e.g. size, granularity, and fluorescence intensity (**Figure 2.4.2 B**). Dot-plots can present two-, three-, or multi-parameters of each cell i.e. forward scatter vs. side scatter in two

dimensional (**Figure 2.4.2 C**). In the 2D histogram of side scatter and forward scatter, the data is plotted into four quadrants that describe lower and higher intensity of side and forward scatter lights in each quadrant. Data analysis of flow cytometry is usually specific to experimental objectives. The current FACS technology has the ability to measure 18 different fluorescent dyes simultaneously, but the fluorescent dyes have to be pre-conjugated to the antibodies [22].

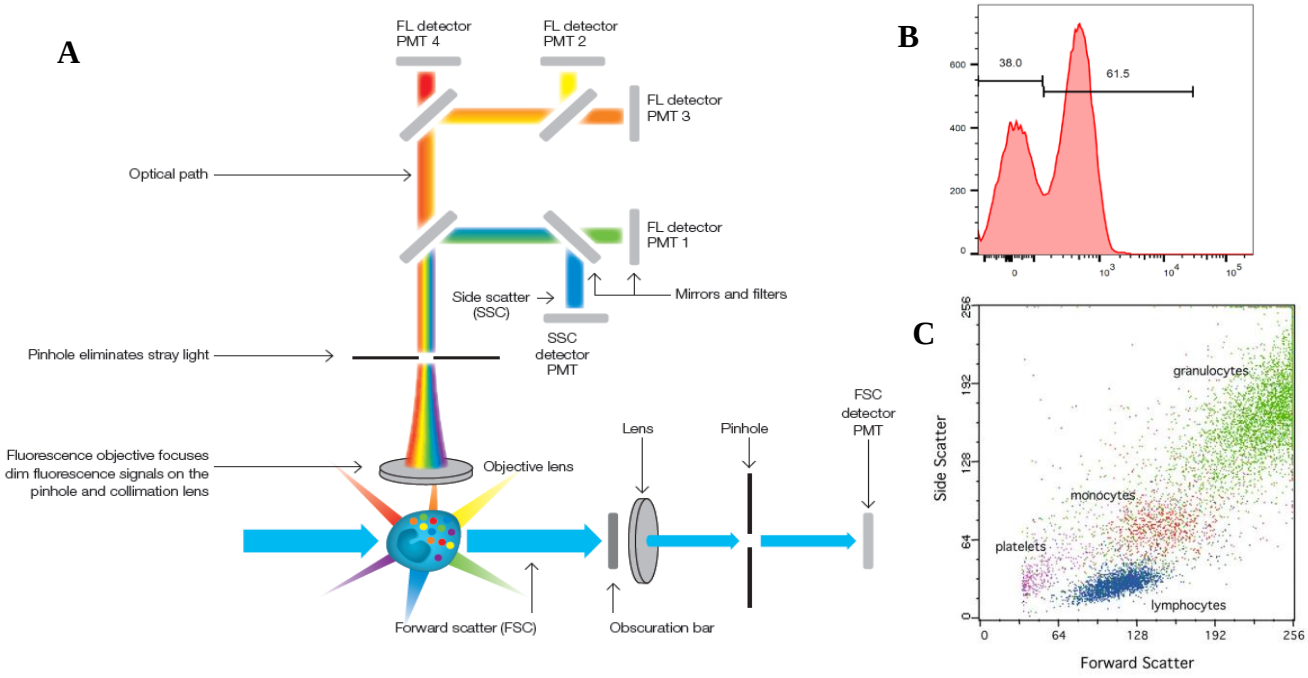

Figure 2.4.2. A. Schematic of flow cytometry setup, FL=fluorescence, PMT=photomultiplier tube, SSC=side scatter, FCS=forward scatter, blue arrow=light path **B**. Example of a one-dimensional histogram of cells within the lymphocyte gate, **C**. Example of dot plot of forward versus side scatter (figures adapted from [16,23]).

References

1. Cooper, G. S., Bynum, M. L. K., and Somers, E. C. Recent insights in the epidemiology of autoimmune disease: improved prevalence estimates and understanding of clustering of diseases. *J. Autoimmun*. 2009. 33, 197-207.
2. Lerner, A., Jeremias, P., and Matthias, T. The world incidence and prevalence of autoimmune disease is increasing. Int. *J. Celiac Dis*. 2015. 3, 151-155.
3. Brunton, L. L., Lazo, J. S., and Parker, K. L. (Editor). Goodman and Gilman's: The Pharmacological Basis of Therapeutics 11st Ed. Krensky, A. M., Vincenti, F., and Bennett, W. M. Chapter 52, Immunosuppressants, Tolerogens, and Immunostimulants. McGraw-Hill. USA. 2006. p. 1406. DOI: 10.1036/0071422803
4. Wiseman, AC. Immunosuppression medications. *Clin. J. Am. Soc. Nephrol*. 2016. 112), 332-343.
5. Lallana, E. C., and Fadul, C. E. Toxicities of immunosuppressive treatment of autoimmune neurologic diseases. *Curr. Neuropharmacol*. 2011. 9, 468-477.

6. Reinhardt, J. K., Klemd, A. M., Danton, O., Mieri, M. D., Smiesko, M., Huber, R., Bürgi, T., Gründemann, C., and Hamburger, M. Sesquiterpene lactones from *Artemisia argyi:* absolute configuration and immunosuppressant activity. *J. Nat. Prod*. 2019. 82, 1424-1433.
7. Zimmermann-Klemd, A. M., Reinhardt, J. K., Morath, A., Schamel, W. W., Steinberger, P., Leitner, J., Huber, R., Hamburger, M., and Gründemann, C. Immunosuppressive activity of *Artemisia argyi* extract and isolated compounds. *Front. Pharmacol*. 2020. 11, 1-13.
8. Potterat, O., and Hamburger, M. Combined use of extract library and HPLC-based activity profiling for lead discovery: potential, challenge, and practical considerations. *Planta Med*. 2014. 80, 1171-1181.
9. Murphy, K. Janeway's Immunobiology 8th Ed. 2012. Garland Science, Taylor & Francis Group. USA. p2-16, 28, 32-33, 148-151, 611-612-653, 767-770.
10. Kumar, B. V., Connors, T. J., and Farber, D. L. Human T cell development, localization, and function throughout life. *Immunity*. 2018, 48, 202-213.
11. Rabb, H. The T cell as a bridge between innate and adaptive immune systems: implications for the kidney. *Kidney Int.* 2002. 61, 1935-1946.
12. Chen, L., and Flies, D. B. Molecular mechanisms of T cell co-stimulation and co-inhibition. *Nat. Rev. Immunol.* 2013. 13, 227-242.
13. Koretzky, G. A. Multiple roles of CD4 and CD8 in T cell activation. *J. immunol.* 2010. 185, 2643-2644.
14. Alonso-Camino, V., Sanchez-Martin, D., Compte, M., Sanz, L., and Alvarez-Vallina, L. Lymphocyte display: a novel antibody selection platform based on T cell activation. *PloSOne*. 2009. 4, e7174.
15. Azarsiz, E., Karaca, N., Ergun, B., Durmuscan, M., Kutukculer, N., and Aksu, G. In vitro T lymphocyte proliferation by carboxyfluorescein diacetate succinimidyl ester method is helpful in diagnosing and managing primary immunodeficiencies. *J. Clin. Lab. Anal.* 2017. 32, e22216.
16. Nijkamp, F. P., and Parnham, M. J. (Editor). Principles of Immunopharmacology, 2nd. Dunne, J. F., and Maecker, H. T. Chapter B3, Flow Cytometry. Birkhauser Verlag. Germany. 2005. p.183-187.
17. Jaroszeski, M. J., and Radcliff, G. Fundamental of Flow cytometry. Molecular Biology. 1999. 11, page 37-54.
18. Quah, B. J. C., and Parish, C. R. The use of carboxyfluorescein diacetate succinimidyl ester (CFSE) to monitor lymphocyte proliferation. *J. Vis. Exp*. 2010. 44, e2259.
19. Vermes, I., Haanen, C., and Reutelingsperger, C. Flow cytometry of apoptotic cell death. *J of Immunological Methods*. 2000. 243, 167-190.
20. Vermes, I., Haanen, C., Steffens-Nakken, H., and Reutelingsperger, C. A novel assay for apoptosis flow cytometric detection of phosphatidylserine expression on early apoptotic cells using fluorescein labelled annexin V. *J. Immunol. Methods*. 1995. 184, 39-51.
21. Rieger, A. M., Nelsom, K. L., Konowalchuk, J. D., and Barreda, D. R. Modification annexin V/propidium iodide apoptosis assay for accurate assessment of cell death. *J. Vis. Exp.* 2011. 50, e2597.
22. Murphy, K., and Weaver, C. Janeway's Immunobiology 9th Ed. Garland Science, Taylor & Francis Group. USA. 2017. p.767-770.
23. Bio-Rad. Flow Cytometry Basic Guide. bio-rad-antibodies.com/flowguide.

3. RESULT AND DISCUSSION

3.1. HPLC-Based activity profiling for $GABA_A$ receptor modulators in *Murraya exotica*

Nova Syafni, Fahimeh Moradi-Afrapoli, Ombeline Danton, Anke Wilhelm, Marco Stadler, Steffen Hering, Olivier Potterat, and Matthias Hamburger

Natural Product Communication, 14 (2019) 41-45, DOI:

https://doi.org/10.1177/1934578X1901400112

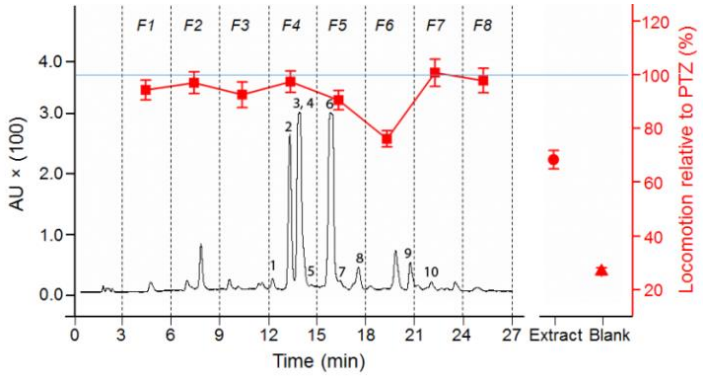

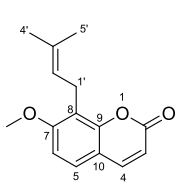

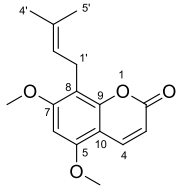

HPLC-based activity profiling utilizing a zebrafish-larvae locomotor activity assay has enabled the localization of active compounds for $GABA_A$ receptor modulators. Osthol (**9**) was identified as the main active compound. Osthol (**9**) and its related structural compound (coumurrayin, **10**) were tested in the *Xenopus oocyte* assay. Compound **9** potentiated $GABA_A$-induced chloride currents by 487 ± 42%, with an EC_50 of 46 ± 10 μM, while **10** showed negligible effects on chloride currents. Both compounds showed favourability for oral bioavailability and BBB permeability based on *in silico* evaluation of physicochemical properties.

Extraction of plant material for isolation, isolation of all compounds, recording and elucidating all isolated compounds, in silico calculation on ACDLabs/Percepta, writing the manuscript were my contributions to this publication.

Nova Syafni

NPC Natural Product Communications

2019
Vol. 14
No. 1
41 - 45

HPLC-Based Activity Profiling for $GABA_A$ Receptor Modulators in *Murraya exotica*

Nova Syafni[a,b], Fahimeh Moradi-Afrapoli[a], Ombeline Danton[a], Anke Wilhelm[c], Marco Stadler[d], Steffen Hering[d], Olivier Potterat[a] and Matthias Hamburger[a*]

[a]*Pharmaceutical Biology, University of Basel, Klingelbergstrasse 50, 4056 Basel, Switzerland*

[b]*Faculty of Pharmacy/Sumatran Biota Laboratory, Andalas University, 25163 Padang, West Sumatra, Indonesia*

[c]*Faculty of Natural and Agricultural Sciences, University of the Free State, 9300 Bloemfontein, Republic of South Africa*

[d]*Department of Pharmacology and Toxicology, University of Vienna, Althanstrasse 14, 1090 Vienna, Austria*

matthias.hamburger@unibas.ch

Received: August 31st, 2018; Accepted: October 17th, 2018

A dichloromethane extract from twigs and leaves of *Murraya exotica* produced allosteric potentiation of gamma aminobutyric acid (GABA) induced chloride currents in a microelectrode assay in *Xenopus laevis* oocytes expressing GABA receptors of α_1, β_2, γ_{2s} subunit composition. The activity was tracked by HPLC-based activity profiling utilizing a zebrafish locomotor activity assay. Osthol (**9**) was identified as the main active compound. In addition, five other coumarins and four flavonols were identified. Osthol (**9**) and structurally related coumurrayin (**10**) were tested in the *Xenopus* oocyte assay. Compound **9** potentiated $GABA_A$-induced chloride currents by 487 ± 42%, with an EC_{50} of 46 ± 10 μM, while **10** showed negligible effects on chloride currents. *In silico* evaluation of physicochemical properties showed that **9** and **10** had properties that are favorable for oral bioavailability and BBB permeability.

Keywords: *Murraya exotica*, $GABA_A$ receptor modulation, Zebrafish larvae, *Xenopus laevis* oocyte, HPLC-based activity profiling, Osthol.

Ionotropic gamma aminobutyric acid ($GABA_A$) receptors are important inhibitory neurotransmitter receptors in the central nervous system (CNS) [1]. Human $GABA_A$ receptors are heteropentameric proteins with numerous combinations of 19 different subunits ($\alpha_{1\text{-}6}$, $\beta_{1\text{-}3}$, $\gamma_{1\text{-}3}$, δ, π, ε, θ, and $\rho_{1\text{-}3}$) [2]. The most abundant $GABA_A$ receptor subtype in the brain is composed of 2 α_1, 2 β_2 and 1 γ_2 subunits [3]. $GABA_A$ receptors possess binding sites for the endogenous neurotransmitter GABA, and an allosteric binding site (benzodiazepine binding site) where drugs such as benzodiazepines and other compounds interact and thereby potentiate the effects of the neurotransmitter. Also, there is evidence for additional allosteric binding sites [4]. Currently used benzodiazepines and non-benzodiazepines (e.g. zolpidem) lack of $GABA_A$ receptor subtype selectivity and, therefore, possess a number of adverse effects such as sedation and addiction [1,4]. There is thus a need for new allosteric $GABA_A$ receptor modulators with subtype selectivity and ideally novel binding modes.

A structurally diverse range of natural products are known to interact with $GABA_A$ receptors in various ways, as orthosteric agonists (e.g. muscimol), as orthosteric antagonists (e.g. bicuculline), as non-competitive channel blockers (e.g. picrotoxin), or as allosteric agonists at the benzodiazepine binding site (e.g. valerenic acid) [5]. Compounds such as piperine interact with a benzodiazepine-independent allosteric binding site [6]. Given the need for novel chemotypes of $GABA_A$ receptor modulators, and considering the structural diversity and uniqueness of natural products as compared to synthetic drugs, we screened an in-house library of plant extracts for allosteric modulation of human $GABA_A$ receptors ($\alpha_1\beta_2\gamma_{2s}$ subunit composition) expressed in *Xenopus laevis* oocytes [7]. A dichloromethane extract from leaves and twigs of *Murraya exotica* L. (Rutaceae) enhanced the $GABA_A$-induced chloride ion current (I_{GABA}) by 102 % when tested at 100 μg/mL. The activity was confirmed in a larval zebrafish locomotor assay [8]. The maximal tolerable concentration (MTC) of the extract was determined, and the MTC (20 μg/mL) used as the highest test concentration. Lowering of pentylenetetrazol (PTZ)-induced larval locomotion was recorded at 5, 10, and 20 μg/mL of extract.

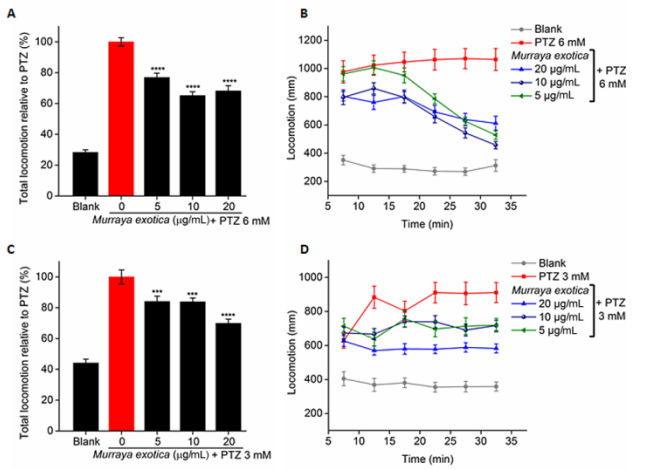

Figure 1: PTZ-induced locomotor activity of zebrafish larvae pretreated for 3 h with a dichloromethane extract of *M. exotica* at concentrations of 5, 10 and 20 μg/mL. **A**) Total locomotion (total distance travelled) in 25 min relative to PTZ (6 mM, red bar). Recording of locomotion started 5 min after addition of PTZ; **B**) Distance travelled by larvae during 5-min intervals of the observation period (PTZ 6 mM); **C**) Total locomotion (total distance travelled) in 25 min relative to PTZ (3 mM, red bar); **D**) Distance travelled by larvae during 5-min intervals of the observation period (3 mM PTZ).

Total distance (in mm) travelled by the larvae within 25 min (5 to 30 min after exposure of larvae to 6 mM PTZ) was recorded and compared with that of the PTZ-only group (Figure 1A). The extract lowered PTZ-induced locomotion in a concentration-dependent manner. At the highest concentration of 20 μg/mL locomotion was 68.2 ± 3.4% of the PTZ-only group (red bar). The positive control

diazepam (4 μM) lowered the larval locomotion to 72.0 ± 2.4%. Patterns of larval movement were visualized by plotting the distance travelled from 5 to 30 min after exposure to 6 mM PTZ, whereby 5-min intervals were recorded (Figure 1B). The assay was also performed with 3 mM PTZ to ensure that lowering of larval locomotion in the later phases of observation was not due to toxicity (Figure 1C and 1D) [8]. The extract thus lowered PTZ-provoked locomotion over the entire tracking period [9]. Given that zebrafish larvae used in the assay (7 days postfertilization, dpf) possess a functional blood-brain barrier (BBB) [10,11], one could thus assume that the activity seen in the initial *Xenopus* oocyte assay was due to BBB permeable compounds with drug-like properties [12,13,14]. As a next step, HPLC-based activity profiling of the extract was performed with the aid of the larval zebrafish locomotor assay [8]. The HPLC chromatogram recorded at 315 nm and the corresponding activity profile are shown in Figure 2. A decrease of larval locomotion was found for fraction F6 (18 to 21 min).

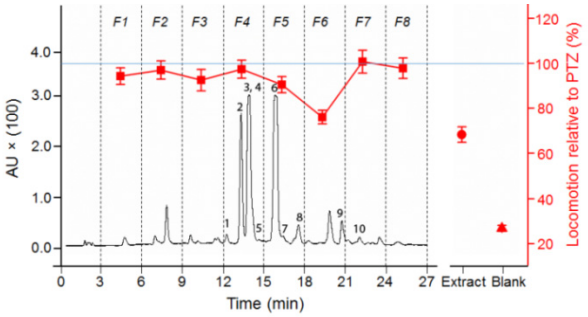

Figure 2: HPLC-based activity profiling of the extract. Separation of 360 μg of extract on an analytical HPLC column was monitored at 315 nm. Eight micro-fractions (F1-F8) of 3 min each were collected (indicated with dashed lines). Lowering of PTZ-induced locomotor activity by micro-fractions is shown above (expressed as % activity relative to the PTZ-only group, n = 32). Locomotor activity after treatment with extract and blank is shown to the right of the chromatogram. Peak numbering corresponds to compounds **1-10**.

The active time-window showed two main peaks (t_R = 19.9 min and t_R = 20.8 min). The latter was identified after preparative isolation as osthol (**9**). The earlier eluting peak was a mixture of several structurally related compounds which could not be purified due to the limited amount of material. However, the UV spectrum and NMR data of the mixture were indicative of coumarins [15]. In addition, compounds outside of the active time-window were isolated to obtain preliminary information on structural features responsible for activity/inactivity [6]. Five coumarins, osthenon (**1**), hainanmurpanin (**2**), meranzin (**4**), phebalosin (**6**), and coumurrayin (**10**), along with four flavonoids, 3,5,7,8,3',4',5'-hepta-methoxyflavone (**3**), 3,5,6,7,3',4',5'-heptamethoxyflavone (**5**), 3,5,6,7,8,3',4'-heptamethoxyflavone (**7**), and 3,5,6,7,8,3',4',5'-octamethoxyflavone (**8**) were purified and their structures unambiguously assigned by NMR and MS data, and by comparison with literature data [16-24] (Figure 3). Spectroscopic data of compounds are provided as Supporting Information.

Osthol (**9**) from the active time-window, and methoxy derivative **10** from the later eluting inactive fraction F7 were submitted to *in vitro* automated two-microelectrode voltage clamp assay on *Xenopus* oocytes expressing $\alpha_1\beta_2\gamma_{2s}$ receptors. Compound **9** showed considerable GABAergic activity (EC_{50} = 46 ± 10 μM, potentiation of I_{GABA} by 487 ± 42%), whereas **10** was inactive at concentrations up to 300 μM. The positive control diazepam (1 μM) enhanced I_{GABA} by 231.3 ± 22.6%. Osthol (**9**) had been recently identified in a screening of a compound library of natural coumarins as a positive allosteric $GABA_A$ receptor modulator targeting the benzodiazepine binding site [25].

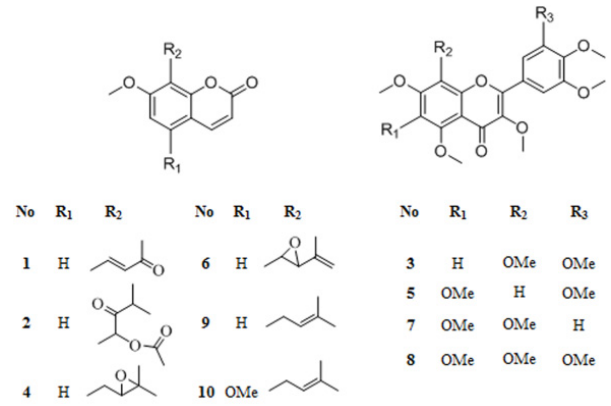

Figure 3: Structures of isolated compounds.

Important physicochemical and ADME properties as defined by Lipinski [12,13] and Veber [14] were calculated for **9** and **10** to possibly explain the lack of activity of **10** (Table 1). However, the data indicated that both compounds fulfilled criteria for oral bioavailability and permeability of the blood-brain-barrier (BBB). In the case of active osthol (**9**), BBB permeation was supported by the observed activity in the larval zebrafish assay. However, the lack of activity of **10**, as compared to active **9**, could not be explained by the pharmacophore model that has been proposed for coumarins [25].

As to polymethoxyflavones **3**, **5**, **7** and **8**, their lack of activity indirectly confirmed earlier findings that for simple natural flavones and flavonols the presence of free phenolic groups is required for interaction with ionotropic GABA receptors [26-28].

Experimental

General: Pentylenetetrazol (PTZ) (purity ≥ 98 %) was from Sigma-Aldrich, and diazepam (purity ≥ 98 %) was from Lipomed. HPLC-grade acetonitrile (Scharlau) and water (Barnstead EASY-pure II water purification system) were used for HPLC separations. HPLC solvents contained 0.1% formic acid (Scharlau) for analytical separations. DMSO (Scharlau) was used for dissolving the samples for HPLC analysis. Deuterated solvents for NMR were purchased from Armar Chemicals. Solvents used for extraction, column chromatography, centrifugal partition chromatography (CPC), and recrystallization were of technical grade (Romil Pure Chemistry) and were redistilled before use. Silica gel (63-200 μm, Merck) was used for column chromatography.

Table 1: *In silico* prediction of physicochemical and ADME properties.

Compound	QikProp (Schrödinger)							ACD/Percepta Platform (ACD/Labs)		
	MW[a]	donor HB[b]	accpt HB[c]	logP o/w[d]	PSA[e]	*rotor[f]	log BB[g]	Pe Caco-2 (cm/s)[h]	HIA[i]	PPB[j]
9	244.3	0	3.3	3.14	46.1	3	-0.28	2.44E-06	100%	95%
10	274.3	0	4.0	3.27	53.1	4	-0.37	2.44E-06	100%	94%

[a]Molecular weight (g/mol). [b]Hydrogen bond donors. [c]Hydrogen bond acceptors. [d]Octanol-water partition coefficient. [e]Polar surface area (Å). [f]Rotatable bonds. [g]Blood/brain partition coefficient. [h]Caco-2 permeability, Pe (cm/s). [i]Maximum achievable human intestinal absorption. [j]Plasma protein bound fraction.

Optical rotation was measured with a P -2000 digital polarimeter (Jasco) equipped with a sodium lamp (589 nm) and a 10 cm temperature-controlled microcell.

NMR spectra were recorded with a Bruker Avance III spectrometer operating at 500.13 MHz for ^1H and 125.77 MHz for ^{13}C. ^1H NMR experiments and 2D homonuclear and heteronuclear NMR spectra were measured with a 1 mm TXI probe at 18°C. ^{13}C NMR spectra were obtained in 3 or 5 mm tubes at 23°C. Data were analyzed using ACD/Spectrus Processor 2017.1.3. HPLC-PDA-MS analyses were performed with a Shimadzu LC-PDA-MS/MS instrument consisting of a degasser, quaternary pump (LC-20AD), column oven (CTO-20AC), PDA detector (SPD-M20A), and triple quadrupole mass spectrometer (LCMS-8030), connected via a T-split to an ELSD 3300 detector (Alltech). A SunFire C18 column (3.5 μm, 3.0 x 150 mm) equipped with a guard column (3.0 x 10 mm) (Waters) was used for analytical separations. Data acquisition and processing were performed using lab solution software (Shimadzu).

Centrifugal partition chromatography (CPC) was performed on an Armen Instrument with coil volume 100 mL connected to a pump model 210 (Varian), 218 UV detector (Varian) and a fraction collector model 704 (Varian).

Flash chromatography was carried out on a Sepacore MPLC system consisting of two C-605 pumps, C-635 UV detector, and C-660 fraction collector (all Büchi), or with a Puriflash 4100 system (Interchim). A glass column (70 x 460 mm), and prepacked silica gel cartridges (Interchim) 12 g (50 μm), 40 g (15 μm) and 125 g (30 μm) were used.

Semi-preparative HPLC was carried out with a Waters 2690 instrument consisting of a degasser, binary high pressure mixing pump, column oven, and a Waters 996 photodiode array detector. A SunFire Prep C18 column (5 μm, 10 x 150 mm) equipped with a guard column (10 x 10 mm) (Waters) was used for separation.

Evaporation of micro-fractions was done with a Genevac EZ-2 plus vacuum centrifuge (Avantec).

The movement of zebrafish larvae was tracked with DanioVision observation chamber equipped with an IR sensitive camera and a temperature controller unit (Noldus Information Technology). The locomotor activity was analyzed with EthoVision XT11 software (Noldus Information Technology).

***Plant Material*:** Dried leaves and twigs of *Murraya exotica* L. were purchased in October 2008 from the Juhuayuan Herbal Market in Kunming, Yunnan Province, and identified by Yunnan Baiyao from Group Co. LTD, Kunming, China. A voucher specimen has been deposited at the Division of Pharmaceutical Biology, University of Basel, under identification number 43553.

Two-microelectrode voltage clamp assay with Xenopus laevis oocytes: Recombinant $GABA_A$ receptors ($\alpha_1\beta_2\gamma_{2s}$) were expressed in *X. laevis* oocytes by cRNA injection, as previously described [28]. Two-microelectrode voltage clamp measurements were performed between day 1 and 5 after cRNA injection, using a TURBO TEC 03X amplifier (npi Electronic) at a holding potential of -70 mV. Data acquisition was with pCLAMP 10 software (Molecular Devices). Currents were low-pass filtered at 1 kHz and sampled at 3 kHz. The bath solution contained 90 mM NaCl, 1 mM KCl, 1 mM $MgCl_2$, 1 mM $CaCl_2$, and 5 mM HEPES (pH 7.4). Electrode filling solution contained 3 M KCl. Test solutions (100 μL) were applied to the oocytes at a speed of 200 μL/s by means of the Screening Tool automated fast perfusion system (npi Electronic). GABA EC_{4-6} was determined through a concentration-response experiment with 0.1 to 1 mM GABA solutions. Stock solutions of tested extract (10 mg/mL) and pure compounds (100 mM) in DMSO were diluted with a bath solution containing GABA EC_{4-6} to obtain appropriate working solutions according to a validated protocol. Enhancement of the I_{GABA} was defined as $(I_{GABA + Comp}/I_{GABA}) - 1$, where I(GABA + Comp) is the current response in the presence of a given compound, and I_{GABA} is the control of the GABA-induced chloride current. Data were analyzed using Origin 7.0 SR0 software (OriginLab Corporation) and are given as the mean ± SE of at least two oocytes from ≥ 2 batches. Diazepam (purity ≥ 98%; Sigma) was used as a positive control at 1 μM.

Zebrafish larvae locomotor activity model: Experiments were approved by the Kantonales Veterinaeramt Basel-Stadt (license number 1995 continuation; approval date 03 February, 2015), and conducted in accordance with EU directive 2011/63/EU. Wild-type zebrafish of the ABC × TU strain were kept under standard conditions [29]. Fertilized eggs were collected via natural spawning, and incubated at 28.5°C in E3 medium containing 5 mM NaCl, 0.17 mM KCl, 0.33 mM $CaCl_2$, and 0.33 mM $MgSO_4$ in water (0.5 mL methylene blue 0.05% w/v was added to 1 liter medium as a disinfectant, and pH was corrected to 7.4 by K_2CO_3 0.5 M). Stock solution of the extract (10 mg/mL in DMSO) was diluted with E3 medium to obtain the appropriate working solution. Toxicity assessments were performed prior to the activity screening. Larvae (6 dpf) were placed in 96-well plates (1 larva per well), and aliquots of 50 μL working solutions were spiked into each well to afford a final volume of 250 μL. Larvae (n = 12) were incubated with the extract at 50, 25, 12.5, and 6.25 μg/mL. Locomotor impairments, including loss of larval response after a light touch of the tail, loss of posture, body deformation, and death were monitored and compared with the blank (same number of untreated larvae) after 3, 6, and 24 h. After the first toxicity assessment, intermediate concentrations were tested to accurately define the MTC at which not more than 2 of 12 larvae were impaired. For activity screening, MTC was considered as the highest test concentration. The lower concentrations were obtained by serial dilutions. Larvae (7dpf, n = 16) were incubated for 3 h at 28.5°C with the test solutions. Then, 20 μL of PTZ solution were added to each well to reach a final test concentration (6 mM or 3 mM). Microplates were placed in the movement-tracking chamber. Tracking of the larval movements started after 5 min, and continued until 30 min. Total distance travelled by the larvae within 25 min (between min 5 and 30) was considered as the total locomotor activity. Patterns of larval movements were obtained by plotting movement vs. time, whereby total distance traveled was calculated over 5-min intervals. A PTZ-only group (16 larvae treated only with PTZ) and a blank group (16 larvae maintained only in the medium) were placed in each microplate. Diazepam (4 μM) was used as the positive control. All tests were repeated in two independent experiments (n = 32). Statistical analyses were performed with IBM SPSS Statistics version 20 using the Kruskal-Wallis test followed by the Mann-Whitney test to determine significant differences between treatment groups and the PTZ only group.

Micro-fractionation for activity profiling: HPLC-based activity profiling of dichloromethane extract *M. exotica* was performed with a zebrafish larvae locomotor activity assay as previously reported [7,8,30] with minor modifications. Micro-fractionation was carried out in two identical repeats whereby in each of those, 36 μL extract (10 mg/mL in DMSO) was injected onto an analytical HPLC column (SunFire C18, 3.5 μm, 3 x 150 mm) eluted with H_2O +

0.1% formic acid (A), and MeCN + 0.1% formic acid (B); 20→90% B (0-24 min), 100% B (24-29 min). The flow rate was 0.4 mL/min. Three-min micro-fractions between t_R 3 and 27 min were collected into a 96-well deep-well plate. Corresponding micro-fractions from the two injections were combined. After drying the plate in an EZ-2 Plus evaporator (GeneVac), micro-fractions in the wells were dissolved with 11.25 μL of DMSO, and the plate was shaken at 1400 rpm for 30 min for complete dissolution (stock solutions). Afterwards, E3 medium was added to each stock solution up to a final volume of 900 μL. Corresponding micro-fractions from two injections were combined (working solutions). Aliquots of 50 μL of working solutions were added to each well of a 96-well microliter plate containing one zebrafish larva and 200 μL of E3 medium (final DMSO concentration of 0.5%). Sixteen larvae were used for testing of each micro-fraction, and the activity was assessed in duplicate experiments (n = 32).

Extraction and isolation: Powdered *M. exotica* leaves and twigs (135 g) were extracted with 2 x 300 mL DCM for 24 h each under stirring at room temperature. The extracts were combined and evaporated under reduced pressure to afford 22.5 g of dry extract. The extract was chromatographed on a silica gel column (70 x 460 mm) at a flow rate of 25 mL/min, using a step gradient (*n*-hexane, *n*-hexane/EtOAc, EtOAc, EtOAc/MeOH and MeOH). A total of 43 fractions were collected. Compounds detected in the active time window of the HPLC activity profiling were localized in fractions 13 (90.1 mg) and 14 (160.0 mg). Both fractions were further separated on a silica gel cartridge 40 g [*n*-hexane/EtOAc (9:1, 0.9 L), (9:2, 0.3 L) at a flow rate of 10 mL/min]. Compound **9** (16.8 mg) was eluted between 40-53 min, and compound **10** (5.9 mg) between 60-77 min. Both compounds were recrystallized from *n*-hexane/chloroform.

Fractions 19, 20-22, 28, and 35-37 were recrystallized in hexane-chloroform to afford **4** (43.0 mg), **6** (100.0 mg), **5** (6.0 mg) and **3** (90.0 mg), respectively.

Fractions 18 (252.0 mg), 24 (275.0 mg), and 25 (347.0 mg) were further separated by CPC with *n*-hexane/EtOAc/MeOH/water (5:1:7:5, *v/v/v/v*) in ascending mode, with a switch to descending mode towards the end of the separation. The flow rate was 5 mL/min, loading speed was 500 rpm, and eluting speed 2000 rpm. The separation time was 120, 60, and 78 min, respectively, corresponding to 75, 32 and 32 min in ascending mode, followed by 45, 28 and 46 min in descending mode, respectively. Fractions were collected every 2 min. The separation was monitored by TLC and HPLC-PDA-MS analysis of the fractions.

In the case of fraction 18, CPC fractions collected between 30 and 76 min were combined and further separated by semi-preparative RP-HPLC [H_2O + 0.1% formic acid (A), MeCN + 0.1% formic acid (B); 50→68% B (0-24 min), 100% B (24-29 min); flow rate 4 mL/min], to afford compounds **1** (0.3 mg, t_R 12.0 min) and **10** (0.2 mg, t_R 16.7 min).

For fraction 24, CPC fractions were collected from 32 to 34 min (38.9 mg), and from 34 to 38 min (15.8 mg). The first fraction was further separated by flash chromatography on a silica gel cartridge (12 g). A gradient of EtOAc/*n*-hexane (20% to 40% EtOAc in 130 min) was used at a flow rate of 8 mL/min. Compound **2** (4.0 mg) was recrystallized from *n*-hexane/chloroform. Purification of the second fraction by semi-preparative RP-HPLC [H_2O + 0.1% formic acid (A), MeCN + 0.1% formic acid (B); 20→90% B (0-20 min), 100% B (20-25 min); flow rate 4 mL/min] afforded compound **8** (1.0 mg, t_R 14.1 min).

For fraction 25, CPC fractions were collected from 52 to 54 min. The residue (9.2 mg) was separated by semi-preparative RP-HPLC [H_2O + 0.1% formic acid (A), MeCN + 0.1% formic acid (B); 50→60% B (0-24 min), 100% B (24-29 min); flow rate 4 mL/min] to afford compound **7** (0.2 mg, t_R 7.6 min).

In silico predictions: Physicochemical and ADME properties for **9** and **10** were calculated with QikProp (QikProp, version 4.6, Schrödinger, LLC, 2015) and Percepta (ACD/Labs, ACD/Percepta Platform, version 12.10, 2012). These software packages use trained QSAR models for calculating predefined physicochemical descriptors for drug-likeness (according to Lipinski's rule of five [12,13] and Veber's rule [14]) and for determination of properties that are relevant from a pharmacokinetic viewpoint (e.g. plasma protein binding, Caco-2 permeability, and Log BB)

Supplementary data: Spectroscopic data of compounds **1**-**10**, including ^{1}H NMR data and ^{13}C NMR data (extracted from HSQC-DEPT and HMBC spectra for compounds **1**,**2**,**4**,**7**,**9**, and **10**)

Acknowledgments – We thank Dr. Teresa Faleschini and Orlando Fertig for technical assistance, and Dr. Heinz Georg Belting, Biozentrum, University of Basel, for access to the zebrafish facility. Dr. Martin Smieško, Division of Molecular Modeling, and Dr. Mouhssin Oufir, Division of Pharmaceutical Biology, University of Basel, are gratefully acknowledged for the *in silico* calculations. Financial support for N.S. was provided by a scholarship from the Indonesia Endowment Fund for Education (LPDP).

References

[1] Olsen RW, Sieghart W. (**2008**) International Union of Pharmacology. LXX. Subtypes of γ-aminobutyric acid$_A$ receptors: classification on the basis of subunit composition, pharmacology, and function. Update. *Pharmacological Reviews*, ***60***, 243-260.

[2] Simon J, Wakimoto H, Fujita N, Lalande M, Barnard EA. (**2004**) Analysis of the set of GABA$_A$ receptor genes in the human genome. *The Journal of Biological Chemistry*, ***40***, 41422-41435.

[3] Uusi-Oukari M, Korpi ER. (**2010**) Regulation of GABA$_A$ receptor subunit expression by pharmacological agents. *Pharmacological Review*, ***62***, 97-135.

[4] Sieghart W. (**2015**) Allosteric modulation of GABA$_A$ receptors via multiple drug-binding sites. *Advances in Pharmacology*, ***23***, 53-96.

[5] Khom S, Baburin I, Timin E, Hohaus A, Trauner G, Kopp B, Hering S. (**2007**) Valerenic acid potentiates and inhibits GABA$_A$ receptors: molecular mechanism and subunit specificity. *Neuropharmacology*, ***53,*** 178-187.

[6] Zaugg J, Baburin I, Strommer B, Kim H-J, Hering S, Hamburger M. (**2010**) HPLC-based activity profiling: discovery of piperine as a positive GABA$_A$ receptor modulator targeting a benzodiazepine-independent binding site. *Journal of Natural Products*, ***73***, 185-191.

[7] Kim HJ, Baburin I, Khom S, Hering S, Hamburger M. (**2008**) HPLC-Based activity profiling approach for the discovery of GABA$_A$ receptor ligands using an automated two microelectrode voltage clamp assay on *Xenopus oocytes*. *Planta Medica*, ***74***, 521-526.

[8] Moradi-Afrapoli F, Ebrahimi SN, Smiesko M, Hamburger M. (**2017**) HPLC-based activity profiling for GABA$_A$ modulators in extract: Validation of an approach utilizing a larval zebrafish locomotor assay. *Journal of Natural Products*, ***80***, 1548-1557.

[9] Baraban SC, Taylor MR, Castro PA, Baier H. (**2005**) Pentylenetetrazole induced changes in zebrafish behavior, neural activity and c-fos expression. *Neuroscience*, ***131***, 759-768.

[10] Jeong J-Y, Kwon H-B, Ahn J-C, Kang D, Kwon S-H, Park JA, Kim K-W. (**2008**) Functional and developmental analysis of the blood-brain barrier in zebrafish. *Brain Research Bulletin*, ***75***, 619-628.
[11] Fleming A, Diekmann H, Goldsmith P. (**2013**) Functional characterization of the maturation of the blood-brain barrier in larval zebrafish. *Plos One*, ***8***, 1-12.
[12] Lipinski CA, Lombardo F, Dominiv BW, Feeney PJ. (**1997**) Experimental and computational approaches to estimate solubility and permeability in drug discovery and development settings. *Advanced Drug Delivery Reviews*, ***23***, 3-25.
[13] Lipinski CA, Lombardo F, Dominiv BW, Feeney PJ. (**2001**) Experimental and computational approaches to estimate solubility and permeability in drug discovery and development settings. *Advanced Drug Delivery Reviews*, ***46***, 3-26.
[14] Veber DF, Johnson SR, Cheng H-Y, Smith BR, Ward KW, Kopple KD. (**2002**) Molecular properties that influence the oral bioavailability of drug candidates. *Journal of Medicinal Chemistry*, ***45***, 2615-2623.
[15] Murray RDH, Méndez J, Brown SA. (**1982**) Identification and structural elucidation. In The Natural Coumarins. John Wiley & Sons Ltd, Bristol, England, 22–38.
[16] Ito C, Furukawa H. (**1987**) Constituents of *Murraya exotica* L. Structure elucidation of new coumarins. *Chemical and Pharmaceutical Bulletin*, ***35***, 4277-4285.
[17] Imai F, Kinoshita T, Sankawa U. (**1989)** Constituents of leaves of *Murraya paniculata* collected in Taiwan. *Chemical and Pharmaceutical Bulletin*, ***37***, 358-362.
[18] Yan R, Shen J, Liu X, Zou Y, Xu X. (**2018**) Preparative isolation and purification of hainanmurpanin, meranzin, and phebalosin from leaves of *Murraya exotica* L. using supercritical fluid extraction combined with consecutive high-speed countercurrent chromatography. *Journal of Separation Science*, ***41,*** 2092-2101.
[19] Joshi BS, Kamat VN. (**1970**) Isolation of 3,3',4',5,5',7,8-heptamethoxyflavone from *Murraya exotica. Phytochemistry*, ***9***, 889.
[20] Dreyer DL. (**1968**) Chemotaxonomy of the Rutaceae. IV. Constituents of *Murraya paniculata* (Linn.) Jack. *Journal of Organic Chemistry*, ***33***, 3574-3576.
[21] Ito C, Fujiwara K, Koizumi M, Furukawa H. (**1998**) Isolation and characterization of an antibacterial substance from *Citrus* plant. *Journal of the Chinese Chemical Society*, ***45***, 89-91.
[22] Machida K, Osawa K. (**1989**) On the flavonoid constituents from the peels of *Citrus hassaku* Hort. *ex* Tanaka. *Chemical and Pharmaceutical Bulletin*, ***37***, 1092-1094.
[23] Joshi BS, Kamat VN. (**1969**) Structure of exoticin, a flavone from the leaves of *Murraya exotica* Linn. *Indian Journal of Chemistry*, ***7***, 636.
[24] Ramstad E, Lin W-NC. (**1968**) Coumurrayin, a new coumarin from *Murraya paniculata* (L.) Jack. *Tetrahedron Letters*, ***7***, 811-813.
[25] Singhuber J, Baburin I, Ecker GE, Kopp B, Hering S. (**2011**) Insights into structure-activity relationship of $GABA_A$ receptor modulating coumarins and furanocoumarins. *European Journal of Pharmacology*, ***668***, 57-68.
[26] Hanrahan JR, Chebib M, Johnston GAR. (**2015**) Interactions of flavonoids with ionotropic GABA receptors. *Advances in Pharmacology*, ***72***, 189-200.
[27] Wasowski C, Marder M. (**2012**) Flavonoids as $GABA_A$ receptor ligands: the whole story? *Journal of Experimental Pharmacology*, ***4***, 9-24.
[28] Rueda DC, De Mieri M, Hering S, Hamburger M. (**2014**) HPLC-based activity profiling for $GABA_A$ receptor modulators in *Adenocarpus cincinnatus*. *Journal of Natural Products*, ***96***, 640-649.
[29] Westerfield M. (**2007**) A Guide for the laboratory use of zebrafish (*Danio rerio*). University of Oregon Press, Eugene, USA.
[30] Potterat O, Hamburger M. (**2013**) Concepts and technologies for tracking bioactive compounds in natural product extracts: generation of libraries, and hyphenation of analytical processes with bioassay. *Natural Product Reports*, ***30***, 546-564.

Natural Product Communications
2019
Volume 14, Number 1, Pages 41-45

HPLC-Based Activity Profiling for GABAA Receptor Modulators in *Murraya exotica*

Nova Syafni, Fahimeh Moradi-Afrapoli, Ombeline Danton, Anke Wilhelm, Marco Stadler, Steffen Hering, Olivier Potterat, and Matthias Hamburger

Supplementary data

SUPPORTING INFORMATION

HPLC-Based Activity Profiling for $GABA_A$ Receptor Modulators in *Murraya exotica*

Nova Syafni[a,b], Fahimeh Moradi-Afrapoli[a], Ombeline Danton[a], Anke Wilhelm[c], Marco Stadler[d], Steffen Hering[d], Olivier Potterat[a] and Matthias Hamburger[a]*

[a] *Pharmaceutical Biology, University of Basel, Klingelbergstrasse 50, 4056 Basel, Switzerland*
[b] *Faculty of Pharmacy/Sumatran Biota Laboratory, Andalas University, 25163 Padang, West Sumatra, Indonesia*
[c] *Faculty of Natural and Agricultural Sciences, University of Free State, 9300 Bloemfontein, Republic of South Africa*
[d] *Department of Pharmacology and Toxicology, University of Vienna, Althanstrasse 14, 1090 Vienna, Austria*

*Correspondence:
matthias.hamburger@unibas.ch
+41-61-267-1425. Fax: +41-61-267-1474.

7-Methoxy-8-[(1E-)-3-oxo-1-butenyl]-2H-1-benzopyran-2-one
(**Syn.: Osthenone**) (**1**)[b]
CAS Nr. 112789-90-9
$C_{14}H_{12}O_4$, LC-ESI-MS, *m/z* = 244.07

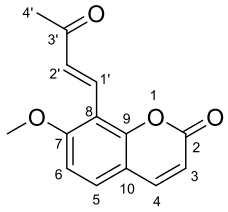

1

Table S1. NMR spectroscopic data (500 MHz, $CDCl_3$) of compound **1**

position	δ_C[a]	δ_H (*J* in Hz)
2	160.9, C	
3	113.4, CH	6.31, d (9.5)
4	143.2, CH	7.64, d (9.8)
5	129.9, CH	7.45, d (8.9)
6	107.6, CH	6.91, d (8.9)
7	161.6, C	
8	112.3, C	
9	154.0, C	
10	112.9, C	
1’	131.1, CH	7.99, d (16.5)
2’	132.3, CH	7.36, d (16.8)
3’	199.3, C	
4’	27.6, CH_3	2.44, s
7-OMe	56.2, CH_3	4.00, s

[a] ^{13}C chemical shifts deduced from HSQC and HMBC NMR spectra.
[b] δ_H reference data can be found in Ito C, Furukawa H.(**1987**) Constituents of *Murraya exotica* L. structure elucidation of new coumarins. *Chemical and Pharmaceutical Bulletin*. ***35***, 4277 - 4285.

(+) [1-(7-Methoxy-2-oxochromen-8-yl)-3-methyl-2-oxobutyl] acetate
(**Syn.: Hainanmurpanin**) (**2**)[b]
CAS Nr. 95360-22-8
$C_{16}H_{18}O_6$, LC-ESI-MS, *m/z* = 318.11
$[\alpha]^{25}_D$ = +96° (*c* 0.1, $CHCl_3$)

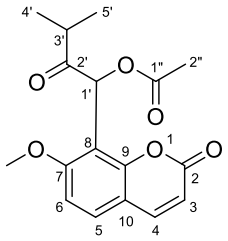

2

Table S2. NMR spectroscopic data (500 MHz, $CDCl_3$) of compound **2**

position	δ_C[a]	δ_H (*J* in Hz)
2	159.6, C	
3	113.5, CH	6.21, d (9.5)
4	143.3, CH	7.62, d (9.8)
5	130.2, CH	7.48, d (8.9)
6	108.0, CH	6.88, d (8.9)
7	160.8, C	
8	111.8, C	
9	153.6, C	
10	113.0, C	
1’	69.4, CH	6.93, s
2’	207.7, C	
3’	36.1, CH	2.80, m
4’	17.9, CH_3	0.99, d (6.7)
5’	18.9, CH_3	1.13, d (7.0)
1’’	169.5, C	
2’’	20.6, CH_3	2.11, s
7-OMe	56.4, CH_3	3.87, s

[a] ^{13}C chemical shifts deduced from HSQC and HMBC NMR spectra.
[b] δ_H reference data can be found in:

1. Imai F, Kinoshita T, Sankawa U. (**1989**) Constituents of the Leaves of *Murraya paniculata* Collected in Taiwan. *Chemical and Pharmaceutical Bulletin. **37***, 358-362.
2. Yan R, Shen J, Liu X, Zou Y, Xu X. (**2018**) Preparative isolation and purification of hainanmurpanin, meranzin, and phebalosin from leaves of *Murraya exotica* L. using supercritical fluid extraction combined with consecutive high-speed countercurrent chromatography. *Journal of Separation Science. **41***, 2092-2101.

3,5,7,8-Tetramethoxy-2-(3,4,5-trimethoxyphenyl)chromen-4-one
(**Syn.: 3,5,7,8,3‘,4‘,5‘-Heptamethoxyflavone/Hibiscetin heptamethyl ether**) (**3**)[b]
CAS Nr. 21634-52-6
$C_{22}H_{24}O_9$, LC-ESI-MS, *m/z* = 432.14

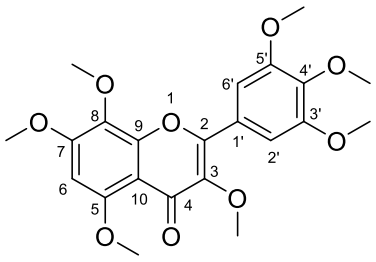

3

Table S3. NMR spectroscopic data (500 MHz, $CDCl_3$) of compound **3**

position	δ_C	δ_H (*J* in Hz)
2	151.9, C	
3	141.3, C	
4	174.3, C	
5	156.4, C	
6	92.2, CH	6.41, s
7	156.4, C	
8	130.8, C	
9	150.9, C	
10	109.2, C	
1’	126.1, C	
2’	105.6, CH	7.53, s
3’	153.1, C	
4’	139.9, C	
5’	153.1, C	
6’	105.6, CH	7.53, s
3-OMe	60.0, CH_3	3.91, s
5-OMe	56.5, CH_3	3.98, s
7-OMe	56.3, CH_3	3.99 , s
8-OMe	61.0, CH_3	3.92 [a], s
3’-OMe	56.1, CH_3	3.92 [a], s
4’-OMe	61.4, CH_3	3.93 [a], s
5’-OMe	56.1, CH_3	3.92 [a], s

[a] Overlapping signals.
[b] δ_H and δ_C reference data can be found in:

1. Joshi BS, Kamat VN. (**1970**) Short Communication: Isolation of 3, 3’, 4’, 5, 5’, 7, 8-Heptamethoxyflavone from *Murraya exotica*. *Phytochemistry*. ***9***, 889.
2. Ferracin RJ, das G. F. da Silva MF, Fernandes JB, Paulo C, Vieira PC. (**1998**) Flavonoids from the fruits of *Murraya paniculata*, *Phytochemistry*. ***47***, 393-396.

(-) 8-[(3,3-Dimethyloxiran-2-yl)methyl]-7-methoxychromen-2-one
(**Syn.: Meranzin**) (**4**)[c]
CAS Nr. 23971-42-8
$C_{15}H_{16}O_4$, LC-ESI-MS, *m/z* = 260.10
$[\alpha]^{25}_D$ = -69° (*c* 0.1, $CHCl_3$)

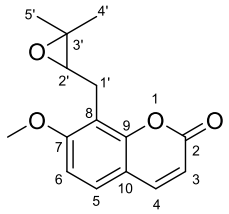

4

Table S4. NMR spectroscopic data (500 MHz, $CDCl_3$) of compound **4**

position	δ_C[a]	δ_H (*J* in Hz)
2	160.8, C	
3	112.9, CH	6.16, d (9.1)
4	143.6, CH	7.58, d (9.5)
5	127.1, CH	7.31, 1H, d, (8.5)
6	107.4, CH	6.82, d (8.5)
7	160.6, C	
8	114.1, C	
9	153.3, C	
10	113.0, C	
1’	22.4CH_2	3.15, dd (15.9, 8.2)
		2.94 [b]
2’	62.8CH	2.95 [b]
3’	59.0, C	
4’	24.6, CH_3	1.23, s
5’	19.0, CH_3	1.43, s
7-OMe	56.1, CH_3	3.88, s

[a] ^{13}C chemical shifts deduced from HSQC and HMBC NMR spectra.
[b] Overlapping signals.
[c] δ_H reference data can be found in:

1. Ito C, Furukawa H. (**1987**) Constituents of *Murraya exotica* L. structure elucidation of new coumarins. *Chemical and Pharmaceutical Bulletin*, ***35***, 4277-4285.
2. Do Q-T, Lamy C, Renimel I, Sauvan N, André P, Himbert F, Morin-Allory L, Bernard P. (**2007**) Reverse pharmacognosy: identifying biological properties for plants by means of their molecule constituents: application to meranzin. *Planta Medica*, ***73***, 1235-1240.

3,5,6,7-Tetramethoxy-2-(3,4,5-trimethoxyphenol)chromen-4-one
(**Syn.: 3,5,6,7,3',4',5'-Heptamethoxyflavone**) (**5**)[b]
CAS Nr. 17245-30-6
$C_{22}H_{24}O_9$, LC-ESI-MS, *m/z* = 432.14

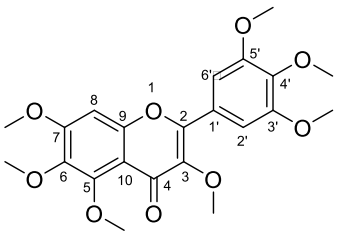

5

Table S5. NMR spectroscopic data (500 MHz, $CDCl_3$) of compound **5**

position	δ_C	δ_H (*J* in Hz)
2	153.1, C	
3	141.1, C	
4	173.6, C	
5	152.4, C	
6	139.8, C	
7	157.7, C	
8	96.0, CH	6.73, s
9	153.5, C	
10	113.1, C	
1'	125.9, C	
2'	105.9, CH	7.35, s
3'	153.1, C	
4'	140.2, C	
5'	153.1, C	
6'	105.9, CH	7.35, s
3-OMe	60.1, CH_3	3.88, s
5-OMe	62.2, CH_3	4.01, s
6-OMe	61.6, CH_3	3.91, s
7-OMe	56.3, CH_3	3.97, s
3'-OMe	56.4, CH_3	3.94 [a]
4'-OMe	61.0, CH_3	3.93 [a]
5'-OMe	56.4, CH_3	3.94 [a]

[a] Overlapping signals.
[b] δ_H and δ_C reference data can be found in:

1. Dreyer DL. (**1968**) Chemotaxonomy of the Rutaceae. IV. Constituents of *Murraya paniculata* (Linn.) Jack. *The Journal of Organic Chemistry*. ***33***, 3574-3576.
2. Nakayama M, Fukui K. (**1970**) Synthetic of the flavone derivatives. XVIII. The syntheses of 5,7,3'-trihydroxy-3,8,4',5'-tetramethoxyflavone and related compounds. *Bulletin of the Chemical Society of Japan.* ***43***, 3276-3278.

(+) 7-Methoxy-8-(-3-prop-1-en-2-yloxiran-2-yl)chromen-2-one
(**Syn.: Phebalosin**) (**6**)[a]
CAS Nr. 6545-99-9
$C_{15}H_{14}O_4$, LC-ESI-MS, *m/z* = 258.09
$[\alpha]^{25}_D$ = +3° (*c* 0.1, $CHCl_3$)

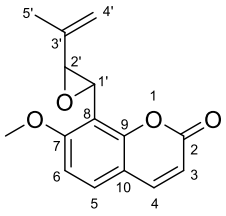

6

Table S6. NMR spectroscopic data (500 MHz, $CDCl_3$) of compound **6**

position	δ_C	δ_H (*J* in Hz)
2	160.3, C	
3	113.4, CH	6.18, d (9.5)
4	143.4, CH	7.58, d (9.8)
5	129.0, CH	7.38, d (8.9)
6	107.6, CH	6.83, d (8.9)
7	161.9, C	
8	112.8, C	
9	153.8, C	
10	112.9, C	
1’	51.7, CH	3.92, d (2.4)
2’	60.6, CH	3.87, d (2.4)
3’	141.3, C	
4’	113.5, CH_2	5.24, m
		5.02, m
5’	17.4, CH_3	1.82, s
7-OMe	56.3, CH_3	3.91, s

[a] δ_H reference data can be found in:

1. Ito C, Furukawa H. (**1987**) Constituents of *Murraya exotica* L. structure elucidation of new coumarins. *Chemical and Pharmaceutical Bulletin*. ***35***, 4277-4285.
2. Ito C, Furukawa H, Ishii H, Ishikawa T, Haginiwa J. (**1990**) The chemical composition of *Murraya paniculata*. The structure of five new coumarins and one new alkaloid and the stereochemistry of murrangatin and related coumarins. *Journal of the Chemical Society, Perkin Transactions 1*. ***7***, 2047-2055.

2-(3,4-Dimethoxyphenyl)-3,5,6,7,8-pentamethoxy-4H-chromen-4-one
(**Syn.: 3,5,6,7,8,3‘,4‘-heptamethoxyflavone**) (**7**)[c]
CAS Nr. 1178-24-1
$C_{22}H_{24}O_9$, LC-ESI-MS, *m/z* = 432.14

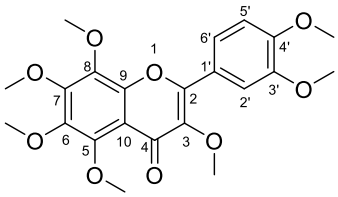

7

Table S7. NMR spectroscopic data (500 MHz, $CDCl_3$) of compound **7**

position	δ_C[a]	δ_H (*J* in Hz)
2	150.1, C	
3	139.4, C	
4	176.1, C	
5	146.8, C	
6	142.0, C	
7	149.6, C	
8	136.4, C	
9	C	
10	C	
1’	120.6, C	
2’	111.3, CH	7.82, d (1.8)
3’	147.7, C	
4’	149.3, C	
5’	111.2, CH	7.02, d, (8.5)
6’	121.8, CH	7.84, dd (8.4, 2.0)
3-OMe	59.7, CH_3	3.90, s
5-OMe	62.2, CH_3	3.99, s
6-OMe	61.6, CH_3	3.96, s
7-OMe	61.5, CH_3	4.10, s
8-OMe	61.7, CH_3	4.01, s
3’-OMe	55.9, CH_3	3.98[b], s
4’-OMe	55.9, CH_3	3.98 [b], s

[a] ^{13}C chemical shifts deduced from HSQC and HMBC NMR spectra.
[b] Overlapping signals.
[c] δ_H reference data can be found in:

1. Wang X, Li F, Zhang H, Geng Y, Yuan J, Jiang T. (**2005)** Preparative isolation and purification of polymethoxylated flavones from Tangerine peel using high-speed counter-current chromatography. *Journal of chromatography A*. ***1090***, 188-192.
2. Ito C, Fujiwara K, Koizumi M, Furukawa H. (**1998)** Isolation and characterization of an antibacterial substance from *Citrus* plant. *Journal of the Chinese Chemical Society*. ***45***, 89-91.
3. Machida K, Osawa K. (**1989**) On the flavonoid constituents from the peels of *Citrus hassaku* HORT. *Ex* TANAKA. *Chemical and Pharmaceutical Bulletin*. ***37***, 1092-1094.

3,5,6,7,8-Pentamethoxy-2-(3,4,5-Trimethoxyphenyl)chromen-4-one
(**Syn.: exoticin / 3,5,6,7,8,3‘,4‘,5‘-octamethoxyflavone**) (**8**)[b]
CAS Nr. 13336-94-8
$C_{23}H_{26}O_{10}$, LC-ESI-MS, *m/z* = 462.15

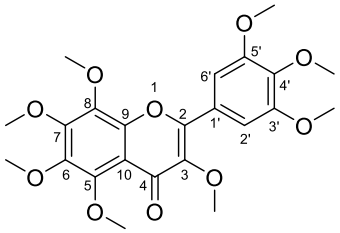

8

Table S8. NMR spectroscopic data (500 MHz, $CDCl_3$) of compound **8**

position	δ_C	δ_H (*J* in Hz)
2	152.7, C	
3	141.1, C	
4	173.9, C	
5	148.2, C	
6	143.9, C	
7	151.4, C	
8	137.7, C	
9	146.7, C	
10	115.0, C	
1’	126.0, C	
2’	105.6, CH	7.51, s
3’	153.1, C	
4’	140.2, C	
5’	153.1, C	
6’	105.6, CH	7.51, s
3-OMe	60.0, CH_3	3.90, s
5-OMe	62.3, CH_3	3.97, s
6-OMe	61.0, CH_3	3.94 [c], s
7-OMe	61.7, CH_3	4.09, s
8-OMe	61.9, CH_3	4.00, s
3’-OMe	56.1, CH_3	3.93 [a], s
4’-OMe	61.8, CH_3	3.94, s
5’-OMe	56.1, CH_3	3.93 [a], s

[a] Overlapping signals.
[b] δ_H reference data can be found in Joshi BS, Kamat VN. (**1969**) Structure of exoticin, a flavone from the leaves of *Murraya exotica* Linn. *Indian Journal of Chemistry.* ***7***, 636.

7-Methoxy-8-(3-methylbut-2-enyl)chromen-2-one
(**Syn.: Osthol**) (**9**)[b]
CAS.: 484-12-8
$C_{15}H_{16}O_3$, LC-ESI-MS, *m/z* = 244.11

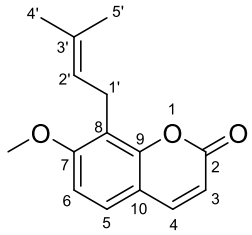

9

Table S9. NMR spectroscopic data (500 MHz, $CDCl_3$) of compound **9**

position	δ_C[a]	δ_H (*J* in Hz)
2	161.3, C	
3	112.7, CH	6.20, d (9.5)
4	143.6, CH	7.59, d (9.5)
5	126.1, CH	7.27, d (8.9)
6	107.4, CH	6.83, d (8.5)
7	160.1, C	
8	117.7, C	
9	152.5, C	
10	113.2, C	
1’	21.9, CH_2	3.53, d (7.3)
2’	121.2, CH	5.23, m
3’	132.3, C	
4’	25.6, CH_3	1.66, s
5’	17.9, CH_3	1.84, s
7-OMe	55.9, CH_3	3.92, s

[a] ^{13}C chemical shifts deduced from HSQC and HMBC NMR spectra.
[b] δ_H reference data can be found in Ito C, Furukawa C. (**1987**) Constituents of *Murraya exotica* L. structure elucidation of new coumarins. *Chemical and Pharmaceutical Bulletin.*, ***35***, 4277-4285.

5,7-Dimethoxy-8-(3-methylbut-2-enyl)chromen-2-one
(**Syn.: Coumurrayin**) (**10**)[b]
CAS Nr. 17245-25-9
$C_{16}H_{18}O_4$, LC-ESI-MS, *m/z* = 274.12

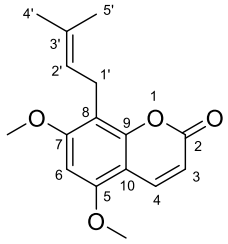

10

Table S10. NMR spectroscopic data (500 MHz, $CDCl_3$) of compound **10**

position	δ_C[a]	δ_H (*J* in Hz)
2	161.6, C	
3	110.5, CH	6.11, d, (9.8)
4	138.5, CH	7.96, d (9.8)
5	155.2, C	
6	90.4, CH	6.33, s
7	161.0, C	
8	110.5, C	
9	153.9, C	
10	103.9, C	
1’	21.4, CH_2	3.44, d (7.3)
2‘	121.8, CH	5.21, m
3’	132.0, C	
4’	25.7, CH_3	1.67, s
5’	17.7, CH_3	1.83, s
5-OMe	55.8, CH_3	3.92, s
7-OMe	55.8, CH_3	3.91, s

[a] ^{13}C chemical shifts deduced from HSQC and HMBC NMR spectra.
[b] δ_H reference data can be found in Ramstad E, Lin W-NC, Lin T-J, Koo W-Y. (**1968**) Coumurrayin, A new coumarin from *Murraya paniculata* (L.) Jack. *Tetrahedron Letters*. ***7***, 811-813.

3.2. Clerodane diterpenes from *Casearia corymbosa* as allosteric modulators at the neurosteroid binding site of $GABA_A$ receptors

Nova Syafni, Maria Teresa Faleschini, Ombeline Danton, Matthias Hamburger

To be submitted

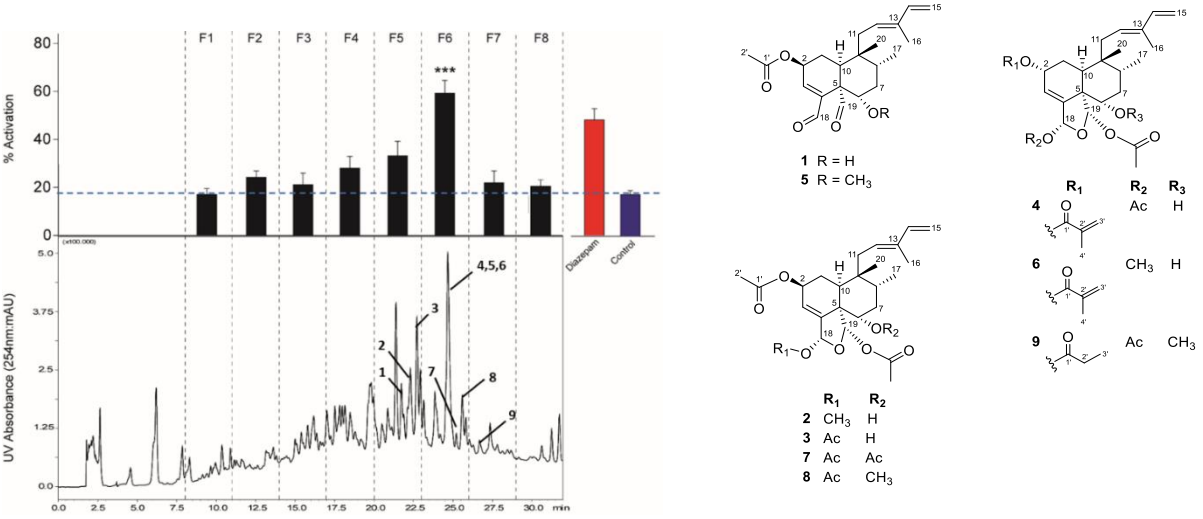

Nine clerodane-type diterpenoids have been isolated from EtOAc extract of *Casearia corymbosa* leaves; five of them are new (**1**, **5** - **7**, and **9**). The absolute configuration of all isolated compounds was established by ECD. All compounds were ested in the FLIPR assay. Five active compounds (**1**, **3**, **5**, **7**, and **8**) exhibited $GABA_A$ receptors potentiation, although only three compounds (**3**, **7**, and **8**) exhibited EC_{50} values of 0.5, 4.57, and 1.36 µM, respectively. Compound **8** was further investigated for the identification of $GABA_A$ receptor binding sites. It observed decreasing activation in combination with PREGS at the highest concentration and could be the first report of a non-steroidal compound interacting in the neurosteroid site of action.

Screening the extracts in the FLIPR assay, upscaled the extraction of plant material, isolation of all compounds, recording and elucidating the structures of isolated compounds, testing the isolated compounds in FLIPR assay, writing the manuscript, and preparing the figures and tables of phytochemical part were my contribution to this publication.

Nova Syafni

Clerodane Diterpenes from *Casearia corymbosa* as Allosteric Modulators at the Neurosteroid Binding site of $GABA_A$ Receptors

Nova Syafni[†,§,‡], Maria Teresa Faleschini[†,‡], Ombeline Danton[†], Matthias Hamburger[†,*]

[†]Department of Pharmaceutical Biology, University of Basel, Klingelbergstrasse 50, 4056 Basel, Switzerland

§Faculty of Pharmacy and Sumatran Biota Laboratory, University of Andalas, Kampus Limau Manis, Padang, West Sumatra, Indonesia.

‡These authors contributed equally

KEYWORDS: *Casearia corymbosa*, Clerodane diterpenoid, $GABA_A$ receptor modulator, Neurosteroid binding site, FLIPR assay

ABSTRACT: An EtOAc extract of *Casearia corymbosa* leaves led to an allosteric potentiation of the GABA induced chloride current in Chinese Hamster Ovary (CHO) cells stably expressing $GABA_A$ receptor with $\alpha_1\beta_2\gamma_2$ subunit composition. The activity was tracked by HPLC-based activity profiling, and four known (**2**, **3, 4** and **8**) and five new clerodane-type diterpenoids (**1**, **5** - **7**, and **9**) were isolated. Compounds **1** – **8** were obtained from the active time window. The absolute configuration of all compounds was established by ECD. Compounds **3**, **7**, and **8** exhibited EC_{50} of 0.5, 4.57, and 1.36 μM, respectively. When combined with diazepam, etazolate, and allopregnanolone, compound **8** led to an additive potentiation of GABA induced chloride currents in CHO cells. The effect of **8** was not inhibited by flumazenil, but abrogated by pregnenolone sulfate.

The major inhibitory neurotransmitter in the mammalian central nervous system (CNS) is gamma amino butyric acid (GABA).[1,2] GABA type A receptors play an important role in modulating excitatory signals in the CNS. They are heteropentameric ion channels which, upon opening, are permeable to chloride ions. A total of 19 $GABA_A$ receptor subunits have been identified [α (1-6), β (1-3), γ (1-3), δ, ε, θ, π, ρ (1-3)] which assemble to 11 receptor subtypes. These subtypes differ with respect to their distribution in the CNS and in their sensitivity to various ligands. The most abundant $GABA_A$ receptor subtype consists of two α_2, two β_2 and one γ_2 subunit. Besides binding sites for the endogenous neurotransmitter, $GABA_A$ receptors possess several allosteric binding sites, such as the benzodiazepine, barbiturate, alcohol, and neurosteroid binding sites. $GABA_A$ receptors are the target for anxiolytic, hypnotic, anesthetic and anticonvulsant drugs.

Various assay formats have been exploited for the discovery of $GABA_A$ receptor ligands, such as radio-immunoassays, fluorescent labelling, radioactivity-based flux and microphysiometry assays.[3,4,5,6] Two-microelectrode electrophysiological assays with *Xenopus laevis* oocytes transiently expressing $GABA_A$ receptors of desired subunit composition have been widely used for the functional assessment of allosteric modulators, and larval zebrafish locomotor assays have served for the *in vivo* characterization of natural products.[7,8,9,10] We recently validated a FLIPR (fluorometric imaging plate reader) assay for the discovery of allosteric $GABA_A$ receptor modulators in plant extracts.[11] The assay utilizes Chinese hamster ovary (CHO) cells stably expressing $GABA_A$ receptor with $\alpha_1\beta_2\gamma_2$ subunit composition.[12] The FLIPR assay allows for an observation of real-time membrane potential changes associated with activation of the ion channel.[13,14]

Casearia corymbosa Kunth (Salicaceae) is a tree distributed in the Mesoamerican region between Mexico and Venezuela. Clerodane-type diterpenes possessing insect antifeedant and other

biological activities have been identified.[15] We here report on the activity-directed identification of diterpenoids acting as allosteric $GABA_A$ receptor modulators, and on experiments characterizing the allosteric binding site of the major active compound.

RESULT AND DISCUSSION

A library of 708 ethyl acetate extracts from plants was screened with the aid of a recently validated FLIPR assay using stably transfected CHO cells expressing $GABA_A$ receptors of $\alpha_1\beta_2\gamma_2$ subunit composition.[11] The EtOAc extract from leaves of *Casearia corymbosa* potentiated the GABA-induced chloride current in a concentration-dependent manner, reaching >75% at 20 µg/mL (Figure S1). HPLC-based activity profiling of the active extract enabled the localization of the main activity in fraction F6 and, to a lesser extent, in fraction F5 (Figure 1).[16,17]

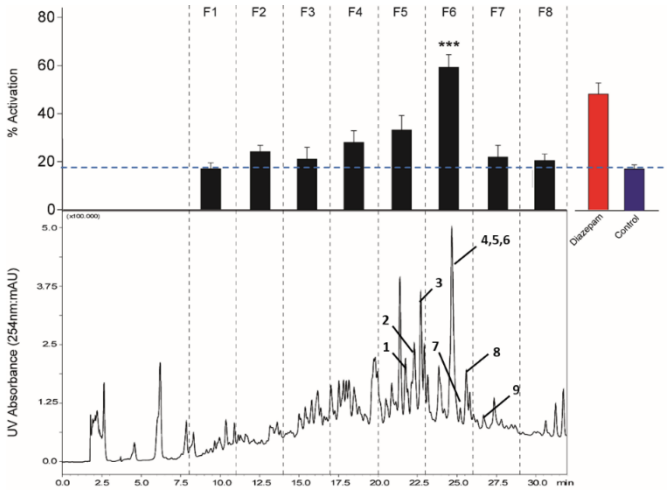

Figure 1. HPLC-based activity profile of the EtOAc extract. The lower panel shows the HPLC chromatogram (UV 254 nm), and the % potentiation of chloride currents by microfractions F1 - F8 is given above (n=8, mean ± SEM). The red and blue bars represent activation by 20 µM diazepam (in the presence of 2 µM GABA), and by 2 µM GABA (control), respectively. Dashed lines indicate microfractions collected for the bioassay (3.00 minutes each), and numbers correspond to compounds **1** to **9**. *** Statistical significance $p \leq 0.001$.

The extract was submitted to preparative column chromatography on silica gel, and 20 fractions were collected. All fractions were analyzed by HPLC-PDA-ELSD-ESIMS, and fractions 8, 9 and 10 were found to contain compounds localized in the active time windows. These fractions were further separated by semi-preparative HPLC, and compounds **1**-**9** were obtained. Of these, **1**-**8** were located in the active time windows of F5 and F6 (Figure 1).

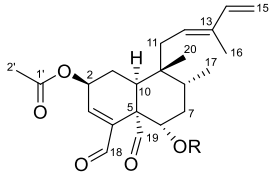

1 R = H
5 R = CH_3

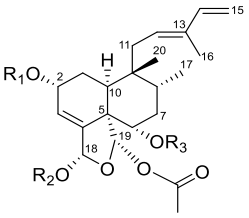

	R_1	R_2	R_3
4	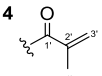	Ac	H
6	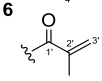	CH_3	H
9	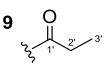	Ac	CH_3

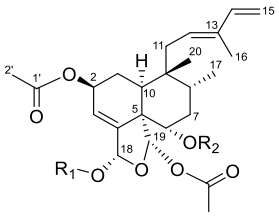

	R_1	R_2
2	CH_3	H
3	Ac	H
7	Ac	Ac
8	Ac	CH_3

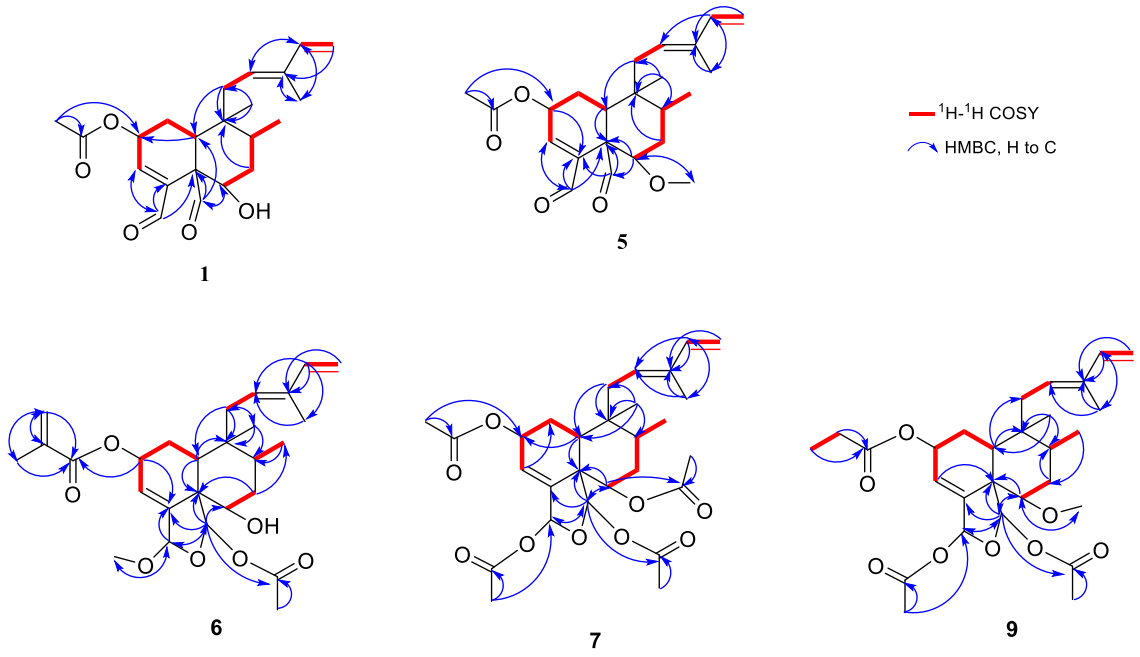

Figure 3. Key correlations from COSY and HMBC of compounds **1**, **5** –**7**, and **9**.

Four compounds corresponded to previously reported graveospene H (**2**), and corymbotins A (**8**), D (**3**), and F (**4**).[15,18] They were all clerodane-type diterpenes with a decalin moiety, a branched side chain at C-9, and four remaining carbons attached to C-4, C-5, C-8 and C-9.[19] However, the absolute configuration of **3**, **4** and **8** had not been reported previously. A comparison of their ECD spectra with those of clerodane-type diterpenes from *Casearia graveolens*[18] established the absolute configuration of **3** and **8** as (2*S*,5*S*,6*S*,8*R*,9*R*,10*S*,18*R*,19*S*), and as (2*R*,5*S*,6*S*,8*R*,9*R*,10*S*,18*R*,19*S*) for compound **4** (Figures S27 and S28).

Compound **1** had a molecular formula of $C_{22}H_{30}O_5$ [HRESIMS *m/z* 397,1987 $[M+Na]^+$; calcd for $C_{22}H_{30}O_5Na^+$, 397.1986]. Based on the ^1H and 2D NMR spectra (Table 1), the skeleton of **1** was established as a clerodane diterpene with, as for corymbotins A, D and F (**8**, **3** and **4**), the compound had a $\Delta_{3,4}$ double bond [δ_H 6.89 (H-3), δ_c 151.3 (C-3); δ_c 145.9 (C-4)], and a branched

six-carbon side chain with a conjugated diene attached to C-9 [δ_H 2.00 and 2.19 (H_2-11), δ_C 31.2 (C-11); δ_H 5.27 (H-12), δ_C 126.2 (C-12); δ_C 137.1 (C-13); δ_H 6.37 (H-14), δ_C 141.3 (C-14); δ_H 5.11 and 4.95 (H_2-15), δ_C 111.0 (C-15); and δ_H 1.72 (H_3-16), δ_C 12.0 (C-16)]. In addition, the NMR spectra indicated the presence of two aldehyde groups [δ_H 9.40 (H-18), δ_C 194.5 (C-18) and δ_H 10.00 (H-19), δ_C 202.1 (C-19)]. HMBC correlations from H-18 to C-3 (δ_C 151.3), C-4 (δ_C 145.9), and C-5 (δ_C 56.2), and from H-19 to C-5 (δ_C 56.2) and C-6 (δ_C 73.1) (Figure 3) indicated that they were attached to C-4 and C-5, respectively. An HMBC correlation from H-2' (δ_H 2.12) to C-2 (δ_C 69.9) and C-1' (δ_C 170.0) indicated the attachment of an acetyloxy moiety at C-2. The relative configuration of **1** was established on the basis of diagnostic NOESY cross-peaks between H-2/H-10, H-10/H-19, H-19/H-11, H-20/H-1α, H-1β/H-6, H-1β/H-8, and H-6/H-8. The absolute configuration was determined by a comparison of experimental and calculated ECD spectra of the (2*S*,5*S*,6*S*,8*R*,9*R*,10*S*) stereoisomer (Figure 4). Two negative Cotton effects (CEs) at 216 nm (Δε -7.8) and 239 nm (Δε -7.5) indicated the absolute configuration of **1** as (2*S,*5*S,*6*S,*8*R,*9*R,*10*S*), and the structure of this new compound was thus established as (5*S*,8*R*,9*R*,10*S*)-2*S*-acetoxy-6*S*-hydroxy-clerod-3,12,14-trien-18,19-dial.

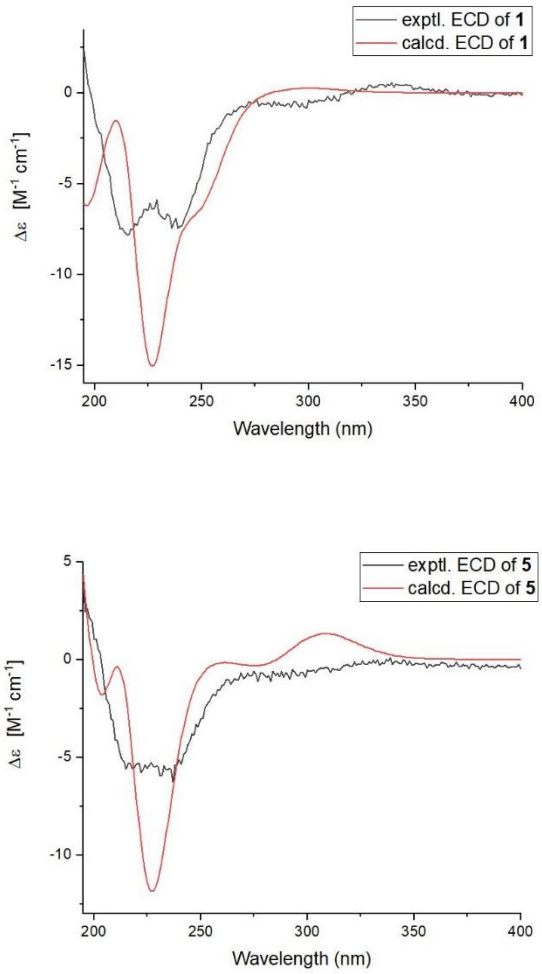

Figure 4. Experimental and calculated ECD spectra of compounds **1** and **5**.

Compound **5** had a molecular formula of $C_{23}H_{32}O_5$ (HRESIMS *m/z* 411.2145 $[M + Na]^+$, calcd for $C_{23}H_{32}O_5Na^+$, 411.2142). The NMR data were very similar to those of **1**. The major difference was in a methoxy group [δ_H 3.32 and δ_C 57.1 ppm] that showed an HMBC correlation with C-6 (δ_C 82.6). The relative configuration was established based on NOESY correlations between H-2/H-10, H-10/H-19, H-19/H-6, H-1*β*/H-6, H-6/H-8, H-17/H-11, and H-20/H-1α. The ECD spectrum resembled that of **1**, as it showed two negative Cotton effects at 215 nm (Δε -5.6) and

237 nm (Δε -6.3). The spectrum matched with the calculated ECD spectrum of the (2*S*,5*S*,6*S*,8*R*,9*R*,10*S*) stereoisomer (Figure 4), and the structure of **5** was established as (5*S*,8*R*,9*R*,10*S*)-2*S*-acetoxy-6*S*-methoxy-clerod-3,12,14-trien-18,19-dial, a new natural product.

A molecular formula of $C_{27}H_{38}O_7$ was calculated for compound **6** (HRESIMS m/z 497.2514 [M + Na]$^+$, calcd for $C_{27}H_{38}O_7Na^+$, 497.2510). 1D and 2D NMR spectral data indicated a structure similar to graveospene H (**2**). However, the acetyloxy moiety in compound **2** was replaced by a methacrylate ester at C-2 [δ_C 166.7 (C-1'); δ_C 136.7 (C-2'); δ_H 5.58 and 6.12 (H_2-3'), δ_C 125.2 (C-3'); δ_H 1.98 (H_3-4'), δ_C 18.0 (C-4')], while an HMBC cross-peak between H-2 (δ_H 5.51) and C-1' (Figure 3) indicated the attachment at C-2. NOESY cross-peaks between H-10/H-20, H-20/H-8, H-11/H-17, H-8/H-6, H-6/H-19, H-6/H-18, H-19/H-18, and H-8/H-20 established the relative configuration of the scaffold. The absolute configuration was determined by ECD.[18] The positive CE at 207 nm (Δε +29.9), together with a negative CE at 232 nm (Δε -9.0) (Figure S27), indicated a (2*R,*5*S,*6*S,*8*R,*9*R,*10*S,*18*S,*19*S*) configuration. Compound **6** was a new natural product and called graveospene J.

The structure of compound **7** was established with the aid of HRESIMS (*m/z* 541.2409 [M + Na]$^+$, calcd for $C_{28}H_{38}O_9Na^+$, 541.2408), 1D and 2D NMR data (Table 2, Figure 3). NMR data showed that it was similar to compound **3**, with an acetyloxy moiety (δ_H 2.08, δ_C 21.1; δ_C 170.1) instead of a hydroxyl group at C-6. The relative configuration was determined based on NOESY cross-peaks between H-2/H-10, H-1β/H-6, H-6/H-19, H-6/H-18, H-6/H-8, H-8/H-20, H-17/H-11, and H-20/H-1α. The ECD spectrum showed two negative CEs at 196 (Δε -12.5) and 230 (Δε -12.5) nm (Figure S28), indicating a (2S,5*S,*6*S,*8*R,*9*R,*10*S,*18*S,*19*S*) configuration. Thus, the structure of **7** was established as (2*S*,6*S*)-diacetoxyzuelanin, a new natural product.

Compound **9** (HRESIMS *m/z* 527.2618 $[M + Na]^+$, calcd for $C_{28}H_{40}O_8Na^+$, 527.2616) had a molecular formula $C_{28}H_{40}O_8$. 1D and 2D NMR data (Table 2, Figure 3) closely resembled those of **8**, the only difference being in the presence of a propylate residue at C-2 [δ_C 173.8 (C-1'); δ_H 2.42 (H_2-3'), δ_C 27.9 (C-2'); δ_H 1.21 (H_3-3'), δ_C 9.1 (C-3')]. NOESY correlations between H-10/H-20, H-20/H-8, H-8/H-6, 6-OCH_3/H-19, 6-OCH_3/H-18, and H-19/H-18 determined the relative configuration, and CEs at 202 (Δε +26.19) and 234 (Δε -8.3) nm in the ECD spectrum (Figure S 28) established the absolute configuration as 2*R*,5*S*,6*S*,8*R*,9*R*,18*R*,19*S*. The structure of **9** was thus established as (2*R*)-propanoyloxy-(6*R*)-methoxyzuelanin, a new natural product.

Table 1. ^{1}H and ^{13}C NMR Spectroscopic Data for Compounds **1** and **5** ($CDCl_3$; 500.13 MHz for ^{1}H and 125.77 MHz for ^{13}C NMR; δ in ppm).

Position	**1**		**5**	
	δ_C[a]	δ_H (mult *J* in Hz)	δ_C[a]	δ_H (mult *J* in Hz)
1α 1β	25.6, CH_2	2.22[b] 1.67, dd (10.4, 2.1)	25.9, CH_2	2.16, m 1.63, m
2	69.9, CH	5.64, ddd (10.5, 6.6, 2.1)	70.2, CH	5.59, ddd (10.5, 6.6, 2.1)
3	151.3, CH	6.89, br s	143.2, CH	6.73, br s
4	145.9, C	-	147.1, C	-
5	56.2, C	-	55.1, C	-
6	73.1, CH	3.96, br dd (11.4, 5.7)	82.6, CH	3.52, m
7	37.4, CH_2	1.96[b]	32.4, CH_2	1.76[b] 2.05, m
8	35.6, CH	1.81, m	35.7, CH	1.77[b]
9	39.5, C	-	39.8, C	-
10	44.4, CH	2.29, dd (13.7, 2.1)	44.5, CH	2.40, dd (14.0, 2.4)
11	31.2, CH_2	2.00[b] 2.19[b]	31.2, CH_2	1.73[b] 2.25, dd (15.9, 8.5)
12	126.2, CH	5.27, br t (6.9)	126.3, CH	5.27, m
13	137.1, C	-	136.7, C	-
14	141.3, CH	6.37, dd (17.2, 10.8)	141.6, CH	6.39, dd (17.4, 10.7)
15	111.0, CH_2	4.95, d (11.0) 5.11, d (17.4)	110.7, CH_2	4.95 d (10.7) 5.09, d (17.4)
16	12.0, CH_3	1.72, s	12.1, CH_3	1.71, s
17	15.3, CH3	0.97[b]	15.6, CH_3	1.01, d (6.1)
18	194.5, CH	9.40, s	190.1, CH	9.30, s
19	202.1, CH	10.00, s	202.0, CH	10.37, s
20	25.7, CH_3	0.98[b]	25.1, CH_3	0.90, s
1’	170.0, C	-	170.0, C	-
2’	20.7, CH_3	2.12, s	20.8, CH_3	2.10, s
6-OR	-	3.41, br s	57.1, CH_3	3.32, s

[a] ^{13}C NMR data extracted from HSQC and HMBC spectra, [b] Overlapping signals.

Table 2. ^{1}H and ^{13}C NMR Spectroscopic Data for Compounds **6, 7** and **9** ($CDCl_3$; 500.13 MHz for ^{1}H and 125.77 MHz for ^{13}C NMR; δ in ppm).

Position	**6**		**7**		**9**	
	δ_C[a]	δ_H (mult *J* in Hz)	δ_C	δ_H (mult *J* in Hz)	δ_C	δ_H (mult *J* in Hz)
1α 1β	27.0, CH_2	1.93[b] 1.93[b]	26.1, CH_2	2.21[b] 1.82[b]	30.3, CH_2	1.95[b] 1.91[b]
2	66.8, CH	5.51[b]	70.5, CH	5.60, dddd (9.5, 7.0, 2.8, 1.8)	66.1, CH	5.49, br t (4.3)
3	121.5, CH	6.11, dd (4.0, 0.9)	125.2, CH	5.91, br s	121.2, CH	5.93, br d (3.7)
4	146.3, C	-	143.4, C	-	146.0, C	-
5	53.6, C	-	52.0, C	-	52.9, C	-
6	72.9, CH	3.78, dd (12.1, 4.1)	74.8, CH	5.17, dd (12.2, 4.3)	81.9, CH	3.29[b]
7	37.5, CH_2	1.65[b] 1.72, dd (3.7, 3.7)	33.4, CH_2	1.64[b] 1.81[b]	31.5, CH_2	1.46, ddd (12.8, 12.8, 12.8) 1.88[b]
8	36.7, CH	1.78[b]	36.1, CH	1.94[b]	36.1, CH	1.73[b]
9	37.9, C	-	38.4, C	-	37.7, C	-
10	37.1, CH	2.41, dd (10.1, 7.0)	42.2, CH	2.45, dd (14.0, 2.8)	37.0, CH	2.35, dd (13.1, 4.0)
11	30.4, CH_2	1.76[b] 2.24, dd (16.8, 8.5)	29.9, CH_2	1.72[b] 2.25[b]	27.1, CH_2	1.71[b] 2.25, dd (16.6, 8.7)
12	129.2, CH	5.40, br dd (7.9, 3.1)	128.5, CH	5.38, br dd (7.6, 2.1)	129.3, CH	5.42, dd (8.2, 2.4)
13	135.5, C	-	135.8, C	-	135.3, C	-
14	141.3, CH	6.26, dd (17.4, 10.7)	141.1, CH	6.32, dd (17.2, 10.8)	141.3, CH	6.31, dd (17.2, 10.8)
15	110.7, CH_2	4.92 d (10.7) 5.09, d (17.4)	111.0, CH_2	4.95, d (10.7) 5.11, d (17.4)	110.7, CH_2	4.94, d (10.7) 5.10, d (17.1)
16	11.8, CH_3	1.67[b]	11.8, CH_3	1.68[b]	11.8, CH_3	1.68, s
17	15.5, CH_3	0.94, d (6.7)	15.3, CH_3	0.94, d (6.7)	15.7, CH_3	0.97, d (7.0)
18	104.6, CH	5.53[b]	94.8, CH	6.49, dd (1.5, 1.5)	96.2, CH	6.67, dd (1.5, 1.2)
19	96.7, CH	6.49, s	97.0, CH	6.54, s	97.7, CH	6.50, s
20	24.9, CH_3	0.81, s	24.9, CH_3	0.87, s	24.9, CH_3	0.83, s
1’	166.7, C	-	169.7, C	-	173.8, C	-
2’	136.7, C	-	21.1, CH_3	2.08[b]	27.9, CH_2	2.42, qd (7.6, 1.2)
3’	125.2, CH_2	5.58, dq (1.7, 1.4) 6.12, dq (1.7, 0.9)	170.1, C	-	9.1, CH_3	1.21, dd (7.6, 7.6)
4’	18.0, CH_3	1.98, dd (1.4, 0.9)	21.1, CH_3	2.08[b]	-	-
6-OR	-	-	170.7, C	-	57.4, CH_3	3.31, s
18-OR1	55.6, CH_3	3.41, s	21.1, CH_3	2.08[b]	170.1, C	-
2	-	-	169.3, C	-	21.2, CH_3	2.10, s
19-OR1	169.6, C	-	21.1, CH_3	1.96, s	169.5, C	-
2	21.4, CH_3	1.92, s	26.1, CH_2	2.21[b] 1.82[b]	21.6, CH_3	1.95, s

[a] ^{13}C NMR data extracted from HSQC and HMBC spectra, [b]Overlapping signals.

Compounds **1** – **9** were first tested at a single concentration of 20 µM in the FLIPR assay (Figure 5). The results showed that **3**, **7**, and **8** significantly enhanced the GABA-induced Cl^- currents. Diterpenoids **1** and **5** were found to have moderate activity (% activation ~40%), while compounds **2**, **4**, **6**, and **9** displayed no activity. Concentration-response and EC_{50} values were thus determined for compounds **1**, **3**, **5**, **7**, and **8**.

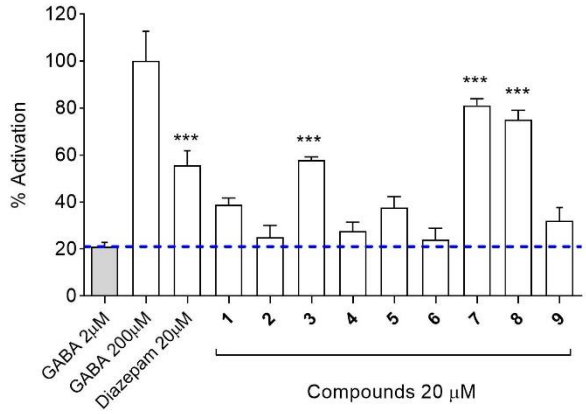

Figure 5. Percentage of activation for compounds **1-9** (in presence of 2 µM GABA), along with 2 µM GABA (control), 200 µM GABA (100%), and 20 µM diazepam (in presence of 2 µM GABA), (n=4, mean ± SEM). Final DMSO concentration in the assay was 0.1%. The *** above the bars indicate statistical significance with $p \leq 0.001$.

Compounds **3**, **7**, and **8** displayed significant positive allosteric modulation of the GABA-induced Cl^- currents, with EC_{50} values of 0.51, 4.57, and 1.36 μM, respectively (Figure 6). Compounds **1** and **5** did not display a clear concentration-dependent effect (data not shown) and thus were not pursued further. When compared to other known allosteric $GABA_A$ receptor modulators previously tested in the FLIPR assay, such as the piperine (EC_{50}: 5.76 μM), magnolol (EC_{50}: 4.81 μM), and valerenic acid (EC_{50}: 12.56 μM)[20], diterpenoids **3**, **7**, and **8** were more potent.

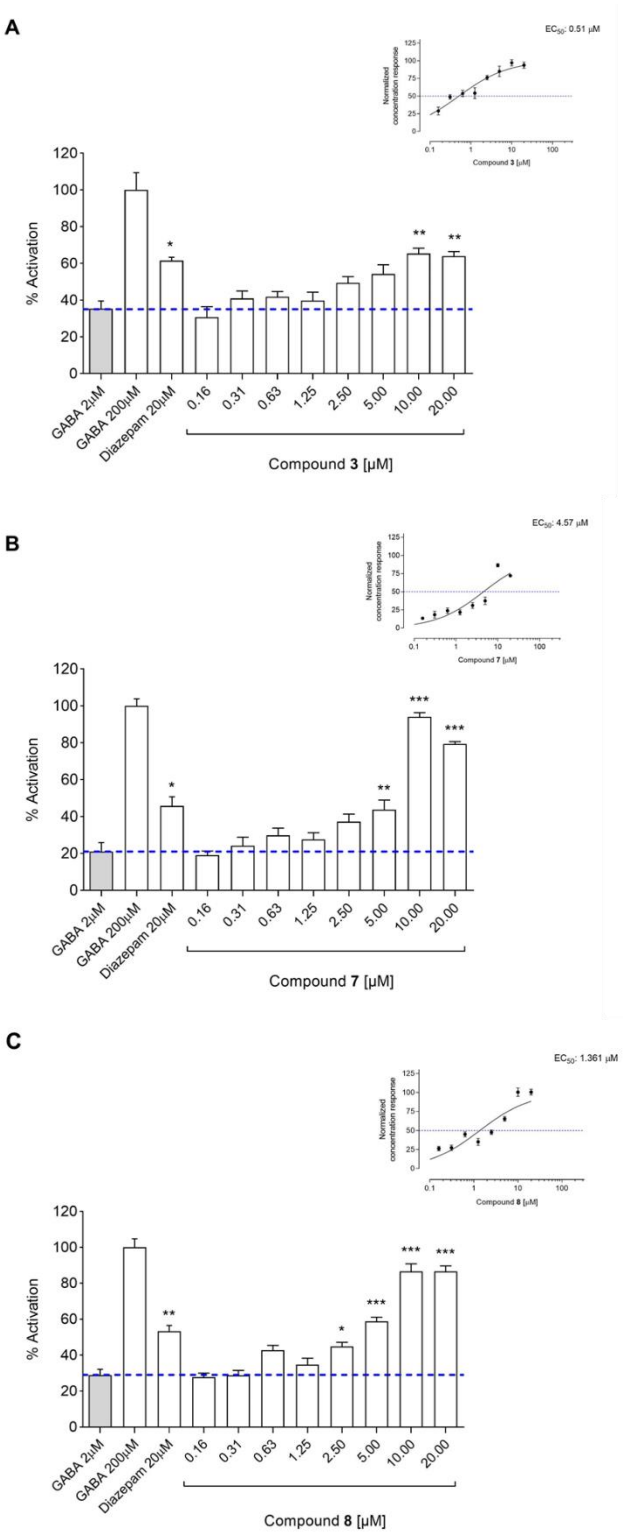

Figure 6. Percentage of activation for compounds **3** (**A**), **7** (**B**) and **8** (**C**) (in presence of 2 µM GABA), along with 2 µM GABA (control), 200 µM GABA (100%), and 20 µM diazepam (in presence of 2 µM GABA), (n=10, mean ± SEM). The plots above each bar graph show the corresponding concentration-response curves with calculated EC_{50} values. Final DMSO

concentration in the assay was 0.1% response curves with calculated EC_{50} values. Final DMSO concentration in the assays was 0.1%. The *, ** and *** above the bars indicate statistical significance with $p \leq 0.05$, $p \leq 0.01$ and $p \leq 0.001$, respectively.

$GABA_A$ receptors possesses several binding sites. [21] Classical orthosteric and allosteric agonists and antagonists bind to the extracellular domains, while binding sites for lipids and neurosteroids are located in the transmembrane domain (TMD). Direct channel blockers bind within the ion pore formed by the $GABA_A$ receptor pentamer.[20,21] We investigated the possible binding site of diterpenoid **8** utilizing known receptor agonists/antagonists for the different allosteric binding sites.

In a first step the assay conditions for the binding sites and agonist/antagonist combinations were optimized. The activation by diazepam (2 μM) was abolished by flumazenil (0.001 – 100 μM) in a concentration dependent manner (Figure S29), and activation by the neurosteroid allopregnanolone (0.5 μM) was abrogated by increasing concentrations of pregnenolone sulfate (PREGS, 0.001 – 100 μM, Figure S30).[22,23] The barbiturate binding site was validated with the aid of the positive modulator etazolate (Figure S31), since no antagonists of this binding site are known. In contrast, no activation was seen in the presence of ethanol at concentrations up to 640 mM (Figure S32). This is in line with reports that $GABA_A$ receptors containing γ_2-subunits are only weakly sensitive to ethanol.[22,23]

To assess a possible interaction at the benzodiazepine binding site, compound **8** (5 μM) was tested together with increasing concentrations of the antagonist flumazenil (0.001 – 10 μM) (Figure 7A). The activation by **8** was not abrogated even at the highest flumazenil concentration. When combining increasing concentrations of compound **8** (0.5 – 8 μM) with diazepam (2 μM) an additive effect was observed (Figure 7B). These data indicated that the diterpenoid was interacting with a binding site that was independent of the benzodiazepine site.

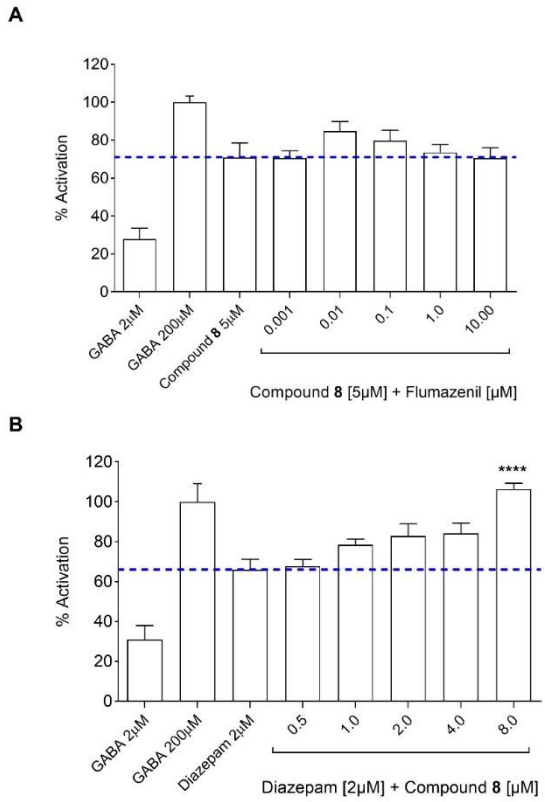

Figure 7. Percentage of activation by (**A**) **8** (5 µM) and increasing concentrations of flumazenil (in presence of 2 µM GABA), and (**B**) diazepam (2 µM) and increasing concentrations of **8** (in presence of 2 µM GABA), together with 2 µM GABA (control), 200 µM GABA (100%) and 2 µM diazepam (in presence of 2 µM GABA; positive control), (n=4, mean ± SEM). Final DMSO concentration in the assays was 0.2%. The **** above the bars indicate statistical significance with $p \leq 0.0001$.

The potentiation of GABA-induced Cl^- currents by etazolate (2 µM) was further increased by increasing concentrations of **8** (0.5 – 8 µM) (Figure 8), indicating that the diterpenoid interacted with an allosteric site other than the barbiturate binding site of the $GABA_A$ receptor.

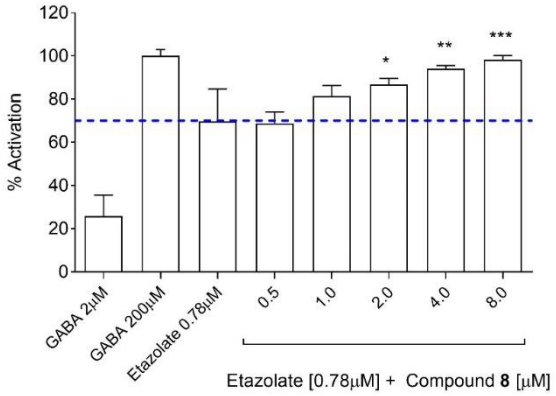

Figure 8. Percentage of activation by etazolate (0.78 µM) and increasing concentrations of 8 (in presence of 2 µM GABA), along with 2 µM GABA (control), 200 µM GABA (100%), and 0.78 µM etazolate (in presence of 2 µM GABA; positive control), (n=4, mean ± SEM). Final DMSO concentration in the assay was 0.2%. The *, ** and *** above the bars indicate statistical significance with $p \leq 0.05$, $p \leq 0.01$ and $p \leq 0.001$, respectively.

To assess a possible interaction at the benzodiazepine binding site, compound **8** (5 µM) was tested together with increasing concentrations of the antagonist flumazenil (0.001 – 10 µM) (Figure 7A). The activation by **8** was not abrogated even at the highest flumazenil concentration. When combining increasing concentrations of compound **8** (0.5 – 8 µM) with diazepam (2 µM) an additive effect was observed (Figure 7B). These data indicated that the diterpenoid was interacting with a binding site that was independent of the benzodiazepine site.

Neurosteroids and general anesthetics are known to bind on sites located in the transmembrane domain (TMD) of the $GABA_A$ receptor.[24,25] To assess a possible interaction at the neurosteroid binding sites, diterpenoid **8** (10 µM) was tested in combination with the negative allosteric modulator pregnenolone sulfate (PREGS). A decrease of activation was seen with the highest concentration of PREGS (10 µM). Intriguingly, when **8** (0.5 – 4.0 µM) was tested together with the positive allosteric modulator allopregnanolone (0.25 µM) the activation increased in a concentration dependent manner (Figure 9A and B).

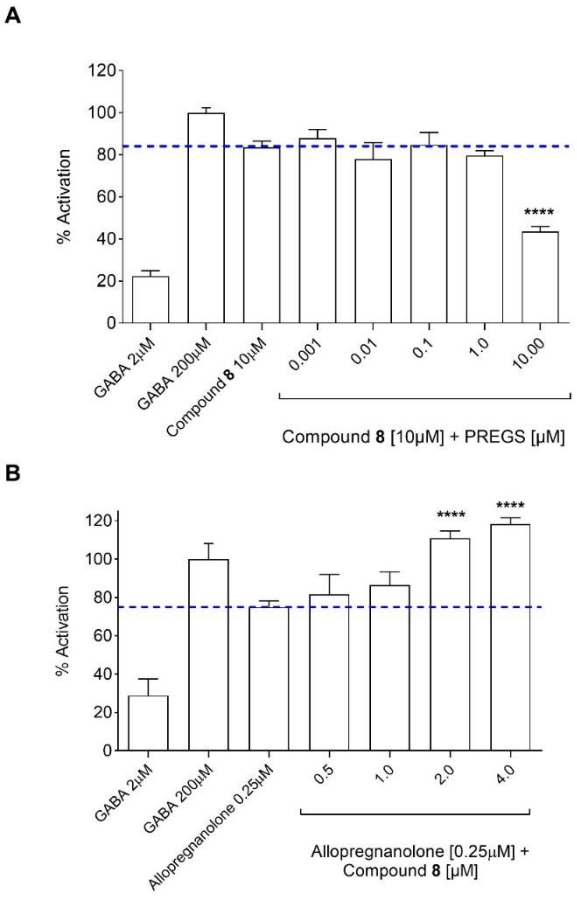

Figure 9. Percentage of activation (**A**) with compound **8** (10 µM) and increasing concentrations of PREGS (in presence of 2 µM GABA), and (**B**) with allopregnanolone (0.25 µM) and increasing concentrations of **8** (in presence of 2 µM GABA), along with 2 µM GABA (control), 200 µM GABA (100%), and 0.25 µM allopregnanolone (in presence of 2 µM GABA; positive control) (n=4, mean ± SEM). Final DMSO concentration in the assay was 0.2%. The **** above the bars indicate statistical significance with $p \leq 0.0001$.

Cryo-electron microscopic structures of $GABA_A$ receptors have been recently published[26,27,28] and the existence of functional binding sites for neurosteroids on the α_1 subunit and at the interface of the β_3/α_1 subunits has been reported[29]. The existence of multiple sites may explain the somewhat puzzling observation of an abrogation of the effect of **8** by PREGS, on the one hand, and the additive effect of **8** and the positive allosteric modulator allopregnanolone, on the other hand. Further investigations are needed to better understand the

interaction of **8** with these binding sites. To the best of our knowledge, this is the first report of a non-steroidal compound interacting with the neurosteroid binding sites of $GABA_A$ receptors.

EXPERIMENTAL SECTION

General Experimental Procedures. Optical rotations were measured in chloroform on a P-2000 digital polarimeter (Jasco) equipped with a sodium lamp (589 nm) and a 10 cm temperature-controlled microcell. Electronic circular dichroism (ECD) spectra were recorded on a Chirascan CD spectrometer with 1 mm path precision cells (110 QS, Hellma Analytics), at a concentration of 0.1 – 0.2 mg/mL in acetonitrile (CH_3CN). NMR spectra were measured with a Bruker Avance III spectrometer operating at 500.13 MHz for ^1H and 125.77 MHz for ^{13}C. ^1H NMR, COSY, HSQC, HMBC, and NOESY spectra were measured with a 1 mm TXI probe at 23°C. ^{13}C NMR spectra were obtained in 3 or 5 mm tubes with a BBO probe at 23°C. $CDCl_3$ for NMR was from Armar Chemicals (Döttingen).

HPLC-PDA-ELSD-ESIMS analyses were performed with an instrument consisting of a degasser, quaternary pump (LC-20AD), column oven (CTO-20AC), PDA detector (SPD-M20A), and triple quadrupole mass spectrometer (LCMS-8030) (all Shimadzu), connected via a T-split to an ELSD 3300 detector (Alltech). A SunFire C_{18} column (3.5 µm, 150 × 3.0 mm i.d., with guard column 10 mm × 3.0 mm i.d.) was used (Waters). Data acquisition and processing were performed with Lab Solution software (Shimadzu).

Time-based microfractionation into 96-deepwell plates was carried out with the analytical HPLC system. Instead of the mass spectrometer a FC 204 fraction collector (Gilson) was connected.

Semi-preparative HPLC was carried out with an HP 1100 Series instrument consisting of a quaternary pump, autosampler, column oven, and a G13115B diode array detector (all Agilent). A SunFire Prep C18 column (5 μm, 10 x 150 mm) equipped with a guard column (10 x 10 mm)

(Waters) and, for normal phase, a Nucleodur Prep 100-5 CN column (5 μm, 10 x 150 mm) equipped with a guard column (10 x 10 mm) (Macherey-Nagel) were used for separation.

HPLC-grade acetonitrile (Scharlau Chemie) and water from Milli-Q water purification system (Merck Millipore) with 0.1% formic acid were used for reverse phase. Extra pure *n*-heptane (Scharlau) and HPLC-grade 2-propanol (Macron Fine Chemicals) were used for normal phase (semipreparative CN column). Solvents used for extraction and column chromatography were of technical grade (Romil Pure Chemistry) and were redistilled before use. Silica gel (0.063 − 0.200 mm, Merck) were used for flash column chromatography on a Puriflash 4100 system (Interchim). HRESIMS data were measured on a LQT XL Orbitrap mass spectrometer (Thermo Scientific) via direct injection.

Evaporation of micro-fractions was done with a EZ-2 plus vacuum centrifuge (Genevac).

Plant Material. Leaves of *Casearia corymbosa* Kunth. were collected by Alex Espinosa in El Cope, 5 Km from Ilegar al Pablado, Panama. The material was authenticated by Alex Espinosa, Taxonomist at Ciflorpan, and voucher specimens have been deposited at the Herbarium of the University of Panama (PMA), Panama (voucher number 7166), and at the Division of Pharmaceutical Biology, University of Basel, Switzerland (voucher # 853).

Microfractionation. *C. corymbosa* EtOAc extract was separated by analytical RP-HPLC [0.1% aqueous formic acid (A), 0.1% formic acid in CH_3CN (B), 0-30 min (5-100% B); 30-37 min (100% B); flow rate 0.5 mL/min; injection volume 3 x 40 µL of a solution of 10 mg/mL in DMSO. From t_R 8 to 32 min fractions of 3 minutes each were collected into a 96-deep-well plate with conical bottom (Biotage), and dried for 12 h at 37°C in a Genevac EZ-2 vacuum evaporator. The residues were redissolved prior to the bioassay.

Extraction and Isolation. Powdered *C. corymbosa* leaves (60 g) were macerated at rt under stirring with 3 x 300 mL EtOAC for two days each to afford 5.8 g of crude extract. The extract was separated on a silica gel column (49 x 460 mm) using a step gradient (*n*-hexane, *n*-hexane/EtOAc, EtOAc, EtOAc/MeOH and MeOH). The flow rate was 30 mL/min, and 20

fractions were collected. Fractions were analyzed by HPLC-PDA-ESIMS, and compounds detected in the active time windows of the HPLC activity profile were localized in fractions 7 to 16.

Fractions 8 (51 mg) and 9 (110 mg) were submitted to semi-preparative RP-HPLC [H_2O + 0.1% formic acid (A), CH_3CN + 0.1% formic acid (B); isocratic 64% B (1-30 min); flow rate 4.0 mL/min]. Fractions 8 and 9 yielded, respectively, eight (A1-A8) and seven (B1-B7) subfractions. Subfractions of interest were separated by semi-preparative HPLC on a CN column with isopropyl alcohol (A) and heptane (B) as mobile phase. Fraction A5 (10 mg) [isocratic 99% B (1-30 min); flow rate 4.0 mL/min] afforded compound **8** (2.1 mg, t_R 26.3 min). Fraction A6 (10 mg) [isocratic 97% B (1-30 min); flow rate 3.0 mL/min] gave compound **9** (0.3 mg, t_R 24.5 min).

Fraction B1 (10 mg) [isocratic 95% B (1-30 min); flow rate 3.0 mL/min] yielded compound **3** (0.3 mg, t_R 21.6 min). Fraction B3 (10 mg) [isocratic 97% B (1-30 min); flow rate 3.0 mL/min] afforded compound **7** (0.6 mg, t_R 18.2 min). Fraction B4 (60 mg) [isocratic 97% B (1-30 min); flow rate 3.0 mL/min] afforded compounds **5** (0.6 mg, t_R 17.2 min) and **8** (4 mg, t_R 23.1 min).

Fraction 10 (800 mg) was submitted to preparative RP-HPLC [H_2O + 0.1% formic acid (A), MeOH + 0.1% formic acid (B), isocratic 75% B (1-30 min); flow rate 20 mL/min] to afford two fractions (C1 and C2). Fraction C1 (80 mg) was submitted to semi-preparative RP-HPLC [H_2O + 0.1% formic acid (A), CH_3CN + 0.1% formic acid (B), isocratic 54% B (1-30 min); flow rate 4.0 mL/min] to yield seven subfractions (C1a-C1g). Fraction C1d (6.1 mg) and C1e (12.6 mg) were separated by semi-preparative HPLC on a CN column with 2-propanol (A) and *n*-heptane (B) as mobile phase. Fraction C1d [isocratic 97% B (1-30 min); flow rate 3.0 mL/min] afforded compound **2** (1.6 mg, t_R 13.6 min) and compound **1** (1.0 mg, t_R 5.2 min). Fraction C1e [isocratic 96% B (1-30 min); flow rate 3.0 mL/min] afforded compound **3** (6.0 mg, t_R 23.3 min) and compound **1** (0.8 mg, t_R 6.4 min). Fraction C2 (100 mg) was submitted to semi-preparative HPLC on a CN column [2-propanol (A), *n*-heptane (B), isocratic 97% B (1-

35 min); flow rate 3.0 mL/min] to obtain compounds **6** (2.5 mg, t_R 14.2 min) and **4** (15 mg, t_R 31.4 min).

(5*S*,8*R*,9*R*,10*S*)-2*S*-acetoxy-6*S*-hydroxy-clerod-3,12,14-trien-18,19-dial (**1**): $[\alpha]_D^{25}$ -59.1 (c 0.02, CH_2Cl_2); ECD (CH_3CN) 216 (Δε -7.8), 239 (Δε -7.5), 299 (Δε – 0.9) nm; ^{13}C NMR and ^1H NMR data, see Table 1; HRESIMS *m/z* 397. 1987 $[M + Na]^+$ (calcd for $C_{22}H_{30}O_5Na^+$, 397.1986)

Graveospene H (**2**): $[\alpha]_D^{25}$ -48.0 (c 0.03, CH_2Cl_2); ECD (CH_3CN) 206 (Δε + 0.1), 228 (Δε -11.1) nm; ^{13}C NMR and ^1H NMR data, see Table S1; HRESIMS *m/z* 471.2355 $[M + Na]^+$ (calcd for $C_{25}H_{36}O_7Na^+$, 471.2354).

Corymbotin D (**3**): $[\alpha]_D^{25}$ -31.4 (c 0.04, CH_2Cl_2); ECD (CH_3CN) 207 (Δε + 1.6), 231 (Δε -10.0) nm; ^{13}C NMR and ^1H NMR data, see Table S1, Supporting Information ; HRESIMS *m/z* 499.2303 $[M + Na]^+$ (calcd for $C_{26}H_{36}O_8Na^+$, 499.2303).

Corymbotin F (**4**): $[\alpha]_D^{25}$ +57.1 (c 0.02, CH_2Cl_2); ECD (CH_3CN) 207 (Δε + 31.9), 231 (Δε -10.1) nm; ^{13}C NMR and ^1H NMR data, see Table S2, Supporting Information; HRESIMS *m/z* 525.2458 $[M + Na]^+$ (calcd for $C_{28}H_{38}O_8Na^+$, 525.2459).

(5*S*,8*R*,9*R*,10*S*)-2*S*-acetoxy-6*S*-methoxy-clerod-3,12,14-trien-18,19-dial (**5**): $[\alpha]_D^{25}$ -62.5 (c 0.01, CH_2Cl_2); ECD (CH_3CN) 215 (Δε -5.6), 237 (Δε -6.3), 299 (Δε – 0.9) nm; ^{13}C NMR and ^1H NMR data, see Table 1; HRESIMS *m/z* 411.2145 $[M + Na]^+$ (calcd for $C_{23}H_{32}O_5Na^+$, 411.2142).

Graveospene J (**6**): $[\alpha]_D^{25}$ +57.9 (c 0.02, CH_2Cl_2); ECD (CH_3CN) 207 (Δε + 29.9), 232 (Δε -9.0) nm; ^{13}C NMR and ^1H NMR data, see Table 2; HRESIMS *m/z* 497.2514 $[M + Na]^+$ (calcd for $C_{27}H_{38}O_7Na^+$, 497.2510).

(2*S*,6*S*)-diacetoxyzuelanin (**7**): $[\alpha]_D^{25}$ -51.5 (c 0.03, CH_2Cl_2); ECD (CH_3CN) 196 (Δε -12.5), 230 (Δε -12.5) nm; ^{13}C NMR and ^1H NMR data, see Table 2; HRESIMS *m/z* 541.2409 $[M + Na]^+$ (calcd for $C_{28}H_{38}O_9Na^+$, 541.2408).

Corimbotin A (**8**): $[\alpha]_D^{25}$ -44.2 (c 0.05, CH_2Cl_2); ECD (CH_3CN) 204 (Δε +2.8), 232 (Δε -10.3) nm; ^{13}C NMR and ^{1}H NMR data, see Table S2, Supporting Information; HRESIMS *m/z* 513.2460 $[M + Na]^+$ (calcd for $C_{27}H_{38}O_8Na^+$, 513.2459).

(2*R*)-propanoyloxy-(6*R*)-methoxyzuelanin (**9**): $[\alpha]_D^{25}$ +53.8 (c 0.01, CH_2Cl_2); ECD (CH_3CN) 202 (Δε + 26.1), 234 (Δε -8.3) nm; ^{13}C NMR and ^{1}H NMR data, see Table 2; HRESIMS *m/z* 527.2618 $[M + Na]^+$ (calcd for $C_{28}H_{40}O_8Na^+$, 527.2616).

Computational Methods. Conformational analysis was performed with Schrödinger MacroModel 9.8 (Schrödinger, LLC, New York, USA) employing the OPLS2005 (optimized potential for liquid simulations) force field in water for ECD calculations. The five conformers with the lowest energy were selected for geometrical optimization and energy calculation applying DFT with the Becke's nonlocal three parameter exchange and correlation functional, and the Lee-Yang-Parr correlation functional level (CAM-B3LYP), using the 6-31G(d,p) basis set and the SCRF method with the CPMC model for solvation (MeOH) with the Gaussian 09 program package.[30] Excitation energy (denoted by wavelength in nm), rotator strength (Rstr), dipole velocity (Rvel), and dipole length (Rlen) were calculated in CH_3CN by TD-DFT/CAM-B3LYP/6-31G(d,p). ECD curves were obtained on the basis of rotator strengths with a half-band of 0.3 eV using SpecDis v1.71.[31] ECD spectra were calculated from the spectra of individual conformers according to their contribution calculated by Boltzmann weighting.

FLIPR assay. Chinese Hamster Ovary (CHO) cells stably expressing $GABA_A$ receptor with $\alpha_1\beta_2\gamma_2$ subunit composition were passaged following an established protocol.[11,12] The Chinese Hamster Ovary (CHO) cell line stably expressing the $\alpha_1\beta_2\gamma_2$ $GABA_A$ receptor subtype was cloned by B'Sys. Cells were cultured in DMEM F-12 nutrient mixture supplemented with 10% FBS, 1% penicillin/streptomycin, under antibiotic pressure with 200 µg/mL hygromycin B, 5 µg/mL puromycin and 100 µg/mL zeocin. Cells were incubated in humidified air at 37 °C and 5% CO_2, until 80–90% cell confluency. Passage numbers used in this study were from 10 to 30. Briefly, cells of approx. 80-90% confluency were seeded in a 96-black walled plate at a

density of 60,000 cells/well in 100 µL culture medium. The plate was incubated in humidified air at 37 °C and 5% CO_2 for 24 hours to allow cells to adhere. Then, 100 µL of FLIPR red dye solution (10.4 mL assay buffer and red FLIPR assay reagent) was added to each well. The plate was further incubated for 30 minutes to allow the dye to penetrate into the cell membrane (assay plate). During the incubation time, a compound plate (clear 96-well plate) with controls, extracts, microfractions, compounds, and blanks was prepared (200 µL/well). Test solutions of extracts, microfractions, and compounds were prepared in buffer (consisting of 10% HBSS and 2% HEPES in sterilized H_2O) and DMSO.

For the extract library screening, 2 µL of a 10 mg/mL DMSO stock solution of the extracts were added to 198 µL of buffer, and transferred into the compound plate. Final test concentration for extracts was 20 µg/mL, with a final DMSO concentration in the assay of 0.1%. For extracts tested active (> 35 % potentiation) serial dilutions were prepared from the stock solution to obtain final test concentrations of 0.16, 0.31, 0.63, 1.25, 2.50; 5.00, 10.00 and 20.00 µg/mL.

For the testing of microfractions, 10 µL DMSO were added to each well of the 96-deepwell plate, followed by 990 µL HHBS buffer. The plate was shaken for 10 min at 500 rpm on a MixMate plate shaker (Eppendorf). 100 µL of each well were mixed in Eppendorf tubes with 100 µL HHBS buffer (1:1 dilution), and the solutions were transferred into the compound plate. Aliquots of 50 µL were transferred from the compound plate to the assay plate during the fluorescent measurement.

To test the pure compounds, stock solutions of 20 mM in DMSO were prepared. Compounds were assayed at a final concentration range of 0.16 to 20.00 µM (8x dilution series) or alternatively from 0.01 to 20.00 µM (12x dilution series). Aliquots of 200 µL from each dilution were transferred into wells of the compound plate and tested.

A series of controls was included in each assay. GABA at 200 µM was used to represent 100% activation of the receptor, while GABA at 2 µM represented the minimum activation

(EC_{10}). The positive control was diazepam at 20 μM in presence of GABA 2 μM, and buffer with 0.1% DMSO was used as a blank. GABA solutions (2 and 200 μM) were prepared from a 100 mM stock solution. In order to achieve a final test concentration of 20 μM diazepam in the assay plate, a 100 μM working solution was prepared from a stock solution (1 mg/mL in methanol).

All test solutions were placed in the appropriate position in the compound plate (200 μL). Right after the final incubation period of the assay plate, the compound and assay plates were placed into a FlexStation 3 (Molecular Devices). The FlexStation parameters used in this study were as previously published.[11] Fluorescence was recorded for 500 sec. For the first 25 sec, the background fluorescence of the assay plate was measured (background signal). At 25 sec, 50 μL of test solutions (dilutions from compounds, extracts, microfractions, diazepam, and blanks) were transferred from the compound plate into the assay plate. The fluorescence was then recorded until 295 sec. At 295 sec, 25 μL of GABA solutions (final concentration of 2 or 200 μM) were transferred into each well of the assay plate and fluorescence was recorded until 500 sec. The change in fluorescence intensity measured between 270 and 330 sec was used for the calculation of percentage activation.

Identification of allosteric binding site. For the benzodiazepine binding site, a serial dilution of flumazenil (0.001 to 100 μM, 100 mM stock solution in DMSO) with diazepam at a fixed concentration of 2 μM was prepared in the compound plate and tested in the FLIPR assay according to the above protocol, with addition of 2 μM GABA at 295 sec. Then, compound **8** at a concentration of 5 μM was tested with increasing concentrations of flumazenil (0.001 to 10 μM). For an additive potentiation, increasing concentrations of compound **8** (0.5, 1.0, 2.0, 4.0, and 8.0 μM, from a 16 mM stock solution in DMSO) were tested together with diazepam at a fixed concentration of 2 μM.

Titrations of etazolate (0.78 to 25 μM, prepared from a 25 mM stock solution) were used to evaluate the barbiturate binding site. For an additive potentiation, increasing concentrations of

compound **8** (0.5 to 8.0 μM) were tested together with a fixed concentration of etazolate at 0.78 μM.

For the neurosteroid binding site, a serial dilution of PREGS (0.001 to 100.0 μM, prepared from a 100 mM stock solution) was tested together with allopregnanolone at a fixed concentration of 0.5 μM. Then, compound **8** at a fixed concentration of 10 μM was tested in the presence of increasing concentrations of PREGS (0.001 to 10 μM). For an additive potentiation, increasing concentrations of compound **8** (0.5, 1.0, 2.0, and 4.0 μM) were tested in presence of a fixed concentration of 0.25 μM allopregnanolone. For all binding site experiments, 2 μM GABA was added at 295 sec. In addition, controls of GABA 2 μM, GABA 200 μM, and 0.2% DMSO were used in each assay plate.

Statistical analysis. GraphPad Prism version 5 (GraphPad Software) was used for the calculations and graphical plots. Grubbs's test of the GraphPad outlier calculator was used (alpha = 0.05) to determine data outliers. After removal of outliers, percentage activation (%) was calculated by normalizing the readouts of the controls and test samples with that of 200 μM GABA. To compute the statistical significance, average total activation of each test sample was compared to the EC_{10} (2 μM GABA) by one-way analysis of variance, followed by Dunnett's multiple comparison test. The statistical significance indicated with *, **, ***, and **** respectively, represents $p \leq 0.05$, $p \leq 0.01$, $p \leq 0.001$, and $p \leq 0.0001$.

AUTHOR INFORMATION

Corresponding Author

*Matthias Hamburger

matthias.hamburger@unibas.ch

Pharmaceutical Biology, University of Basel

Klingelbergtrasse 50, 4056 Basel, Swiss

Author Contributions

NS performed screening the extract library, isolation, structure elucidation, testing the isolated compounds. MTS performed the bioassays screening the extract library, microfractionation, testing the isolated compound, binding site assay and analysing the data. OD assisted in NMR and did ECD calculation. MH designed and supervised the project. NS wrote the draft manuscript which was finalized by MH. All authors read and approved the final manuscript.

Funding Sources

NS is supported by a scholarship from LPDP (Indonesia Endowment Fund for Education).

ACKNOWLEDGMENT

The provision of plant material by Prof. Mahabir Gupta, CIFLORPAN, Panama, is gratefully acknowledged. Thanks are due to Orlando Fertig for technical assistance, and to Dr. Andrea Treyer for HRMS measurements.

ABBREVIATIONS

$GABA_A$ gamma amino butyric acid type A, FLIPR fluorescence imaging plate reader, CN-HPLC Cyano column high performance liquid chromatography, PREGS pregnenolone sulfate.

REFERENCES

(1) Uusi-Oukari, M.; Korpi, E. R.; Pharmacol. Rev. 2010, 62, 97-135.

(2) Sigel, E.; Steinmann, M. E.; J. Biol. Chem. 2012, 287, 40224-40231.

(3) Smith, A. J.; Simpson, P. B. Anal. Bioanal. Chem. 2003, 377, 843-851.

(4) Möhler, H.; Richards, J. G. Nature. 1981, 294, 763-765.

(5) Smith, A. J.; Alder, L.; Silk, J.; Adkins, C.; Fletcher, A. E.; Scales, T.; Kerby, J.; Marshall, G.; Wafford, K. A.; McKernan, R. M.; Atack, J. R. Mol. Pharmacol. 2001, 59, 1108-1118.

(6) Smith, A. J.; McKernan, R. M.; Atack, J. R. Eur. J. Pharmacol, 1998, 359, 261-269.

(7) Baburin, I.; Bey;, S.; Hering, S. Pflüg. Arch. 2006, 453, 117-123.

(8) Zaugg, J.; Baburin, I.; Strommer, B.; Kim, H-J.; Hering, S.; Hamburger, M. J. Nat. Prod. 2010, 73, 185-191.

(9) Zaugg, J.; Eickmeier, E.; Rueda, D. C.; Hering, S.; Hamburger, M. Fitoterapia. 2011, 82, 434-440.

(10) Moradi-Afrapoli, F.; Ebrahimi, S. N.; Smiesko, M. ; Hamburger, M. J. Nat. Prod. 2017, 80, 1548-1557.

(11) Faleschini, M. T.; Maier, A.; Fankhauser, S.; Thasis, K.; Hebeisen, S.; Hamburger, M.; Butterweck, V. Planta Med. 2019, 85, 925-933.

(12) Joesch, C.; Guevarra, E.; Parel. S. P.; Bergner, A.; Zbinden, P.; Konrad, D.; Albercht, H. J, Biomol Screen. 2008, 13, 218-228.

(13) Arkin, M. R.; Connor, P. R.; Emkey, R.; Garbison, K. E.; Heinz, B. A.; Wiernicki, T. R.; Johnston, P. A.; Kandasamy, R. A.; Rankl, N. B.; Sittampalam, S. FLIPR Assays for GPCR and Ion Channel Targets. In Assay Guidance Manual [Internet]; Sittampalam, G. S.; Coussens, N. P.; Brimacombe, K.; Grossman, A.; Arkin, M.; Auld, D.; Austin, C.; Bael, J.; Bejcek, B.; Caaveiro, J. M.. M.; Chung, T. D. Y.; Dahlin, J. L.; Devanaryan, V.; Foley, T. L.; Glicksman, M.; Hall, M. D.; Haas, J. V.; Inglese, J.; Iversen, P. W.; Kahl, S. D.; Kales, S. C.; Lal-Nag, M.; Li, Z.; McGee, J.; McManus, O.; Riss, R.; Trask, O. J. jr.; Weidner, . R.; Wildey, M. J.; Xia, M.; Xu, X.; eds.: Bethesda, MD, Eli Lilly & Company and the National Center for Advancing Translational Science, 2004.

(14) Baxter, D. F.; Kirk, M.; Garcia, A. F.; Raimondi, A.; Holmqvist, M. H., Flint, K. K.; Bojanic, D.; Distefando, P. S.; Curtis, R.; Xie, Y. J. Biomol. Screen. 2002, 7, 79-85.

(15) Chen, T-B., Wiemer, D. F. J. Nat Prod. 1991, 54, 1612-1618

(16) Potterat, O.; Hamburger, M. Nat. Prod. Rep. 2013, 30, 546-564.

(17) Potterat, O.; Hamburger, M. Planta Med. 2014, 80, 1171-1181.

(18) Liu, F., Ma, J., Shi, Z., Zhang, Q., Wang, H., Li, D., Song, Z., Wang, C., Jin, J., Xu, J., Tuerhong, M., Abudukeremu, M., Shuai, L., Lee, D., Guo, Y. J. Nat. Prod. 2020, 83, 36-44.

(19) Li, R.; Morris-Natschke, S. L. M.; Lee, K-H. Nat. Prod. Rep. 2016, 33, 1166-1226.

(20) Khayenko, V.; Maric, H., M. Front. Mol. Neurosci. 2019, 12, 1-10.

(21) Olsen, R., W. Neuropharmacology. 2018, 136, 10-22.

(22) Wallner, M.; Hanchar, H., J.; Olsen, R., W. Proceedings of the National Academy of Sciences. 2003, 100, 15218-15223.

(23) Olsen, R., W., Hanchar, H., J., Meera, P., Wallner, M. Alcohol, 2007. 41, 210-209.

(24) Alvarez, L., D., Pecci, A. J Steroid Biochem. 2018, 182, 72-80.

(25) Alvarez, L., D., Pecci, A., Estrin, D., A. J. Med. Chem. 2019, 62, 5250-5260.

(26) Zhu, S.; Noviello, C. M.; Walsh Jr, R. M.; Kim, J. J.; Hibbs, R. E. Nature. 2018, 559, 67-71.

(27) Laverty, D.; Desai, R.; Uchanski, T. ; Masiuli, S.; Stec, W. J.; Malinauskas, T.; Zivanov, J.; Pardon, E.; Steyaert, J.; Miller, K. W.; Aricescu, A. R. Nature. 2019, 565, 516-520.

(28) Masiulis, S.; Desai, R.; Uchanski, T. ; Martin, I. S.; Laverty, D.; Karia, D.; Malinauskas, T.; Zivanov, J.; Pardon, E.; Kotecha, A.; Steyaert, J.; Miller, K. W.; Aricescu, A. R. Nature. 2019, 565, 454-459.

(29) Chen, Z-W.; Bracamontes, J. R.; Budelier, M. M.; Germann, A. L.; Shin, D. J.; Kathiresan, K.; Qian, M-X.; Manion, B.; Cheng, W. W. L.; Reichert, D. E.; Akk, G.; Covey, D. F.; Evers, A. S. PLoS Biol. 2019, 17, 1-27.

(30) Frisch, M. J.; Trucks, G. W.; Schlegel, H. B.; Scuseria, G. E.; Robb, M. A.; Cheeseman, J. R.; Scalmani, G.; Barone, V.; Mennucci, B.; Petersson, G. A.; Nakatsuji, H.; Caricato, M.; Li, X.; Hratchian, H. P.; Izmaylov, A. F.; Bloino, J.; Zheng, G.; Sonnenberg, J. L.; Hada, M.; Ehara, M.; Toyota, K.; Fukuda, R.; Hasegawa, J.; Ishida, M.; Nakajima, T.; Honda, Y.; Kitao, O.; Nakai, H.; Vreven, T.; Montgomery, J. A.; Peralta, J. E.; Ogliaro, F.; Bearpark, M.; Heyd, J. J.; Brothers, E.; Kudin, K. N.; Staroverov, V. N.; Kobayashi, R.; Normand, J.; Raghavachari, K.; Rendell, A.; Burant, J. C.; Iyengar, S. S.; Tomasi, J.; Cossi, M.; Rega, N.; Millam, J. M.; Klene, M.; Knox, J. E.; Cross, J. B.; Bakken, V.;

Adamo, C.; Jaramillo, J.; Gomperts, R.; Stratmann, R. E.; Yazyev, O.; Austin, A. J.; Cammi, R.; Pomelli, C.; Ochterski, J. W.; Martin, R. L.; Morokuma, K.; Zakrzewski, V. G.; Voth, G. A.; Salvador, P.; Dannenberg, J. J.; Dapprich, S.; Daniels, A. D.; Farkas, O.; Foresman, J. B.; Ortiz, J. V.; Cioslowski, J.; Fox, D. J. *Gaussian 09, Revision A02*, Gaussian, Inc.: Wallingford CT, 2009.

(31) Bruhn, T.; Schaumlöffel, A.; Hemberger, Y.; Bringmann, G. *SpecDis version 1.71* University of Wuerzburg: Wuerzburg, Germany, 2013.

Supporting Information

Clerodane Diterpenes from *Casearia corymbosa* as Allosteric Modulators at the Neurosteroid Binding site of $GABA_A$ Receptors

Nova Syafni[†,§,‡], Maria Teresa Faleschini[†,‡], Ombeline Danton[†], Matthias Hamburger[†,*]

[†]Department of Pharmaceutical Biology, University of Basel, Klingelbergstrasse 50, 4056 Basel, Switzerland

§Faculty of Pharmacy and Sumatran Biota Laboratory, University of Andalas, Kampus Limau Manis, Padang, West Sumatra, Indonesia.

[‡]These authors contributed equally

KEYWORDS: $GABA_A$ receptor modulator, HPLC-based activity profiling, FLIPR assay, *Casearia corymbosa*, Clerodane diterpenoid.

Corresponding Author

*Matthias Hamburger

matthias.hamburger@unibas.ch

Pharmaceutical Biology, University of Basel

Klingelbergstrasse 50, 4056 Basel, Swiss

Table of contents

Figure S 1. Percentage of activation for 2 μM GABA (control), 200 μM GABA (100%), and diazepam (20 μM, in presence of 2 μM GABA), along with increasing concentrations of *Casearia corymbosa* extract (in presence of 2 μM GABA) (n=8, mean ± SEM). Final DMSO concentration in the assays was 0.1%. The * and *** above the bars indicate statistical significance with $p \leq 0.05$ and $p \leq 0.001$, respectively. 107

Table S 1. ^{1}H and ^{13}C NMR Spectroscopic Data for Compounds **2** and **3** ($CDCl_3$; 500.13 Hz for ^{1}H and 125.77 for ^{13}C NMR; δ in ppm)..... 108

Table S 2. ^{1}H and ^{13}C NMR Spectroscopic Data for Compounds **4** and **8** ($CDCl_3$; 500.13 Hz for 1H and 125.77 for ^{13}C NMR; δ in ppm). 109

Figure S 2. ^{1}H NMR spectrum of compound **1** in $CDCl_3$ (500 MHz). 110

Figure S 3. ^{1}H-^{1}H COSY spectrum of compound **1** in $CDCl_3$ (500 MHz). 111

Figure S 4. HSQC spectrum of compound **1** in $CDCl_3$ (500 MHz). 112

Figure S 5. HMBC spectrum of compound **1** in $CDCl_3$ (500 MHz). 113

Figure S 6. ^{1}H-^{1}H NOESY spectrum compound **1** in $CDCl_3$ (500 MHz). 114

Figure S 7. ^{1}H NMR spectrum of compound **5** in $CDCl_3$ (500 MHz). 115

Figure S 8. ^{1}H-^{1}H COSY spectrum of compound **5** in $CDCl_3$ (500 MHz). 116

Figure S 9. HSQC spectrum of compound **5** in $CDCl_3$ (500 MHz). 117

Figure S 10. HMBC spectrum of compound **5** in $CDCl_3$ (500 MHz). 118

Figure S 11. ^{1}H-^{1}H NOESY spectrum of compound **5** in $CDCl_3$ (500 MHz). 119

Figure S 12. ^{1}H NMR spectrum of compound **6** in $CDCl_3$ (500 MHz). 120

Figure S 13. ^{1}H-^{1}H COSY spectrum of compound **6** in $CDCl_3$ (500 MHz). 121

Figure S 14. HSQC spectrum of compound **6** in $CDCl_3$ (500 MHz). 122

Figure S 15. HMBC spectrum of compound **6** in $CDCl_3$ (500 MHz). 123

Figure S 16. ^{1}H-^{1}H NOESY spectrum of compound **6** in $CDCl_3$ (500 MHz). 124

Figure S 17. ^{1}H NMR spectrum of compound **7** in $CDCl_3$ (500 MHz). 125

Figure S 18. ^{1}H-^{1}H COSY spectrum of compound **7** in $CDCl_3$ (500 MHz). 126

Figure S 19. HSQC spectrum of compound **7** in $CDCl_3$ (500 MHz). 127

Figure S 20. HMBC spectrum of compound **7** in $CDCl_3$ (500 MHz). 128

Figure S 21. ^{1}H-^{1}H NOESY spectrum of compound **7** in $CDCl_3$ (500 MHz). 129

Figure S 22. ^{1}H NMR spectrum of compound **9** in $CDCl_3$ (500 MHz). 130

Figure S 23. ^{1}H-^{1}H COSY spectrum of compound **9** in $CDCl_3$ (500 MHz). 131

Figure S 24. HSQC spectrum of compound **9** in $CDCl_3$ (500 MHz). 132

Figure S 25. HMBC spectrum of compound **9** in CDCl3 (500 MHz). 133

Figure S 26. 1H-1H NOESY spectrum of compound **9** in CDCl3 (500 MHz). 134

Figure S 27. Experimental ECD and UV spectra of compounds **2**-**4** and **6** in CH_3CN..... 135

Figure S 28. Experimental ECD and UV spectra of compounds **7 - 9** in CH_3CN. 136

Figure S 29. Percentage of activation for 2 μM diazepam with increasing concentrations of flumazenil (in presence of 2 μM GABA), along with 2 μM GABA (control), 200 μM GABA (100%), and 2 μM diazepam (in presence of 2 μM GABA), (n=4, mean ± SEM). Final DMSO concentration in the assay was 0.2%. The * and **** above the bars indicate statistical significance with $p \leq 0.05$, and $p \leq 0.0001$, respectively. 137

Figure S 30. Percentage of activation for 0.5 μM allopregnanolone with increasing concentrations of PREGS (in presence of 2 μM GABA), along with 2 μM GABA (control), 200 μM GABA (100%), and 0.5 μM allopregnanolone (in presence of 2 μM GABA) (n=4, mean ± SEM). Final DMSO concentration in the assay was 0.2%. The **** above the bars indicate statistical significance with $p \leq 0.0001$. 137

Figure S 31. Percentage of activation for increasing concentrations of etazolate (in presence of 2 μM GABA), along with 2 μM GABA (control), 200 μM GABA (100%), and 20 μM diazepam (in presence of 2 μM GABA), (n=4, mean ± SEM). Final DMSO concentration in the assay was 0.2%. The ** and **** above the bars indicate statistical significance with $p \leq 0.01$, and $p \leq 0.0001$, respectively..... 138

Figure S 32. Percentage of activation for increasing concentrations of ethanol (in presence of 2 μM GABA), along with 2 μM GABA (control), 200 μM GABA (100%), and 20 μM diazepam (in presence of 2 μM GABA), (n=4, mean ± SEM). 138

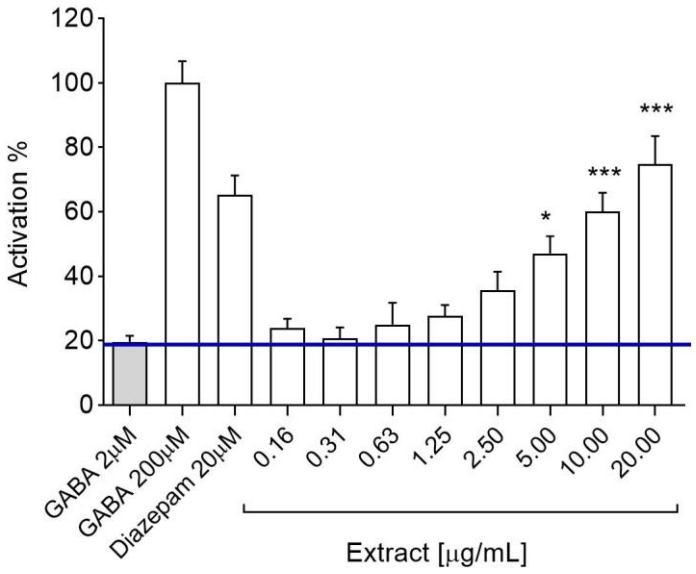

Figure S 1. Percentage of activation for 2 µM GABA (control), 200 µM GABA (100%), and diazepam (20 µM, in presence of 2 µM GABA), along with increasing concentrations of *Casearia corymbosa* extract (in presence of 2 µM GABA) (n=8, mean ± SEM). Final DMSO concentration in the assays was 0.1%. The * and *** above the bars indicate statistical significance with $p \leq 0.05$ and $p \leq 0.001$, respectively.

Table S 1. ^{1}H and ^{13}C NMR Spectroscopic Data for Compounds **2** and **3** ($CDCl_3$; 500.13 Hz for ^{1}H and 125.77 for ^{13}C NMR; δ in ppm).

Position	**2**		**3**	
	δ_C[a]	δ_H (mult *J* in Hz)	δ_C[a]	δ_H (mult *J* in Hz)
1α 1β	26.3, CH_2	2.18[b] 1.66[b]	26.2, CH_2	2.15[b] 1.68[b]
2	71.0, CH	5.58, dddd (9.6, 6.7, 2.4, 1.5)	70.8, CH	5.58, dddd (9.2, 7.0, 2.3, 1.8)
3	123.6, CH	5.98, br s	123.8, CH	5.89, br s
4	145.7, C	-	144.8, C	-
5	53.5, C	-	53.5, C	-
6	74.1, CH	3.96, ddd (11.9, 8.5, 3.7)	73.9, CH	3.97, ddd (11.6, 7.6, 4.3)
7	37.8, CH_2	1.64[b] 1.76, ddd (13.4, 3.7, 3.7)	37.6, CH_2	1.63[b] 1.73[b]
8	36.7, CH	1.84, m	36.7, CH	1.84, m
9	38.5, C	-	38.4, C	-
10	41.5, CH	2.37, dd (14.0, 2.8)	41.6, CH	2.36, dd (14.0, 2.8)
11	30.1, CH_2	1.70, m 2.22[b]	30.0, CH_2	1.66[b] 2.20[b], dd (16.8, 7.9)
12	128.9, CH	5.38, br dd (7.6, 3.1)	128.8, CH	5.36, br dd (6.7, 2.8)
13	135.6, C	-	135.8, C	-
14	141.2, CH	6.30, dd (17.2, 10.8)	141.2, CH	6.29, dd (17.1, 10.7)
15	110.7, CH_2	4.93, d (10.7) 5.08, d (17.4)	110.8, CH_2	4.91, d (10.7) 5.07, d (17.4)
16	11.8, CH_3	1.66[b]	11.8, CH_3	1.64[b]
17	15.5, CH_3	0.93, d (6.7)	15.5, CH_3	0.91, d (6.7)
18	104.2, CH	5.46, dd (1.5, 1.5)	95.2, CH	6.68, dd (1.8, 1.4)
19	96.4, CH	6.44, s	96.8, CH	6.45, s
20	24.9, CH_3	0.84, s	24.8, CH_3	0.83, s
1’	170.5, C	-	170.7, C	-
2’	21.0, CH_3	2.06, s	21.0, CH_3	2.05[b]
6-OR1	-	2.11, d (9.2)	-	2.15[b]
2	-	-		
18-OR1	55.8, CH_3	3.42, s	169.9, C	-
2	-	-	21.0,- CH_3	2.05[b]
19-OR1	169.7, C	-	169.2, C	-
2	21.5, CH_3	1.93, s	21.4, CH_3	1.91, s

[a] ^{13}C NMR data extracted from HSQC and HMBC spectra, [b]Overlapping signals.

Table S 2. ^{1}H and ^{13}C NMR Spectroscopic Data for Compounds **4** and **8** ($CDCl_3$; 500.13 Hz for 1H and 125.77 for ^{13}C NMR; δ in ppm).

Position	4		8	
	δ_C	δ_H (mult *J* in Hz)	δ_C	δ_H (mult *J* in Hz)
1*α* 1*β*	26.7, CH_2	1.94[b] 1.87[b]	26.4, CH_2	2.16[b] 1.69[b]
2	66.7, CH	5.44, br dd (3.8, 3.8)	70.9, CH	5.60, dddd (9.2, 7.0, 2.4, 1.8)
3	121.6, CH	5.96, br d (3.7)	123.4, CH	5.85, br s
4	145.5, C	-	145.3, C	-
5	53.5, C	-	52.9, C	-
6	72.6, CH	3.78, ddd (11.0, 7.0, 4.0)	82.8, CH	3.50, dd (12.1, 3.8)
7	37.3, CH_2	1.61[b] 1.67[b]	31.6, CH_2	1.44, ddd (12.8, 12.8, 12.8) 1.88, ddd (13.7, 3.7, 3.5)
8	36.7, CH	1.74, m	36.2, CH	1.77, m
9	37.6, C	-	38.5, C	-
10	36.9, CH	2.33, dd (13.1, 3.4)	41.5, CH	2.39, dd (13.9, 2.6)
11	30.3, CH_2	2.18, dd (16.9, 8.1) 1.66[b]	29.9, CH_2	1.65[b] 2.20, dd (17.7, 8.2)
12	129.0, CH	5.34, br dd (7.3, 3.1)	129.0, CH	5.36, br dd (7.6, 2.4)
13	135.7, C	-	135.7, C	-
14	141.2, CH	6.21, dd (17.4, 10.7)	141.2, CH	6.29, dd (17.1, 10.7)
15	110.7, CH_2	5.02, d (17.4) 4.86, d (10.7)	110.9, CH_2	4.93, d (11.0) 5.07, d (17.1)
16	12.0, CH_3	1.61[b]	11.9, CH_3	1.64[b]
17	15.5, CH_3	0.88, d (6.7)	15.7, CH_3	0.94, d (7.0)
18	95.6, CH	6.65, br s	95.7, CH	6.61, dd (1.5, 1.5)
19	97.0, CH	6.47, s	97.1, CH	6.42, s
20	25.0, CH_3	0.76, s	25.1, CH_3	0.82, s
1’	166.6, C	-	170.8, C	-
2’	136.6, C	-	21.2, CH_3	2.09[b]
3’	125.5, CH_2	5.57, br s 6.10, br s	-	-
4’	18.3, CH_3	1.94[b]	-	-
6-OR	-	2.88, d (7.6)	57.5, CH_3	3.33, s
18-OR1	170.7, C	-	170.3, C	-
2	21.2, CH_3	2.03, s	21.2, CH_3	2.08[b]
19-OR1	169.3, C	-	169.5, C	-
2	21.6, CH_3	1.86[b]	21.7, CH_3	1.92, s

[a] ^{13}C NMR data extracted from HSQC and HMBC spectrum, [b] Overlapping signals.

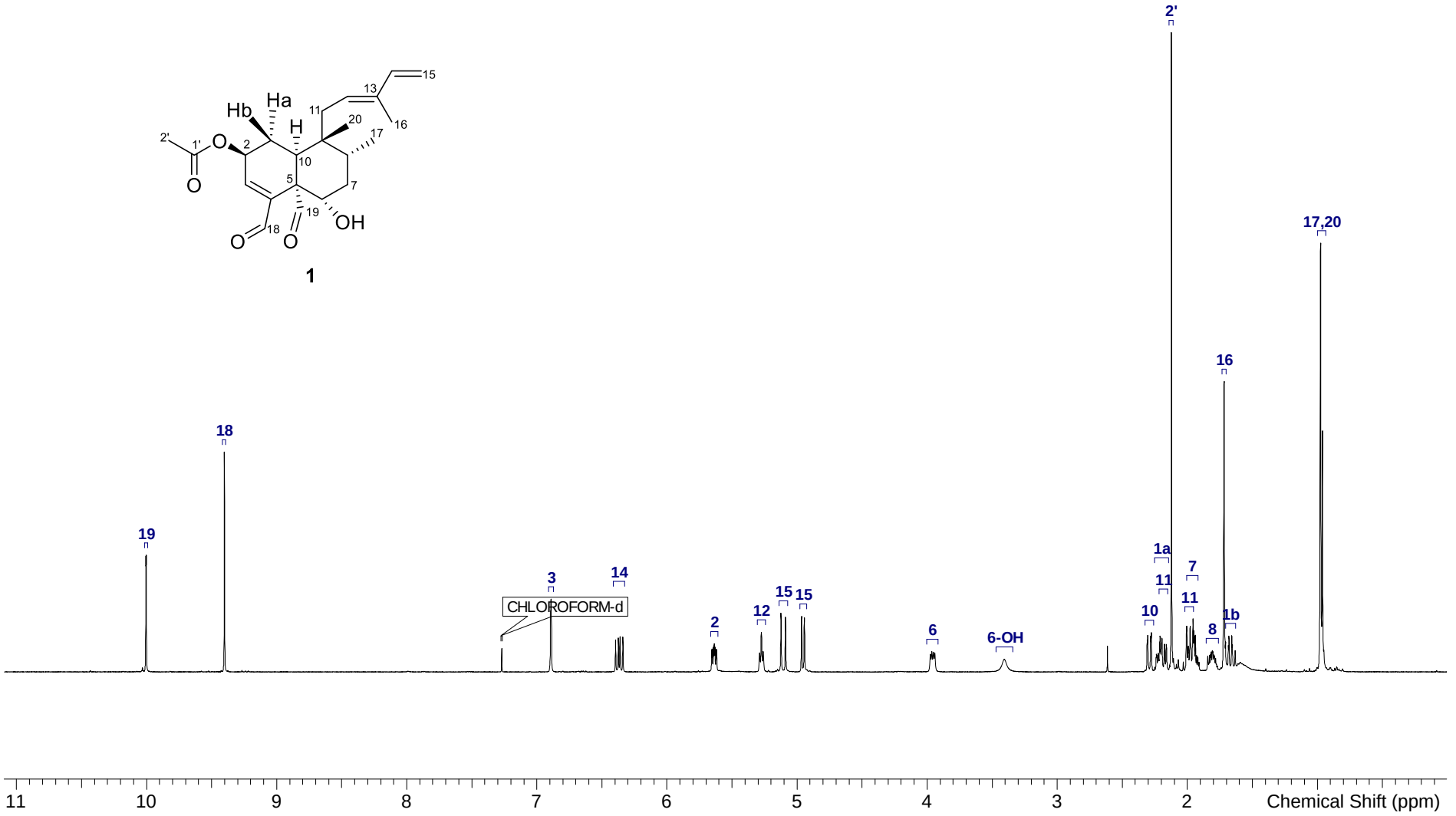

Figure S 2. ^{1}H NMR spectrum of compound **1** in $CDCl_3$ (500 MHz).

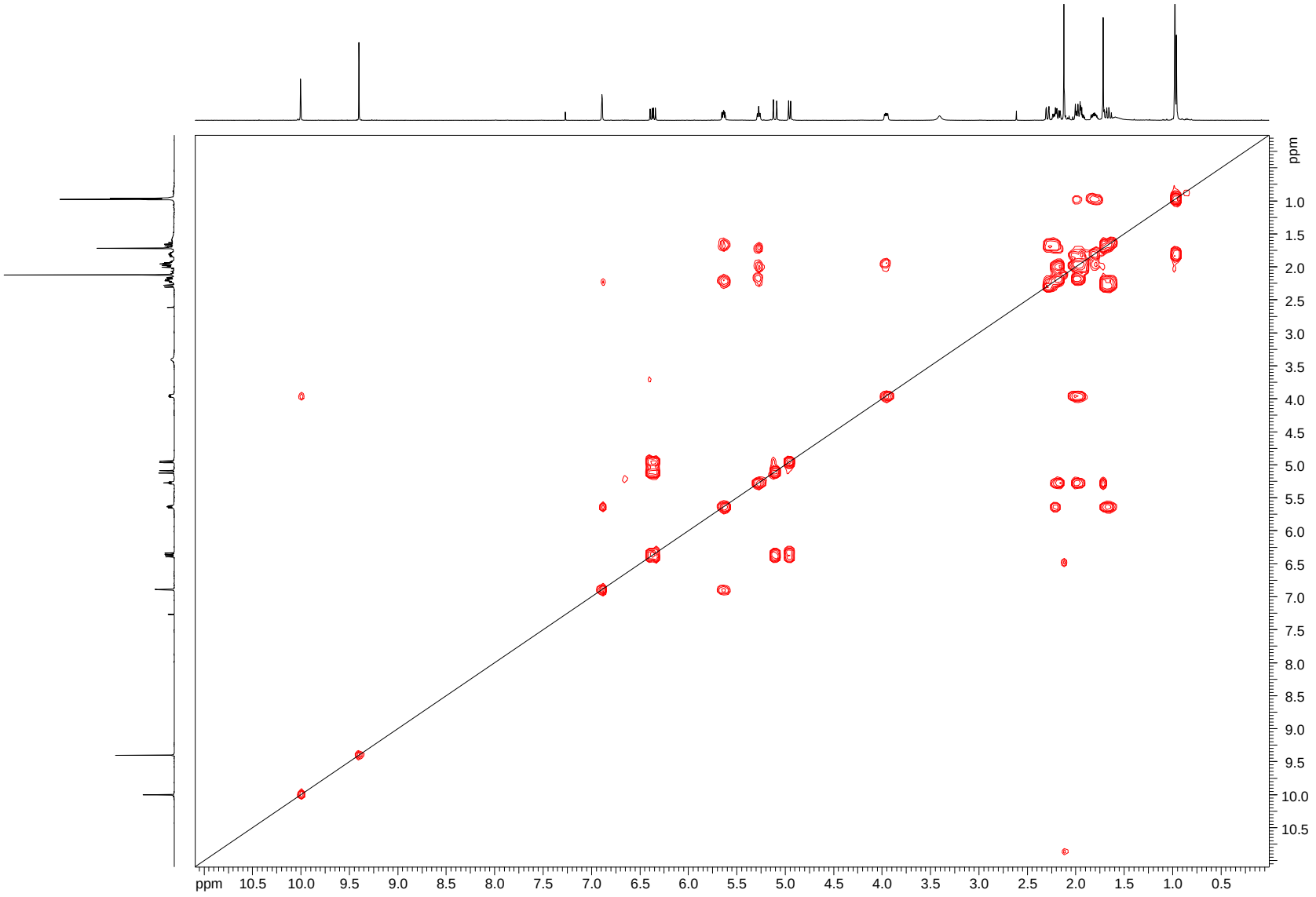

Figure S 3. ^{1}H-^{1}H COSY spectrum of compound **1** in $CDCl_3$ (500 MHz).

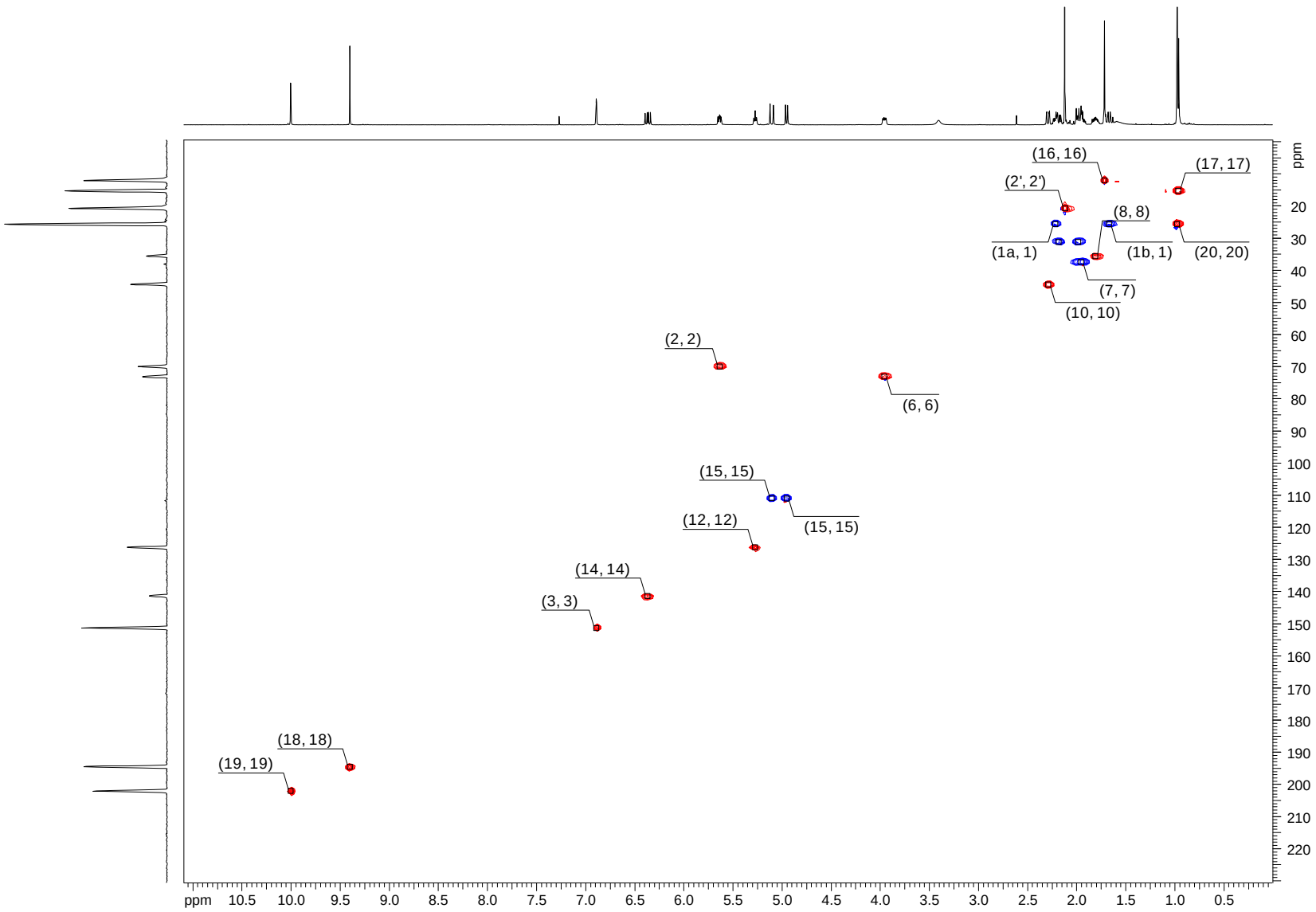

Figure S 4. HSQC spectrum of compound **1** in $CDCl_3$ (500 MHz).

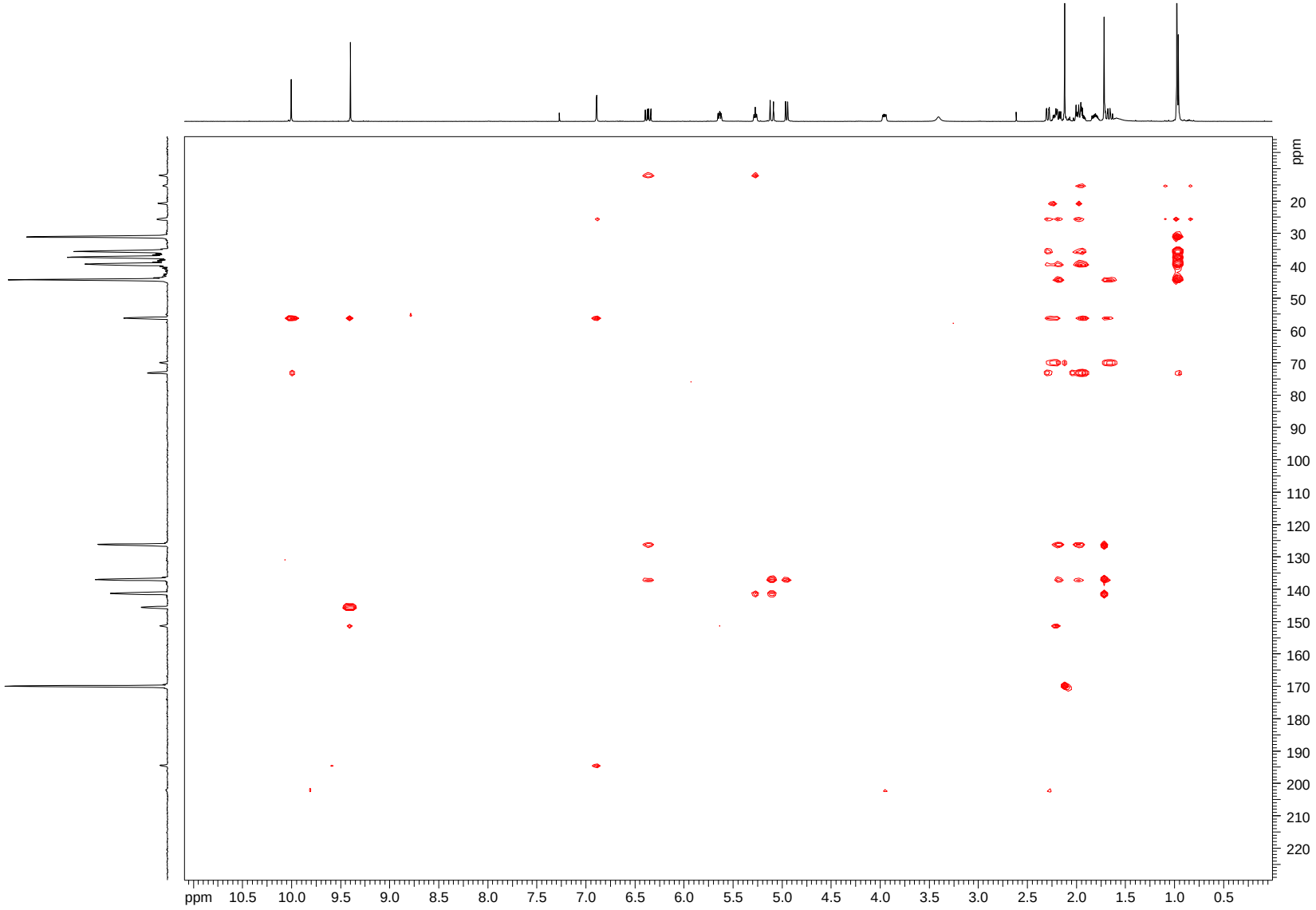

Figure S 5. HMBC spectrum of compound **1** in $CDCl_3$ (500 MHz).

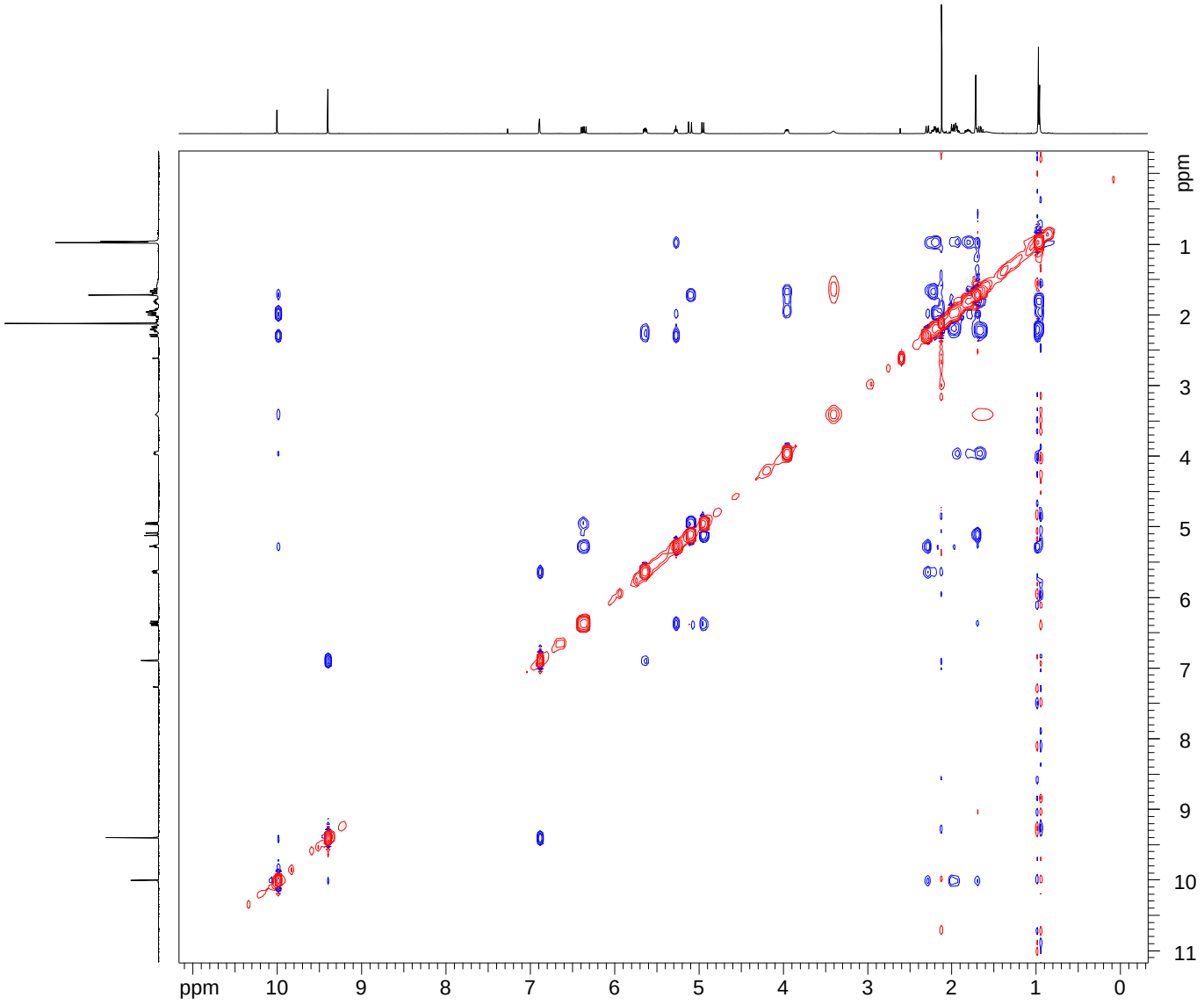

Figure S 6. ^{1}H-^{1}H NOESY spectrum compound **1** in $CDCl_3$ (500 MHz).

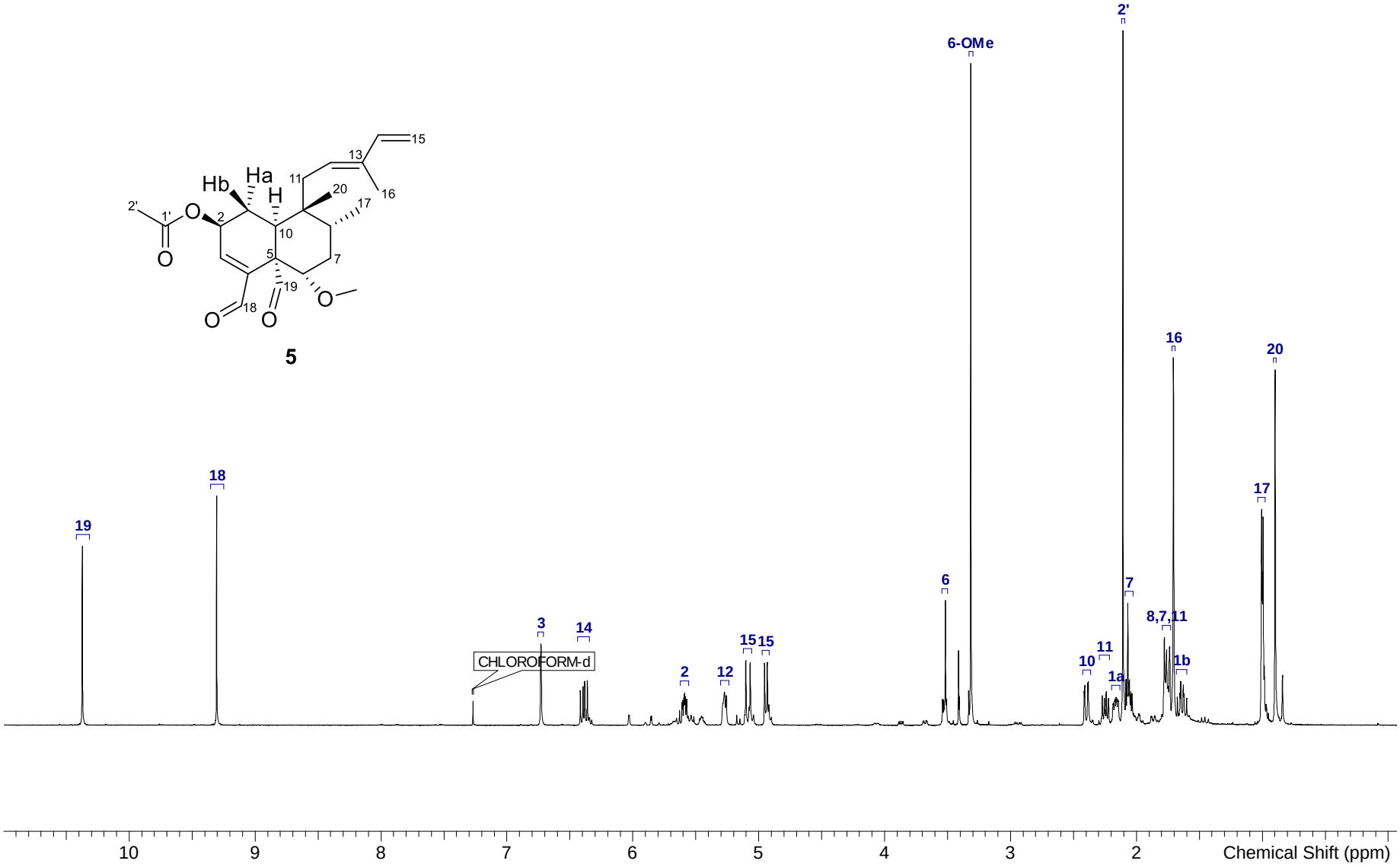

Figure S 7. ^{1}H NMR spectrum of compound **5** in $CDCl_3$ (500 MHz).

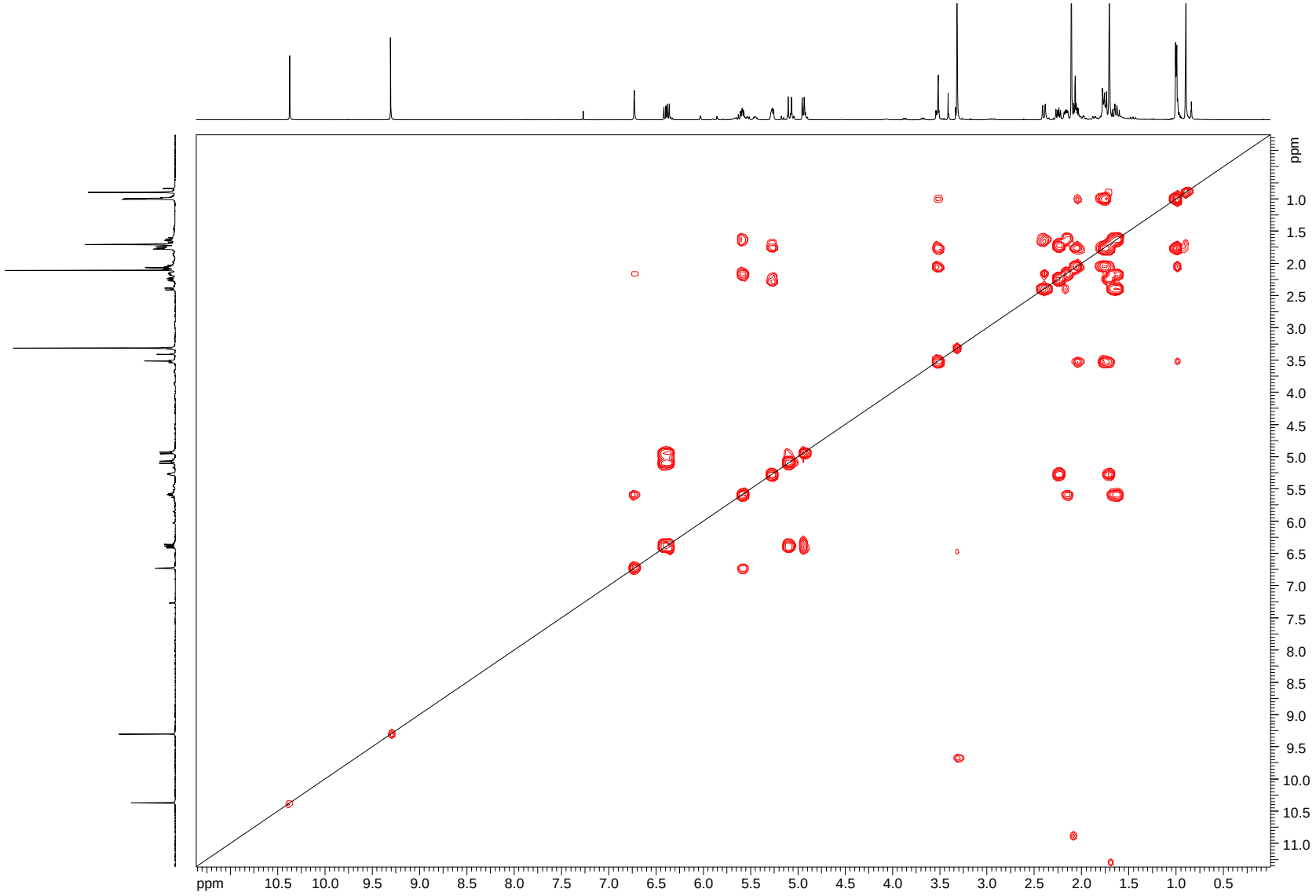

Figure S 8. ^{1}H-^{1}H COSY spectrum of compound **5** in $CDCl_3$ (500 MHz).

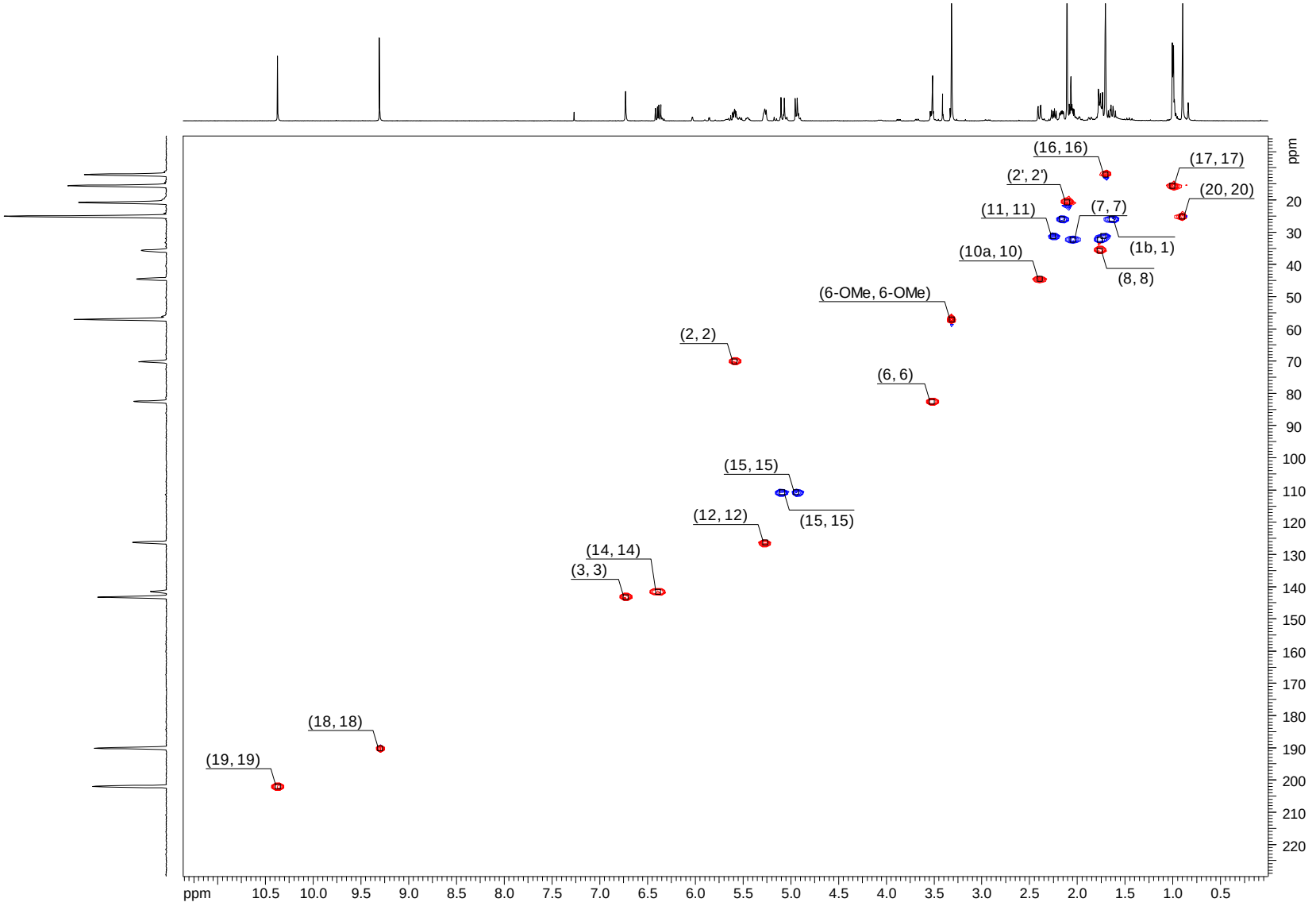

Figure S 9. HSQC spectrum of compound **5** in $CDCl_3$ (500 MHz).

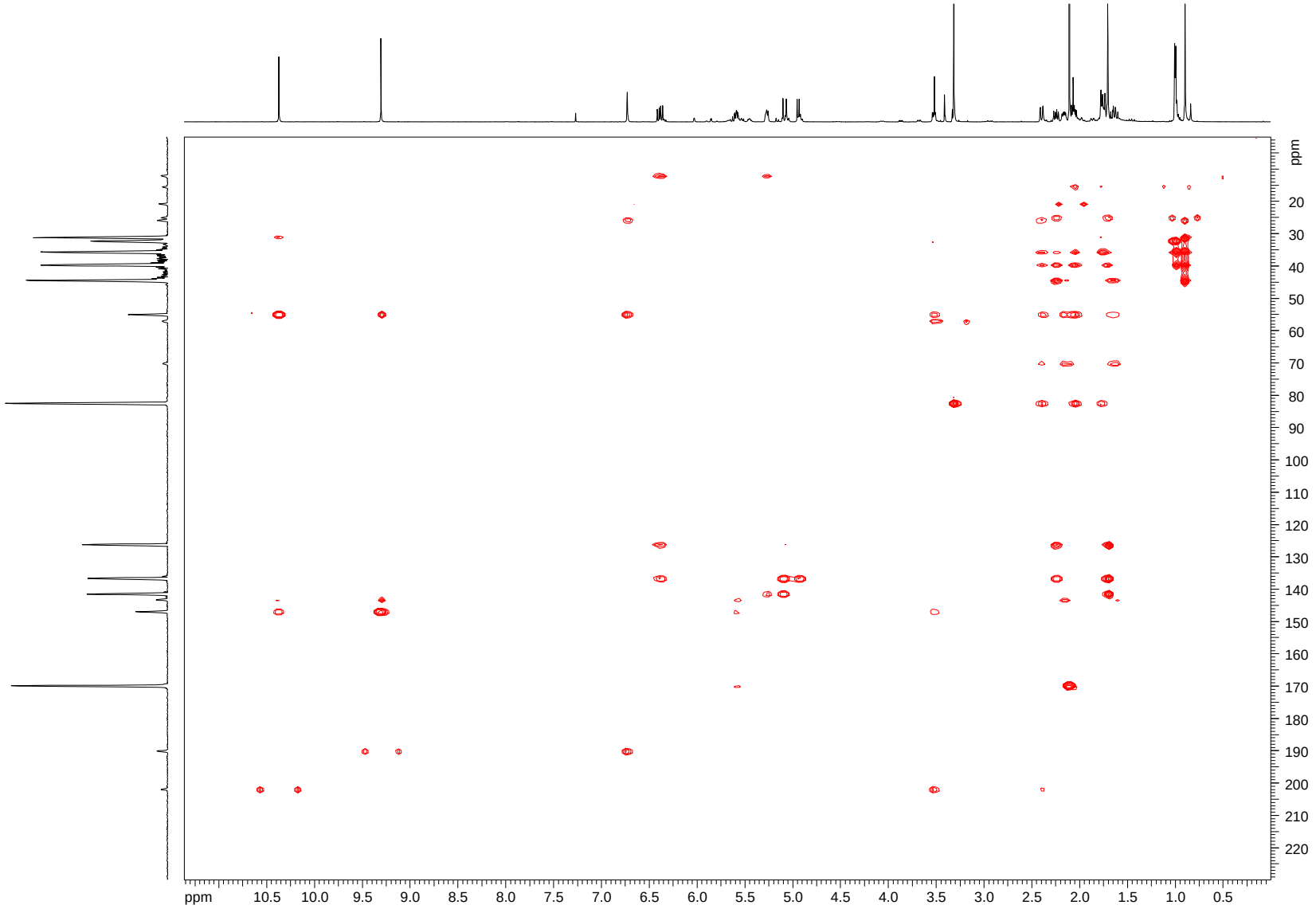

Figure S 10. HMBC spectrum of compound **5** in $CDCl_3$ (500 MHz).

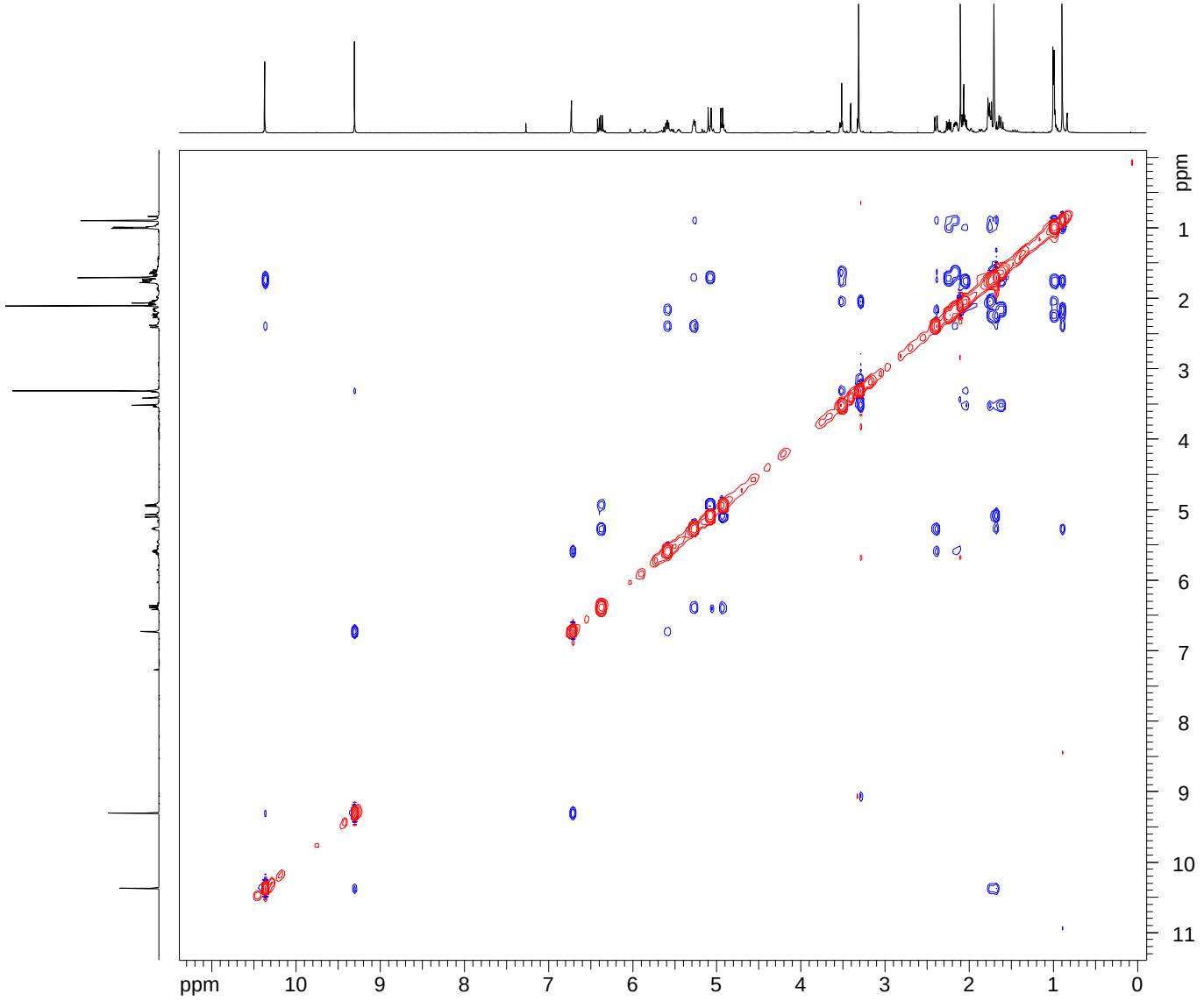

Figure S 11. ^{1}H-^{1}H NOESY spectrum of compound **5** in $CDCl_3$ (500 MHz).

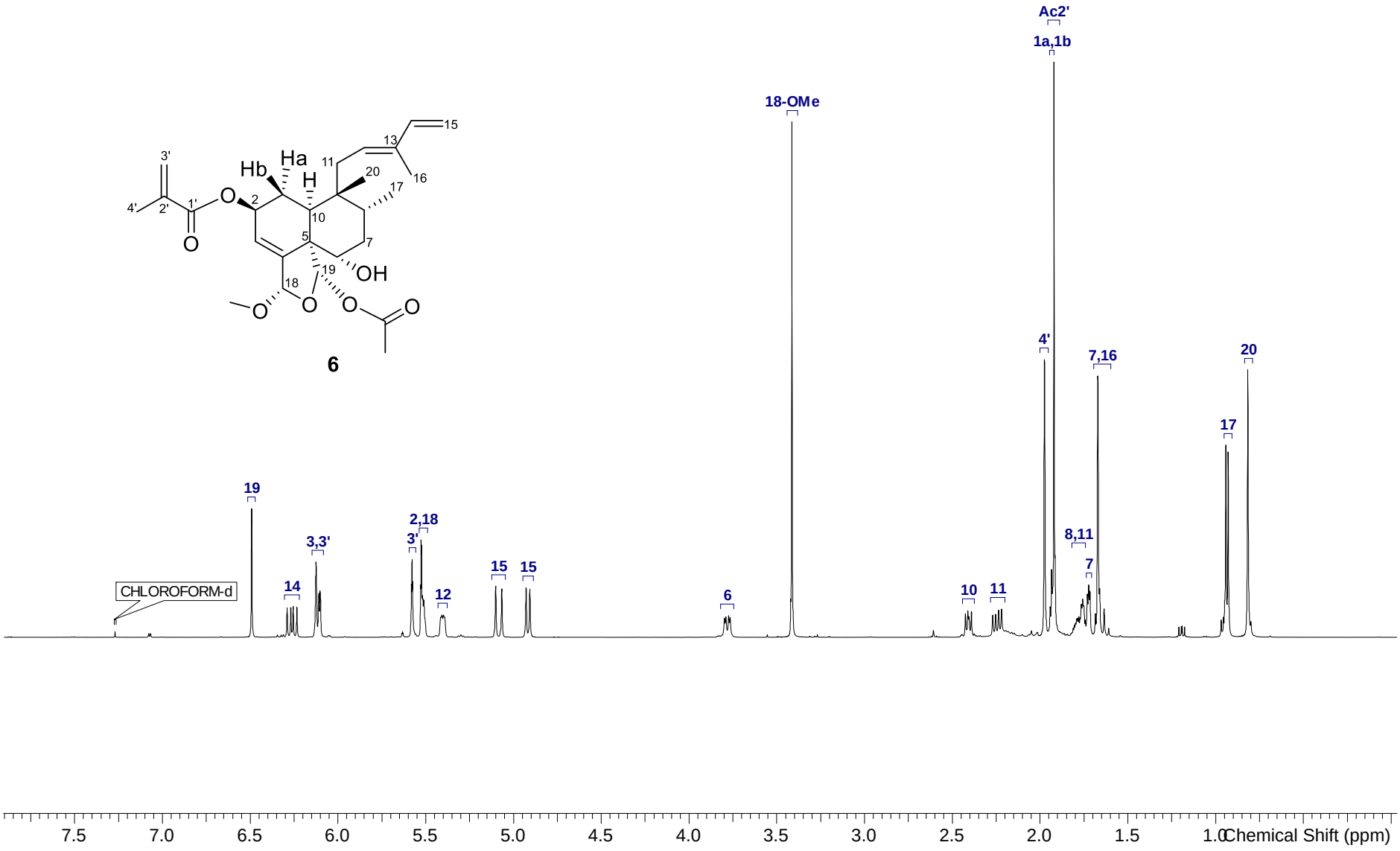

6

Figure S 12. ^{1}H NMR spectrum of compound **6** in $CDCl_3$ (500 MHz).

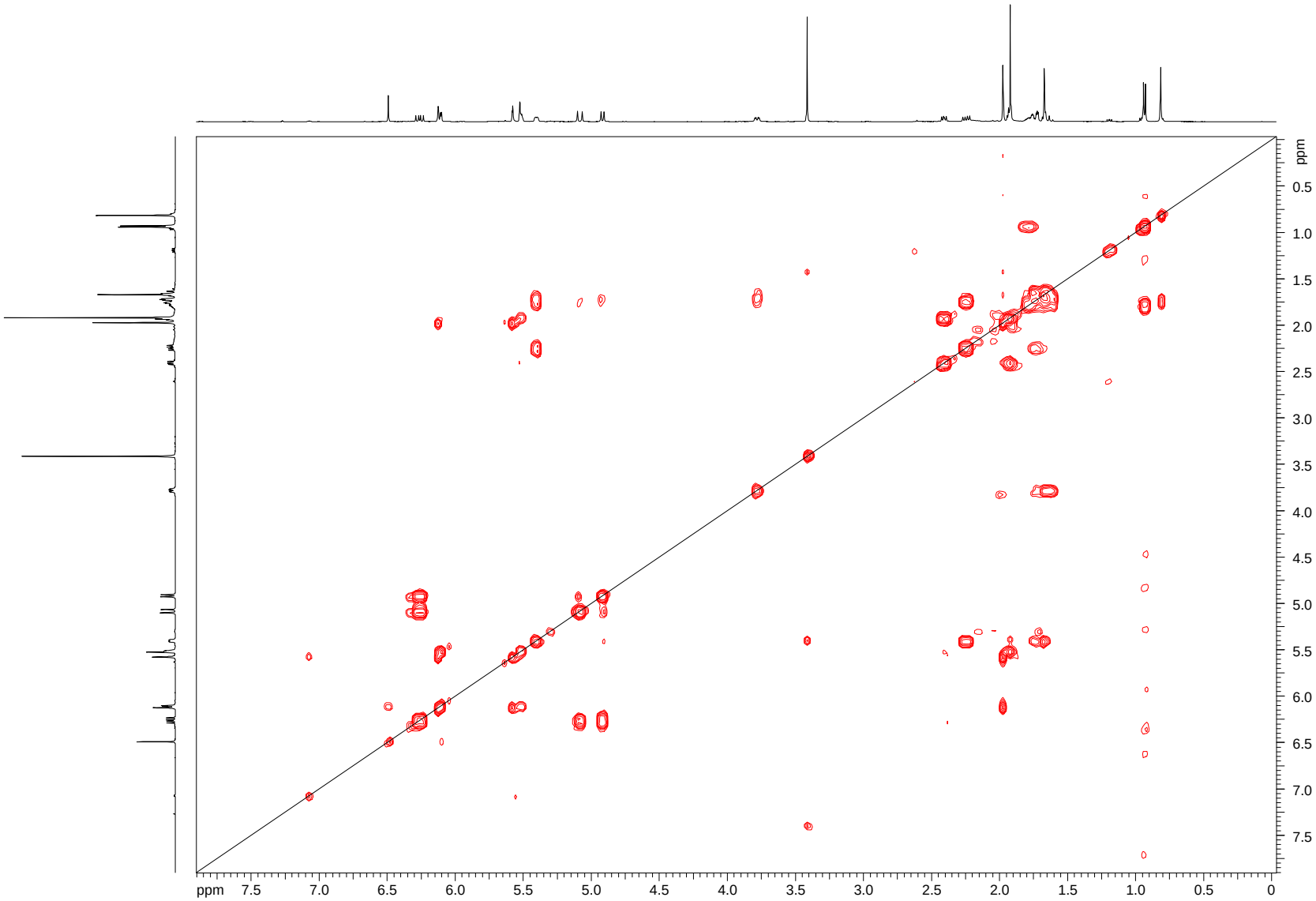

Figure S 13. ^{1}H-^{1}H COSY spectrum of compound **6** in $CDCl_3$ (500 MHz).

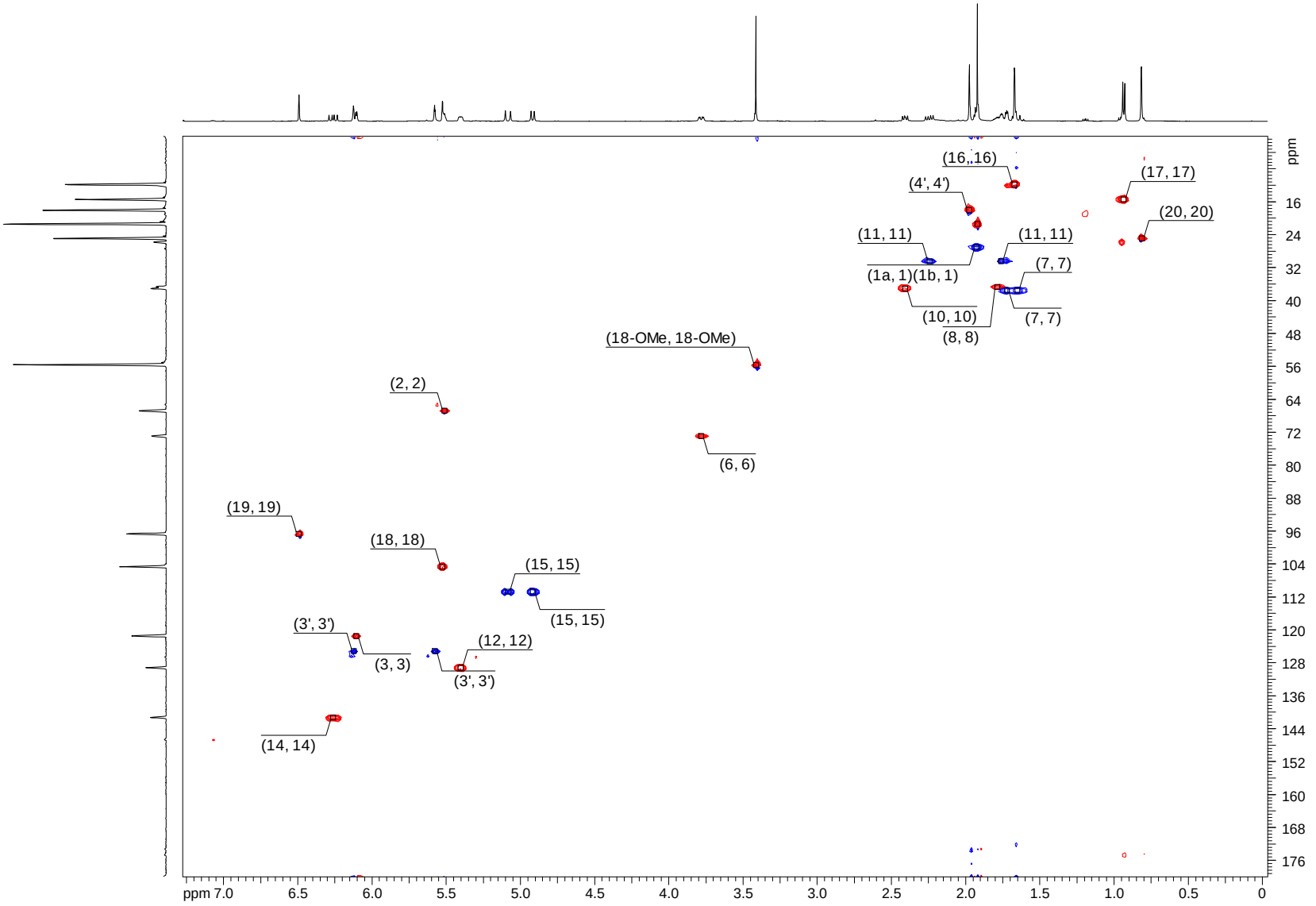

Figure S 14. HSQC spectrum of compound **6** in $CDCl_3$ (500 MHz).

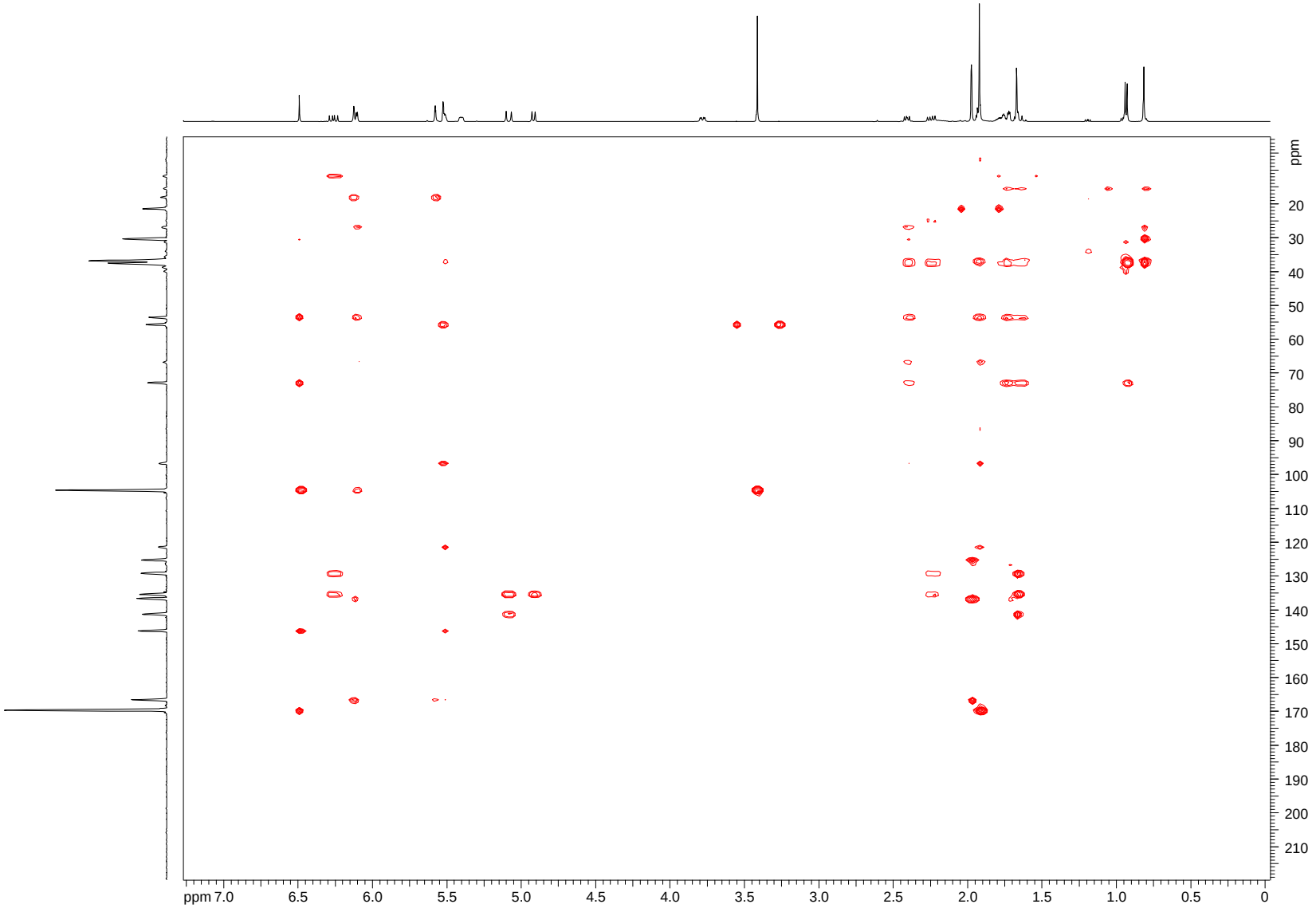

Figure S 15. HMBC spectrum of compound **6** in $CDCl_3$ (500 MHz).

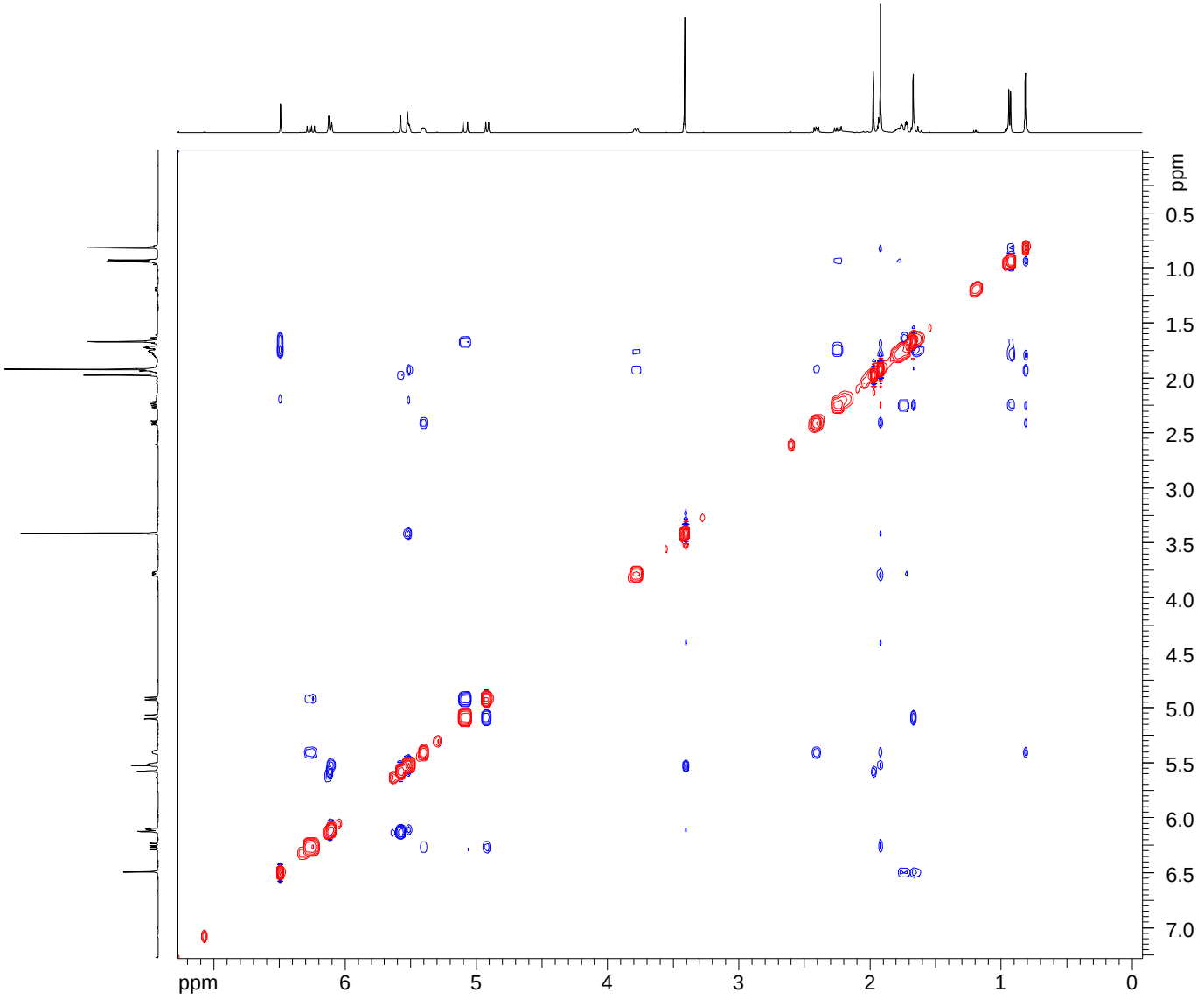

Figure S 16. ^{1}H-^{1}H NOESY spectrum of compound **6** in $CDCl_3$ (500 MHz).

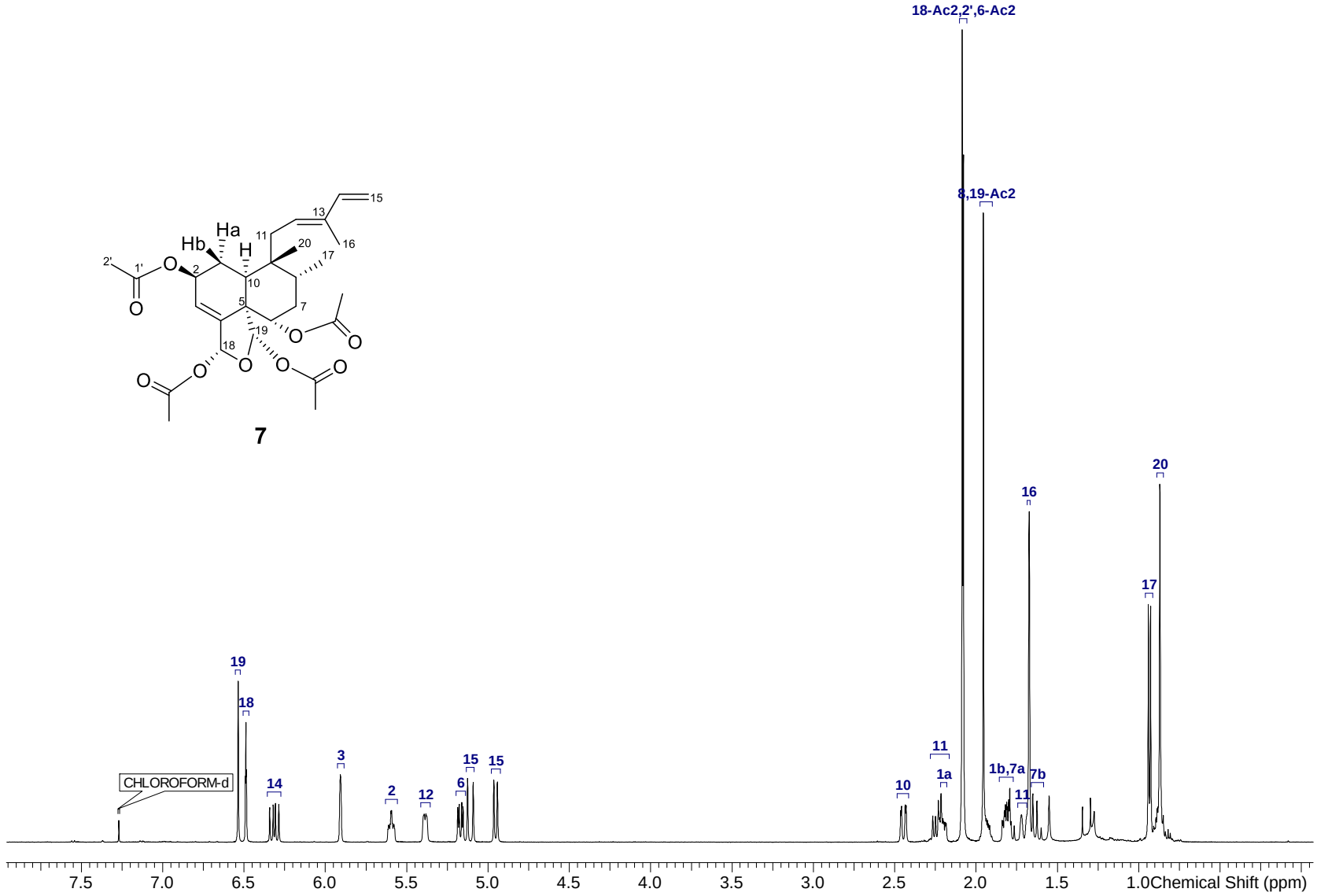

Figure S 17. ^{1}H NMR spectrum of compound **7** in $CDCl_3$ (500 MHz).

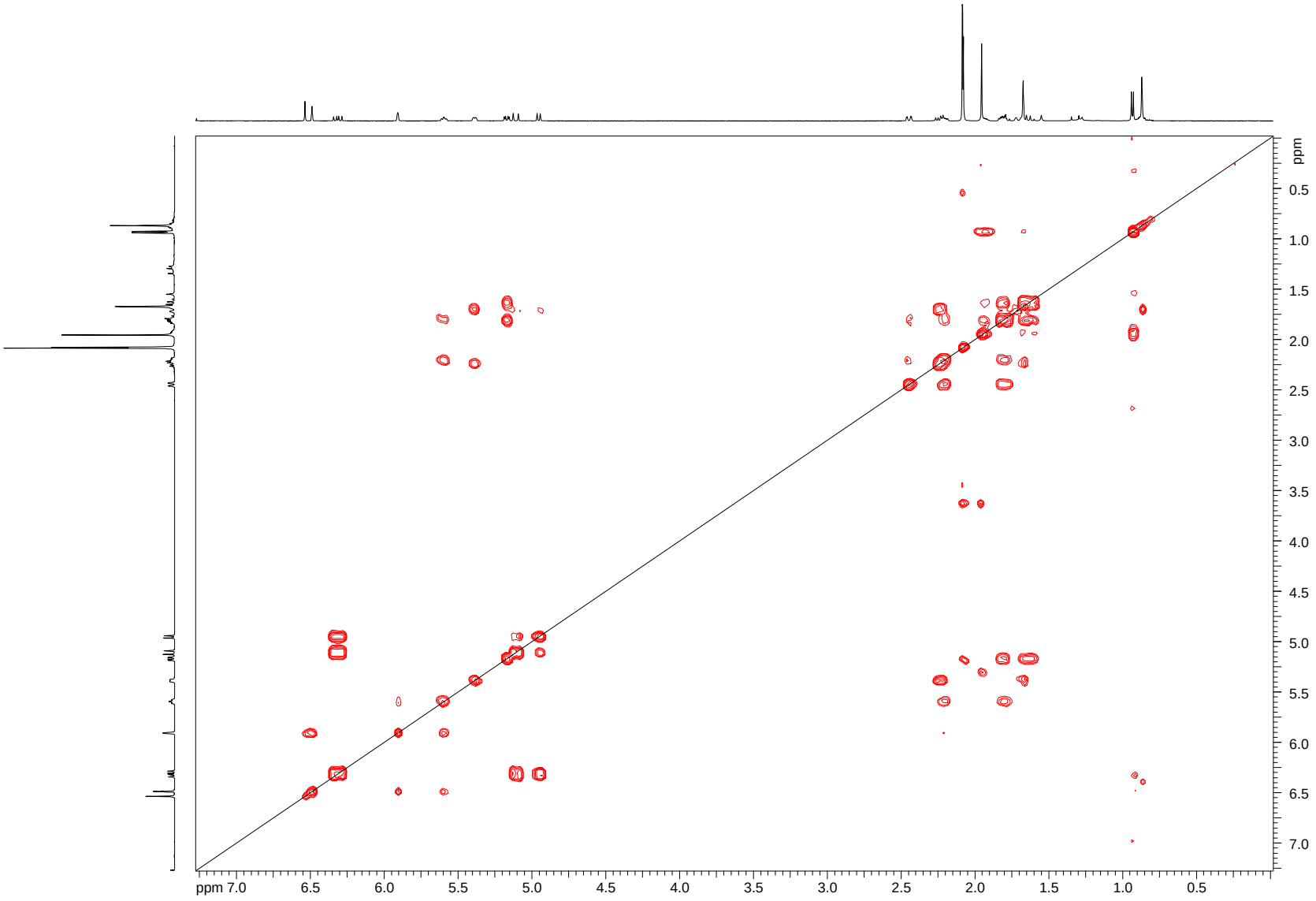

Figure S 18. ^{1}H-^{1}H COSY spectrum of compound **7** in $CDCl_3$ (500 MHz).

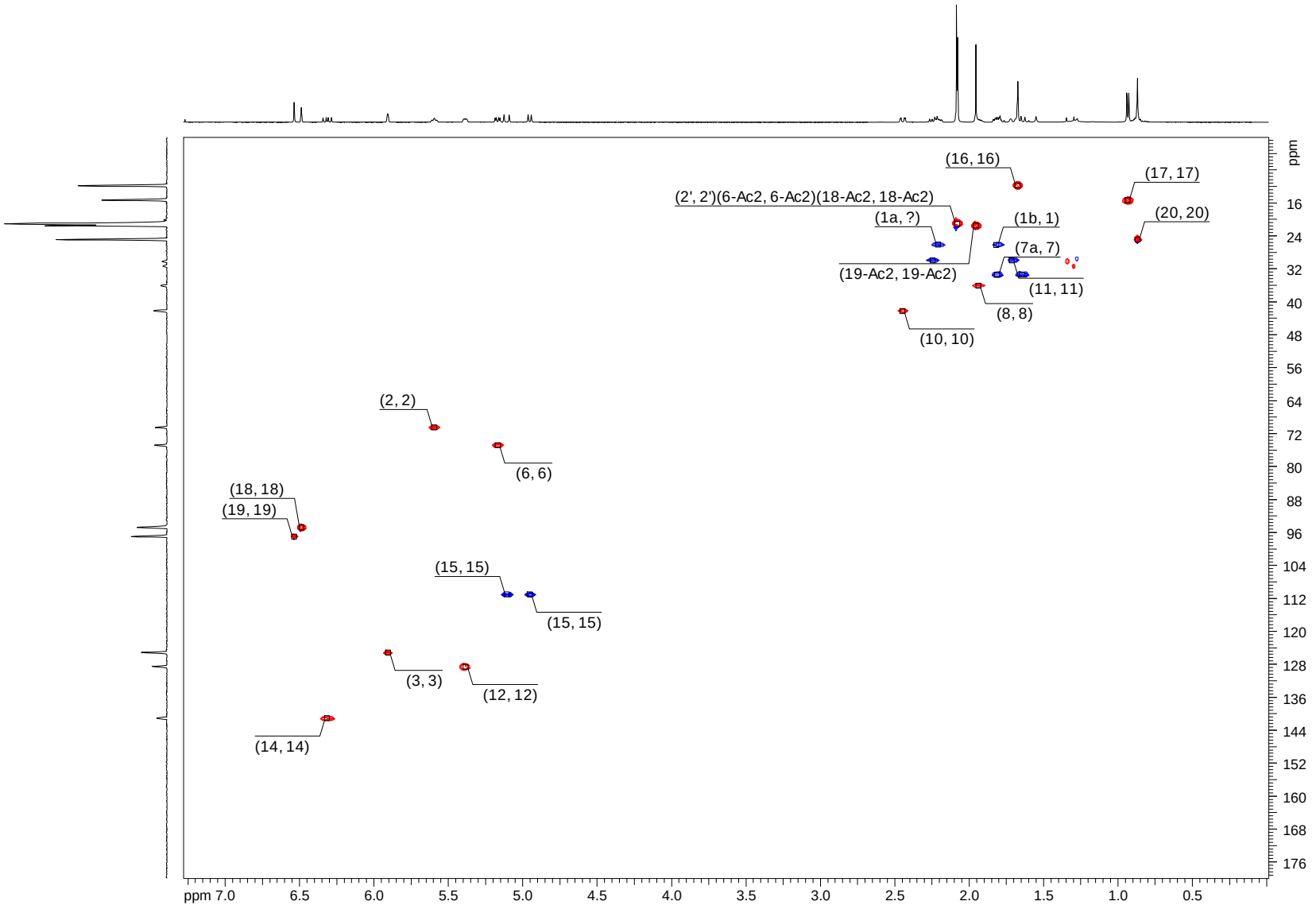

Figure S 19. HSQC spectrum of compound **7** in $CDCl_3$ (500 MHz).

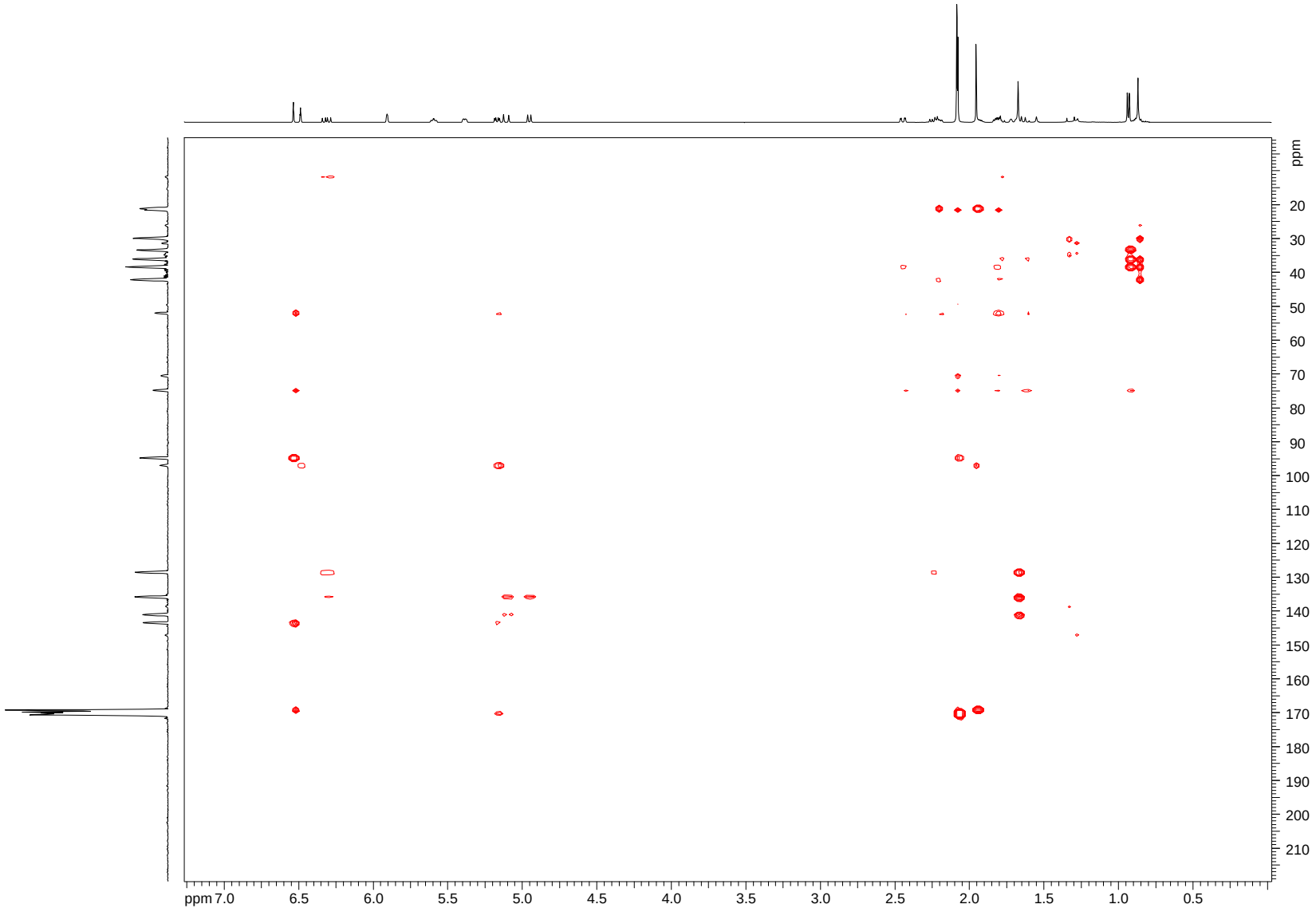

Figure S 20. HMBC spectrum of compound **7** in $CDCl_3$ (500 MHz).

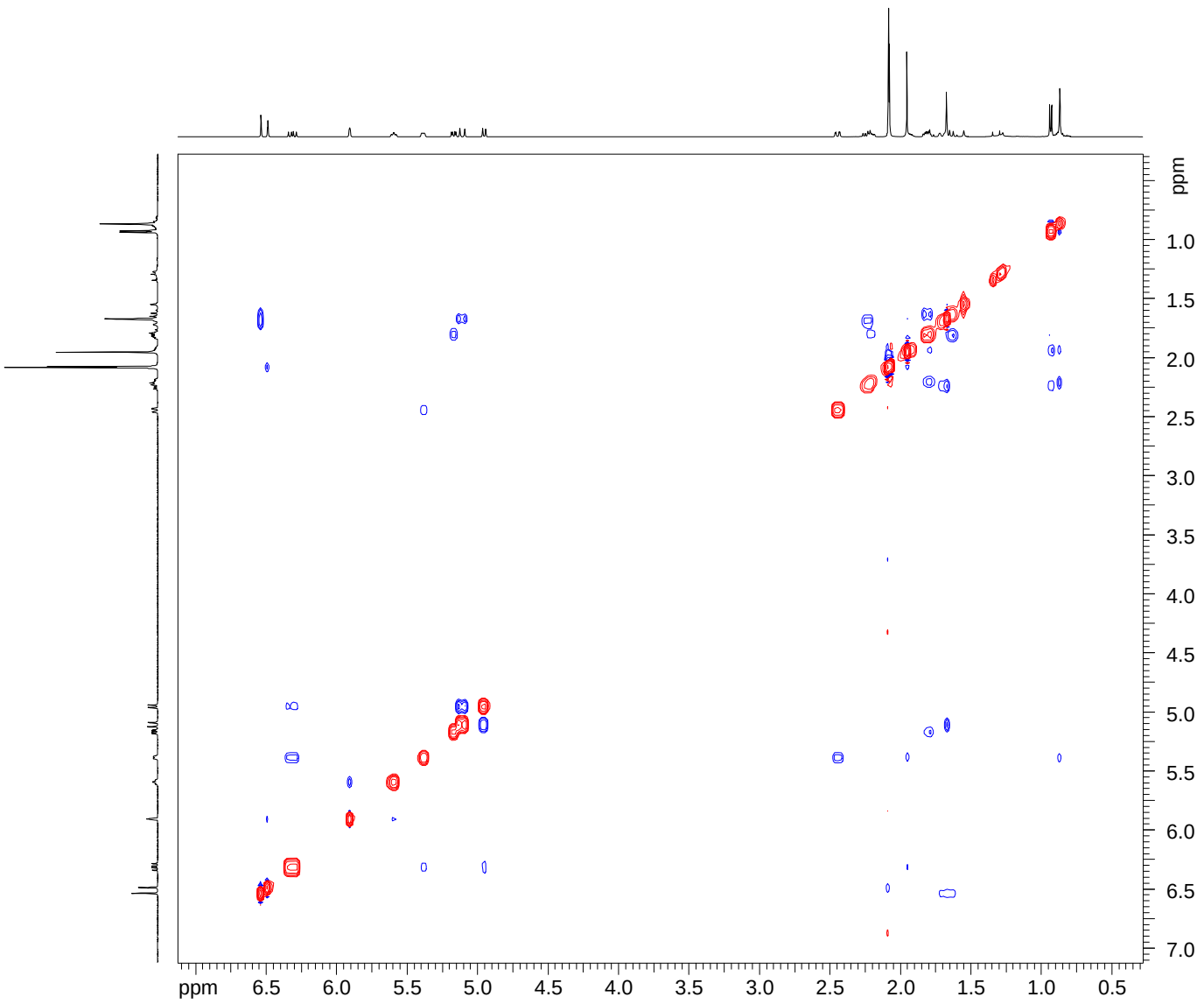

Figure S 21. ^{1}H-^{1}H NOESY spectrum of compound **7** in $CDCl_3$ (500 MHz).

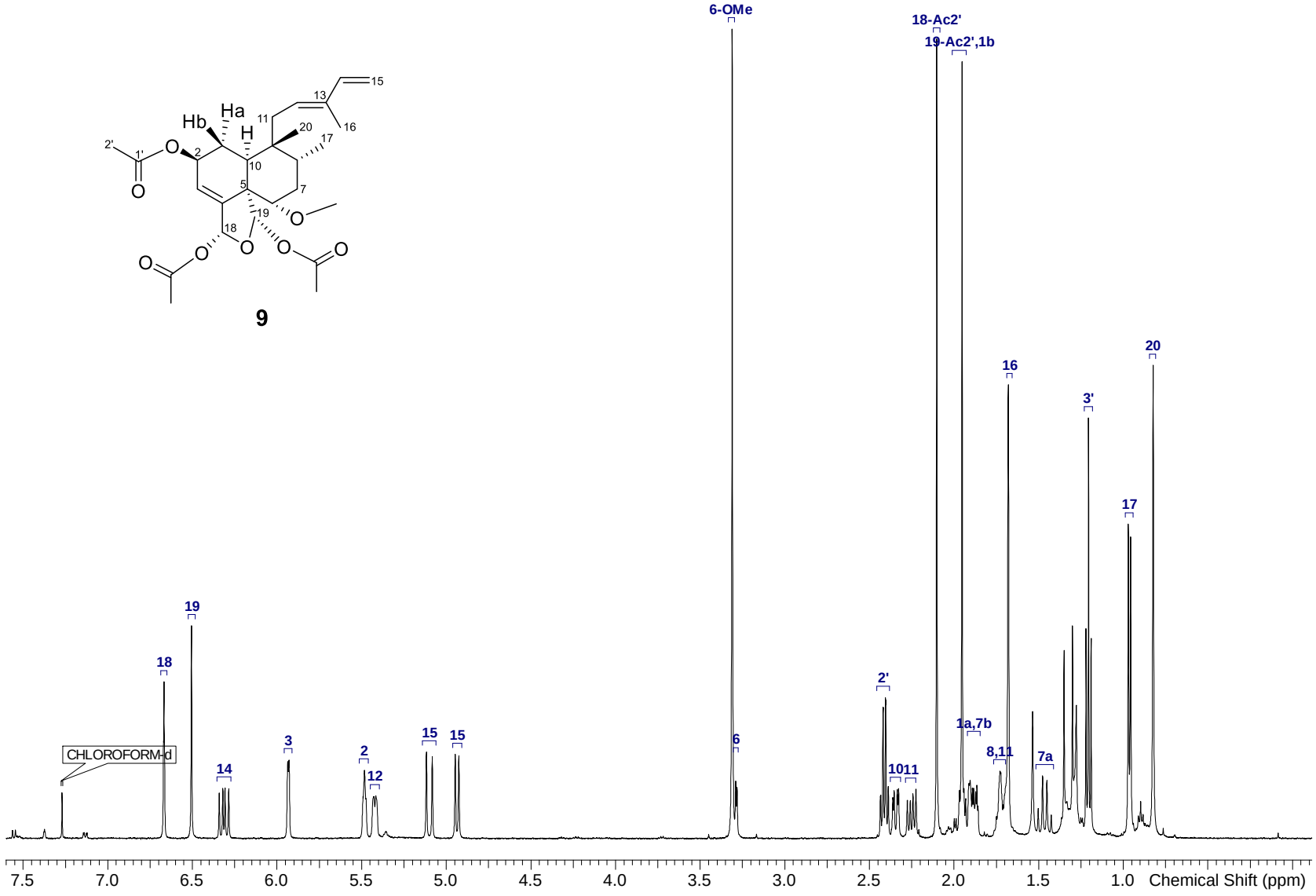

Figure S 22. ^{1}H NMR spectrum of compound **9** in $CDCl_3$ (500 MHz).

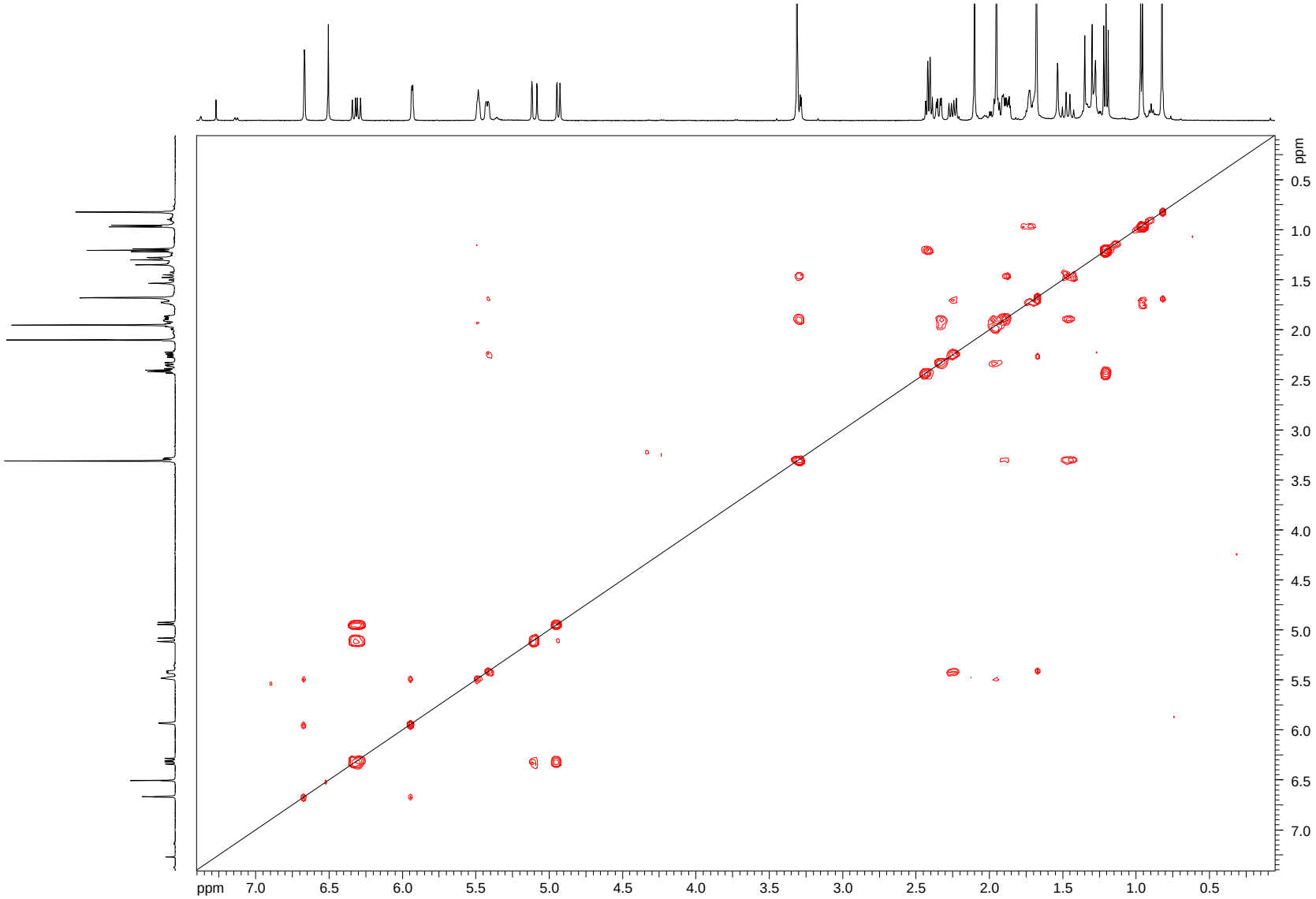

Figure S 23. ^{1}H-^{1}H COSY spectrum of compound **9** in $CDCl_3$ (500 MHz).

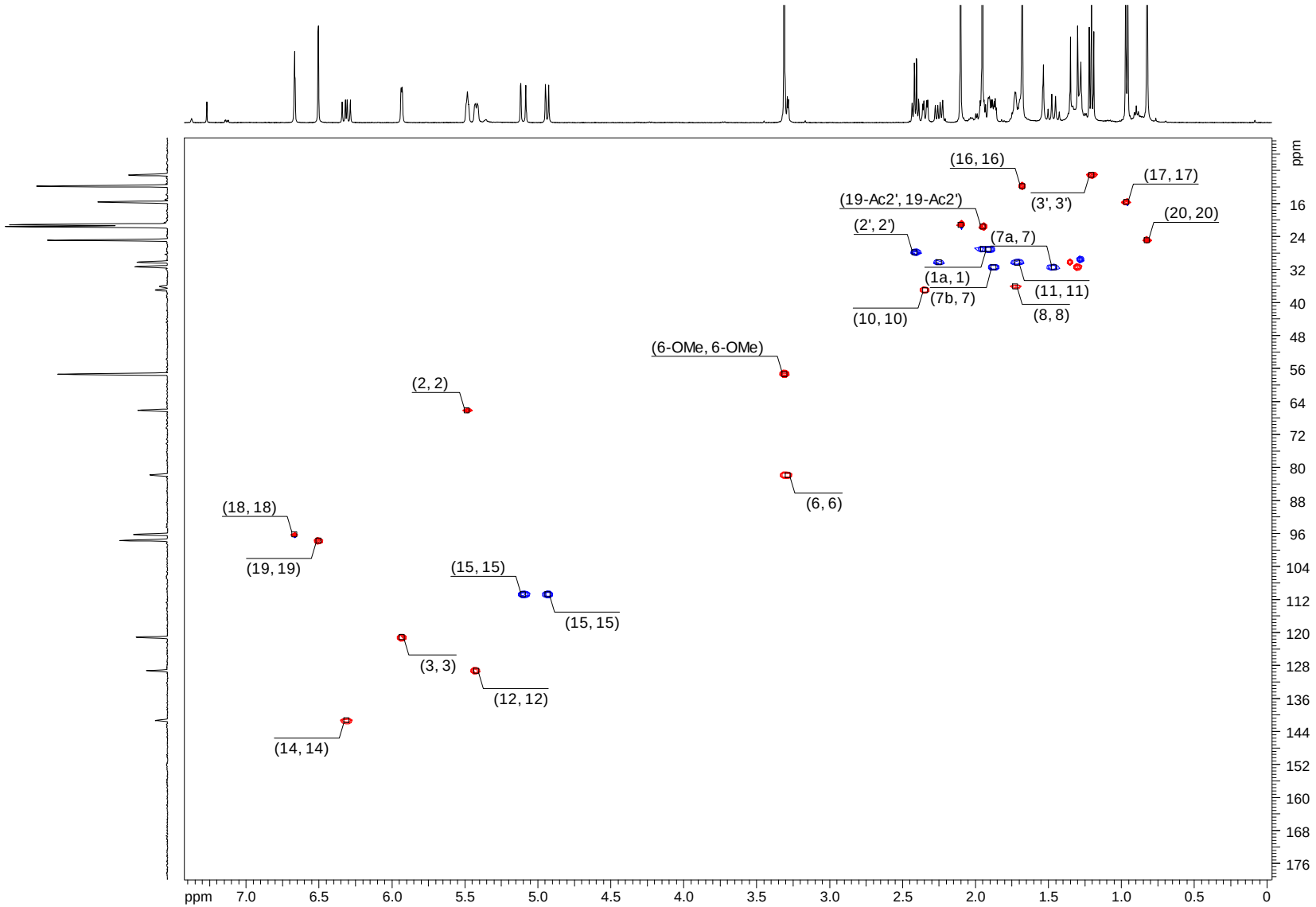

Figure S 24. HSQC spectrum of compound **9** in $CDCl_3$ (500 MHz).

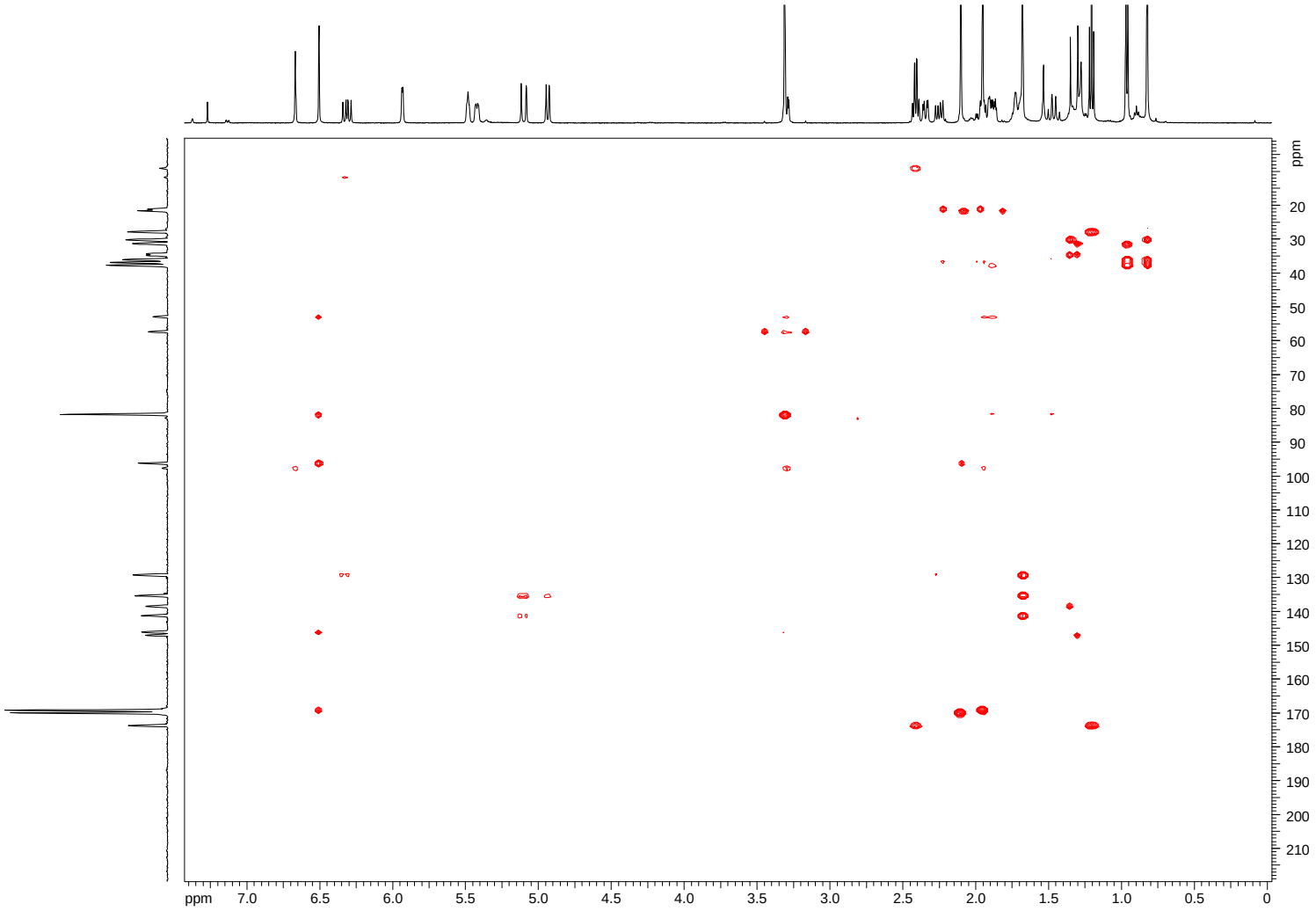

Figure S 25. HMBC spectrum of compound **9** in CDCl3 (500 MHz).

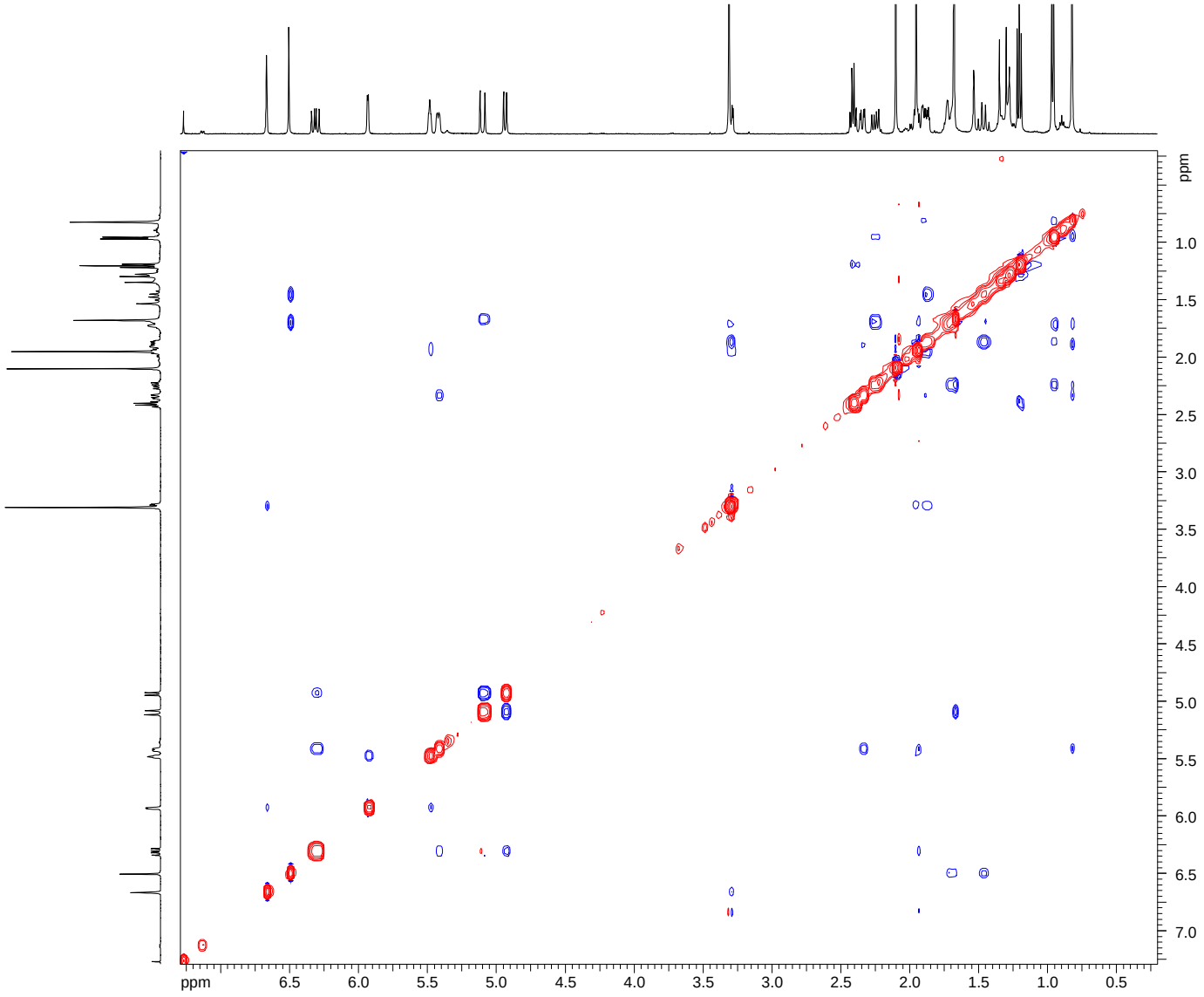

Figure S 26. ^{1}H-^{1}H NOESY spectrum of compound **9** in $CDCl_3$ (500 MHz).

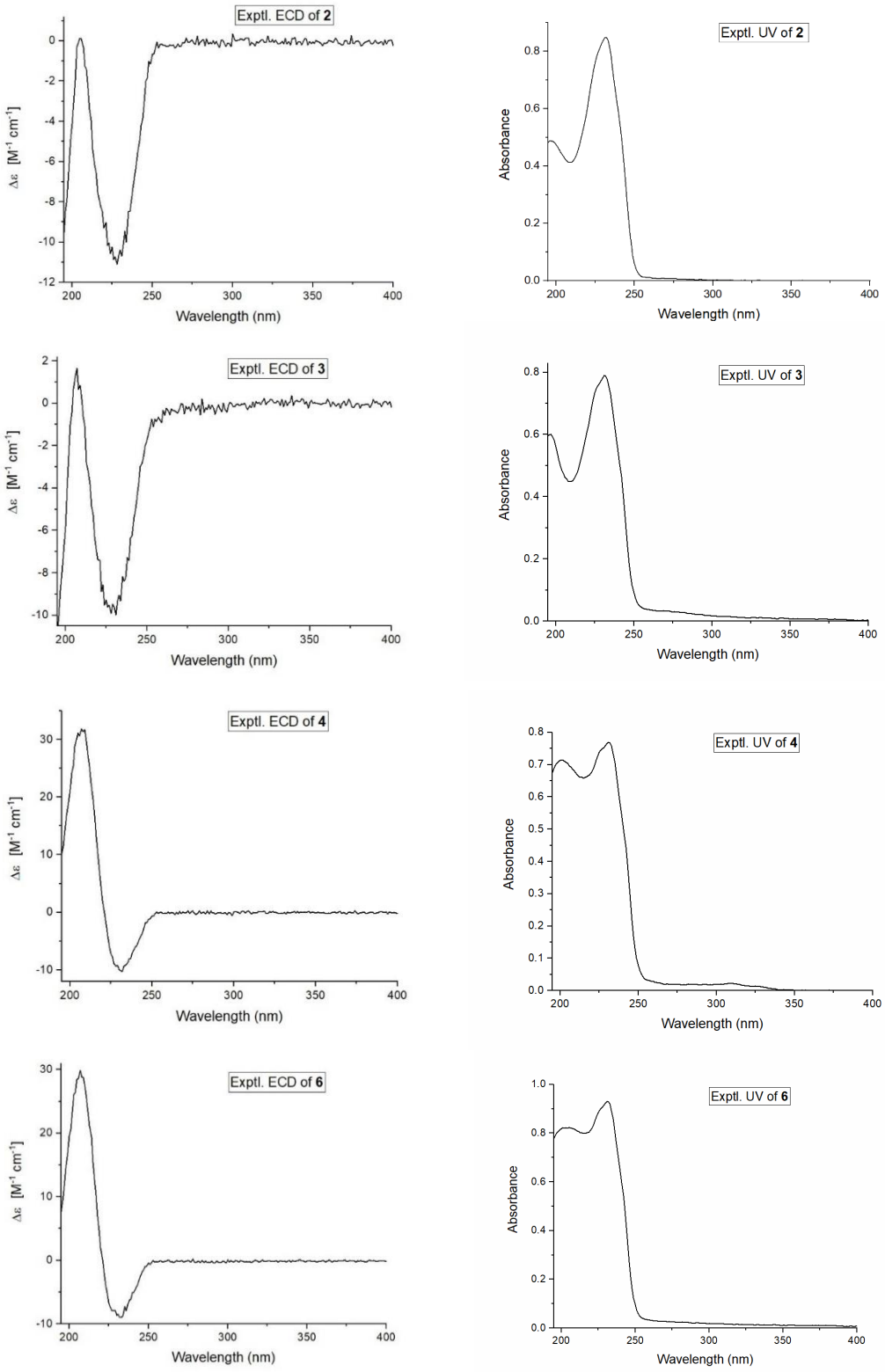

Figure S 27. Experimental ECD and UV spectra of compounds **2**-**4** and **6** in CH_3CN.

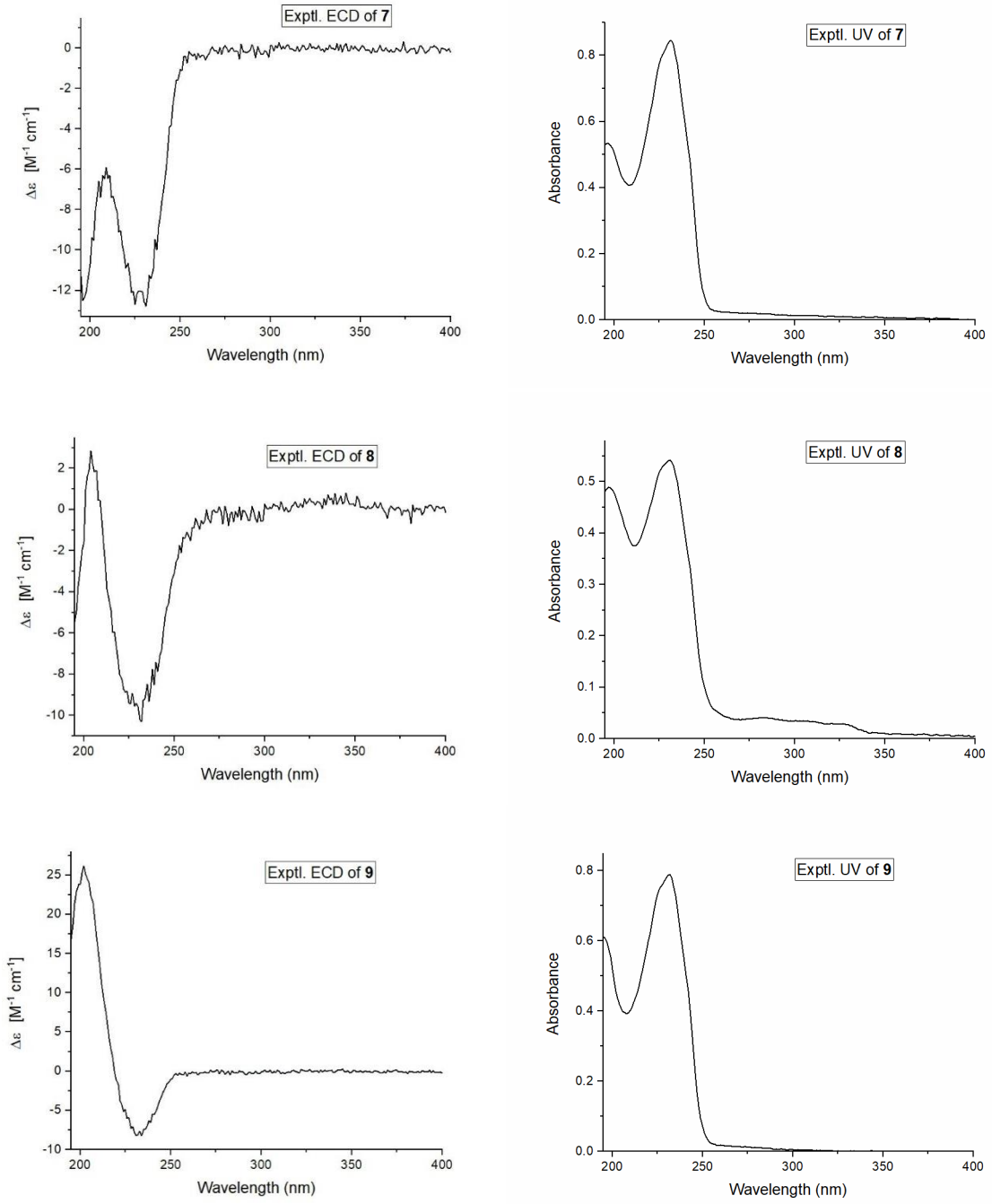

Figure S 28. Experimental ECD and UV spectra of compounds **7 - 9** in CH_3CN.

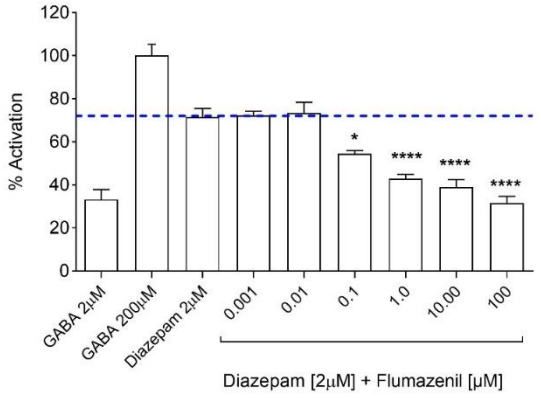

Figure S 29. Percentage of activation for 2 μM diazepam with increasing concentrations of flumazenil (in presence of 2 μM GABA), along with 2 μM GABA (control), 200 μM GABA (100%), and 2 μM diazepam (in presence of 2 μM GABA), (n=4, mean ± SEM). Final DMSO concentration in the assay was 0.2%. The * and **** above the bars indicate statistical significance with $p \leq 0.05$, and $p \leq 0.0001$, respectively.

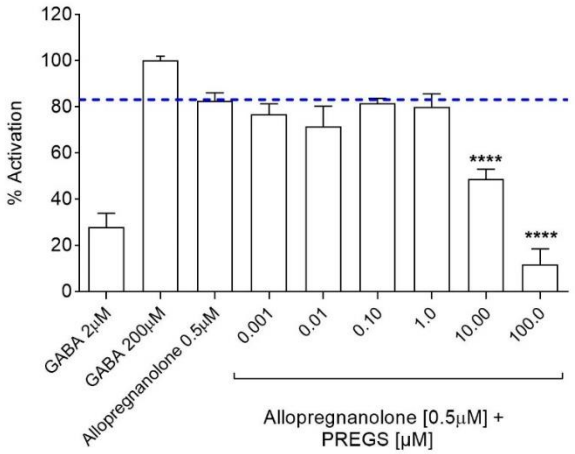

Figure S 30. Percentage of activation for 0.5 μM allopregnanolone with increasing concentrations of PREGS (in presence of 2 μM GABA), along with 2 μM GABA (control), 200 μM GABA (100%), and 0.5 μM allopregnanolone (in presence of 2 μM GABA) (n=4, mean ± SEM). Final DMSO concentration in the assay was 0.2%. The **** above the bars indicate statistical significance with $p \leq 0.0001$.

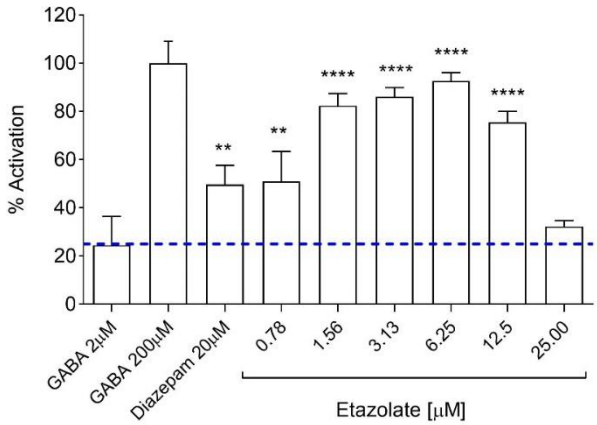

Figure S 31. Percentage of activation for increasing concentrations of etazolate (in presence of 2 µM GABA), along with 2 µM GABA (control), 200 µM GABA (100%), and 20 µM diazepam (in presence of 2 µM GABA), (n=4, mean ± SEM). Final DMSO concentration in the assay was 0.2%. The ** and **** above the bars indicate statistical significance with $p \leq 0.01$, and $p \leq 0.0001$, respectively.

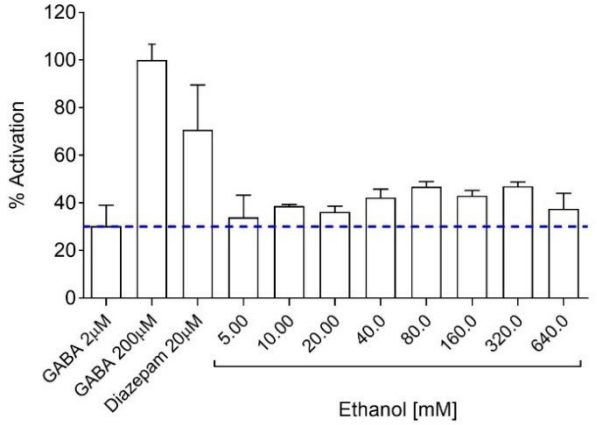

Figure S 32 Percentage of activation for increasing concentrations of ethanol (in presence of 2 µM GABA), along with 2 µM GABA (control), 200 µM GABA (100%), and 20 µM diazepam (in presence of 2 µM GABA), (n=4, mean ± SEM).

3.2. Immunosuppressant flavonoids from *Scutellaria baicalensis*

Nova Syafni, Seema Devi, Amy M. Zimmermann-Klemd, Jakob K. Reinhardt, Ombeline Danton, Carsten Gründemann, Matthias Hamburger

Submitted

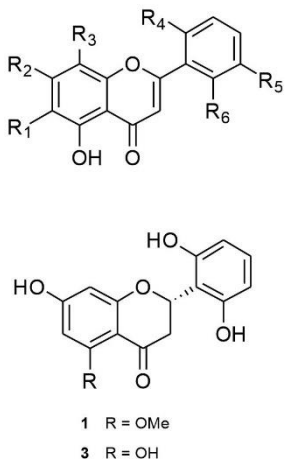

Compound	R_1	R_2	R_3	R_4	R_5	R_6
2	H	OH	OMe	OH	OH	OMe
4	H	OMe	OMe	OH	H	OH
5	OMe	OMe	OMe	OH	H	OH
6	H	OH	OMe	H	H	OH
7	H	OH	H	H	H	OH
8	H	OH	OMe	OH	H	OMe
9	OMe	OH	H	H	H	OH
10	H	OMe	OMe	OH	H	OMe
11	H	OH	OMe	H	H	H
12	OMe	OH	OMe	H	H	H
13	H	OH	H	H	H	H
14	OMe	OMe	OMe	OH	H	OMe
15	H	OMe	OMe	H	H	OH
16	OMe	OH	H	H	H	H
17	OMe	OMe	OMe	H	H	OH

Compounds wogonin (**11**), chrysin (**13**), skullcapflavone (**14**), and oroxylin A (**16**) were identified by their inhibition of T-cell proliferation (IC_{50} values at 20.2, 22.2, 12.1, and 39.0 μM, respectively) at non-cytotoxic concentrations. Compounds **2**, **4**, **8**, and **12** were mediate active immunosuppressant compounds with IC_{50} values of 55.9, 45.9, 61.6, and 50.2 μM, respectively. Most of the isolated flavonoids possessed an unusual substitution pattern on the B-ring, with an absence of substituents at C-3 and C-4.

Extraction of plant material, isolated all of the compounds, recorded and elucidated the structures of isolated compounds, writing the manuscript, in silico calculation on ACDLabs/Percepta, preparing HPLC-based activity profiling figure, compound structure figures, and tables were my contribution to this publication.

Nova Syafni

Immunosuppressant Flavonoids from *Scutellaria baicalensis*

Nova Syafni[1,2], Seema Devi[3], Amy M. Zimmermann-Klemd[3], Jakob K. Reinhardt[1], Ombeline Danton[1], Carsten Gründemann[4], Matthias Hamburger[1*]

[1]Pharmaceutical Biology, Department of Pharmaceutical Sciences, University of Basel, Basel, Switzerland

[2]Faculty of Pharmacy and Sumatran Biota Laboratory, University of Andalas, Padang, West Sumatra, Indonesia

[3]Center for Complementary Medicine, Institute for Infection Prevention and Hospital Epidemiology, Faculty of Medicine, University of Freiburg, Freiburg, Germany

[4]Translational Complementary Medicine, Department of Pharmaceutical Sciences, University of Basel, Basel, Switzerland

*** Correspondence:**
Prof. Matthias Hamburger
matthias.hamburger@unibas.ch

Abstract

A library of extracts from plants used in Traditional Chinese Medicine was screened for the *in vitro* inhibitory potential on the proliferation of human T lymphocytes. A dichloromethane extract from roots of *Scutellaria baicalensis* inhibited proliferation with an IC_{50} of 12.9 μg/mL. To localize compounds responsible for the activity, the extract was submitted to HPLC-based activity profiling, and two priority windows of activity were seen. Twelve compounds (**5-16**) were identified from the active time windows, and structurally related flavones **2**, **4**, and **17,** and flavanones **1** and **3** were isolated from adjacent fractions. All flavonoids possessed an unusual substitution pattern on the B-ring, with an absence of substituents at C-3 and C-4. Compounds **11**, **13**, **14**, and **16** inhibited T-cell proliferation (IC_{50} values at 12.1 to 39 μM) at non-cytotoxic concentrations.

Keywords: *Scutellaria baicalensis*, T-lymphocyte proliferation, Immunosuppressant activity, HPLC-based activity profiling, Flavonoids

INTRODUCTION

The immune system is built to discriminate self from non-self antigens. The loss of immunological tolerance to antigens can produce autoreactive immune responses (Santori, 2015). Immunosuppressive agents are an option for treating this condition. Since T-lymphocytes are a self-centered network in the immune system, most immunosuppressant drugs target the mechanism of enormous diversity in T-cells receptor and signaling pathways. An over-stimulated CD28 pathway (costimulatory pathways in T-cells) causes excessive proliferation and differentiation of naïve T-cells. The dysfunction of these costimulatory pathways triggers autoimmune diseases such as type-I diabetes and rheumatoid arthritis (Khan and Ghazanfar, 2018).

We recently screened an extract library prepared from 435 traditional Chinese herbal drugs for their ability to inhibit T-cell proliferation without concomitant cytotoxicity (Reinhardt et al., 2019; Zimmermann-Klemd et al., 2020). One of the promising hits in this screening was a dichloromethane (DCM) extract from roots of *Scutellaria baicalensis* Georgi (Lamiaceae) which exhibited an IC_{50} of

12.9 μg/mL. Huang Qin (黄芩; roots of *Scutellaria baicalensis*) is a widely used herbal drug in Traditional Chinese Medicine, and monographs have been published in the Chinese Pharmacopoeia (2015), the European Pharmacopoeia (EP 9.0), the British Pharmacopoeia (BP 2018), and the United States Pharmacopeia (USP 2020). The drug has been traditionally used for the treatment of nausea and vomiting in febrile diseases, dysentery, epistaxis, hemorrhage, inflammation, and respiratory infections (Tang and Eisenbrand, 2011). Flavonoids are the major secondary metabolites in the roots, and flavone glycosides (wogonin glucoside, baicalin, oroxyloside) and their aglycones (wogonin, baicalein, oroxyloside) have been identified (Wang et al., 2018). We here report on the activity-driven identification of compounds responsible for the immunosuppressant activity of the extract, and on the further evaluation of their activity.

MATERIALS AND METHODS

2.1 General

HPLC-grade acetonitrile (Scharlau) and water (Barnstead EASY-pure II water purification system) were used for HPLC separations. For analytical separations HPLC solvents contained 0.1% formic acid (Scharlau). DMSO (Scharlau) was used for dissolving the samples for HPLC analysis. Solvents used for extraction, column chromatography, and recrystallization were of technical grade (Romil Pure Chemistry) and were redistilled before use. Silica gel 60 F_{254} coated aluminum TLC plates and silica gel (0.063 − 0.200 mm) for column chromatography were from Merck. TLC plates were visualized under UV light and by spraying with 1% vanillin (Roth) in EtOH, followed by 10% sulfuric acid (Scharlab) in EtOH and heating at 110°C. Reagent grade aluminium chloride (Sigma-Aldrich) and reagent grade 36% hydrochloric acid (Hänseler) were used to prepare UV/vis shift reagents. HPLC-grade methanol (Scharlau) was used for UV, optical rotation and ECD measurements. Deuterated solvent (DMSO-d_6) for NMR was purchased from Armar Chemicals. Evaporation of microfractions was done with a Genevac EZ-2 plus vacuum centrifuge (Avantec).

HPLC-PDA-ELSD-MS analyses and HPLC-based microfractionation were performed with an instrument consisting of a degasser, quaternary pump (LC-20AD), column oven (CTO-20AC), PDA detector (SPD-M20A), and triple quadrupole mass spectrometer (LCMS-8030) (all Shimadzu), connected via a T-split to an ELSD 3300 detector (Alltech). A SunFire C18 column (3.5 μm, 3.0 x 150 mm) equipped with a guard column (3.0 x 10 mm) (Waters) was used for analytical separations. Data acquisition and processing were performed using lab solution software (Shimadzu).

Flash chromatography was carried out on a Puriflash 4100 system (Interchim). A glass column (25 x 460 mm i.d.) was used. Semi-preparative HPLC was carried out with an Agilent 1100 Series instrument with a PDA detector, and with a Waters 2690 instrument consisting of a degasser, binary high pressure mixing pump, column oven, and a Waters 996 photodiode array detector. A SunFire Prep C18 column (5 μm, 10 x 150 mm) equipped with a guard column (10 x 10 mm) (Waters) was used for separation.

NMR spectra were recorded with a Bruker Avance III spectrometer operating at 500.13 MHz for ^{1}H and 125.77 MHz for ^{13}C. ^{1}H NMR experiments and 2D homonuclear and heteronuclear NMR spectra were measured with a 1 mm TXI probe at 18°C. ^{13}C NMR spectra were obtained in 3 or 5 mm tubes with a BBO probe at 23°C. Data were analyzed using ACD/Spectrus Processor 2017.1.3.

Optical rotations were measured in MeOH on a P-2000 digital polarimeter (Jasco) equipped with a sodium lamp (589 nm) and a 10 cm temperature-controlled microcell. Electronic circular dichroism (ECD) spectra were recorded, at a concentration of 0.1 mg/mL in MeOH, on a Chirascan CD spectrometer with 1 mm path precision cells (110 QS, Hellma Analytics). UV/vis absorption spectra were recorded with a Lambda 35 spectrometer (PerkinElmer), either in pure MeOH and after addition of $AlCl_3$/HCl (Harborne et al, 1975).

2.2 Plant Material

Dried roots of *Scutellaria baicalensis* were purchased in November 2017 from Lian Chinaherb (Wollerau, Switzerland). A voucher specimen has been deposited at the Division of Pharmaceutical Biology, University of Basel, under plant number 1020.

2.3 Microfractionation for Activity Profiling

For microfractionation of the extract an FC 204 fraction collector (Gilson) adapted for 96-deepwell plates was connected to the LC-MS 8030 system (Shimadzu). Three injections of the extract (10 mg/mL in DMSO) were carried out: 2 x 30 µL (corresponding in total to 0.6 mg of extract) with only the PDA detector for collection of microfractions, and 1 x 10 µL with PDA-ELSD-ESI-MS detection for recording of on-line spectroscopic data. Water with 0.1% formic acid (A) and acetonitrile with 0.1% formic acid (B) were used as mobile phase. The gradient was 20% to 100% B in 30 min, followed by 10 min at 100% B. Microfractions of 1 min each were collected from minute 2 to minute 35, whereby corresponding microfractions of the two runs were collected into the same well. The deepwell plate was dried in a Genevac EZ-2 evaporator, and residues re-dissolved in DMSO prior to the bioassay.

2.4 Extraction and Isolation

Powdered *S. baicalensis* roots (160 g) were extracted at room temperature and under stirring with 2 x 400 mL DCM for two days each. The combined extracts were evaporated under reduced pressure to afford 1.4 g of dry residue. The extract was chromatographed on a silica gel column (25 x 460 mm) at a flow rate of 25 mL/min, using a step gradient (*n*-hexane, *n*-hexane/EtOAc, EtOAc, EtOAc/MeOH and MeOH). A total of 35 fractions were collected. Compounds detected in the active time window of the HPLC activity profile were localized in fractions 10, 13, 16, 18, 21, and 26, respectively. These fractions were further purified by semi-preparative HPLC and recrystallization.

Compound **11** (26.0 mg) was obtained from fraction 16 (47.2 mg) via recrystallization from a methanol/ethanol mixture. Fraction 10 (31.4 mg) was separated by semi-preparative RP-HPLC [H_2O + 0.1% formic acid (A), MeCN + 0.1% formic acid (B); 44% B (0-20 min); flow rate 4 mL/min] to afford **16** (17.0 mg, t_R 15.1 min). Fraction 13 (8.5 mg) (semi-preparative RP-HPLC [H_2O + 0.1% formic acid (A), MeCN + 0.1% formic acid (B); isocratic 42% B (0-25 min); flow rate 4 mL/min]) afforded compound **13** (2.1 mg, t_R 14.1 min), and fraction 18 (16.0 mg) [H_2O + 0.1% formic acid (A), MeCN + 0.1% formic acid (B); 43-45% B (0-25 min); flow rate 4 mL/min] yielded compounds **11** (1.6 mg, t_R 12.0 min), **12** (3.5 mg, t_R 12.5 min), **15** (5.8 mg, t_R 13.5 min), and **17** (5.4 mg, t_R 15.6 min). Fraction 21 (70.4 mg) (semi-preparative RP-HPLC [H_2O + 0.1% formic acid (A), MeCN + 0.1% formic acid (B); 38-42% B (0-25 min); flow rate 4 mL/min]) yielded compounds **10** (6.0 mg, t_R 14.9 min), and **14** (50.0 mg, t_R 18.2 min), fraction 26 (25.5 mg) [H_2O + 0.1% formic acid (A), MeCN + 0.1% formic acid (B); 38-42% B (0-25 min); flow rate 4 mL/min] afforded compounds **3** (1.1 mg, t_R 12.9 min), **4** (0.6 mg, t_R 17.9 min), **5** (1.3 mg, t_R 21.3 min), **8** (3.4 mg, t_R 24.3 min), **6** (0.3 mg, t_R 26.1 min), **7** (0.2 mg, t_R 27.4 min), and **9** (1.0 mg, t_R 28.0 min), and fraction 29 (17.5 mg) [H_2O + 0.1% formic acid (A), MeCN + 0.1% formic acid (B); 21-24% B (0-24 min); flow rate 4 mL/min] gave compounds **1** (0.5 mg, t_R 9.1 min) and **2** (1.0 mg, t_R 19.1 min).

(2S)-7,2',6'-Trihydroxy-5-methoxyflavanone (**1**): yellowish amorphous solid, $[\alpha]_D^{25}$ = 11.2 (*c* 0.03, MeOH); ECD (MeOH, *c* 0.1 mg/mL , 1 mm path length)) λ_{max} ($\Delta\varepsilon$): 223 (+3.5), 278 (-1.3), 332 (+0.9); ^{1}H and ^{13}C NMR, see Table S1, Supplementary Material; ESIMS *m/z* 303 $[M+H]^+$.
5,7,3',6'-Tetrahydroxy-8,2'-dimethoxyflavone (Viscidulin III) (**2**): pale yellow amorphous solid, ^{1}H and ^{13}C NMR, see Table S2, Supplementary Material; ESIMS *m/z* 347 $[M+H]^+$.

(2S)-5,7,2',6'-Tetrahydroxyflavanone (**3**): yellowish amorphous solid, $[\alpha]_D^{25}$ = 20.7 (*c* 0.02, MeOH); ECD (MeOH, *c* 0.2 mg/mL, 1 mm path length)) λ_{max} ($\Delta\varepsilon$): 223 (+2.9), 284 (-1.9), 325 (+0.5); ^{1}H and ^{13}C NMR, see Table S1, Supplementary Material; ESIMS *m/z* 289 $[M+H]^+$.
5,2',6'-Trihydroxy-7,8-dimethoxyflavone (**4**): ^{1}H and ^{13}C NMR, see Table S3, Supplementary Material; ESIMS *m/z* 331 $[M+H]^+$.
5,2',6'-Trihydroxy-6,7,8-trimethoxyflavone (**5**): yellow amorphous solid, ^{1}H and ^{13}C NMR, see Table S3, Supplementary Material; ESIMS *m/z* 361 $[M+H]^+$.
5,7,2'-Trihydroxy-8-methoxyflavone (Scutevulin) (**6**): pale yellow amorphous solid, ^{1}H and ^{13}C NMR, see Table S3, Supplementary Material; ESIMS *m/z* 301 $[M+H]^+$.
5,7,2'-Trihydroxyflavone (**7**): yellow amorphous solid, ^{1}H and ^{13}C NMR, see Table S3, Supplementary Material; ESIMS *m/z* 271 $[M+H]^+$.
5,7,6'-Trihydroxy-8,2'-dimethoxyflavone (**8**): yellow amorphous solid, ^{1}H and ^{13}C NMR, see Table S2, Supplementary Material; ESIMS *m/z* 331 $[M+H]^+$.
5,7,2'-Trihydroxy-6-methoxyflavone (Tenaxin II) (**9**): yellow amorphous solid, ^{1}H and ^{13}C NMR, see Table S4, Supplementary Material; ESIMS *m/z* 301 $[M+H]^+$.
5,6'-Dihydroxy-7,8,2'-trimethoxyflavone (Rivularin) (**10**): yellow amorphous solid, ^{1}H and ^{13}C NMR, see Table S2, Supplementary Material; ESIMS *m/z* 345 $[M+H]^+$.
Wogonin (**11**): yellow needles, ^{1}H and ^{13}C NMR, see Table S4, Supplementary Material; ESIMS *m/z* 285 $[M+H]^+$.
5,7-Dihydroxy-6,8-dimethoxyflavone (**12**): yellow amorphous solid, ^{1}H and ^{13}C NMR, see Table S4, Supplementary Material; ESIMS *m/z* 315 $[M+H]^+$.
Chrysin (**13**): yellow amorphous solid, ^{1}H and ^{13}C NMR, see Table S4, Supplementary Material; ESIMS *m/z* 255 $[M+H]^+$.
Skullcapflavone II (**14**): yellow amorphous solid, ^{1}H and ^{13}C NMR, see Table S2, Supplementary Material; ESIMS *m/z* 375 $[M+H]^+$.
Skullcapflavone I (**15**): yellow amorphous solid, ^{1}H and ^{13}C NMR, see Table S5, Supplementary Material; ESIMS *m/z* 315 $[M+H]^+$.
Oroxylin A (**16**): yellow amorphous solid, ^{1}H and ^{13}C NMR, see Table S5, Supplementary Material; ESIMS *m/z* 285 $[M+H]^+$.
5,2'-Dihydroxy-6,7,8-trimethoxyflavone (Tenaxin I) (**17**): yellow amorphous solid, ^{1}H and ^{13}C NMR, see Table S5, Supplementary Material; ESIMS *m/z* 345 $[M+H]^+$.

2.5 Preparation and Cultivation of Human Peripheral Lymphocytes

Peripheral blood mononuclear cells (PBMCs) were isolated from the blood of healthy adult donors obtained from the Blood Transfusion Centre (University Medical Centre, Freiburg, Germany). Venous blood was centrifuged on a LymphoPrep gradient (density: 1.077 g/cm^3, 20 min, 500*g*, 20 ºC; Progen). After centrifugation, cells were wash twice with phosphate-buffered saline (PBS) and subsequently cultured in RPMI 1640 medium supplemented with 10% heat-inactivated fetal calf serum (GE Healthcare Life Sciences), 2 mM L-glutamine, 100 U/mL penicillin, and 100 U/mL streptomycin (all from Life Technologies). The cells were cultured at 37 ºC in a humidified incubator with a 5% CO_2/95% air atmosphere.

2.6 T Cell Proliferation Assay

Lymphocytes were isolated, washed twice in cold PBS, and resuspended in PBS at concentration of 5 x 10^6 cells/mL. Cells were stained for 10 min at 37 ºC with carboxyfluorescein diacetate succinimidyl ester (CFSE; 5 µM: Sigma-Aldrich, St. Louis, MO, USA). The staining was stopped by washing twice with complete medium. Stained lymphocytes (2 x 10^6 cells/mL) were stimulated with anti-human CD3 (clone HIT3a) and anti-human CD28 (clone 28.2) mAbs (each 100 ng/mL; eBioscience) in the presence

of either medium, cyclosporine A (CsA; 4.16 μM; Novartis Pharma), camptothecin (CPT; 300 μM; Tocris), or plant extracts/single compounds (concentration range 0.01 – 100 μg/mL) and incubated for 72 h. The negative control remained unstimulated. Flow cytometric analysis of the cell division was performed using a FACS Calibur instrument (BD Biosciences).

2.7 Determination of Apoptosis and Necrosis of T Cells

Lymphocytes were isolated, washed twice in cold PBS, and resuspended in medium at a concentration of 2 x 10^6 cells/mL. Cells were stimulated with anti-human CD3 (clone HIT3a) and anti-human CD28 (clone 28.2) mAbs (each 100 ng/mL; eBioscience) in the presence of either medium, camptothecin (CPT; 300 μM; Tocris), 0.5% Triton-X 100, or plant extracts/single compounds (concentration range 0.01 – 100 μg/mL) and cultivated for 48 h. The negative control remained unstimulated. Cultured cells were washed with PBS and stained with annexin V-FITC using the apoptosis-detection kit (eBioscience) according to the manufacturer's instructions. Propidium iodide (eBioscience) was added, and cells were stained for 15 min at room temperature in the dark. Apoptosis and necrosis rates were determined by flow cytometric analysis using a FACS Calibur instrument (BD Biosciences).

2.8 Testing of Microfractions

The dried microfractions in 96-deepwell plates were redissolved in 25 μL of DMSO by sonication and mixing with a pipette. Of each stock solution, 1 μL was diluted in 100, 300, 900, 2700, 8100, and 24300 μL of cell suspension, respectively, and tested for inhibition of T-lymphocyte proliferation as described above. Each microfraction was scored based on the number of dilutions showing ≥50% inhibition of proliferation relative to the positive control. Dilutions showing inhibition ≥50% were scored with 1, and those with inhibition ≤ 50% were considered as inactive and scored with 0.

2.9 *In Silico* Predictions

Physicochemical and ADME properties for all isolated compounds were calculated with Percepta (ACD/Labs, ACD/Percepta Platform, 12.10, 2012).

2.10 Analysis of Data

For statistical analysis, data were processed with Microsoft Excel and SPSS software (Version 22.0, IBM, Armonk, USA). Statistical significance was determined with the SPSS software by one-way ANOVA followed by Dunnett's *post hoc* pairwise comparisons. Values are presented as mean ± standard deviation differences from controls (*$p < 0.05$).

RESULTS AND DISCUSSION

HPLC-Based Activity Profiling and Isolated Compounds

The dichloromethane (DCM) extract from the roots of *S. baicalensis* inhibited T-lymphocyte proliferation with an IC_{50} of 12.9 μg/mL (**Figure S1**, **Supplementary Material**) without concomitant cytotoxicity. Compounds responsible for the activity of the extract were localized with the aid of HPLC-based activity profiling (Potterat and Hamburger, 2014). The extract was submitted to analytical HPLC, and one-minute microfractions were collected and tested. An overlay of the activity profile and the HPLC chromatogram is shown in **Figure 1**. Fractions eluted at t_R 14 and 17 min were scored with the highest activity, followed by at the fraction at t_R 10 min. The fraction at t_R 31 min was not considered given that no peak was detected in the chromatogram.

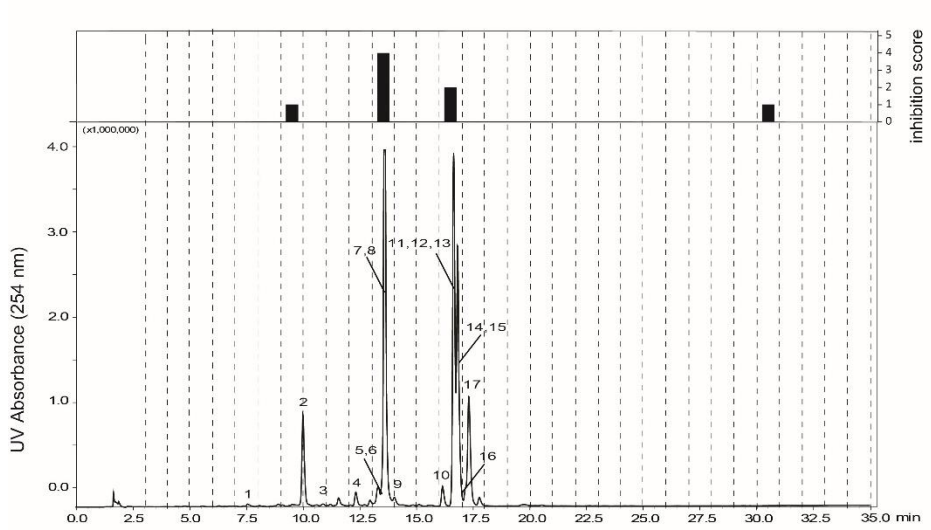

Figure 1. UV chromatogram at 254 nm of the DCM extract of *S. baicalensis* roots (SunFire C18, 3.5 µm, 3.0 x 150 mm i.d.); solvent A: water + 0.1% formic acid, solvent B: acetonitrile + 0.1% formic acid, 20% to 100% B in 30 min, 100% B for 5 min; flow rate 0.5 mL/min; microfractions of 1 min each. The bars above the chromatogram show the inhibition scores of microfractions.

Preparative flash chromatography of the extract on a silica gel column afforded 41 fractions. Compounds that were initially detected in the windows of activity of the activity profile were tracked by HPLC-PDA-MS analysis of these fractions, and purified by semi-preparative RP-HPLC.

The UV spectra of compounds **1 - 17** exhibited absorption maxima in the region of 260 - 284 nm, and either a broad shoulder at 300 - 380 nm or a second absorption maximum between 313 and 340 nm, suggesting the presence of flavonoids (Harborne et al, 1975). The ESIMS (positive ion mode) showed $[M+H]^+$ adduct ions at *m/z* 255 - 375 which were in line with the molecular weight of typical flavonoid aglycones. The ^{1}H NMR spectra of compounds **1 - 17** exhibited resonances between δ_H 5.50 and 7.00 ppm that were characteristic for protons of ring A, while signals between δ_H 6.00 to 8.00 ppm were characteristic for the protons on ring B (Harborne et al., 1975). With exception of **3**, **7**, and **13**, the spectra showed singlets at δ_H 3.50 - 4.10 ppm (3H each) that were indicative of one to four aromatic methoxy groups. Flavones **2**, and **4 - 17**, and flavanones **1** and **3** were readily differentiated based on characteristic ^{1}H and ^{13}C NMR signals attributable to ring C (**Figure 2**; **Table S1 - S5**, **Supplementary Material**). In flavones, H-3 appeared as a singlet at δ_H 6.20 - 7.10 ppm and C-3 at δ_C 100.0 - 111.0 ppm, the quaternary carbon C-2 at δ_C 159.0 - 164.0 ppm, and carbonyl carbon C-4 at δ_C 181.0 - 184.0 ppm. In flavanones, H-2 appeared at δ_H 5.80 (dd, J = 15.0 and 2.0 Hz), and the diastereotopic methylene protons at C-3 as two dd at δ_H 2.00 - 4.00 (J = 14.0 - 18.0 and 2.0 - 4.0 Hz). The resonances of C-2 and C-3 were at δ_C 40.0 and 71.0 ppm, respectively, and carbonyl carbon C-4 at δ_C 188.8 - 197.6 ppm. Complete NMR spectral assignments were achieved by 1D and 2D NMR. The flavones appearing in the active time windows of the activity profile (**Figure 1**) were identified as viscidulin III (**2,** Tomimori et al., 1984a; Zhang et al., 1994), 5,2',6'-trihydroxy-6,7,8-trimethoxyflavone (**5,** Kikuchi et al., 1991), scutevulin (**6**, Tomimori et al., 1984a; Malikov and Yuldashev, 2002), 5,7,2'-trihydroxyflavone (**7**), 5,7,6'-trihydroxy-8,2'-dimethoxyflavone (**8**) (Tomimori et al., 1984b), tenaxin II (**9**, Tomimori et al., 1983), rivularin (**10**, Zhang et al., 1994), wogonin (**11**, Li et al., 2017), 5,7-dihydroxy-6,8-dimethoxyflavone (**12**, Horie et al., 1995), chrysin (**13**, Takagi et al., 1980), skullcapflavone II (**14**, Takido et al., 1975), skullcapflavone I (**15**, Horie et al., 1979), and oroxylin A (**16**, Huang et al., 2003). Two flavones, 5,2',6'-trihydroxy-7,8-dimethoxyflavone (**4**, Chemesova et al., 1993) and tenaxin I (**17**,

Tomimori et al., 1983), and two flavanones, (*2S*)-7,2',6'-trihydroxy-5-methoxyflavanone (**1**, Tomimori et al., 1984b) and (*2S*)-5,7,2',6'-tetrahydroxyflavanone (**3**, Kubo et al., 1981), were located in adjacent fractions of the activity profile. The position of hydroxy or methoxy groups at C-5 in flavanones **1** and **3** was established with the aid of UV/Vis shift reagents (Harborne et al., 1975). In the UV/vis absorption spectrum of **3**, addition of $AlCl_3$/HCl led to a bathochromic shift of band II (24 nm), whereas the no shift was observed in case of **1**. The absolute configuration of flavanones **1** and **3** was determined by ECD (**Figure S2**, **Supplementary Material**). The ECD spectrum of **1** exhibited positive cotton effects at 223 and 332 nm, and a negative cotton effect at 278 nm. Positive cotton effects at 223 and 325 nm along with a negative cotton effect at 284 nm were observed for **3**. Thus, both compounds had a (*2S*) configuration (Tomimori et al., 1984; Kubo et al., 1981).

All compounds possess an unusual substitution pattern of the B-ring, with an absence of substituents at C-4', but substituents at C-2' and C-6' (Harborne et al., 1975). Likewise, substituents at C-6 or C-8 are also not very common in flavonoids (Wang et al., 2018).

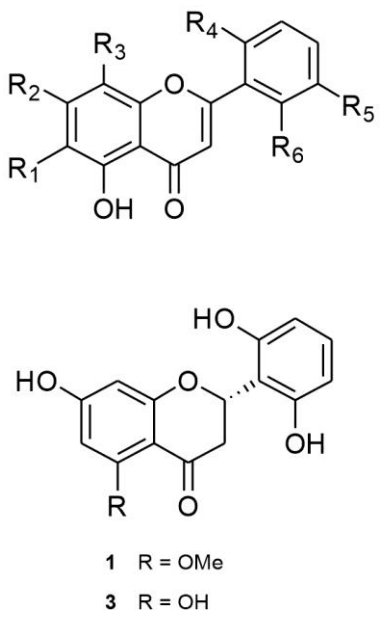

Compound	R_1	R_2	R_3	R_4	R_5	R_6
2	H	OH	OMe	OH	OH	OMe
4	H	OMe	OMe	OH	H	OH
5	OMe	OMe	OMe	OH	H	OH
6	H	OH	OMe	H	H	OH
7	H	OH	H	H	H	OH
8	H	OH	OMe	OH	H	OMe
9	OMe	OH	H	H	H	OH
10	H	OMe	OMe	OH	H	OMe
11	H	OH	OMe	H	H	H
12	OMe	OH	OMe	H	H	H
13	H	OH	H	H	H	H
14	OMe	OMe	OMe	OH	H	OMe
15	H	OMe	OMe	H	H	OH
16	OMe	OH	H	H	H	H
17	OMe	OMe	OMe	H	H	OH

Figure 2. Structures of isolated compounds

Immunosuppressant Activity

All flavonoids in the active time windows of the activity profile (**Figure 1**) are flavones with rare substitution patterns. Compounds that were available in sufficient amounts (**2**, **4**, and **8 - 17**) were tested for a concentration-dependent inhibition of T-cell proliferation (**Figure 3**; **Figure S3** and **Table S6**, **Supplementary Material**). FACS analysis of forward and side scatter and cell proliferation were used to assess toxicity and immunosuppressive activity. Compounds **9** and **10** were weakly active, as they showed notable inhibition of T-cell proliferation only at concentrations ≥ 25 µg/ml. Compounds **2**, **4**, **8**, and **12** showed intermediate activity, with IC_{50}'s of 55.9, 45.9, 61.6, and 50.2 µM, respectively. High immunosuppressant activity was determined for compounds **11**, **13**, **14**, and **16**, with IC_{50} values of 20.2, 22.2, 12.1, and 39.0 µM, respectively. All compounds showed cytotoxicity at high concentrations. Compounds **1**, **3**, and **5 - 7** could not be tested due to the limited amount of material.

For a number of structurally diverse flavonoids an inhibition of T-lymphocyte proliferation has been reported. Examples include simple flavones such as luteolin and apigenin (Verbeek et al., 2004),

methoxyflavones such as hispidulin and nepetin (Thitilertdecha et al., 2019), prenylated flavones such as artelastin (Cerqueire et al., 2003), simple flavonols such as quercetin (Sternberg et al., 2008; Hushmendy et al., 2009) and fisetin (Song et al., 2013), prenylated flavonol glycosides such as baohuoside-1 (Ma et al., 2005; Ma et al., 2004) and icariin (Shen et al., 2015), acylated kaempferol derivatives (Kuo et al., 2005), isoflavones such as genistein (Traganos et al., 1992), flavonolignans such as silibinin (McClure et al., 2012) and delphinidin (Dayoub et al., 2017), a widely occurring anthocyanin.

Attempts have been made previously at establishing structure-activity relationships for immunosuppressant flavonoids. For example, a $\Delta^{2,3}$-double bond and a carbonyl group at C-4 were considered as relevant for activity, and flavones decreased T-cell proliferation of murine and human T-cells more strongly than flavonols (Verbeek et al., 2004; Kim et al., 1991). With respect to substituents at the B-ring, the activity increased from monohydroxy to di- and trihydroxy substituted flavonoids (Kim et al., 1991). However, given the highly diverse substitution patterns of the A- and B-rings in our compound series it was not possible to draw firm conclusions on structure-activity relationships.

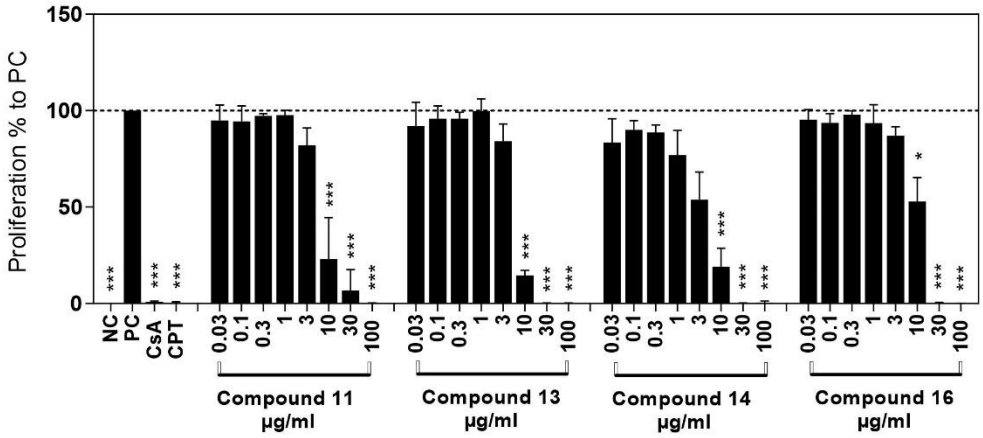

Figure 3. Inhibition of T cell proliferation by compounds **11**, **13**, **14**, and **16**. Data of three independent experiments are depicted as means ± standard deviation in comparison to the untreated, stimulated cells as positive control (PC; 100% ± SD). Unstimulated cells were used as the negative control (NC), cyclosporine A (CsA; 5µg/ml) was used as a known inhibitor of T cell proliferation, and camptothecin (CPT; 300 µM) was used as a known inducer of apoptosis. The asterisks represent significant differences from PC (*$p \leq 0.05$, ***$p \leq 0.001$.

3.3 Physicochemical and ADME properties of compounds

Given that no clear structure-activity relationship could be derived for our series of flavonoids the physicochemical and ADME properties, as defined by Lipinski and Veber rules (Lipinski et al., 1997; Lipinski et al., 2001; Veber et al., 2002), were calculated (**Table S7**, **Supplementary Material**). None of the flavonoids exhibited any violations of Lipinski's Rule of Five, with clog P values between 1.73 and 3.11, a molecular weight ranging from 270 to 346 g/M, with 2 to 4 H donor and 4 to 8 H acceptor sites, 1 to 4 rotatable bonds, and 3 rings. ADME profiling showed that predicted solubility ranged from 0.33 mg/ml (soluble) to 0.005 mg/ml (highly insoluble). Caco-2 permeability ranged from 122 x 10^6

cm/s (highly permeable) to 3 x 10^6 cm/s (moderately permeable), and a 100% human intestinal absorption (HIA) was predicted for all compounds. Predicted plasma protein binding (PPB) of compounds was moderate to extensive (76% to 97%), while CNS penetration was weak to absent. Taken together, flavanone **1** had the best overall ADME properties when considering solubility, permeability and plasma protein binding, followed by flavanone **2**, and flavones **4**, **5**, **9** and **10**. The other compounds showed low solubility and extensive plasma protein binding. The most active flavones **11** and **14** both had high predicted permeability and intestinal absorption, but a very low calculated solubility, and strong to extensive plasma protein binding.

CONCLUSION

With the aid of an HPLC-based activity profiling approach the compounds in a lipophilic extract of *S. baicalensis* responsible for a non-cytotoxic inhibition of human T lymphocyte proliferation were located and identified. Skullcapflavone II (**14**) and wogonin (**11**) were the major compounds responsible for the activity of the extract, given their abundance and IC_{50} values, while oroxylin A (**16**) and chrysin (**13**) contributed to a somewhat lesser extent. While the *in vitro* active compounds show no Lipinski violations, some unfavorable ADME properties, such as low solubility and high plasma protein binding certainly limit their potential as pure compounds. In contrast, a further exploration is warranted under the perspective of *S. baicalensis* as a source for phytomedicines. It has been shown that ADME properties of poorly soluble and poorly bioavailable pharmacologically active natural products are significantly improved if they are tested and/or administered in the form of an herbal extract (Nahrstedt and Butterweck, 2010; Oberthür et al., 2003; Gertsch, 2011).

ETHICS STATEMENT

Patients gave their written consent to donate blood for scientific research. All experiments conducted on human material were approved by the Ethics Committee of the University of Freiburg (55/14).

CONFLICT OF INTEREST

The authors declare that the research was conducted in the absence of any commercial or financial relationships that could be construed as a potential conflict of interest.

AUTHOR CONTRIBUTIONS

NS performed isolation, structure elucidation, and *in silico* calculation. SD and AM performed the bioassays and analyzed the data. JK performed the initial microfractionation. OD assisted in NMR and ECD analysis. CG and MH designed and supervised the project. NS wrote the draft manuscript which was finalized by MH and CG. All authors read and approved the final manuscript.

FUNDING

NS thanks the Indonesia Endowment Fund for Education (LPDP) for a fellowship. C.G. is supported by PRIAM-BS (Verein Stiftungsprofessur für Integrative und Anthroposophische Medizin an der Universität Basel).

ACKNOWLEDGMENTS

Technical assistance of Orlando Fertig is gratefully acknowledged.

REFERENCES

- Cerqueira, F., Cordeiro-Da-Silva, A., Araujo, N., Cidade, H., Kijjoa, A., and Nascimento, M. S. J. (2003). Inhibition of lymphocyte proliferation by prenylated flavones: Artelastin as a potent inhibitor. *Life Sci*. 73, 2321-2334. doi: https://doi.org/10.1016/S0024-3205(03)00627-1
- Chemesova, I. I., Iinuma, M., Budanstev, A. L. (1993). Investigation of the flavonoid composition of *Scutellaria adenostegia. Chem. Nat. Compd*. 29, 133-134. doi: https://doi.org/10.1007/BF00631041
- Dayoub, O., Lay, S. L., Soleti, R., Clere, N., Hilairet, G., Dubois, S., Gagnadoux, F., Boursier, J., Martinez, M. C., and Andriantsitohaina, R. (2017). Estrogen receptor α/HDAC/NFAT axis for delphinidin effects on proliferation and differentiation of T lymphocytes from patients with cardiovascular risks. *Sci. Rep.* 7, 1-17. doi: 10.1038/s41598-017-09933-4
- Gertsch, J. (2011). Botanical drugs, synergy, and network pharmacology: forth and back to intelligent mixtures. *Planta Med*. 77, 1086-1098. doi: http://dx.doi.org/10.1055/s-0030-1270904
- Harborne, J. B., Mabry, T. J., and Mabry, H. (1975). The Flavonoids. New York: Academic Press.
- Horie, T., Kawamura, Y., Yamamoto, H., Kitou, T., and Yamashita, K. (1995). Synthesis of 5,8-dihydroxy-6,7-dimethoxyflavones and revised structures for some natural flavones. *Phytochemistry*. 39, 1201-1210. doi: https://doi.org/10.1016/0031-9422(95)00070-N
- Horie, T., Tsukayama, M., Masumura, M., Nakayama, M., and Hayashi, S. (1979). The synthesis of 5,2'-dihydroxy-6,8-dimethoxyflavone and its isomers: a revised structure of skullcapflavone I. *B. Chem. Soc. Jpn.* 52, 2950-2952. doi: https://doi.org/10.1246/bcsj.52.2950
- Huang, W-H., Chien, P-Y., Yang, C-H., and Lee, A-R. (2003). Novel synthesis of flavonoids of *Scutellaria baicalensis* Georgi. *Chem. Pharm. Bull*. 51, 339-340. doi: 10.1248/cpb.51.339
- Hushmendy, S., Jayakumar, L., Hahn, A. B., Bhoiwala, D., Bhoiwala, D. L., and Crawford, D. R. (2009). Select phytochemicals suppress human T-lymphocytes and mouse splenocytes suggesting their use in autoimmunity and transplantation. *Nutr Res*. 29, 568-578. doi: 10.1016/j.nutres.2009.08.003
- Khan, U., and Ghazanfar, H. (2018). "T lymphocytes and autoimmunity", in International Review of Cell and Molecular Biology, 342. Elsevier Inc. page 140. ISSN 1937-6448. doi: https://doi.org/10.1016/bs.ircmb.2018.05.008
- Kikuchi, Y., Miyaichi, Y., Yamaguchi, Y., Kizu, H., Tomimori, T., and Vetschera, K. (1991). Studies on the constituents of *Scutellaria* species. XIV. On the constituents of the root and the leaves of *Scutellaria alpine* L. *Chem. Pharm. Bull*. 39, 199-201.
- Kim, C-J., and Cho, S. K. (1991). Pharmacological activities of flavonoids (III) structure-activity relationships of flavonoids in immunosuppression. *Arch. Pharm. Res*. 14, 147-159. doi: https://doi.org/10.1007/BF02892020

- Kubo, M., Kimura, Y., Odani, T., Tani, T., and Namba, K. (1981). Studies on Scutellariae radix. *Planta Med*. 43, 194-201. doi: 10.1055/s-2007-971499
- Kuo, Y-C., Lu, C-K., Huang, L-W., Kuo, Y-H., Chang, C., Hsu, F-L., and Lee, T-H. (2005). Inhibitory effects of acylated kaempferol glycosides from the leaves of *Cinnamomum kotoense* on the proliferation of human peripheral blood mononuclear cells. *Planta Med*. 71, 412-415. doi: 10.1055/s-2005-864134
- Li, T., Weng, T., Wang, J., Wei, Z., Zhao, L., and Li, Z. (2017). A practical and efficient approach to the preparation of bioactive natural product wogonin. *Org. Process Res. Dev*. 21, 171-176. doi: https://doi.org/10.1021/acs.oprd.6b00249
- Li, X-C., Ferreira, D., and Ding, Y. (2010). Determination of absolute configuration of natural products: theoretical calculation of electronic circular dichroism as a tool. *Curr. Org. Chem*. 14, 1678-1697. doi: 10.2174/138527210792927717
- Lipinski, C. A., Lombardo, F., Dominy, B. W., and Feeney, P. J. (1997). Experimental and computational approaches to estimate solubility and permeability in drug discovery and development settings. *Adv. Drug Deliv. Rev.* 23, 3-25. doi: https://doi.org/10.1016/S0169-409X(96)00423-1
- Lipinski, C. A., Lombardo, F., Dominy, B. W., and Feeney, P. J. (2001). Experimental and computational approaches to estimate solubility and permeability in drug discovery and development settings. *Adv. Drug Deliv. Rev.* 46, 3-26. doi: 10.1016/s0169-409x(00)00129-0
- Lu, L., Guo, Q., and Zhao, L. (2016). Overview of oroxylin A: a promising flavonoid compound. *Phytother. Res*. 30, 1765-1774. doi: https://doi.org/10.1002/ptr.5694
- Ma, A., Qi, S., Xu, D., Daloze, P., and Chen, H. (2005). Baohuoside-1 inhibits activated T cell proliferation at G_1 - S phase transition. *Transpl Immunol*. 15, 55-62. doi: https://doi.org/10.1016/j.trim.2005.05.002
- Ma, A., Qi, S., Xu, D., Zhang, X., Daloze, P., and Chen, H. (2004). Baohuoside-1, a novel immunosuppressive molecule, inhibits lymphocyte activation *in vitro* and *in vivo*. *Transplantation*. 78, 831-838. doi: 10.1097/01.tp.0000137786.56231.41
- Malikov, V. M., and Yuldashev, M. P. (2002). Phenolic compounds of plants of the *Scutellaria* L. genus. Distribution, structure, and properties. *Chem. Nat. Compd*. 38, 358-406. doi: https://doi.org/10.1023/A:1021638411150
- McClure, J., Lovelace, E. S., Elahi, S., Maurice N. J., Wagoner, J., Dragavon, J., Mittler, J. E., Kraft, Z., Stamatatos, L., Horton, H., De Rosa, S. C., Coombs, R. W., and Polyak, S. J. (2012). Silibinin inhibits HIV-1 infection by reducing cellular activation and proliferation. *PloS One*. 7, e41832. doi: https://doi.org/10.1371/journal.pone.0041832
- Nahrstedt, A., and Butterweck, V. (2010). Lessons learned from herbal medicinal products: the example of St. John's Wort. *J. Nat. Prod.* 73, 1015-1021. doi: https://doi.org/10.1021/np1000329
- Oberthür, C., Heineman, C., Elsner, P., Benfeldt, E., and Hamburger, M. (2003). A comparative study on the skin of pure tryptanthrin and tryptanthrin in *Isatis tinctoria* extract by dermal microdialysis coupled with isotope dilution ESI-LC-MS. *Planta Med*. 69, 385-389. doi: 10.1055/s-2003-39718
- Potterat, O., and Hamburger, M. (2014). Combined use of extract libraries and HPLC-based activity profiling for lead discovery: potential, challenges, and practical considerations. *Planta Med*. 80, 1171-1181. doi: 10.1055/s-0034-1382900
- Quah, B. J. C., and Parish, C. R. (2010). The use of carboxyfluorescein diacetate succinimidyl ester (CFSE) to monitor lymphocyte proliferation. *J. Visualized Exp*. 44, 1-4. doi: 10.3791/2259
- Reinhardt, J. K., Klemd, A. M., Danton, O., Mieri, M.D., Smiesko, M., Huber, R., Bürgi, T., Gründemann, C., and Hamburger, M. (2019). Sesquiterpene lactones from *Artemisia argyi*: absolute configuration and immunosuppressant activity. *J. Nat. Prod*. 82, 1424-1433. doi: https://doi.org/10.1021/acs.jnatprod.8b00791

- Santori, F. R. (2015). The immune system as self-centered network of lymphocytes. *Immunol. Lett.* 166, 109-116. doi: 10.1016/j.imlet.2015.06.002
- Shen, R., Deng, W., Li, C., and Zeng, G. (2015). A natural flavonoid glucoside icariin inhibits Th1 and Th17 cell differentiation and ameliorates experimental autoimmune encephalomyelitis. *Int. Immunopharmacol.* 24, 224-231. doi: 10.1016/j.intimp.2014.12.015
- Song, B., Guan, S., Lu, J., Chen, Z., Huang, G., Li, G., Xiong, Y., Zhang, S., Yue, Z., and Deng, X. (2013). Suppressive effects of fisetin on mice T lymphocytes *in vitro* and *in vivo*. *J Surg Res*. 185, 399-409. doi: https://doi.org/10.1016/j.jss.2013.05.093
- Sternberg, Z., Chadha, K., Lieberman, A., Hojnacki, D., Drake, A., Zamboni, P., Rocco, P., Grazioli, E., Weinstock-Guttman, B., and Munschauer, F. (2008). Quercetin and interferon-β modulate immune response(s) in peripheral blood mononuclear cells isolated from multiple sclerosis patients. *J Neuroimmunol*. 205, 142-147. doi: 10.1016/j.jneuroim.2008.09.008
- Takagi, S., Yamaki, M., and Inoue, K. (1980). Studies on the water-soluble constituents of the roots of *Scutellaria baicalensis* Georgi (Wogon). *Yakugaku Zasshi*. 100, 1220-1224. doi: 10.1248/yakushi1947.100.12_1220
- Takido, M., Aimi, M., Takahashi, S., Yamanouchi, S., Torii, H., and Dohi, S. (1975). Studies on the constituents in the water extracts of crude drugs. I. On the roots of *Scutellaria baicalensis* Georgi (Wogon) (1). *Yakugaku Zasshi*. 95, 108-113. doi: https://doi.org/10.1248/yakushi1947.95.1_108
- Tang, W., and Eisenbrand, G. (2011). Handbook of Chinese Medicinal Plants, Vol. 2. Weinheim: Wiley-VCH Verlag.
- Tomimori, T., Miyaichi, Y., Imoto, Y., Kizu, H., and Suzuki C. (1984a). Studies on the constituents of *Scutellaria baicalensis* species. IV. On the flavonoid constituents of the root of *Scutellaria baicalensis* George (4). *Yakugaku Zasshi*. 104, 529-534. doi: 10.1248/yakushi1947.104.5_529
- Tomimori, T., Miyaichi, Y., Imoto, Y., Kizu, H., and Tanabe, Y. (1984b). Studies on the Constituents of *Scutellaria* Species. III. On the flavonoid constituents of the root of *Scutellaria baicalensis* Georgi (3). *Yakugaku Zasshi*. 104, 524-528. doi: https://doi.org/10.1248/yakushi1947.104.5_524
- Tomimori, T., Miyaichi, Y., Imoto, Y., Kizu, H., and Tanabe, Y. (1983). Studies on the constituents of *Scutellaria* species. II. On the flavonoid constituents of the root of *Scutellaria baicalensis* Georgi (2). *Yakugaku Zasshi*. 103, 607-611. doi: https://doi.org/10.1248/yakushi1947.103.6_607
- Thitilertdecha, P., Tantithavorn. V., Poungpairoj, P., and Onlamoon, N. (2019) Determination of suppressive effect on human T-cell activation by hispidulin, nepetin, and vanilic acid. *Immunopharm Immunot*. 41, 591-598. doi: https://doi.org/10.1080/08923973.2019.1675165
- Traganos, F., Ardelt, B., Halko, N., Bruno, S., and Darzynkiewicz, Z. (1992). Effects of genistein on the growth and cell cycle progression of normal human lymphocytes and human leukemic MOLT-4 and HL-60 cells. *Cancer Res*. 52, 6200-6208.
- Verbeek, R., Plomp, A. C., van Tol, E. A. F., van Noort, J. M. (2004). The flavones luteolin and apigenin inhibit *in vitro* antigen-specific proliferation and interferon-gamma production by murine and human autoimmune T cells. *Biochem. Pharmacol*. 68, 621-629. doi: https://doi.org/10.1016/j.bcp.2004.05.012
- Veber, D. F., Johnson, S. R., Cheng, H-Y., Smith, B. R., Ward, K. W., and Kopple, K. D. (2002). Molecular properties that influence the oral bioavailability of drug candidates. *J. Med. Chem.* 45, 2615-2623. doi: https://doi.org/10.1021/jm020017n
- Wang, Z-L., Wang, S., Kuang, Y., Hu, Z-M., Qiao, X., and Ye, M. (2018). A comprehensive review on phytochemistry, pharmacology, and flavonoid biosynthesis of *Scutellaria baicalensis*. *Pharm. Biol*. 56, 465-484. doi: 10.1080/13880209.2018.1492620
- Zhang, Y-Y., Guo, Y-Z., Onda, M., Hashimoto, K., Ikeya, Y., Okada, M., and Maruno, M. (1994). Four flavonoids from *Scutellaria baicalensis*. *Phytochemistry*. 35, 511-514. doi: https://doi.org/10.1016/S0031-9422(00)94792-7

- Zimmermann-Klemd, A. M., Reinhardt, J. K., Morath, A., Schamel, W. W., Steinberger, P., Leitner, J., Huber, R., Hamburger, M., and Gründemann, C. (2020). Immunosuppressive activity of *Artemisia argyi* extract and isolated compounds. *Front. Pharmacol*. 11, 1-13. doi: https://doi.org/10.3389/fphar.2020.00402

Supplementary Material

Immunosuppressant Flavonoids from *Scutellaria baicalensis*

Nova Syafni[1,2], Seema Devi[3], Amy M. Zimmermann-Klemd[3], Jakob K. Reinhardt[1], Ombeline Danton[1], Carsten Gründemann[4], Matthias Hamburger[1*]

[1]Pharmaceutical Biology, Department of Pharmaceutical Sciences, University of Basel, Basel, Switzerland

[2]Faculty of Pharmacy and Sumatran Biota Laboratory, University of Andalas, Padang, West Sumatra, Indonesia

[3]Center for Complementary Medicine, Institute for Infection Prevention and Hospital Epidemiology, Faculty of Medicine, University of Freiburg, Freiburg, Germany

[4]Translational Complementary Medicine, Department of Pharmaceutical Sciences, University of Basel, Basel, Switzerland

*** Correspondence:**
Prof. Matthias Hamburger
matthias.hamburger@unibas.ch

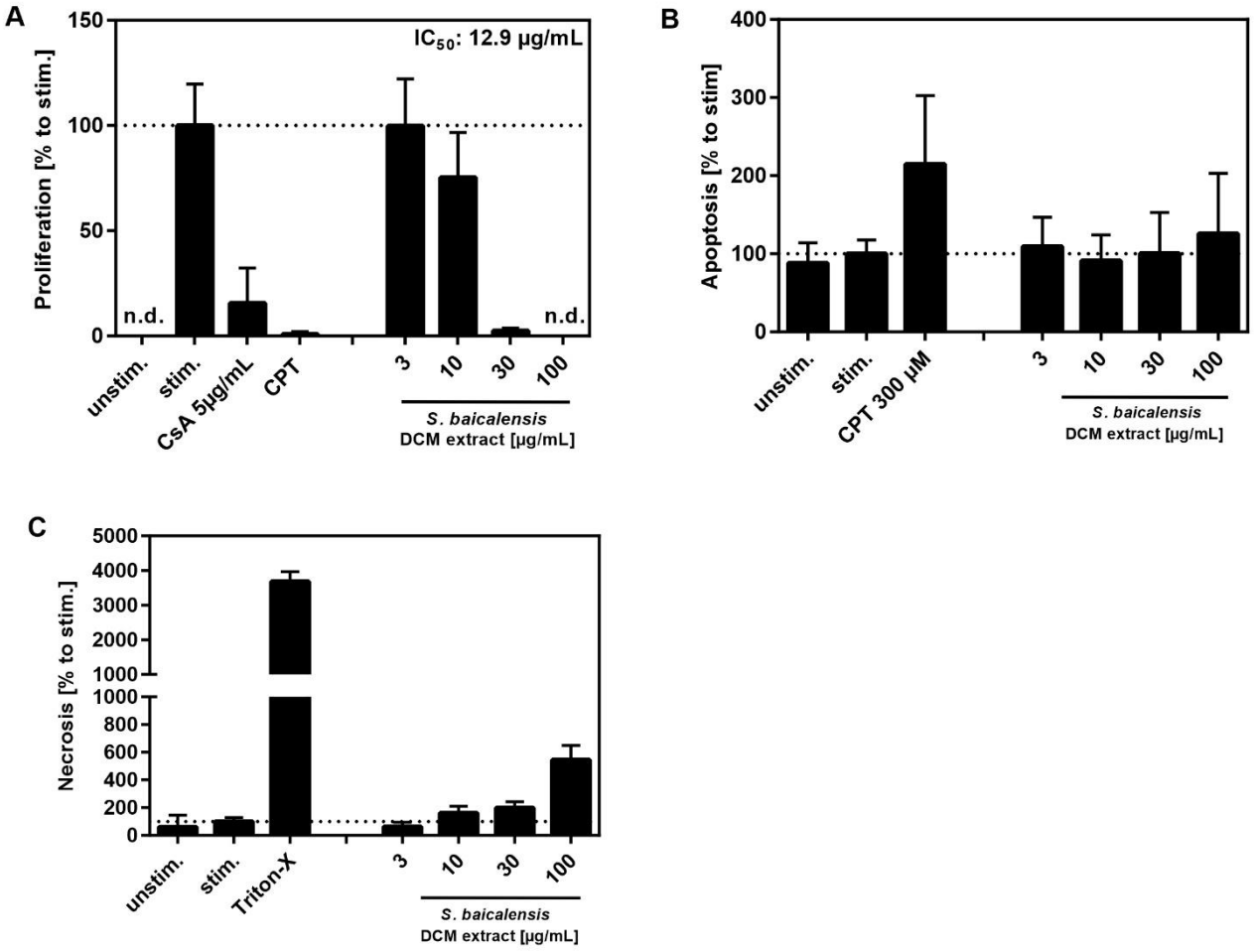

Figure S1. Inhibition of the DCM extract of *Scutellaria baicalensis* on proliferation of human T lymphocytes. The extract inhibited proliferation in a concentration dependent manner (**A**). Induction of apoptosis (**B**) and necrosis (**C**) was not observed at a concentration of 30 µg/mL (n = 2, mean ± SD relative to stimulated cells) where an almost complete inhibition of cell proliferation was observed.

Table S1. ^{1}H and ^{13}C NMR Spectroscopic Data for Compounds **1** and **3** (DMSO-d_6; 500.13 Hz for ^{1}H and 125.77 for ^{13}C NMR; δ in ppm).

position	**1**		**3**	
	δ_C[a]	δ_H (mult *J* in Hz)	δ_C[a]	δ_H (mult *J* in Hz)
2	71.1, CH	5.75, dd (14.2, 2.3)	71.9, CH	5.83[b]
3	41.7, CH_2	2.16, dd (16.5, 2.4) 3.70[b]	39.4, CH_2	2.39, dd (17.4, 3.1) 3.88, dd (17.4, 14.0)
4	188.8, C	-	197.6, C	-
5	162.3, C	-	164.5, C	-
6	93.7, CH	5.97, br s	95.4, CH	5.79[b]
7	166.4, C	-	167.7, C	-
8	95.9, CH	5.80, br s	96.2, CH	5.82[b]
9	165.4, C	-	164.1, C	-
10	103.2, C	-	101.7, C	-
1’	110.8, C	-	110.9, C	-
2’	157.4, C	-	157.6, C	-
3’	106.7, CH	6.33, d (8.2)	107.4, CH	6.34, d (8.2)
4’	129.3, CH	6.91, t (7.9)	130.5, CH	6.96, t (8.2)
5’	106.7, CH	6.33, d (8.2)	107.4, CH	6.34, d (8.2)
6’	157.4, C	-	157.6, C	-
5-R	55.2, CH_3	3.69, s	-	-

[a] ^{13}C Chemical shifts deduced from HSQC and HMBC NMR spectra, [b] Overlapping signals.

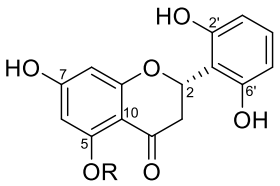

1 R = CH_3
3 R = H

Table S2. ^{1}H and ^{13}C NMR Spectroscopic Data for Compounds **2**, **8**, **10** and **14** (DMSO-d_6; 500.13 Hz for ^{1}H and 125.77 for ^{13}C NMR; δ in ppm).

	2		**8**		**10**		**14**	
position	δ_C[a]	δ_H (mult *J* in Hz)	δ_C[a]	δ_H (mult *J* in Hz)	δ_C[a]	δ_H (mult *J* in Hz)	δ_C[a]	δ_H (mult *J* in Hz)
2	161.8, C	-	161.2, C	-	162.2, C	-	162.2, C	-
3	111.4, CH	6.25, s	111.6, CH	6.23, s	111.8, CH	6.29, s	111.5, CH	6.32, s
4	181.8, C	-	181.7, C	-	182.1, C	-	182.1, C	-
5	156.4, C	-	156.1, C	-	156.8, C	-	148.3, C	-
6	99.1, CH	6.31, s	98.8, CH	6.30, s	95.8, CH	6.57[b]	135.4, C	-
7	157.8, C	-	157.0, C	-	158.3, C	-	152.2, C	-
8	127.9, C	-	127.3, C	-	128.5, C	-	132.2, C	-
9	-, C[c]	-	150.4, C	-	149.8, C	-	146.3, C	-
10	103.5, C	-	103.2, C	-	104.1, C	-	106.0, C	-
1’	115.0, C	-	108.9, C	-	109.1, C	-	108.9, C	-
2’	146.2, C	-	158.1, C	-	158.4, C	-	158.0, C	-
3’	142.5, C	-	102.0, CH	6.62, dd (8.2, 4.3)	102.1, CH	6.60[b]	102.0, CH	6.59, d (8.2)
4’	119.7, CH	6.89, d (8.9)	132.0, CH	7.31, t (8.4)	132.2, CH	7.30, t (7.3)	132.0, CH	7.29, t (8.2)
5’	111.0, CH	6.59, d (8.9)	108.6, CH	6.63, dd (8.2, 4.3)	108.7, CH	6.63[b]	108.7, C	6.65, d (8.2)
6’	148.4, C	-	158.1, C	-	156.9, C	-	157.0, C	-
5-R	-	12.52, s	-	12.53, s	-	12.66, s	-	12.62, br s
6-R	-	-	-	-	-	-	60.2, CH_3	3.83, s
7-R	-	-	-	-	56.3, CH_3	3.91, s	61.3, CH_3	4.01, s
8-R	60.6, CH_3	3.72, s	60.5, CH_3	3.72, s	60.8, CH_3	3.72, s	61.3, CH_3	3.81, s
2’-R	60.3, CH_3	3.75, s	55.6, CH_3	3.76, s	55.7, CH_3	3.76, s	55.5, CH_3	3.75, s
6’-R	-	-	-	-	-	-	-	8.46, s

[a] ^{13}C chemical shifts deduced from HSQC and HMBC NMR spectra, [b] Overlapping signals, [c] Signal not visible.

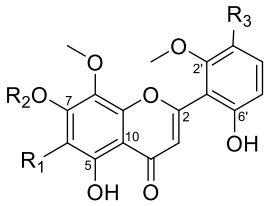

	R_1	R_2	R_3
2	H	H	OH
8	H	H	H
10	H	CH_3	H
14	OCH_3	CH_3	H

Table S3. ^{1}H and ^{13}C NMR Spectroscopic Data for Compounds **4 - 7** (DMSO-d_6; 500.13 Hz for ^{1}H and 125.77 for ^{13}C NMR; δ in ppm).

	4		**5**		**6**		**7**	
position	δ_C[a]	δ_H (mult *J* in Hz)	δ_C[a]	δ_H (mult *J* in Hz)	δ_C[a]	δ_H (mult *J* in Hz)	δ_C[a]	δ_H (mult *J* in Hz)
2	162.8, C	-	159.1, C	-	161.1, C	-	-, C[c]	-
3	111.5, CH	6.26, s	111.5, CH	6.30, s	108.3, CH	7.07, s	108.9, CH	7.11, s
4	182.1, C	-	182.9, C	-	181.8, C	-	-, C[c]	-
5	156.6, C	-	-, C[c]	-	160.4, C	-	-, C[c]	-
6	95.6, CH	6.58, s	135.7, C	-	99.6, CH	6.20, s	-, CH	6.13, br s
7	158.2, C	-	152.3, C	-	156.6, C	-	-, C[c]	-
8	128.5, C	-	132.5, C	-	128.4, C	-	93.9, C	6.39, br s
9	149.7, C	-	-, C[c]	-	-, C[c]	-	-, C[c]	-
10	104.0, C	-	-, C[c]	-	102.5, C	-	-, C[c]	-
1’	108.2, C	-	108.1, C	-	117.4, C	-	-, C[c]	-
2’	156.8, C	-	-, C[c]	-	155.9, C	-	-, C[c]	-
3’	106.4, CH	6.45, d (8.2)	106.4, CH	6.44, d (8.2)	117.4, CH	7.07, br d (8.9)	117.4, CH	7.03, br d (7.9)
4’	131.8, CH	7.12, t (8.1)	132.0, CH	7.10, t (8.2)	132.4, CH	7.35, ddd (8.9, 7.6, 1.2)	132.4, CH	7.33, t (6.7)
5’	106.4, CH	6.45, d (8.2)	106.4, CH	6.44, d (8.2)	118.6, CH	6.95, dd (7.5, 7.5)	118.3, CH	6.91, t (7.6)
6’	156.8, C	-	-, C[c]	-	127.9, CH	7.85, dd (7.9, 1.5)	128.4, CH	7.81, dd (7.8, 1.2)
5-R	-	12.71, s	-	12.71, s	-	12.58, s	-	-
6-R	-	-	60.4, CH_3	3.83, s	-	-	-	-
7-R	56.2, CH_3	3.91, s	61.3, CH_3	4.00, s	-	-	-	-
8-R	60.8, CH_3	3.73, s	61.6, CH_3	3.81, s	60.5, CH_3	3.80, s	-	-

[a] ^{13}C chemical shifts deduced from HSQC and HMBC NMR spectra, [b] Overlapping signals, [c] Signal not visible.

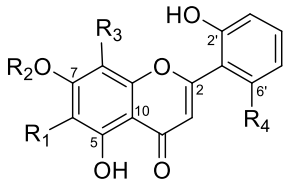

	R_1	R_2	R_3	R_4
4	H	CH_3	OCH_3	OH
5	OCH_3	CH_3	OCH_3	OH
6	H	H	OCH_3	H
7	H	H	H	H

Table S4. ^{1}H and ^{13}C NMR Spectroscopic Data for Compounds **9**, and **11** - **13** (DMSO-d_6; 500.13 Hz for ^{1}H and 125.77 for ^{13}C NMR; δ in ppm).

	9		**11**		**12**		**13**	
position	δ_C[a]	δ_H (mult *J* in Hz)	δ_C[a]	δ_H (mult *J* in Hz)	δ_C[a]	δ_H (mult *J* in Hz)	δ_C[a]	δ_H (mult *J* in Hz)
2	161.3, C	-	164.7, C	-	163.0, C	-	163.5, C	-
3	107.8, CH	7.06	105.4, CH	6.94, s	104.5, CH	6.94, s	104.9, CH	6.88, s
4	182.0, C	-	183.7, C	-	182.3, C	-	182.1, C	-
5	-, C[c]	12.97 (OH)	158.0, C	-	148.3, C	-	161.3, C	-
6	132.0, C	-	99.5, CH	6.30, s	131.6, C	-	99.1, CH	6.20, d (1.8)
7	160.5, C	-	159.0, C	-	-, C[c]	-	165.3, C	-
8	94.1, CH	6.49, s	129.4, C	-	127.9, C	-	94.0, CH	6.49, d (1.8)
9	153.2, C	-	151.3, C	-	-, C[c]	-	157.3, C	-
10	103.2, C	-	105.4, C	-	102.9, C	-	103.5, C	-
1’	117.6, C	-	133.7, C	-	130.7, C	-	130.6, C	-
2’	158.0, C	-	126.7, CH	8.03, d (7.0)	126.0, CH	8.05, dd (7.6, 1.8)	126.2, CH	8.03, d (7.0)
3’	117.0, CH	7.06[b]	129.6, CH	7.58[b]	129.0, CH	7.60[b]	128.9, CH	7.57[b]
4’	132.0, CH	7.34, t (7.3)	132.5, CH	7.59[b]	131.8, CH	7.62[b]	131.6, CH	7.60[b]
5’	118.3, CH	6.92, t (7.5)	129.6, CH	7.58[b]	129.0, CH	7.60[b]	128.9, CH	7.57[b]
6’	127.8, CH	7.81, d (7.6)	126.7, CH	8.03, d (7.0)	126.0, CH	8.05, dd (7.6, 1.8)	126.2, CH	8.03, d (7.0)
5-R	-	12.97, s	-	12.48, s	-	12.63, s	-	12.78, br s
6-R	59.2, CH_3	3.75, s	-	-	60.0, CH_3	3.79, s	-	-
7-R	-	-	-	10.81, br s	-	-	-	-
8-R	-	-	61.4, CH_3	3.85, s	61.0, CH_3	3.89, s	-	-

[a] ^{13}C chemical shifts deduced from HSQC and HMBC NMR spectra, [b] Overlapping signals, [c] Signal not visible.

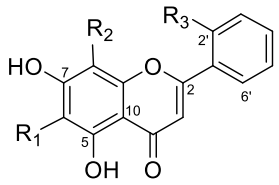

	R_1	R_2	R_3
9	OCH_3	H	OH
11	H	OCH_3	H
12	OCH_3	OCH_3	H
13	H	H	H

Table S5. ^{1}H and ^{13}C NMR Spectroscopic Data for Compounds **15 - 17** (DMSO-d_6; 500.13 Hz for ^{1}H and 125.77 for ^{13}C NMR; δ in ppm).

	15		**16**		**17**	
position	δ_C[a]	δ_H (mult *J* in Hz)	δ_C[a]	δ_H (mult *J* in Hz)	δ_C[a]	δ_H (mult *J* in Hz)
2	161.4, C	-	163.6, C	-	161.8, C	-
3	108.6, CH	7.10, s	105.1, CH	6.95, s	108.6, CH	7.12, s
4	182.2, C	-	182.7, C	-	182.6, C	-
5	156.3, C	-	153.3, C	-	158.4, C	-
6	95.7, CH	6.57, s	132.0, C	-	135.6, C	-
7	158.0, C	-	158.1, C	-	152.6, C	-
8	128.4, C	-	94.8, CH	6.63, s	132.9, C	-
9	148.7, C	-	152.9, C	-	148.3, C	-
10	103.7, C	-	104.8, C	-	106.2, C	-
1’	117.2, C	-	131.2, C	-	117.0, C	-
2’	156.8, C	-	126.8, CH	8.05, dd (7.6, 1.5)	156.7, C	-
3’	117.0, CH	7.07, d (7.9)	129.6, CH	7.56[b]	117.0, CH	7.08, d (8.2)
4’	132.8, CH	7.41, td (7.7, 1.2)	132.4, CH	7.6 [b]	132.9, CH	7.42, td (7.7, 1.2)
5’	119.4, CH	7.03, t (7.6)	129.6, CH	7.56[b]	119.4, CH	7.03, t (7.6)
6’	128.1, CH	7.86, dd (7.9, 1.2)	126.8, CH	8.05, dd (7.6, 1.5)	128.1, CH	7.86, dd (7.7, 1.2)
5-R	-	12.67, s	-	12.92, s	-	12.65, s
6-R	-	-	60.4, CH_3	3.76, s	60.3, CH_3	3.83, s
7-R	56.3, CH_3	3.92, s	-	-	61.2, CH_3	4.02, s
8-R	60.9, CH_3	3.82, s	-	-	61.6, CH_3	3.90, s

[a] ^{13}C chemical shifts deduced from HSQC and HMBC NMR spectra, [b] Overlapping signals.

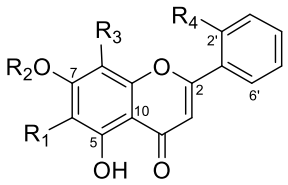

	R_1	R_2	R_3	R_4
15	H	CH_3	OCH_3	OH
16	OCH_3	H	H	H
17	OCH_3	CH_3	OCH_3	OH

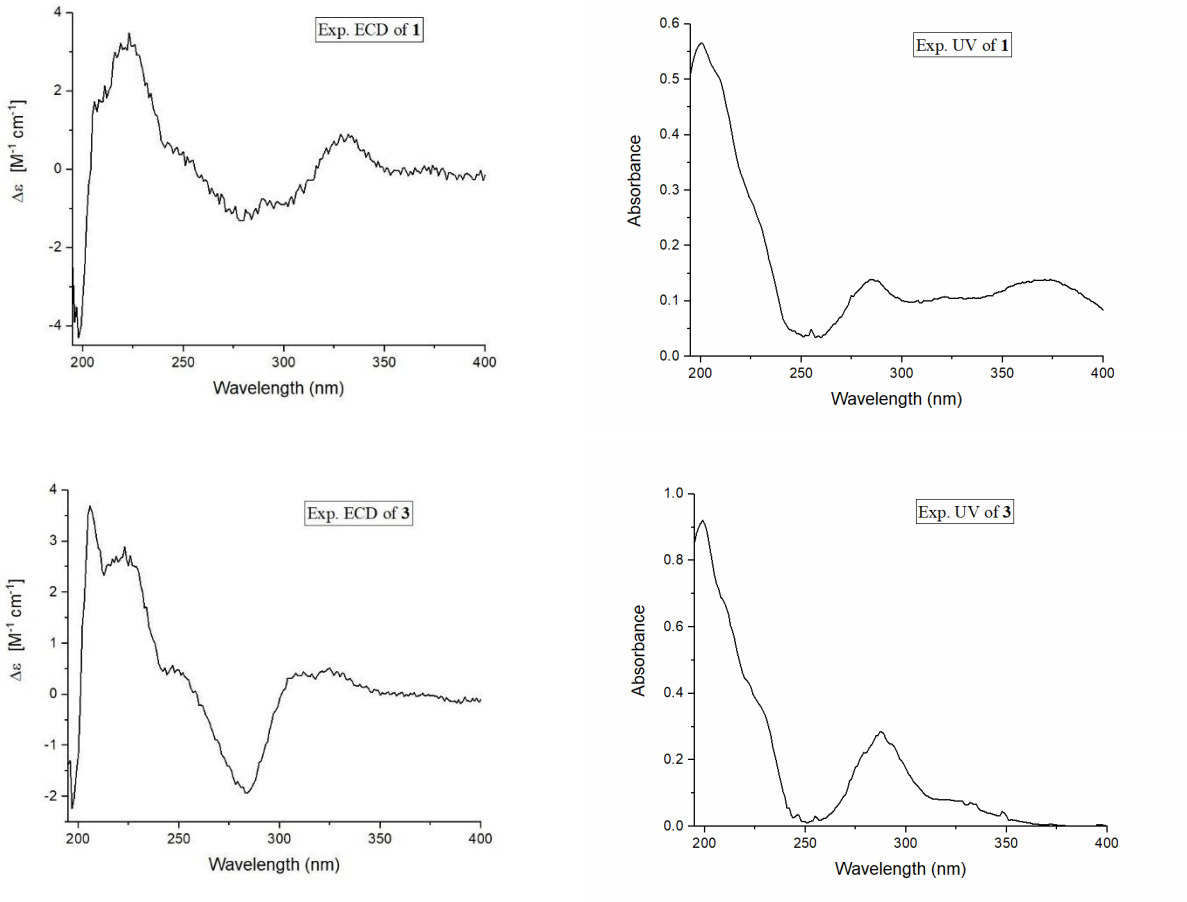

Figure S2. Figure of experimental ECD and UV spectra for compounds **1** and **3** in MeOH.

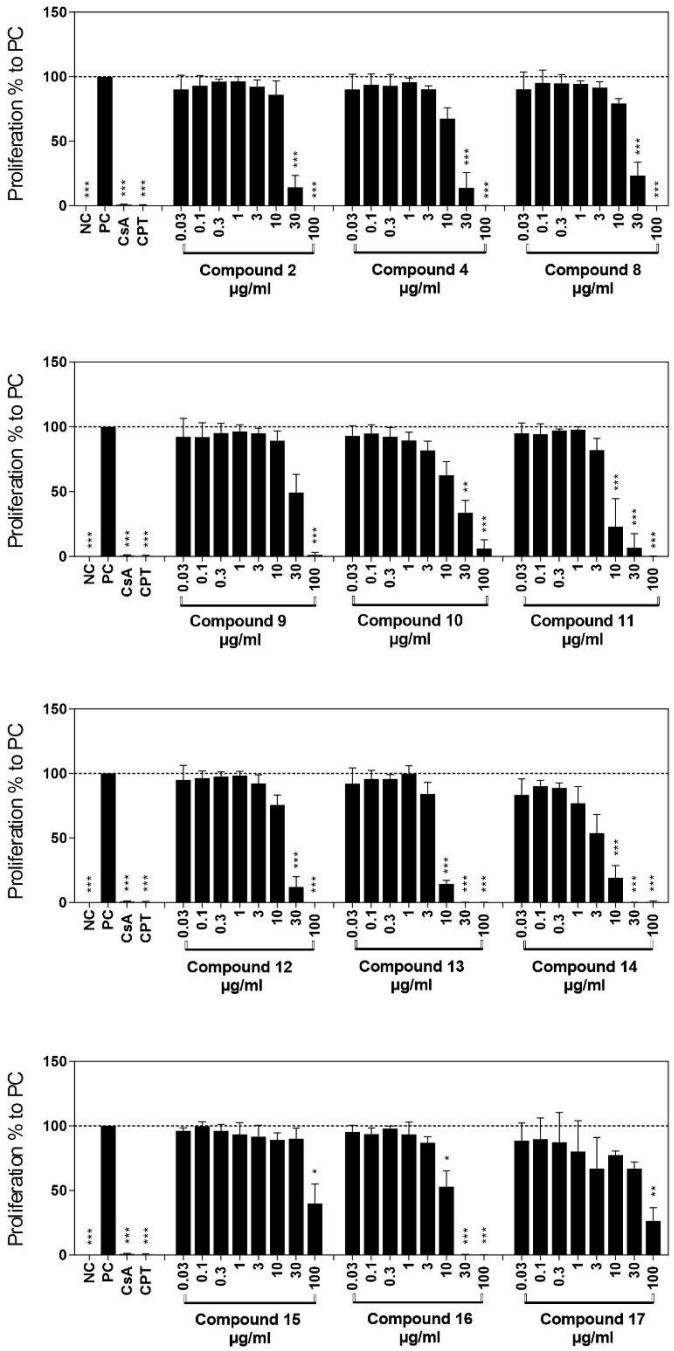

Figure S3. Inhibitory effects of compounds **2**, **4**, and **8-17** on T-cell proliferation. Data of three independent experiments are depicted as means ± standard deviation in relation to the untreated, stimulated cells as positive control (PC; = 100% ± SD). Non-stimulated cells were used as the negative control (NC), cyclosporine A (CsA; 5µg/ml) was used as a known inhibitor of T cell proliferation, and camptothecin (CPT; 300 µM) was used as a known inducer of apoptosis. The asterisks represent significant differences from PC (*$p \leq 0.05$, **$p \leq 0.01$, ***$p \leq 0.001$.

Table S6. Inhibition of T-lymphocyte proliferation (IC_{50}) by testing compounds.

Compound	IC_{50} value (μg/mL)	IC_{50} (μM)
2	19.3	55.9
4	15.2	45.9
8	20.3	61.6
9	33.1	110.2
10	27.7	80.4
11	5.8	20.2
12	15.8	50.2
13	5.7	22.2
14	4.5	12.1
15	Not calculated	-
16	11.1	39.0
17	Not calculated	-

Table S7. Physico-chemical properties and ADME profiling of isolated compounds calculated with Percepta (ACD/Labs, ACD/Percepta Platform).

Compound	Physico-chemical Profiling									ADME Profiling			
	Log P	*MW*	*H Donors*	*H Acceptors*	*Rot Bonds*	*Rings*	*Lipinski*	*Lead-like*	*Solubility (mg/ml)*	*Caco-2 (PE = cm/s)*	*PPB*	*CNS*	*HIA*
1	2.19 (optimal)	302.28 (good)	3 (good)	6 (good)	3 (good)	3 (good)	0 violations (good)	0 violations (good)	0.33 (soluble)	56E-6 (highly permeable)	88% (strongly bound)	score=-3.23 (weak penetrant)	100% (highly absorbed)
2	2.16 (optimal)	346.29 (good)	4 (good)	8 (good)	3 (good)	3 (good)	0 violations (good)	0 violations (good)	0.04 (insoluble)	9E-6 (Highly permeable)	91% (extensively bound)	score=-4.22 (non-penetrant)	100% (highly absorbed)
3	2.35 (optimal)	288.25 (good)	4 (good)	6 (good)	1 (good)	3 (good)	0 violations (good)	0 violations (good)	0.23 (soluble)	27E-6 (highly permeable)	92% (extensively bound)	score=-3.45 (weak-penetrant)	100% (highly absorbed)
4	2.02 (optimal)	330.29 (good)	3 (good)	7 (good)	3 (good)	3 (good)	0 violations (good)	0 violations (good)	0.33 (soluble)	23E-6 (highly permeable)	76% (moderately bound)	score=-3.44 (weak-penetrant)	100% (highly absorbed)
5	1.73 (optimal)	360.31 (good)	3 (good)	8 (good)	4 (good)	3 (good)	0 violations (good)	0 violations (good)	0.2 (soluble)	15E-6 (highly permeable)	79% (moderately bound)	score=-3.75 (non-penetrant)	100% (highly absorbed)
6	2.39 (optimal)	300.26 (good)	3 (good)	6 (good)	2 (good)	3 (good)	0 violations (good)	0 violations (good)	0.08 (insoluble)	30E-6 (highly permeable)	95% (extensively bound)	score=-3.87 (non-penetrant)	100% (highly absorbed)
7	2.54 (optimal)	270.24 (good)	3 (good)	5 (good)	1 (good)	3 (good)	0 violations (good)	0 violations (good)	0.24 (soluble)	28E-6 (highly permeable)	94% (extensively bound)	score=-3.78 (non-penetrant)	100% (highly absorbed)
8	2.51 (optimal)	330.29 (good)	3 (good)	7 (good)	3 (good)	3 (good)	0 violations (good)	0 violations (good)	0.04 (insoluble)	32E-6 (highly permeable)	94% (extensively bound)	score=-3.93 (non-penetrant)	100% (highly absorbed)
9	1.85 (optimal)	302.24 (good)	4 (good)	7 (good)	2 (good)	3 (good)	0 violations (good)	0 violations (good)	0.54 (soluble)	3E-6 (moderately permeable)	88% (undefined)	score=-4.37 (non-penetrant)	100% (highly absorbed)
10	2.61 (optimal)	344.32 (good)	2 (good)	7 (good)	4 (good)	3 (good)	0 violations (good)	0 violations (good)	0.13 (soluble)	92E-6 (highly permeable)	82% (strongly bound)	score=-3.08 (weak-penetrant)	100% (highly absorbed)
11	2.96 (optimal)	284.26 (good)	2 (good)	5 (good)	2 (good)	3 (good)	0 violations (good)	0 violations (good)	0.005 (highly insoluble)	122E-6 (highly permeable)	97% (extensively bound)	score=-3.42 (weak-penetrant)	100% (highly absorbed)
12	2.47 (optimal)	314.29 (good)	2 (good)	6 (good)	3 (good)	3 (good)	0 violations (good)	0 violations (good)	0.002 (highly insoluble)	85E-6 (highly permeable)	95% (extensively bound)	score=-3.61 (non-penetrant)	100% (highly absorbed)
13	3.11 (optimal)	254.24 (good)	2 (good)	4 (good)	1 (good)	3 (good)	0 violations (good)	0 violations (good)	0.04 (insoluble)	98E-6 (highly permeable)	96% (extensively bound)	score=-3.39 (weak-penetrant)	100% (highly absorbed)
14	2.24 (optimal)	374.34 (good)	2 (good)	8 (good)	5 (good)	3 (good)	0 violations (good)	0 violations (good)	0.06 (insoluble)	64E-6 (highly permeable)	82% (strongly bound)	score=-3.36 (weak-penetrant)	100% (highly absorbed)
15	2.52 (optimal)	314.52 (good)	2 (good)	6 (good)	3 (good)	3 (good)	0 violations (good)	0 violations (good)	0.23 (soluble)	86E-6 (highly permeable)	86% (strongly bound)	score=-3.10 (weak-penetrant)	100% (highly absorbed)
16	2.99 (optimal)	284.26 (good)	2 (good)	5 (good)	2 (good)	3 (good)	0 violations (good)	0 violations (good)	0.007 (highly insoluble)	87E-6 (highly permeable)	97% (extensively bound)	score=-3.64 (non-penetrant)	100% (highly absorbed)
17	2.08 (optimal)	344.32 (good)	2 (good)	7 (good)	4 (good)	3 (good)	0 violations (good)	0 violations (good)	0.07 (insoluble)	56E-6 (highly permeable)	84% (strongly bound)	score=-3.38 (weak-penetrant)	100% (highly absorbed)

MW=Molecular weight (g/mol). Caco-2=Caco-2 permeability. PPB=Plasma protein bound. CNS=Central nervous system. HIA=Human intestinal absorption.

4. CONCLUSION AND OUTLOOK

HPLC-based activity profiling has been used for tracking active substances in an extract [1,2]. With mg-amount of extract, this approach is available to localize the activity of the extract. Discovery on $GABA_A$ receptor modulators from natural origin applied in this method with some bioassay formats. The $GABA_A$ receptor modulators project was firstly established by utilizing two-microelectrode voltage clamp assay with *Xenopus laevis* oocytes [3]. It was used as a primary screening of extract libraries for the $GABA_A$ receptor modulatory project. This research data, later on, was utilized as a standard for establishing in-house $GABA_A$ receptor modulators assay. For instance, the zebrafish-larvae locomotor assay using plant extracts and natural products have been reported as active in *Xenopus laevis* oocyte transiently expressing $GABA_A$ receptors of $\alpha_1\beta_2\gamma_2$ subunit composition. The plant extracts used are *Magnolia officinalis* and *Valeriana officinalis*, whereas the compounds are magnolol, valerenic acid, piperine, sophoraflavanone G, sanggenon C, dehydroabietic acid, and sandaracopimaric acid [4].

The application of the hit from *Xenopus* oocyte assay was the dichloromethane extract twigs and leaves of *Murraya exotica* L. (Rutaceae) (**Chapter 3.1**). The maximal tolerated concentration (MTC) of the extract was evaluated before it was submitted to the behavioral model with zebrafish-larvae. Zebrafish-larvae locomotor assay then tracked the active compounds of the extract with the aid of HPLC-based activity profiling. The sample was scaled up for extraction and separated with semi-preparative method. Off-line MS and UV data of HPLC profiling the extract were guided to isolate the active compounds. Ten compounds were obtained, including active and non-active compounds. All compounds were submitted to NMR and elucidated their structures. For confirmation, the compounds in the active time window were again tested in the *Xenopus* oocyte assay. Two compounds in the active time window were structurally related, osthol (**9**) and coumurrayin (**10**). However, osthol showed potentiation of $GABA_A$-induced chloride currents, while coumurrayin did not show significant effects on chloride currents. Both compounds were calculated by *in silico* prediction. The result of physicochemical properties exhibited the values of both compounds were in favour of BBB permeability.

In the case of *Casearia corymbosa* (**Chapter 3.2**), FLIPR assay was used for testing $GABA_A$ receptor modulatory activity [5]. The FLIPR assay utilizing CHO cells expressing $GABA_A$ receptors of α1, β2, γ2 subunit composition recorded the fluorescence during membrane potential change associated with ion change activation in real-time [6,7,8]. The

FLIPR protocol was validated using the plant extracts and compounds that exhibited their activity as allosteric $GABA_A$ receptor modulators in *Xenopus* oocyte assay and in-house zebrafish larvae assay. The validated FLIPR assay was used to screen the EtOAc extract library. The active plant extract was submitted to HPLC-based activity profiling, which localized the responsible activity of compounds. Off-line NMR measurement identified that all of the isolated compounds in the active time window and adjacent fraction were clerodane-type diterpenes, of which five out of nine isolated compounds were new compounds. The absolute configurations of isolated compounds were established by the NOESY and ECD. All compounds then were screened in FLIPR assay, five compounds (**1**, **3**, **5**, **7**, and **8**) enhanced GABA potentiation, and the remaining compounds (**2**, **4**, **6**, and **9**) did not show the activities. Compounds **1**, **3**, **5**, **7**, and **8** were further assessed for concentration-response and EC_{50} values. Compounds **3**, **7**, and **8** showed significant potentiation with EC_{50} 0.51, 4.57, and 1.36 μM, respectively. However, The $EC_{50's}$ of compounds **1** and **5** cannot be determined.

Compound **8** was further investigated for allosteric binding sites of $GABA_A$ receptor modulators. $GABA_A$ receptors possess a variety of allosteric binding sites; three sites of action were assessed in FLIPR assay using active drugs for benzodiazepines, neurosteroids, and barbiturates. In order to evaluate a probability of interaction at the benzodiazepine binding site, the combination of compound **8** (5 µM) and increasing concentrations of flumazenil were tested together, the result did not exhibit antagonist effect. Furthermore, combination of diazepam (2 µM) with increasing concentrations of compound **8** observed significant additive potentiation at higher concentration of **8**. In the neurosteroids binding site assessment, compound **8** at 10 µM was mixed with increasing concentrations of PREGS. The result showed that decreasing potentiation was observed at the highest concentration of PREGS (10 µM). Furthermore, increasing concentrations of compound **8** with allopregnanolone (0.25 µM) displayed additive effects at higher concentrations (2 and 4 µM). The barbiturates binding site was evaluated by adding etazolate at 0.78 µM to increasing concentrations of compound **8**. The results showed a significant additive effect. These binding site experiments exhibited additive effects of compounds **8** in positives allosteric $GABA_A$ receptor modulators. The decreasing effects of compound **8** towards combination with PREGS suggests the presence of an alternative binding site of compound **8** within the neurosteroids binding site. This finding is the first report of non-steroidal compounds interacting in the neurosteroid binding domain. In other words, continuing

the investigation of compound **8** using molecular modelling for $GABA_A$ receptor modulators could give us an insight if it might be useful for GABAergic drug discovery.

HPLC-based activity profiling was also applied to track immunosuppressive compounds in the extract from traditional Chinese medicine, the roots of *Scutellaria baicalensis* (**Chapter 3.3**) [9,10]. Beforehand, the screening of the extract showed inhibition towards T cell proliferation without concomitant cytotoxicity. The proliferation of human T lymphocytes was assayed using the dye carboxyfluorescein diacetate succinimidyl ester (CFSE) [11]. Apoptosis and necrosis events in the cells were examined by Annexin V and Propidium Iodide double staining. Then the immunosuppressive activity and toxicity were evaluated with FACS calibur instrument. HPLC-based activity profiling allowed us to localize two time-active windows of immunosuppressive compounds. Seventeen flavonoid compounds were isolated from the active time windows and adjacent fractions. One- and two-dimensional NMR were measured along with UV and MS data to elucidate the structures. All flavonoids possessed unusual substitution patterns of the B-ring, with substituents at C-2' and C-6' instead of at C-3' and C-4'. The isolated compounds with sufficient amounts were tested on T lymphocyte proliferation. Compounds viscidulin III (**2**), 5,2',6'-trihydroxy-7,8-dimethoxyflavone (**4**), 5,7,6'-trihydroxy-8,2'-dimethoxyflavone (**8**), and 5,7-dihydroxy-6,8-dimethoxyflavone (**12**) showed intermediate activity with IC_{50}'s of 55.9, 45.9, 61.6, and 50.2 µM, respectively. Compounds with high immunosuppressive activity were wogonin (**11**), chrysin (**13**), skullcapflavone II (**14**), and oroxylin A (**16**) with IC_{50} values of 20.2, 22.2, 12.1, and 39.0 µM, respectively. Even though we observed a diversity of the substituent pattern of the A- and B-rings of our isolated compounds, there is no clear structure-activity relationship that could be concluded. The physicochemical and ADME properties of the flavonoid compounds were calculated without violating Lipinski's rule, and some unfavourable ADME properties, such as low solubility and high plasma protein binding.

Overall, the results of this works confirmed that HPLC-based activity profiling was an effective approach to localize the active compounds in milligram amount of extract. HPLC-based activity profiling can also provide additional important information for the prioritization of samples for preparative follow-up [12]. It is necessary to have validity, sensitivity, and suitability of the bioassay for the experimental purpose. In the case of $GABA_A$ receptor modulators assays, the functional assay was performed in *Xenopus* oocyte assay and FLIPR

assay. In order to have an initial insight into the blood-brain barrier permeability of GABAergic compounds, the active sample in the functional assay can be applied to *in vivo* zebrafish-larvae locomotor assay. Further analysis and collaboration of molecular modelling the active compounds are needed for confirmation and comprehensive insight from other fields. In the immunosuppressant assay, the activity of pure compounds of traditional Chinese medicine, the roots of *S. baicalensis*, displayed poor solubility and availability, but as a source of phytomedicines are warranted.

References

[1] Potterat, O., and Hamburger, M. Concept and technologies for tracking bioactive compounds in natural product extract: generation of libraries, and hyphenation of analytical processes with bioassays. *Nat. Prod. Rep*. 2013. 30, 546-564.

[2] Potterat, O., and Hamburger, Combined use of extract libraries and HPLC-based activity profiling for lead discovery: potential, challenges, and practical considerations. *Planta Med*. 2014. 80, 1171-1181.

[3] Zaugg, J., Baburin, I., Strommer, B., Kim, H-J., Hering, S., and Hamburger, M. HPLC-based activity profiling: discovery of piperine as a positive $GABA_A$ receptor modulator targeting a benzodiazepine-independent binding site. *J. Nat. Prod*. 2010. 73, 185-191.

[4] Moradi-Afrapoli, F., Ebrahimi, S., N., Smiesko, M., and Hamburger, M. HPLC-based activity profiling for $GABA_A$ receptor modulators in extracts: validation of an approach utilizing a larval zebrafish locomotor assay. *J. Nat. Prod*. 2017. 80, 1548-1557.

[5] Faleschini, MT, Maier, A, Fankhauser, S, Thasis, K, Hebeisen, S, Hamburger, MM, and Butterweck, V. A FLIPR assay for discovery of $GABA_A$ receptor modulators of natural origin. *Planta Med*. 2019. 85; 925-933.

[6] Joesch, C., Guevarra, E., Parel. S. P. Bergner, A., Zbinden, P., Konrad, D., and Albercht, H. Use of FLIPR membrane potential dyes for validation of high-throughput screening with FLIPR and μARCS technologies: identification of ion channel modulators acting on the GABAA receptor. *J. Biomol Screen*. 2008. 13, 218-228.

[7] Baxter, D. F., Kirk, M., Garcia, A. F., Raimondi, A., Holmqvist, M. H., Flint, K. K., Bojavic, D., Distefano, P. S., Curtis, R., and Xie, Y. A novel membrane potential-sensitive fluorescent dye improves cell-based assay for ion channels. *J. Biomol. Screen*. 2002. 7, 79-85.

[8] Arkarin, MR, Connor, PR, Emkey, R, Garbison, KE, Heinz, BA, Wiernicki, TR, Johnston, PA, Kandasamy, RA, Rankl, NB, and Sittampalam, S. FLIPR^{TM} assay for PCR and ion channel targets. Assay Guidance Manual. 2012. 1-33.

[9] Reinhardt, J., K., Klemd, A., M., Danton, O., Mieri, M., D., Smiesko, M., Huber, R., Burgi, T., Grundemann, C., and Hamburger, M. Sesquiterpene lactones from *Artemisia argyi*: absolute configuration and immunosuppressant activity. *J. Nat. Prod*. 2019. 82, 1424-1433.

[10] Zimmermann-Klemd, A. M., Reinhardt, J. K., Morath, A., Schamel, W. W., Steinberger, P., Leitner, J., Huber, R., Hamburger, M., and Gründemann, C. Immunosuppressive activity of *Artemisia argyi* extract and isolated compounds. *Front. Pharmacol*. 2020. 11; 1-13.

[11] Quah, BJC, and Parish CR. The use of carboxyfluorescein diacetate succinimidyl ester (CFSE) to monitor lymphocyte proliferation. *J. Vis. Exp*. 2010. 44, e2259.

[12] Hamburger, M. HPLC-based activity profiling for pharmacologically and toxicologically relevant natural products – principles and recent examples. Pharmaceutical Biology. 2019. 57(1), 328-334.

ACKNOWLEDGEMENTS

First of all, I would like to express my deepest gratitude Prof. Matthias Hamburger who has continuous support, guide, and expand my science view during my Ph.D. and my future work. It was a privilege to be part of your research group. I would like to thank PD Dr. Martin Smiesko, for being my second supervisor and for the kindness that he has given me. I would like to thank Dr. Emerson Ferreira Queiroz, who has been willing to be co-referee for my defense.

Secondly, I want to express my sincere appreciation to my scholarship, Indonesia Endowment Fund for Education (LPDP) of the Republic of Indonesia, because of this scholarship, I could pursue my Ph.D. at the University of Basel, Switzerland. I want to give my deepest gratitude to Prof. Dayar Arbain, who has introduced me to natural product research, for his continuous support throughout my Ph.D. study and my life in general.

I would like to express my appreciation to all of collaborators without whom I would not have been able to complete my Ph.D. projects: Prof. Dr. Steffen Hering and Dr. Marco Stadler on *Xenopus* oocyte assay; Prof. Dr. Carsten Gründemann, Dr. Amy M. Zimmermann-Klemd, and Seema Devi for the bioactivity testing of immunosuppressant activity.

I would like to say my gratitude to Manuela Rogalski for helping me in all administrative matters; you are amazing. I would like to thank you to Prof. Olivier Potterat for your guidance and trust to work with your projects, as wll as carefully double checked the Zusammenfassung (translated by Vanessa Fabienne Abegg) and also Dr. Eliane Garo for the experience in doing practicum of the plant system. I greatly appreciate Dr. Mouhssin Oufir on guidance and support in terms of research, IT, and life. To Orlando, who was always there when I needed technical assistance in the laboratory, thank you very much.

A special thanks to Ramzi, who spent his time correcting and proofreading my dissertation. I would like to acknowledge Dr. Alen Bozicevic, who companied and helped me at the beginning of my Ph.D. life, and Dr. Fahimeh Moradi-afrapoli, who guided me during my first year working in the lab and for helping me to get through my social life. I would like to thank Dr. Maria Teresa Faleschini, who had been patiently helping me in conducting research in the FLIPR assay, and Dr. Ombeline Danton, who assisted me in elucidating the structure of my isolated compounds, taught me working with ACDLabs and for being my friend and

travelling companion. My appreciation goes to all of my colleagues in the lab, Jakob, Resa, Vanessa, Tanja, Lara, Moris, Dr. Andrea Trayer, Antoine, Anne, Halim, Ming, Marzie, Maryam, Dr. Thanasan Nilsu, Dr. Pascaline Rahelivao, Dr. Anke Wilhelm and Heidi, all of you made my research and social life a great fun.

Thank you to my Indonesian friends in Switzerland (especially Dr. Bramasta Nugraha and Yonika Larasati), as well as in other countries, for continuing support and assistance. Last but not least, thank you to my parents and my big family in Indonesia for their endless support; I miss you all.